AN EDGE-CENTRIC PERSPECTIVE FOR BRAIN NETWORK COMMUNITIES

Joshua Ian Faskowitz

Submitted to the faculty of the University Graduate School

in partial fulfillment of the requirements

for the degree

Doctor of Philosophy

in the Department of Psychological and Brain Sciences

and Program in Neuroscience,

Indiana University

May 2021

Accepted by the Graduate Faculty of Indiana University, in partial

fulfillment of the requirements for the degree of Doctor of Philosophy.

Doctoral Committee

_____

Olaf Sporns, Ph.D., Co-Chair

_____

Aina Puce, Ph.D., Co-Chair

_____

Amanda Mejia, Ph.D.

_____

Richard F. Betzel, Ph.D.

April 27th, 2021

ii

ACKNOWLEDGEMENTS

Networks are all around us. This thesis emphasizes (repeatedly!) that the brain can be understood as a network. Here I would like to acknowledge *my network*: my family, friends, colleagues, and mentors. I am merely a node in my network. What really matters are my connections, the set of *edges*, that I have with you all. All that I have been able to achieve is undeniably influenced by the web of relationships and interactions around me.

To my family: I am what I am because of you. Mom and Dad, Bradley and Adam—your loving imprint on me is everlasting. Grandmas, Grandpas, Aunts, Uncles, and Cousins—you all are always in my heart (and brain) and are an inspiration.

To my friends: What can I say? You lot are great. In Bloomington, I feel fortunate to have formed ties with fellow students and scientists. It has been a pleasure to live and learn in this little college town with y'all. To the Bishop crew, thank you for putting up with my antics. And you are great. In California, to my fraternity brothers, collegiate compatriots, classroom buddies, and childhood friends, your connections matter dearly to me—even though I am far away right now. And finally, to Elizabeth, I am lucky to have you in my life. You are so, so great, and cool and smart.

To my colleagues: I cherish being in the lab because of you all. From USC to IU, learning from you daily is the best part of this career. And seeing you all at conferences absolutely makes my day. I am also thankful for the support from my department. To the anonymous reviewers of papers, thank you too! I reckon you have been fair.

To my scientific mentors: My journey to this point, to this place in my network, has been massively shaped by you. I strive to be scientist in the image of Allison, Neda, and Olaf. You are all rockstars. I am thankful for the time and energy you have invested in me.

I would like to thank my dissertation committee, Olaf, Aina, Amanda, and Rick; and Franco, who also supported me at IU. Thank you for your guidance, backing, and thoughtfulness. You all have made grad school such a meaningful experience.

And finally, thank you again to Olaf. You are really the best mentor I could have asked for in grad school. You have made grad school such a delight. I am so happy to be part of your network!

Joshua Ian Faskowitz

AN EDGE-CENTRIC PERSPECTIVE FOR BRAIN NETWORK COMMUNITIES

The brain is a complex system organized on multiple scales and operating in both a local and distributed manner. Individual neurons and brain regions participate in specific functions, while at the same time existing in the context of a larger network, supporting a range of different functionalities. Building brain networks comprised of distinct neural elements (nodes) and their interrelationships (edges), allows us to model the brain from both local and global perspectives, and to deploy a wide array of computational network tools. A popular network analysis approach is community detection, which aims to subdivide a network's nodes into clusters that can used to represent and evaluate network organization. Prevailing community detection approaches applied to brain networks are designed to find densely interconnected sets of nodes, leading to the notion that the brain is organized in an exclusively modular manner. Furthermore, many brain network analyses tend to focus on the nodes, evidenced by the search for modular groupings of neural elements that might serve a common function.

In this thesis, we describe the application of community detection algorithms that are sensitive to alternative cluster configurations, enhancing our understanding of brain network organization. We apply a framework called the stochastic block model, which we use to uncover evidence of non-modular organization in human anatomical brain networks across the life span, and in the informatically-collated rat cerebral cortex. We also propose a framework to cluster functional brain network edges in human data, which naturally results in an overlapping organization at the level of nodes that bridges canonical functional systems. These alternative methods utilize the connection patterns of brain network edges in ways that prevailing approaches do not. Thus, we motivate an alternative outlook which focuses on the importance of information

provided by the brain's interconnections, or edges. We call this an edge-centric perspective. The edge-centric approaches developed here offer new ways to characterize distributed brain organization and contribute to a fundamental change in perspective in our thinking about the brain.

TABLE OF CONTENTS

INTRODUCTION

The brain is a complex system that functions in both a local and distributed manner. We can interrogate brain functioning by focusing on segregated elements such as neural populations, circuits, or areas, to identify correlated or causal function. Additionally, we can interrogate brain functioning by focusing on how collections of localized elements integrate information with other elements, to give rise to a range of different functions. Neuroscientists have come to appreciate that *both* levels of organization are important for exploring how the brain works.

To capture both local and global features of the brain, we can employ the language and tools of networks (Barabási and Pósfai 2016). The flourishing field of network neuroscience (Sporns 2013, Bassett and Sporns 2017) promotes the application of network science tools to complex brain data, to uncover organizational patterns of brain architecture. Through networks, brain organization across scales of investigation can be probed—ranging from webs of neurons linked by synapses (Cook, Jarrell et al. 2019) to sets of parcellated regions whose aggregate electrophysiological or BOLD signals co-activate (Friston 2011).

The network neuroscience approach has advanced our understanding of the brain by providing a framework that allows for the quantification of brain organization (Rubinov and Sporns 2010). Networks allow us to abstract complex systems into two simple components: distinct elements, called *nodes*, and the interrelationships between nodes, called *edges*. By making this abstraction, a system as complicated as the brain becomes amenable to mathematical operations and computational manipulations. Using tools provided by network science and its mathematical foundation called graph theory, we can assess the economic arrangement of brain regions (Bullmore and Sporns 2012), identify elements of the brain that serve as putative hubs (Sporns, Honey et al. 2007), or even partition the wider network into meaningful sub-networks

that associate with specialized functioning (Power, Cohen et al. 2011, Yeo, Krienen et al. 2011, Betzel 2020).

The forthcoming thesis builds upon the model of the brain as a network and provides for a new lens through which to explore brain network organization. Notably, most discoveries in network neuroscience have focused on the nodes, or distinct elements, of the brain. In this thesis, we draw attention to the *edges* of brain networks, and apply network science tools that consider information at the edge level in specialized ways. Specifically, we highlight the importance of considering edge-level information through applications of a network science approach called *community detection*. We apply novel community detection algorithms to both human and animal structural brain data, as well as to functional data from a large neuroimaging consortium. In this thesis, we demonstrate the usefulness of an edge-centric perspective, which is a change in focus from the conventional, node-centric approach. It is our hope that an alternative perspective can open new possibilities and opportunities for probing the brain's architecture.

From brain mapping to brain networks

Location, location, location in the brain

Network neuroscience could be considered a quintessential modern discipline, as it draws on insights of modern complex systems science, and it operates on data with unprecedented resolution and scope. It is true that today's network neuroscience is made possible by the confluence of advancement computational methodology and data availability (Sporns 2017). However, network neuroscience is also built on knowledge ascertained from years of experimental investigation, localizing brain architecture and function across cortex (Catani, de Schotten et al. 2013, Swanson and Lichtman 2016). Without the work of brain mapping, which has

comprehensively annotated the brain with localized information, the connections between regions would be less meaningful. Here we briefly survey the relevant history of modern neuroscience, with a focus on tools and techniques that would pave the way for later network investigations.

Building a map of a system is an act of simplification, visualizing a bevy of features in a low-dimensional manner, and in turn, partitioning a complex system into understandable chunks (Sporns 2015). To delineate regions across the landscape of the brain, features must be observed that vary across locations. Initially, these features came from the microscopic properties of brain tissue. Pioneering work was performed in the latter half of the 19th century by scientists such as Baillarger, Meynert, and Wernicke, using histological preparations to observe anatomical variation in the brain (Catani, de Schotten et al. 2013). In this work, differences in neural tissue properties, i.e., cytoarchitecture or myeloarchitecture, were demarcated with a goal to identify anatomical markers of psychiatric disorders (Collin, Turk et al. 2016). The meticulous observation of the cortical layers, documenting cell size, shape, and arrangement distinguished certain areas, or parcels, of the cortex for the initial maps created by the likes of the Vogt's, Campbell, and Brodmann in the early 20th century (ffytche and Catani 2005, Nieuwenhuys 2013). By the 1920s and 1930s, dynamic properties of the brain could be localized through the recording of electrophysiological signals. Berger initially observed a 10 Hz idling oscillation in posterior parts of the brain, which was further characterized shortly thereafter by Adrian (Hari and Puce 2017). Also, around this time, Penfield was performing seminal work to map the sensorimotor system via electrical stimulation (Ladino, Rizvi et al. 2018). These early mapping studies, conducted without the luxury of high-resolution noninvasive imaging or modern computers, remain influential. Brodmann's regions became a common language for anatomical localization (Brett, Johnsrude et

3

al. 2002) and Penfield's homunculus would be reproduced in textbooks for years[1]. The knowledge gathered from these works further inform contemporary macroscopic mapping studies (van den Heuvel, Scholtens et al. 2015) and theories about brain wiring (Passingham, Stephan et al. 2002, Goulas, Zilles et al. 2018, Hilgetag, Beul et al. 2019).

The rise of magnetic resonance imaging (MRI) has introduced a new age of brain mapping, by providing millimeter resolution data of the brain's structure and function. Structural MRI provides a high-contrast high-resolution picture of the brain, by measuring the relaxation times of water molecules present in neural tissues with differential fatty constitution. These anatomical pictures can be analyzed with neuroimage processing software, such as FreeSurfer (Fischl 2012) and FSL (Jenkinson, Beckmann et al. 2012), to segment the tissues (Zhang, Brady et al. 2001) or to reconstruct layers of the cortex (Dale, Fischl et al. 1999). Using these tools, we can obtain the volume of brain structures (Hibar, Westlye et al. 2016, Whelan, Hibar et al. 2016) or the estimated thickness of the grey matter (Grasby, Jahanshad et al. 2020). A key development in the analysis of anatomical brain images was the effort to create common stereotaxic spaces and nonlinear imaging warping algorithms used for anatomical alignment (Thompson and Toga 1996, Toga, Thompson et al. 2006, Avants, Epstein et al. 2008). Individual brains are idiosyncratic, with common features (such as the central sulcus) surrounded by fingerprint-like gyrification and sulcal patterns (Pizzagalli, Auzias et al. 2017, Pizzagalli, Auzias et al. 2020). Aligning these features to a common reference space allows for features, such as the modulation of cortical thickness (Van Erp, Walton et al. 2018) or the deformation of anatomy (Faskowitz, de Zubicaray et al. 2016, Jahanshad,

---

[1] The pictorial representation of the homunculus has changed since its initial publication. See Catani (2017) for a brief review about this, and on the legacy of the homunculus.

Roshchupkin et al. 2018), to be measured across people. Collectively, the analyses of structural MRI can be used to map anatomical variation, in health and disease.

Functional MRI (fMRI) allows the dynamics of the brain to be observed *in vivo*, and without the invasiveness of PET tracers. The key to fMRI is the blood oxygen level dependent signal (BOLD—coined by Ogawa, Lee et al. (1990)) contrast, which is based on the difference in magnetic susceptibility between oxygenated and deoxygenated blood (Bandettini 2020). Even though the BOLD signal is vascular, its time course has been demonstrated to be a coupled, delayed, lowpass filtered, and prolonged signal of total neural activity at a location (Logothetis, Pauls et al. 2001). With the advent of fMRI, neuroscientists could design blocked and event-related experiments to localize task-related neural processing; creating colorful statistical maps of activation (Buckner, Bandettini et al. 1996) and sensory topography (Engel, Glover et al. 1997) in the process. Thus, fMRI ushered in a new era of cognitive neuroscientific investigation capable of localizing the neural "activation" patterns in response to a range of tasks and cognitive concepts (Poldrack 2006). Through thousands of fMRI experiments, the landscape of the brain has been annotated with activation coordinates, documenting the functional relevance of many brain regions (Fox and Lancaster 2002, Laird, Lancaster et al. 2005, Yarkoni, Poldrack et al. 2011). To date, increasingly sophisticated experiments employing rich stimuli (often with narrative content; see Willems, Nastase et al. (2020)) are used to gain an understanding of the functional layout of dynamic neural responses (Haxby, Connolly et al. 2014, Huth, De Heer et al. 2016, Baldassano, Hasson et al. 2018).

Filling in the gaps by connecting the maps

In the parlance of networks, delineating parts of the cortex into distinct areas amounts to creating a set of nodes, or elemental pieces of the system. Such divisions alone could be sufficient

to describe the static layout of the brain's components. Like a simple map of the European Union's political borders, such a map does well to visualize how the parts of the system are oriented and can provide details about each component, e.g., What is the capital of Germany? Where are the Alps? Where does the neural response to a face appear? What is the average thickness at the temporal pole? But to understand the *function* and *dynamics* of this system, we need to define the relational characteristics between the components, e.g., How balanced is economic trade between countries? In what patterns does immigration flow? How does the visual system communicate with the rest of the brain? Thus, a brain map of components can be enhanced with information about the relationships between the components [2] (Swanson 2000), or what we would call network edges. In tandem with the rise of localized brain mapping, neuroscientists have collected information about the interacting parts of the neural system—forming what we refer to as brain networks.

A significant first step in the quest to document the brain's wiring was taken with the documentation of the complete *C. elegans* nervous system (White, Southgate et al. 1986). This data would be used as a testbed for network science concepts, like *small-worldness* (Watts and Strogatz 1998) and serve as a valuable resource for studies of neuronal behavioral circuits (Schafer 2018). The "Mind of a Worm" was well ahead of its time, as the comprehensive connectivity (let alone, near complete connectivity) of mammals would not be reported until decades later. The aspirational idea of compiling the complete wiring diagram of the human, coined as the *Human Connectome*, was drafted by Sporns and colleagues (Sporns, Tononi et al. 2005). A key idea of this proposal is that brain's wiring fundamentally shapes and constrains the brain's dynamics. Thus, compiling such a comprehensive network would be a fruitful initial step for modeling brain

---

[2]Swanson writes: "The profound question really is not 'what is the brain?' but rather 'what are the basic parts of the nervous system and how are they interconnected functionally?'"

dynamics, just as compiling the genome marked initial progress for understanding the complex function DNA. To date, such detailed data from the human remains elusive and seemingly unattainable with today's *in vivo* methodologies. However, advances in genetic barcoding make the collection of a mammalian connectome a seemingly more realistic endeavor (Huang, Kebschull et al. 2020).

Through the 20th century, ever more sophisticated methods of tract tracing were developed, to document the mammalian brain's wiring (Saleeba, Dempsey et al. 2019). Tract tracing is a method that involves the injection of tracers (e.g., horse radish peroxidase, dextran-amines, or viral vectors) at specific regions, which permeate the efferent or afferent paths from an injection point, thereby documenting the region's connectivity. However, individual injection experiments are laborious and limited in scope. In 1991, Felleman and Van Essen demonstrated a database approach for collating numerous tracing experiments performed on the macaque (of the 1970s and 80s) and presented this information in tabular matrix and wiring diagram form (which notably conveyed the complexity of the macaque visual system) (Felleman and Van 1991). The advantage of such an approach was that it synthesized laboriously acquired information to gain a fuller view of the interconnected anatomy. Soon after, a wealth of neuroanatomical data became available including the connection matrix of the macaque cortex (Young 1993), cat cortex (Scannell and Young 1993), and later, a database of macaque connectivity (Kotter 2004). This new connectivity data was used for multivariate analyses aimed at elucidating the hierarchical organization encoded by these wiring patterns (Scannell, Blakemore et al. 1995), and to find clusters of differentially connected areas (Hilgetag, Burns et al. 2000). Today, tract tracing can be conducted in a systematic and comprehensive manner, resulting in inter-areal neuronal connectivity maps that do not rely on cross-laboratory data collation (Markov, Ercsey-Ravasz et al. 2014, Knox, Harris et al. 2019).

7

Whereas functional imaging studies of the late 1990's and early 2000's involved mapping functionally localized brain activity, many of the present day's studies are increasing focused on describing how regions connect to each other. Using diffusion-weighted MRI, which gauges the directionality of water flow constrained by neural tissue, paths can be computationally traced through the anatomy using a process known as tractography (Conturo, Lori et al. 1999). Tractography is an ill-posed algorithmic process that is prone to error (Jbabdi and Johansen-Berg 2011), yet it remains among our best methods to characterize white matter connections *in vivo* (Jbabdi, Sotiropoulos et al. 2015). Despite the method's shortcomings, generated streamlines form representations of anatomical tracts (Bullock, Takemura et al. 2019) that can differentiate between diagnostic group (Zhu, Jahanshad et al. 2016) or report the tissue integrity of connections (Yeatman, Wandell et al. 2014). Functional connectivity with fMRI is determined by measuring how the slow oscillatory BOLD signals (less than 0.1 Hz) at different parts brain co-activate, potentially signaling neural communication or a common driver of the constituent areas (Avena-Koenigsberger, Misic et al. 2018, Reid, Headley et al. 2019). Although this paradigm first appeared in 1995 as an investigation of co-activation between motor regions (Biswal, Zerrin Yetkin et al. 1995), awareness of functional connectivity accelerated when a distributed set of regions was shown to strongly correlate during passive rest (or display a coherent pattern of oxygen consumption via PET data), possibly reflecting intrinsic functional architecture (Raichle, MacLeod et al. 2001, Greicius, Krasnow et al. 2003, Vincent, Patel et al. 2007).

The network neuroscience work we perform today builds upon a mountain of knowledge gathered from brain mapping studies and the subsequent studies providing the means to connect these maps. This prior work shows us that the brain can be delineated into meaningful regions,

based on microscopic composition (Catani, de Schotten et al. 2013) or macroscopic patterns (Desikan, Ségonne et al. 2006, Smith, Fox et al. 2009). Furthermore, it has been established that spatially distinct (and possibly distant) regions can be structurally and functionally related, forming the web of relationships that constitute a brain network. Collectively, the modern history of neuroscience points to the concepts of segregation and integration (Tononi, Sporns et al. 1994, Sporns 2013): how parts of the brain carve out distinct functionality and broadcast to other elements, as guiding principles to investigate. Given this, we have fruitfully employed network models to describe these concepts.

A brief network science background

Networks are a universal phenomenon and are all around us, in natural, man-made, and artificial contexts. Networks can be applied to study systems that arise naturally, such as food chains of our ecosystem or the communication patterns between animals (Dunne, Williams et al. 2002). Humans construct and behave in networked patterns, which is evidenced by our transportation systems or social gathering tendencies (Stopczynski, Sekara et al. 2014). Finally, networks provide architectures used in computing applications and mathematical proofs. Across networks of different sizes and contexts, common patterns and properties of networks can be found (Watts and Strogatz 1998, Barabasi 2009). The field of network science encompasses the exploration of these patterns and properties, via modeling and analysis of distributed data. Studies within the realm of network science involve real world networks and range from investigations of simple generative models to the complex processes that overlay network structure. Whereas network science describes the scientific investigation of networked data, graph theory provides the foundation for mathematically describing any single network.

Graph theory is a branch of discrete mathematics used to describe core properties of networks. This field encompasses the theorems and algorithms that can be applied to networks, commonly of arbitrary structure. The origination graph theory is credited to Leonhard Euler, who used a mathematical approach to examine the traversal of seven bridges in the city of Konigsberg (Sachs, Stiebitz et al. 1988). When solving a puzzle about a path across these bridges, Euler had the insight to simplify the problem by modeling the landmasses separated by the river as discrete elements, known as *nodes*, and documenting the landmasses connected by a bridge. These connections are termed *edges*. Thus, he formed a rudimentary network, or graph, that documented the arrangement of the geography, encoded as the network's *topology*.

Euler's initial network could be considered as a basic "flavor" of a graph, with the connections denoting the binary presence or absence of a connection. Graphs can be enriched with details, such as edge weights describing the strength of a relationship, or the direction of a relationship. From these simple components, a practically infinite range of graph topologies can be created, ranging from ordered structures like rings or lattices, to highly convoluted, even random, graph structures. Using the formalism of a graph, a range of fundamental characteristics can be derived from the graph's arrangement of nodes and edges. Measurements such as the nodal degree, which describe the number or sum of edges emanating from (or directed towards) a node, or clustering coefficient, which describe the connected triangles emanating from (or directed towards) a node, are simple graph theoretic measurements that mathematically result from the arrangement of nodes and edges. This contrasts with other network assessments, such as the measuring the exponential fit of a degree distribution, which offer a more computational description of the network.

To date, graph theory has become associated with the theorems and proofs applied to networks with arbitrary or statistically governed topology, which are more treatable from a mathematics perspective (Iñiguez, Battiston et al. 2020). On the other hand, network science has come to describe the approach of practitioners describing real-world networks, which are complex, sparse, and potentially noisy. Notably, the network science approach draws on the insights of graph theory and depends on graph theoretic measurements but forgoes the mathematical certainties only possible in arbitrary graph structures. In this way, the lens of network science is more fruitful to use with brain network data, which deviates far from idealized topologies like a random graph or lattice (Sporns 2011).

What have brain networks revealed about brain organization?

Uncovering and understanding the underlying architecture of the brain is a longstanding pursuit for neuroscientists, and the adoption of network modeling and analysis provides new opportunities in this quest. Importantly, network tools allow for elusive concept of brain *organization* to be quantified, characterizing the ways in which neural elements collectively form a complex system (Bullmore and Sporns 2009, Rubinov and Sporns 2010, Telesford, Simpson et al. 2011, Fornito, Zalesky et al. 2016). Through networks, local regions can be placed within the wider context of the whole brain architecture and compared to other patterns within this architecture. In this way, this approach can complement longstanding *a priori* knowledge about specific regions or circuits (Haber and Knutson 2010), by ascertaining where these neuronal elements fit within the context of the greater brain architecture (Passingham, Stephan et al. 2002). Here we briefly highlight key findings using networks which characterize the distributed organization of the brain.

A key feature unique to brain networks is its spatial layout (Stiso and Bassett 2018), confined to the limited space inside of the skull. The brain is thought to have evolved to balance metabolic and volumetric constraints with the capability to transfer information (Laughlin and Sejnowski 2003, Bullmore and Sporns 2012). The organization of a brain network should reflect the tradeoff between the cost of wiring (operationalized frequently as the Euclidean distance between nodes) and capacity to transfer information (Achard and Bullmore 2007). The small-world topology we observe in brain networks—marked by a graph with high clustering coefficients and low shortest path length—is a plausible result of such a tradeoff (Bassett and Bullmore 2017). Notably, brain networks do not adhere to a strict pattern of absolute wiring cost minimization (Kaiser and Hilgetag 2006, Vertes, Alexander-Bloch et al. 2012, Betzel, Avena-Koenigsberger et al. 2016). Deviation from the least-costly organization is thought to be indicative of topological features vital for brain functioning, such as the formation of integrated and segregated functional states (Fukushima and Sporns 2020) or the placement of highly connected nodes (Roberts, Perry et al. 2016).

Hubs

Within a brain network, not all areas are connected in the same manner. Some areas might form connections with a few select regions whereas other areas might form connections far and wide (Betzel and Bassett 2018). The heterogeneity of nodal connection profiles can be captured using the degree distribution of the network, which for brain networks is observed to be heavy-tailed, but not necessarily 'scale-free' as other less physically constrained networks are argued to

be [3]. One implication of such a degree distribution is the likely presence of hubs—highly connected nodes that are topologically central to the network (Sporns, Honey et al. 2007, van den Heuvel and Sporns 2013). Such nodes are located along a disproportionate number of shortest paths in the network and often link functional systems (Zamora-Lopez, Zhou et al. 2010, Gordon, Lynch et al. 2018). One way to formally measure a node's propensity to link to an array of systems is to employ the participation coefficient (Guimera and Nunes Amaral 2005). High participation nodes are thought to promote flexible brain functioning across tasks (Bertolero, Yeo et al. 2018). Importantly, brain network hubs have been observed to disproportionately connect to other hubs, forming a so-called *rich-club* topology (van den Heuvel and Sporns 2011). This club of high degree nodes is thought to support integration of information, with rich connections that are long and costly, but that also participate in a majority of potential communication paths (van den Heuvel, Kahn et al. 2012).

Modules

A hallmark of complex systems is modularity, which describes how a system can be decomposed into subgraphs (sub-networks) that are highly intra-connected and sparsely inter-connected to the rest of the system (Newman and Girvan 2004). This sort of organizational configuration enables segregated information processing and in turn, potentially endows a system with functional flexibility (Kashtan and Alon 2005). Evidence for modular organization in brain networks is widespread and can be found in a range of contexts (Sporns and Betzel 2016). From the microscale *C. elegans* connectome (Sohn, Choi et al. 2011) to the broad networks obtained with fMRI (Meunier, Lambiotte et al. 2009), we can identify highly clustered subgraphs of the

---

[3] Many practitioners have observed, including Betzel and Bassett (2018), a log-normal edge weight distribution.

network. The identification of these subgraphs is commonly performed via modularity maximization (Newman and Girvan 2004), an algorithmic approach to identify highly clustered subgraphs relative to a null connectivity model (Betzel 2020).

The resultant modules, or communities, from modularity maximization are collections of nodes that could potentially serve a common purpose or contain a common trait. For example, modular groups of neurons within the *C. elegans* connectome correspond to specific functional circuits (Sohn, Choi et al. 2011, Jarrell, Wang et al. 2012) and are enriched for correlated gene expression (Arnatkeviciute, Fulcher et al. 2018). For networks that span the whole brain, identified modules from both structural (Chen, He et al. 2008, Hagmann, Cammoun et al. 2008) and functional data (He, Wang et al. 2009, Meunier, Lambiotte et al. 2009) are commonly related to the functional relevance of each node grouping (Crossley, Mechelli et al. 2013). A related approach to studying modularity in brain networks is to assess the modularity heuristic, Q, given fitted or existing communities. The modularity of brain networks has been shown to differ by age (Hughes, Faskowitz et al. 2020, Puxeddu, Faskowitz et al. 2020), track with task performance (Finc, Bonna et al. 2020), and even mediate cognitive maturation (Baum, Ciric et al. 2017). Finally, the modularity of brain networks has been incorporated into studies of brain pathology, used in part for example to examine the spread of induced damage (Zhang, Huang et al. 2019) or assess the global organization of pre-symptomatic brains structure (Voevodskaya, Pereira et al. 2018).

Finding communities in brain networks

Of the many tools that network science provides to analyze brain organization, the search for, and analysis of, modular organization remains a popular and fruitful approach. Several factors make the lens of modular organization an excellent approach for analyzing brain organization. To begin, finding modular groupings of nodes provides computational results that neatly fit into

prevailing framework of *segregated* and *integrated* brain organization (Sporns 2013, Wig 2017, Shine 2019). A modular partition of the network is one way to show that brain is not uniformly connected, but rather clustered into segregated modules that are functionally synchronized (and possibly actively communicating). Deviation from this modular structure, often framed as integration, can be assessed acutely, in response to cognitive demands (Alavash, Tune et al. 2019, Finc, Bonna et al. 2020), or diffusely, as a measurement of general organizational dysfunction or age-related impairment (Chen, He et al. 2008, Hughes, Cassidy et al. 2019). After modularity maximization is performed, a modular partition of the network provides the information used to characterize specialized *hub-like roles* that nodes can play i.e., provincial, connector, and kinless hubs (Guimera and Nunes Amaral 2005, Power, Mitra et al. 2014, Esfahlani, Bertolero et al. 2020). Furthermore, modularity is likely an appropriate description for the brain given its spatial compactness and the *economic constraints* it evolved under (Bassett, Greenfield et al. 2010, Betzel, Medaglia et al. 2017). And finally, at the level of practical algorithmic implementation, modularity can be adapted to multiple types of brain network modalities (Rubinov and Sporns 2011) and can be applied with robust algorithms (Blondel, Guillaume et al. 2008, Jeub, Sporns et al. 2018, Pedersen, Zalesky et al. 2018), making it a highly usable tool for network neuroscience practitioners. Although modularity is entrenched as a key organizational description for brain network organization, we must also understand this approach is limited to describing a specific network topology.

The search for, and analysis of, network modules falls under the wider scope of community detection for networks (Fortunato and Hric 2016). Community detection describes the tools and algorithmic processes used to uncover a network's underlying community structure, or classification of the network into multiple components. Modularity maximization is merely one

way in which to find meaningful communities of a network (Schaub, Delvenne et al. 2017). Whereas modularity maximization searches for clusters of dense connectivity, other approaches use dynamic processes, graph cuts, or statistical models to identify meaningful groupings of nodes, known generally as communities. These different methods lead to node groupings with different interpretations as well. Whereas a community derived with modularity maximization describes a grouping of nodes that are densely interconnected, a community derived with InfoMap (Rosvall and Bergstrom 2008) describes a grouping of nodes that does well to 'contain' a theoretical random walker.

The repeated application of modularity maximization to brain networks yields a somewhat narrow picture of the brain's community structure, finding modular partitions while precluding other community structure topologies such as core-periphery structure. In the context of brain networks, the modular structures are typically disjoint, meaning that no node is assigned to more than one community. Given the limited community structure definition provided by modularity maximization, there exists a potential gap in our understanding of brain organization: the effectiveness and repeated application of modularity maximization has led us to a restricted understanding of community structure in brain networks. The community topology, or topological characteristics of the network's community structure, for brain networks could be richer than the traditional modular organization we have observed to date.

Edge-centric network neuroscience and community structures

A large focus of network neuroscience is on elucidating features of network nodes—what we would call a node-centric approach. Many operations performed on brain networks are done so that the nodes can be annotated with a value and in turn, differentiated from one another or regressed against a trait. In this way, many of the crucial questions we ask in network neuroscience

16

focus on highlighting certain nodes: Which nodes are highly connected (Sporns, Honey et al. 2007)? Which nodes serve at key conduits of information transmission (van den Heuvel and Sporns 2011, Dann, Michaels et al. 2016)? How can nodes be grouped to form coherent clusters, which form a system of regions that perform a cognitive operation (Yeo, Krienen et al. 2011, Crossley, Mechelli et al. 2013)? Where are the nodes that bridge communities, and crucially integrate across systems (Bertolero, Yeo et al. 2015)? In these analyses and many like them, the focus is on the information that can be gleaned from the network structure to enrich the neuroscientific understanding of the nodes, whether they are neurons, neuronal populations, or volumetric areas.

The node-centric focus can be attributed to the historical roots of cognitive neuroscience, which has largely focused on localizing cognitive, behavioral, and disease-related phenomena in space and time. As a result, patches of cortex and subcortex are often affiliated with specific functions, from word processing and language comprehension, to constructs such as cognitive control and task de-activation. The node-centric perspective influences how we think about brain networks; in that we treat nodes as fundamental units of brain function, and edges as the (secondary) interrelationships between these units. This node-centric perspective is also reflected in the way we construct brain networks, treating the challenge of node definition as a primary influence on network statistics (Zalesky, Fornito et al. 2010, Arslan, Ktena et al. 2018, Messe 2020), whereas the edges are simply the measurements that fall between the nodes after a parcellation is selected. The prevailing node-centric approach is neither incorrect nor misguided. However, we can potentially expand our understanding of distributed brain organization using novel network modeling paradigms.

In this thesis, we propose that additional progress can be made by focusing on brain network edges. An edge-centric perspective focuses on interrelationships within a network and on the information that can be read and produced at the edge-level. To demonstrate this perspective, we apply community detection techniques not yet widely adopted in the network neuroscience community. In doing so, this thesis is positioned at the confluence of two underappreciated topics in network neuroscience: the possibility of non-modular community structure and the development of more edge-centric models. In the work presented here, we demonstrate how two advanced community detection approaches, the weighted stochastic block model and edge clustering, can provide an account of the brain's community structure that is not exclusively modular. Both approaches use edge-level information in a manner that is not common for brain investigations. In typical network neuroscience fashion, this thesis relies on advances made in network science that we can apply to brain networks in a principled manner. Following these empirical investigations, this thesis then explains the importance of brain network edges, and further advances how information at the edge-level is important and could yield new perspectives on brain organization.

The organization of this thesis

In this thesis we provide three exploratory investigations of brain network organization using advanced community detection techniques that we consider to be edge-centric. Following these chapters is review of brain network edges, detailing the role they play in understanding brain organization. We conclude with further synthesis of these chapters and a discussion of future edge-centric directions for neuroscience.

The first two chapters of this thesis demonstrate how we can uncover community structure that is not exclusively modular in both human and non-human structural brain networks (Faskowitz, Yan et al. 2018, Faskowitz and Sporns 2020). Whereas modularity maximization is

the traditional approach for partitioning the brain into dense clusters, here we utilize a statistical community detection tool called the stochastic block model (SBM) (Holland, Laskey et al. 1983, Snijders and Nowicki 1997). Stochastic block modeling is a community detection approach that seeks to form communities based on shared edge-connectivity patterns to other communities. The key advantage of the SBM is that it can flexibly identify a range of community topologies, which include modularity, core-periphery, and disassortative structure. In our applications, we rely on a weighted variant of the SBM (Aicher, Jacobs et al. 2013, Aicher, Jacobs et al. 2015), so that we can include heterogenous edge weight patterns found in our anatomical brain network data.

The next chapter of this thesis is a demonstration of a new edge-centric perspective on functional connectivity. A large portion of network neuroscience is devoted to analyzing functional connectivity networks, whose edges are traditionally formed by measuring the similarity between time series at nodes (Friston 2011, Fornito, Zalesky et al. 2016). In our work, we devised an approach to finely resolve an edge's fluctuations across time, which allows us to measure the similarity between edge time series. Inspired by network science advancements in the realm of edge clustering (Evans and Lambiotte 2009, Ahn, Bagrow et al. 2010), we constructed an edge-by-edge representation of the brain called eFC (*edge* functional connectivity). By performing community detection on this novel representation of the data, we obtain clusters of edges that have similar co-fluctuation patterns. The approach detailed in this chapter is decidedly edge-centric, in that it provides a new framework for analyzing edge-edge relationship via the eFC construct and a new avenue for representing edge activity over time. In particular, edge time series as described here can be adapted for several new applications, making it a fruitful construct for new empirical studies.

The last chapter of this thesis is a review of brain network edges, which is intended to highlight the value of edges elucidating brain network organization. This review seeks to understand how the relationships between nodes can be extracted, grouped, and analyzed. Edges can represent the physical connections that support communication, index the similarity of measurements taken at elements, or indicate an attribute inherent in a connection. Furthermore, edges can be grouped to form constructs such as motifs, fingerprints, and topologies that contain network information at different scales. The edge-centric approach does not exclude nodes, but rather represents a shift in focus and framing when employing networks to analyze brain organization.

The contribution of this thesis to the field of network neuroscience centers on a simple, yet underappreciated, aspects of familiar network science concepts applied to the brain. Here, we underscore the importance of information at the edges. Beyond the text of these chapters, we recognize that our published work is now of the network neuroscience literature, and we hope that these methods can be adopted by colleagues. To this end, we have contributed MATLAB code on GitHub that implements the key algorithms and frameworks used. Overall, we hope that the contributions of this thesis will not cease with the work here. We hope that our colleagues will synthesize the ideas presented here with their own work, to uncover new views of the brain's organization.

CHAPTER 1: WEIGHTED STOCHASTIC BLOCK MODELS OF THE HUMAN CONNECTOME ACROSS THE LIFE SPAN

Abstract

The human brain can be described as a complex network of anatomical connections between distinct areas of the cerebral cortex, referred to as the human *connectome*. Fundamental characteristics of connectome organization can be revealed using the tools of network science and graph theory. Of particular interest is the network's community structure, commonly identified by modularity maximization, where communities are conceptualized as densely intra-connected and sparsely inter-connected. Here we adopt a generative modeling approach called weighted stochastic block models (WSBM) that can describe a wider range of community structure topologies by explicitly considering patterned interactions between communities. We apply this method to the study of changes in the human connectome that occur across the life span (between 6-85 years old). We find that WSBM communities exhibit greater hemispheric symmetry and are spatially less compact than those derived from modularity maximization. We identify several network blocks that exhibit significant linear and non-linear changes across age, with the most significant changes involving subregions of prefrontal cortex. Overall, we show that the WSBM generative modeling approach can be an effective tool for describing types of community structure in brain networks that go beyond modularity.

Introduction

The human brain forms a complex network of anatomically interconnected neurons and brain regions, the *connectome* (Sporns 2011) that can be modeled and analyzed with the tools of network science and graph theory (Bassett and Sporns 2017). Modeling the brain as a network allows us to explore local as well as distributed properties of brain organization, using both descriptive (Hagmann, Cammoun et al. 2008) and generative modeling approaches (Betzel, Avena-Koenigsberger et al. 2016). A hallmark of complex networks, including the human connectome, is the presence of subnetworks, also called communities or modules (Sporns and Betzel 2016). The set of communities that comprise a given network is referred to as the network's community structure. This structure is useful for describing both large-scale and local patterns of the network (Sporns 2013). At large-scale, we can measure differential connectivity trends between communities, e.g., across age (Betzel, Byrge et al. 2014) or in relation to cognition (Bassett, Wymbs et al. 2011). Locally, we can use metrics such as the participation coefficient to assess node-wise aspects of the community structure (Sohn, Choi et al. 2011, Baum, Ciric et al. 2017).

In many extant studies, network communities are operationalized as modular subnetworks, i.e., as groups of nodes that are more densely connected within, and more sparsely connected between groups. However, the process of identifying modules in networks, community detection, is an ill-defined problem with no universal definition (Von Luxburg, Williamson et al. 2012, Fortunato and Hric 2016, Peel, Larremore et al. 2017, Rosvall, Delvenne et al. 2017, Schaub, Delvenne et al. 2017). Modular network communities are merely one plausible lens through which to analyze brain network communities. In fact, recent evidence demonstrates that the presence of diverse community structure connectivity patterns beyond modular configurations correlates with

22

behavioral task performance (Betzel, Medaglia et al. 2018) For this investigation, we employ an alternative to the modularity approach by adopting a model from a family of methods called stochastic block models (SBM) (Holland, Laskey et al. 1983, Wang and Wong 1987, Wasserman and Faust 1994, Karrer and Newman 2011). The SBM splits nodes into blocks, within which all nodes are stochastically equivalent in terms of how they connect to the rest of the network. As a generative model, it has a well-defined likelihood function with consistent parameter estimates. It is also highly flexible, capable of modeling a wide variety of community structures, including the conventional modular, but also disassortative, core-periphery or mixed community structures (Figure 1). Recent theoretical developments in SBM models have also enabled them to capture degree distributions (Karrer and Newman 2011), overlapping communities (Airoldi, Blei et al. 2008), and weighted edge weights (Aicher, Jacobs et al. 2013, Peixoto 2018) as well as statistically principled model selection criteria (Xiaoran, Cosma et al. 2014, Yan 2016).
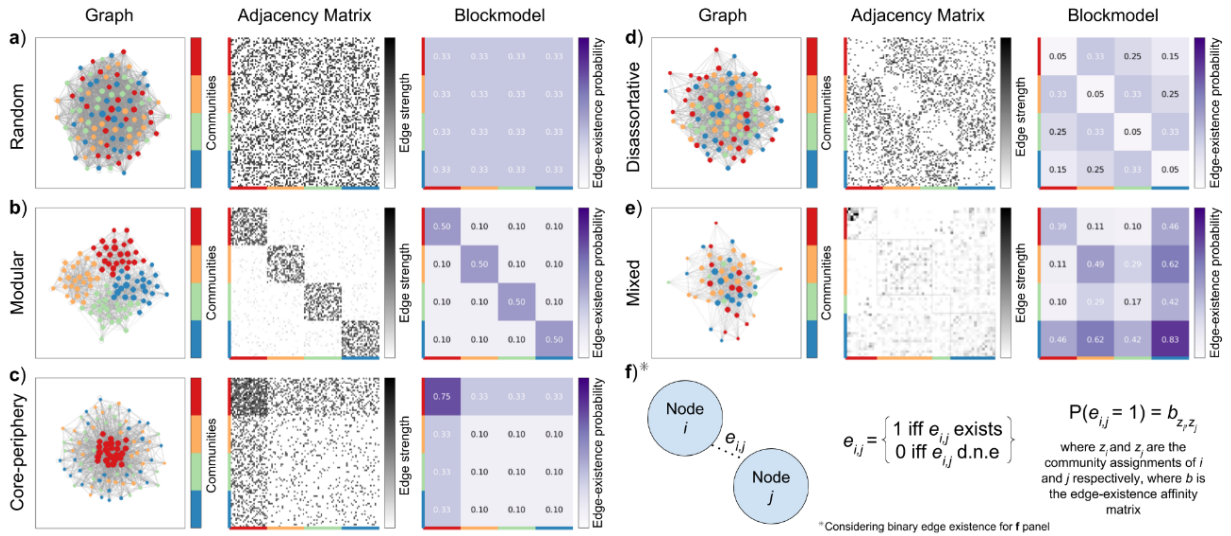
Figure 1 Three representations of network data: graph, adjacency matrix, block model. The graph is visualized as a force-directed (Fruchterman and Reingold 1991) graph layout, the adjacency matrix is visualized as a square matrix with entries for each edge between nodes, and the block model is visualized as a square matrix with entries for each edge-existence parameter between communities. **a)** Random network **b)** Modular network **c)** Core-periphery network **d)** Disassortative network **e)** Mixed network, based on an example fit to brain network data of a single hemisphere **f)** An illustration of a binary (unweighted) edge for each network data representation.

In this study, we employ the stochastic block modeling framework to analyze, cross-sectionally, how brain networks, and the community structure of these networks, are modulated across the human life span. Over the human life span the brain matures nonlinearly, from development to young adulthood, and into old age (Sowell, Thompson et al. 2004). Notably, morphological changes in the cortical grey matter are heterogeneous, as spatially distinct regions of the cortex develop, mature, and decline at different time points and rates (Storsve, Fjell et al. 2014, Gennatas, Avants et al. 2017). Additionally, the white matter architecture that supports connections between these distinct cortical regions develops at variable rates (Imperati, Colcombe et al. 2011, Lebel, Gee et al. 2012, Yeatman, Wandell et al. 2014). To characterize these changes in brain networks across the human life span several recent studies have applied tools of complex

24

network analysis (Zuo, Kelly et al. 2010, Betzel, Byrge et al. 2014, Cao, Wang et al. 2014, Zhao, Cao et al. 2015, Zuo, He et al. 2017). Using resting state functional connectivity MRI networks, studies have shown increases in connectivity between modules increases with age while connectivity within modules decreases (Betzel, Byrge et al. 2014, Chan, Park et al. 2014). The modularity of these networks has been shown to decrease over the life span (Cao, Wang et al. 2014). Concurrently, overall structural connectivity (total number of recovered streamlines) decreases as a function of age (Betzel, Byrge et al. 2014, Lim, Han et al. 2015), hypothesized to be a result of preferential detachment of short structural connections within modules (Lim, Han et al. 2015).

SBMs offer great flexibility as the way in which communities are defined transcends the narrower definition inherent in classical modularity maximization. Despite their methodological advantages, SBMs have only recently been applied to the analysis of brain networks (Pavlovic, Vertes et al. 2014, Moyer, Gutman et al. 2015, Bryant, Zhu et al. 2017, Betzel, Medaglia et al. 2018). Here we apply a weighted variant of the stochastic block model, called the Weighted Stochastic Block Model, or WSBM (Aicher, Jacobs et al. 2013, Aicher, Jacobs et al. 2015, Peixoto 2018), to whole-brain anatomical networks extracted from diffusion imaging and tractography data acquired across a major portion of the human life span. After designing a robust strategy for applying WSBMs to weighted connectome data, we fit WSBMs to group-averaged connectomes, as well as to individual connectome networks. We find patterns of age-related changes that unfold in specific sub-blocks of SBMs, representing bundles of connectome edges that exhibit significant linear or non-linear changes across the life span. We also demonstrate how to measure community structure change across age by conceptualizing community structure as a vector. Finally, we

discuss the patterns of change we detected in this study in the context of previous work reporting on modularity and age-dependent changes in functional connectivity.

Methods

Data description

Our data was generated from 620 human subjects (63% female) from the enhanced Nathan Kline Institute-Rockland Sample (NKI-RS) (Nooner, Colcombe et al. 2012). Institutional Review Board approval was obtained for this project at the Nathan Kline Institute (#226781 and #239708) and at Montclair State University (#000983A and #000983B) in accordance with relevant guidelines. Written informed consent was obtained for all study participants. Written consent and assent were also obtained from minor/child participants and their legal guardian. In the present study, human data used was de-identified and provided open-access via an Amazon S3 Bucket (fcon_1000.projects.nitrc.org/indi/enhanced/neurodata.html). The NKI-RS dataset is a cross-sectional community sample that covers a wide range of the human life span (6-85 years old; std. dev: 20.88). Both T1-weighted (T1w) and diffusion (dMRI) images were collected for each study participant on a 3T Siemens Magnetom Tim Trio scanner (Siemens Medial Solutions USA: Malvern PA, USA) using a 12-channel head coil. T1-weighted magnetization rapid acquisition gradient-echo (MPRAGE) were acquired with the following scan parameters: echo time (TE): 2.52 ms; repetition time (TR): 1900 ms; flip angle (FA): 9 degrees; FOV: 176 sagittal slices at 250 x 250 mm, with 1mm spacing; GRAPPA acceleration factor of 2; acquisition time: 4:18 min. DWI were acquired with the following scan parameters: TE: 85 ms; TR: 2400 ms; FA: 90 degrees; FOV: 64 axial slices of 212 x 212 mm, with 2mm spacing; multi-band acceleration factor: 4; 128 directions in single-shell; b-value $1500s/mm^2$; 9 non-weighted diffusion volumes; anterior >>

posterior phase encoding direction; acquisition time: 5:58 min. A total of 671 dMRI datasets were initially downloaded. Data exclusions included: 13 subjects did not have viable T1w (FreeSurfer failure); 12 dMRI were visually judged as having image artifacts (based on viewing medial axial, coronal, and sagittal slices of fractional anisotropy map) ; 24 tractography reconstructions were visually judged as poor (~3.8% of tractographies generated; based on 6 rotated views of the tractogram and looking for areas of non-smooth streamline paths); 2 streamline count matrices were labeled outliers based on an edge density cutoff (sparsity z-scores of -4.1 and -5.6)—adjacency matrices that failed to reach a binary edge density of 25% were deemed too sparse.

MRI pre-processing

T1w images were run through FreeSurfer's (surfer.nmr.mgh.harvard.edu) *recon-all* pipeline to obtain a cortical surface reconstruction and surface mapping to the FreeSurfer *fsaverage* space. We reconstructed the Yeo17 network parcellation (Yeo, Krienen et al. 2011) (114 cortical nodes, source: github.com/ThomasYeoLab) in the T1w native space using FreeSurfer's nonlinear surface warps. We then applied FSL fast (Zhang, Brady et al. 2001) to the skull-stripped T1w to obtain grey matter (GM), white matter (WM), and cerebral spinal fluid (CSF) partial volume estimation (PVE) maps. The bias-corrected T1w were rigidly aligned to MNI 152 1mm isotropic space using FSL *flirt*. All parcellations and PVE maps were aligned to MNI space by applying the *flirt* linear transformation. PVE maps were thresholded at 0.5, to obtain maps of the majority volume estimates for each voxel.

We first denoised the dMRI using a spatially adaptive denoising algorithm (St-Jean, Coupe et al. 2016). dMRI were then corrected for motion using FSL *eddy_correct*, with the normalized mutual information cost metric. The average unweighted diffusion volume (B0 image) was then linearly aligned to the T1w in MNI 152 2mm space using the FSL *flirt* boundary-based registration

routine (Greve and Fischl 2009). The inverse of this transformation was applied to the T1w to bring the T1w into the dMRI native space. We then used ANTs SyN registration (Avants, Tustison et al. 2011) to nonlinearly correct the dMRI for eddy current distortion in the phase encoding direction. The dMRI images were finally aligned to MNI 152 2mm space by concatenating and applying the *eddy_correct*, ANTs warp, and *flirt* transformations, to interpolate the dMRI only once. dMRI b-vectors were rotated accordingly.

We generated streamline tractography in the MNI 152 2mm isotropic space using Dipy (Garyfallidis, Brett et al. 2014). We first modeled the fiber orientation distribution function (fODF) at each voxel using constrained spherical deconvolution (Tournier, Calamante et al. 2007); fit using a recursive calibration (Tax, Jeurissen et al. 2014) and a spherical harmonic order of 8. We placed 9 random seeds in each voxel of a white matter mask, generated by calculating the intersection of the PVE WM and FreeSurfer WM segmentation. We used Dipy's *LocalTracking* module to deterministically propagate streamlines bidirectionally from each seed. Streamlines were generated at 0.5 mm steps, with a max turning angle of 30 degrees. Streamlines longer than 5mm and terminating in the GM PVE map, while avoiding the CSF PVE map (Smith, Tournier et al. 2012), were retained.

We constructed streamline count adjacency matrices by counting the number of streamlines that terminated in each region of interest (ROI) of the Yeo network parcellation. We disregarded nodes connected by only one streamline as noise and set these entries in the count matrix to zero. We recorded the voxel volume of each ROI of the Yeo parcellation and normalized the streamline count matrices by geometric mean volume of each pair of connected ROIs. This step was taken to remove potential edge-weight bias for larger ROIs. Hence, we recorded the weights of our structural connectivity matrices (connectomes) as streamline density measurements, as in previous

studies (Hagmann, Cammoun et al. 2008, Hagmann, Sporns et al. 2010, Betzel, Medaglia et al. 2018).

Community detection with the stochastic block model

Communities described by the SBM, also called blocks, are groups of nodes that are stochastically equivalent. Hence, nodes in the same community connect to all other nodes with a similar pattern. An SBM block does not require nodes within a block to connect densely to each other, and sparsely to other blocks. Rather, the probability at which nodes in a block connect to other nodes in the same block is a parameter with the same importance as all other block interactions. For classic SBM, the probability of an edge existing between two nodes of block A and block B will be described by a Bernoulli distribution with parameter *theta* that describes the probability of an edge existing between any two nodes of block A and block B. With an SBM of *k* blocks, we can build a $k \times k$ affinity matrix *b* that describes the probability of a connection (edge-existence) between nodes of each block based on the Bernoulli distribution parameterized by the corresponding entry in affinity matrix *b* (see Figure 1f). The between block edge-existence parameters describe the connectivity of each node to each block independently.

Recently, the SBM has been extended to model networks with weighted edges, referred to as the weighted stochastic block model, or WSBM (Aicher, Jacobs et al. 2013, Aicher, Jacobs et al. 2015, Peixoto 2018). With this advancement, we can apply the SBM framework to weighted networks commonly encountered in the network neuroscience literature. Using openly-available code (tuvalu.santafe.edu/~aaronc/wsbm/) (Aicher, Jacobs et al. 2013, Aicher, Jacobs et al. 2015), we fit the WSBM to structural connectivity matrices using a variational-Bayesian approximation approach. For our application, we chose to use the WSBM described by the following generative steps:

- For each node, assign a community membership

- For each pair of communities, assign edge-existence and edge weight parameters

- For each edge, draw from the Poisson distribution with the corresponding edge-existence parameter

- For each existing edge, draw from the normal distribution with the corresponding edge weight parameters

Community structure fitting workflow

Fitting the WSBM on connectome data yields stochastic results (like other community detection algorithms such as modularity maximization). When comparing across different community structures, the correspondence between specific communities could become unclear. Therefore, we first sought to create a representative WSBM partition of our data, to serve as a generalizable model to provide an initial overview of network structure in a specific age window, and to seed further age-dependent analysis. To create a representative matrix to infer the community structure of, we aggregated adjacency matrices from 53 young adult subjects ($25 - 35$ years old; 51% female) and averaged the data subject to several constraints (Figure 2a) (Misic, Betzel et al. 2015, Betzel, Medaglia et al. 2018). Specifically, the edge density of the representative matrix was set to match the average edge density of the input sample. Additionally, the distribution of streamline lengths across the input matrices was maintained, to mitigate bias against hard-to-recover long streamlines (Roberts, Perry et al. 2017).

Fitting WSBM to data requires searching over a large parameter space. Instead of using ad-hoc greedy heuristics, we adopt a multi-step fitting scheme. The first level of fitting involves fitting the model with a uniform prior, to broadly search the parameter space of plausible block partitions. We inferred WSBM structure with uniform block assignment prior parameters for 250

independent trials of the inference process. At each trial, the uniform block assignment is used to seed an expectation maximization algorithm (Aicher, Jacobs et al. 2015) to fit the following WSBM model parameters to the observed data. After 250 trials, the most likely model fit is retained (maximum posterior) and the most likely block assignments for each node are recorded. The second level of fitting involves fitting the model with increasingly stronger priors. The previously inferred block assignment was used to construct a biased block assignment prior parameter. That is, for each node, we assign a 100% higher likelihood for that node to be assigned to the previous most likely block and assign uniform likelihood to the other (k-1) blocks. With this prior, we ran 100 more independent trials. We iterated this second stage 10 times, incrementing the concentration of the most likely nodal prior assignment by 1.5 times (150%, 200%, ... 600%).
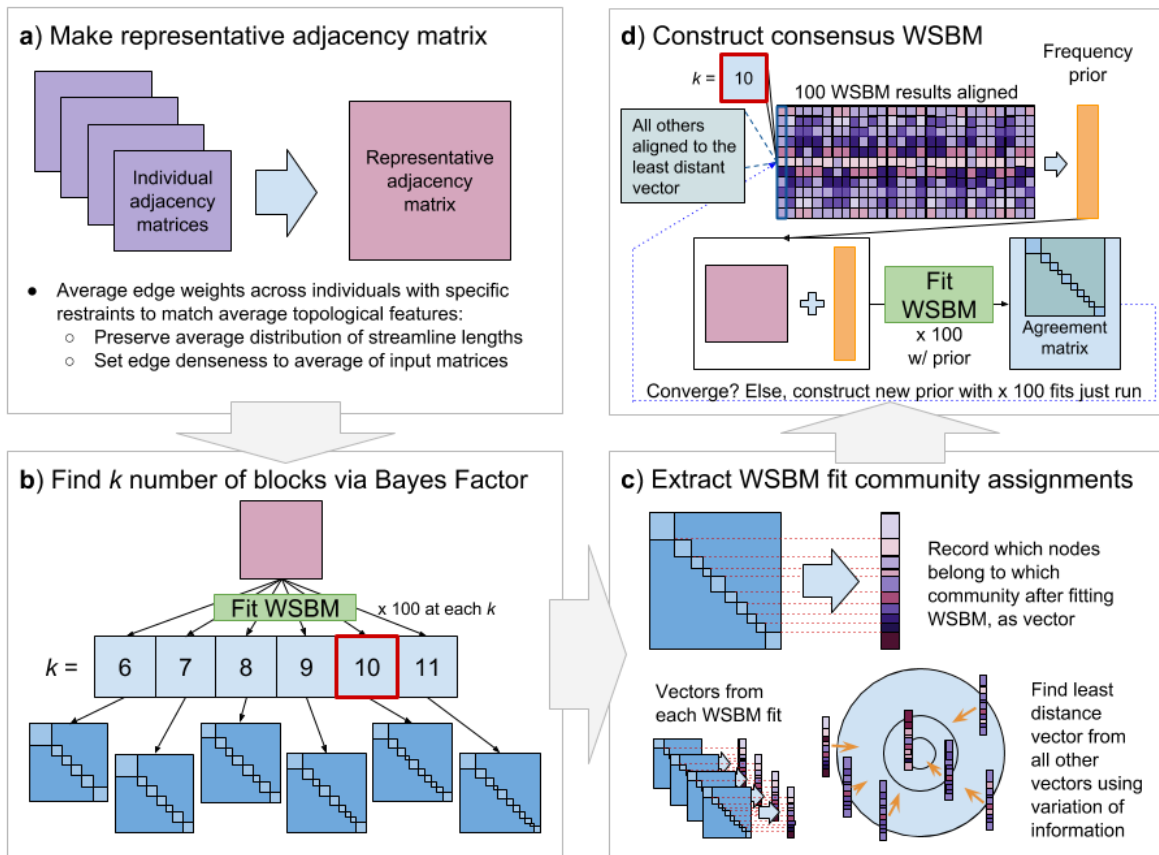
Figure 2 Creation of consensus WSBM model. **a)** A representative adjacency matrix was constructed by averaging across multiple individual matrices. This averaging was performed with specific restraints to mitigate bias. **b)** The number of blocks must be specified *a priori*; to identify an appropriate number of blocks (k), the WSBM was fit 100 times at k=6, 7…11. We recorded the average log-evidence of 100 model fits at each k and used Bayes factor to determine k in a data-driven manner. (Note that the red box indicates the k=10 parameter identified in this study) **c)** At the *k with the highest likelihood*, for each of the 100 fits, we recorded the community assignment for each node as a vector. We then computed the least distant community assignment vector from the 100 fits. **d)** Aligned results of the 100 fits were averaged to create a community assignment prior. This process was repeated until a convergence criterion was met.

We chose the number of communities (k) after repeatedly fitting the WSBM at each value of k=6,7…11 (Figure 2b). We fit the WSBM 100 times at each k and recorded the marginal log-

likelihood (which penalizes model complexity, ensuring that we do not fit the data better simply by increasing the number of parameters) at each fit. Using Bayes factors, we compare the partitions via the difference in marginal log-likelihood of each model fit (Aicher, Jacobs et al. 2015).

Next, we sought to derive a Bayesian consensus WSBM from multiple fits of our data (Lancichinetti and Fortunato 2012). First, we aggregated the results of the 100 WSBM fits at our data-driven selected *k*. Next, we choose a representative partition from these 100 fits by determining the partition least distant from all other partitions (centroid; Figure 2c). To do this, we computed the pairwise distance between all 100 partitions using variation of information (VI) (Meilă 2007, Sohn, Choi et al. 2011). By summing across the rows of this distance matrix, we selected the partition that was least distant (minimum sum) from all others (Meunier, Lambiotte et al. 2009). We then aligned the remaining 99 partitions to the reference partition via the Munkres algorithm (Munkres 1957). The aligned partition matrix (size: 114×100 [nodes × number of fits]) was used to make a new nodal assignment prior, based on the frequencies a node was assigned to each of the *k* communities across 100 fits. This new prior was used as input for 100 more WSBM fits (Figure 2d). This process was repeated until a convergence criterion was met (Kwak, Choi et al. 2009).

We also created an alternative modular community structure to compare against. To match the number of modular communities to the number of communities learned in the WSBM consensus model, we ran the deterministic spectral modularity maximization algorithm for weighted data implemented in the Brain Connectivity Toolbox (function *modularity_und*) across a range of gamma values (gamma: 0.5 to 4.0, at 0.01 steps). This resulted in 351 modular partitions with varying numbers of communities. We identified all partitions with an equal number of

communities to the WSBM consensus model and from these partitions we selected one least distant to the WSBM consensus model (measured by VI).

Finally, we used the consensus community structure models to seed community structure fitting on individual-level brain network data. The WSBM was fit to each subject's adjacency matrix with a prior community affiliation based on the WSBM consensus model concentrated at a level of 3. Thus, for each node, the community assignment of that node in the prior was 3 times more likely than an assignment to any of the other k-1 communities. The WSBM fitting procedure was then conducted as described previously. We collected five independent WSBM fits for each subject and retained the centroid partition of these fits. We also extracted a modular partition for each subject by running the spectral modularity maximization for weighted data, sweeping over levels of gamma from 0.5 to 4.0 in 0.01 increments. We identified modular partitions with k communities and retained the partition closest to the WSBM consensus model as measured by VI, to facilitate unbiased comparison. There is no guarantee that a modular partition with k communities will result from our sweep across gamma values. We excluded subjects for which we did not find a modular partition of k communities from the subsequent individual fits analysis (29 subjects).

Analysis methods

To assess how well our models fit the empirical data, we followed a generative model evaluation framework (Betzel, Avena-Koenigsberger et al. 2016). We generated synthetic data using the inferred edge-existence and edge weight parameters of the WSBM consensus model. To create a comparable generative model from the modular partition, we used the tools of the WSBM fitting toolbox to fit the modular structure with an absolute prior (100% and 0% probabilities), and thus, did not perform model inference. We generated 10,000 synthetic adjacency matrices from

both models. At each iteration, we recorded four binary network statistic distributions of the synthetic data: degree (*d*), clustering coefficient (*c*), betweenness centrality (*b*), and node Euclidean distance (*e*). We compared each synthetic statistic distribution with the empirical distribution of that statistic from the representative adjacency matrix (the data the model was derived from) using the Kolmogorov–Smirnov (KS) statistic, which measures the maximum difference between two empirical cumulative distribution functions. We computed the average KS statistic and conceptualized this as the energy of the synthetic network compared to the empirical network (Betzel, Avena-Koenigsberger et al. 2016).

$$KS\ Energy = mean(KS_d, KS_c, KS_b, KS_e)$$

Lower energy indicates a synthetic network with network statistic distributions that more closely resemble the empirical network statistic distributions. We define energy here as mean KS as opposed to maximum KS, as in (Betzel, Avena-Koenigsberger et al. 2016), so as not to bias the result by any one statistic that might produce systematically higher KS. In the previous study, the max KS was desirable because this metric was used for further optimization of the model. Here, our goal was to measure model performance, without changing the inferred model parameters.

We also sought to evaluate whether the set of inferred parameters of the generative models was meaningful for reducing the energy of the generated synthetic matrices. It could be that the mere modeling of distributions between blocks, regardless of the parameters, would be sufficient to generate synthetic networks with low energy. To test this, we generated 10,000 synthetic adjacency matrices and randomly permuted the intact models' parameters of the edge-existence and edge weight distributions at each iteration.

We next wanted to evaluate the extent to which each community structure preserved hemispheric symmetry. We proceeded under the assumption that at this level of analysis, it would

35

be plausible to expect to find homotopic organization (Zuo, Kelly et al. 2010); that is, that large patterns of organization of the right and left hemisphere organization should appear similar. To measure how the community structure captures laterality, we measured three weighted community-based network statistics: participation coefficient, within-community z-score, and assortativity. These three network measurements produce node-wise statistics that are relative to a given community structure. We measure each statistic given each consensus partition in each of the 620 subjects. For each subject, we compute the KS statistic between the left and right hemispheric distributions of the community-based network statistics.

We evaluated how the connectivity patterns between communities change over time. Our first approach involved measuring the total edge weight between communities. For each of N subject's brain network data, we created a $k \times k$ block matrix recording the total weight between each community of the community structure being analyzed. As our brain network data are symmetric, we analyzed the upper triangle plus main diagonal of the block matrix, totaling (k^2 – k) / 2 + k tests. To examine age-related trends in the values of these block strengths, we employed a multiple linear regression (MLR) analysis to model block strength as a linear combination of predictors. The MLR model was formulated as one of three models: (1) linear, (2) quadratic curve, (3) Poisson curve (as in (Lebel, Gee et al. 2012)):

1) $y = \beta_0 + \beta_1 \times age + \beta_G \times G + \varepsilon$

2) $y = \beta_0 + \beta_1 \times age + \beta_2 \times age^2 + \beta_G \times G + \varepsilon$

3) $y = \beta_0 + \beta_1 \times age \times e^{-\beta_2 \times age} + \beta_G \times G + \varepsilon$

where y is the dependent variable, in this case a vector [number of measurements (n) $\times$ 1] of block strengths between communities i and j, β_1 and β_2 (if necessary) are weights estimated by ordinary least squares regression, G is a matrix [$n \times 2$] nuisance covariates (sex, total network strength)

with β_G $[n \times 2]$ also representing weights estimated by ordinary least squares regression, and ε is a vector $[n \times 1]$ of residual error. We also conducted tests with an additional nuisance parameter indexing motion across the DWI acquisition, which would make G and β_G size $[n \times 3]$. We implemented the MLR by first linearly regressing out the nuisance covariates from the covariate of interest and using the residuals to regress against age. We fit each MLR model to each block strength vector and calculated model accuracy using leave-one-out cross validation (LOOCV). We calculated the root mean-squared-error (RMSE) of each fit and chose the model (linear, quadratic, Poisson) with the lowest error. To obtain a p-value, we randomly permuted age across 10,000 least-squares fit iterations. We retained trends with a computed p-value that passed Bonferroni correction for 55 comparisons (α = 0.0009). For each MLR model we report the coefficient of determination (R^2) calculated from the LOOCV procedure (Yeatman, Wandell et al. 2014):

$$R^2 = 1 - \frac{\sum_{i=1}^{n}(y_i - \acute{y}_i)^2}{\sum_{i=1}^{n}(y_i)^2}$$

where n is the number of measurements, y $[n \times 1]$ is vector of dependent variables, and $\acute{y}$ $[n \times 1]$ is the vector of model predictions.

For our second approach to assess how overall community structure changes across age, we pursued mathematical comparisons that measured all community interactions simultaneously. To do this, we utilized the block matrix, which is a $k \times k$ matrix, in which each entry i, j is a measure of the edges (e.g., total strength, average strength) between communities i and j. Thus, a block matrix provides a condensed information about network connectivity, given a community structure. We unrolled the upper triangle plus main diagonal of the average block matrix into a vector of length $l = \frac{k^2 - k}{2} + k$. We then used this vector as an l dimensional representation of the overall pattern of community structure and measured these vectors similarity and distance to our

consensus models. For this analysis, we used the block matrix of average strength between communities, as opposed to total strength as in the previous analysis, to mitigate the effect of community size for this analysis.

We measured how similar/distant each subject's community structure vector was to the consensus model community structure vector. In the WSBM evaluation, we used the affinity parameters of the WSBM consensus model to obtain the WSBM consensus model vector. For the modular evaluation, we measured the empirical block matrix based on the modular fit to the representative adjacency matrix to obtain the modular consensus model vector. For each of N subjects, we unrolled the upper triangle (including diagonal) of an average strength block matrix given each partition. We compared each of N community structure vectors to the consensus model vector using cosine similarity and city block distance (Aggarwal, Hinneburg et al. 2001). We then used the MLR scheme detailed previously to assess the proportion of the variance in subject-level vector similarity/distance that is due to age.

To analyze individually fit community structures, we employed the previously described vector comparison scheme with individually fit community structures. We recorded the distance of individual vectors to the model prediction vectors, as described previously and employed MLR to measure trends in age versus subject-level vector similarity/distance.

Additionally, we measured nodal versatility across individually fit partition (Shinn, Romero-Garcia et al. 2017). Nodal versatility is an index of how consistently nodes are classified in the same community across repetitions of a community detection algorithm. We used this measure to obtain a versatility index for each of the 114 nodes in use. Instead of measuring nodal versatility across repetitions of an algorithm, we measured the node versatility across subjects to evaluate differences in community detection techniques. We employed a permutation test to create

a distribution of null versatility differences to test for statistical significance. If there is no difference between the methods, exchanging subject A's WSBM community vector for subject A's modular community vector would not affect the node versatility index. Therefore, for each permutation we constructed two complementary node × subject matrices, in which we shuffled the type of community vector included. We computed the node versatility of each node × subject matrix and took the node versatility difference at each node. We measured the empirical versatility difference against the null distribution of versatility differences at each node to obtain a p-value, and report nodes that pass Bonferroni correction for 114 comparisons ($\alpha = 0.0004$).

Results

Model fitting workflow

Our consensus fitting procedure was intended to aggregate the results of 100 WSBM model fits. We found that our method was consistent despite internal stochastic elements of the code; if given the same data, the process produced the same output in each of 20 repetitions. We also ran the process on 100 additional independent runs at $k=10$ to create a new frequency prior and observed that the resulting community structure had a 0.80 normalized mutual information (NMI) to the obtained WSBM consensus model. As a final test, we bootstrap-sampled the results of the 100 fits to create different initial frequency priors. Comparing the results of this process with the obtained WSBM consensus model resulted in NMI measurements with a mean of 0.97 ($\pm$ 0.04, range=0.86-1.0).

Consensus community structure

Using the consensus method outline above, we inferred WSBM community structure from the representative brain network data (edge-existence density=30.1%). We identified 10 bilateral

communities with mixed topology profiles and attributes (Table 1). Sizes of the communities ranged from 6 to 21 nodes. The WSBM model estimates parameters that govern the distribution of edge and edge weight between communities; these parameters are visualized in panels **d** and **e** of Figure 3. Generally, the WSBM modeled a positive relationship between edge existence and edge weight; in other words, block interactions with low edge existence were modeled with low edge weight or high edge existence with high edge weight. One block interaction, *4-10*, stands out as having been modeled with a low edge existence but high edge weight (red arrow, panel **e**, Figure 3). This interaction is predicted to be connected at a probability of 13% and its edges are predicted to have a strength (average streamline density) of 0.29. Three block interactions are notable for having high edge weight and edge-existence parameters: 3-3, 6-6, and 7-7. In the modular community structure, not all communities identified were bilateral; that is, some communities were confined to only one hemisphere. The modular communities range in size from 2-22 nodes. Measuring the total Euclidean distance between nodes of communities in each partition, in each subject, we find that the modular community structure consists of communities much more spatially compact (M=8.29×10^{3}mm, SD=89.01) than the WSBM partition (M=8.68×10^{3}mm, SD=62.54mm; (two-tailed paired t-test with unequal variances; t(1.11×10^3)=88.35, p < 10^{-9}) .

Table 1 How consistently high strength nodes (top 25%) appear in the same community, measured across subject with the intraclass correlation coefficient; confidence interval computed with 500 bootstrap iterations.

Community structure model	Binary degree ICC (95% confidence interval)	Weighted degree ICC (95% confidence interval)
WSBM	0.83 (0.82 – 0.84)	0.74 (0.73 – 0.75)
Modular	0.64 (0.62 – 0.65)	0.59 (0.58 – 0.61)
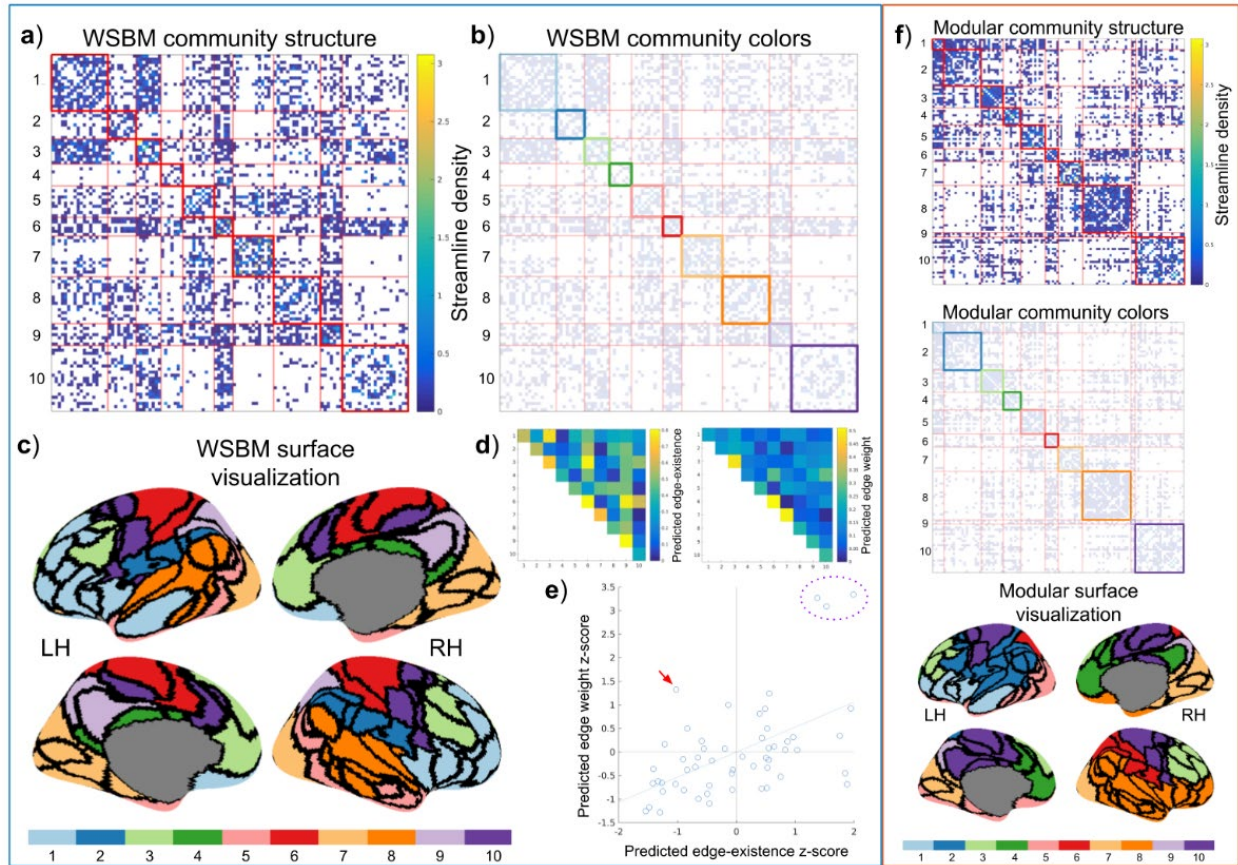
Figure 3 The WSBM consensus model, fit to a representative matrix averaged across 53 young adult subjects. LH = left hemisphere; RH = right hemisphere. **a)** The adjacency matrix ordered by the blocks of the WSBM consensus model. On-diagonal blocks are outlined in red, off-diagonal blocks are outlined in light red. **b)** The adjacency matrix of the young adult data with the on-diagonal blocks colored to match the inflated surface view (in panel **c**). **c)** The community structure of the consensus model visualized on the inflated surface of the left and right hemispheres. **d)** The predicted edge-weight and edge-existence matrices; the entries of these matrices contain the consensus model predictions for the average edge-weight and edge-existence for each block interaction. To calculate the consensus model's average block interaction prediction, these two matrices can be multiplied element-wise. **e)** We plot the paired parameters of the block interactions (z-score transformed). From this plot, we observe a general linear trend between predicted edge-existence and predicted edge weight for each block interaction. We highlight how the WSBM fit densely connected and densely weighted areas (purple dotted circle) as well as non-modular block interactions (red arrow). **f)** Visualization of alternative modular community structure, visualized as adjacency matrices and on the

cortical surface in the same manner as WSBM model. The labeling of these alternative community structures (represented as colors) is aligned to closely match the labeling of the WSBM model using the Munkres algorithm.

We also measured how the high strength nodes were distributed amongst communities in the different community structure models. We recorded in which communities the top 25%-degree (binary degree and weighted degree) nodes for each subject appeared and then measured how consistently these high strength nodes were dispersed among the communities across subjects (Table 2). We find that the WSBM model most consistently groups high degree nodes in a similar pattern across subjects, as measured by the intraclass-correlation coefficient, $ICC(3,1)$ (Shrout and Fleiss 1979).

Table 2 Table of community statistics for the WSBM and modular consensus partitions. Statistics from the representative young adult matrix; across-subject mean ± standard deviation in parentheses.

Label	Mean within-community strength	Mean between-community strength	Mean community participation coef.	Community assortativity
WSBM				
1	0.11 (0.096 ± 0.018)	0.042 (0.04 ± 0.0066)	0.77 (0.73 ± 0.027)	-0.035 (-0.027 ± 0.025)
2	0.095 (0.08 ± 0.027)	0.035 (0.032 ± 0.0076)	0.82 (0.76 ± 0.022)	0.011 (-0.006 ± 0.032)
3	0.33 (0.28 ± 0.076)	0.054 (0.05 ± 0.0093)	0.78 (0.75 ± 0.022)	0.19 (0.16 ± 0.078)
4	0.051 (0.046 ± 0.029)	0.038 (0.033 ± 0.0086)	0.73 (0.64 ± 0.054)	-0.084 (-0.084 ± 0.054)
5	0.11 (0.12 ± 0.032)	0.035 (0.034 ± 0.006)	0.79 (0.73 ± 0.027)	0.032 (0.034 ± 0.033)
6	0.4 (0.37 ± 0.12)	0.056 (0.051 ± 0.009)	0.78 (0.75 ± 0.025)	0.26 (0.24 ± 0.13)
7	0.33 (0.33 ± 0.049)	0.021 (0.022 ± 0.0041)	0.48 (0.45 ± 0.05)	0.25 (0.24 ± 0.055)
8	0.11 (0.1 ± 0.021)	0.033 (0.032 ± 0.0067)	0.77 (0.71 ± 0.03)	0.029 (0.026 ± 0.022)
9	0.19 (0.19 ± 0.098)	0.052 (0.049 ± 0.0086)	0.85 (0.79 ± 0.032)	0.098 (0.082 ± 0.094)
10	0.084 (0.063 ± 0.017)	0.032 (0.027 ± 0.0046)	0.7 (0.66 ± 0.03)	-0.0068 (-0.018 ± 0.019)
Modular				
1	0.2 (0.19 ± 0.057)	0.05 (0.048 ± 0.0095)	0.81 (0.75 ± 0.028)	0.066 (0.051 ± 0.058)
2	0.11 (0.1 ± 0.024)	0.034 (0.03 ± 0.0059)	0.7 (0.63 ± 0.039)	0.015 (0.018 ± 0.028)
3	0.3 (0.25 ± 0.061)	0.042 (0.041 ± 0.0083)	0.72 (0.68 ± 0.034)	0.21 (0.15 ± 0.069)
4	0.27 (0.23 ± 0.07)	0.034 (0.033 ± 0.0073)	0.7 (0.66 ± 0.051)	0.19 (0.14 ± 0.075)
5	0.19 (0.19 ± 0.035)	0.043 (0.041 ± 0.0084)	0.71 (0.66 ± 0.04)	0.062 (0.059 ± 0.049)
6	0.19 (0.18 ± 0.063)	0.046 (0.042 ± 0.011)	0.78 (0.7 ± 0.044)	0.049 (0.05 ± 0.073)
7	0.35 (0.35 ± 0.055)	0.025 (0.026 ± 0.0055)	0.52 (0.49 ± 0.042)	0.28 (0.27 ± 0.061)
8	0.14 (0.14 ± 0.024)	0.029 (0.028 ± 0.0061)	0.57 (0.52 ± 0.055)	0.068 (0.058 ± 0.027)
9	0.5 (0.49 ± 0.48)	0.057 (0.054 ± 0.015)	0.87 (0.81 ± 0.036)	0.35 (0.34 ± 0.45)
10	0.14 (0.1 ± 0.019)	0.026 (0.025 ± 0.0042)	0.55 (0.55 ± 0.038)	0.085 (0.044 ± 0.023)

Model fitting comparison
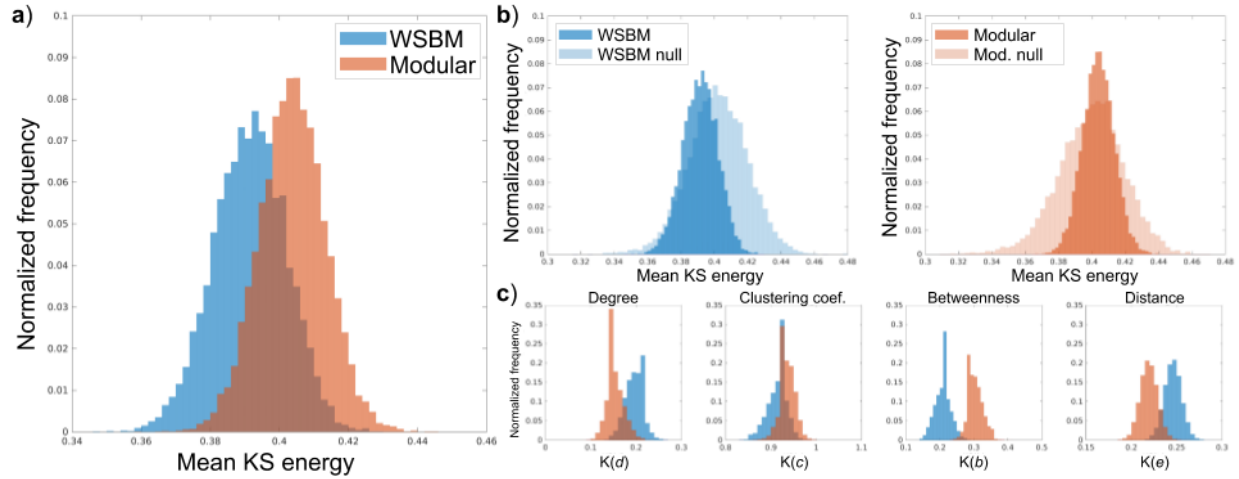
Figure 4 Comparison of WSBM and modular generative capabilities and characteristics. **a)** We compared the mean KS energy between generated synthetic data based on the community structure models and empirical data; we observe that the WSBM generates synthetic data with a lower mean KS statistic—demonstrating that WSBM synthetic networks have network statistic distributions more representative of the empirical data. **b)** We compare each model energy distribution with the energy distribution from a randomized model containing the same affinity parameters; we observe that the mean energy of the WSBM model is significantly lower than the WSBM randomized model; we observe that the mean energy of the modular model is higher than the modular randomized model **c)** We show the KS statistics of each network statistic that comprises the KS energy formulation.

We found significant differences between the community structures identified through WSBM inference and modularity maximization. The mean generative energy of the WSBM model (M=0.391, SD=0.011) was significantly lower than the mean of the modular model (M=0.404, SD=0.009) (two-tailed paired t-test with unequal variances; t(1971)=-88.03, p < 10^{-9}). This WSBM generative energy distribution had a significantly lower mean than the mean of the randomized WSBM generative energy distribution (M=0.402, SD=0.377; t(1630)=52.16 , p < 10^{-9}), whereas the mean of the randomized modular generative energy distribution (M=0.400, SD=0.360) was

lower than its distribution from the intact model ($t(1443)=-17.68$, $p < 10^{-9}$). The individual

distributions averaged over to calculate generative energy are also shown in panel **c** of Figure 4.

We studied how the community structures under investigation capture symmetric network

structure across hemisphere, as measured by node-wise network statistics. We measured the

histogram distances between the left and right hemisphere histograms of participation coefficient,

within-community z-score, and assortativity using the KS statistic. We found the mean of

participation coefficient and node-assortativity KS distributions to be significantly lower for the

WSBM community structure compared to the KS distribution for the modular community

structure. Statistical comparisons are shown in Table 3.

Table 3 Statistical comparisons between community structure-based node statistics

Node-wise network statistic	Mean ± standard deviation	t-statistic	p-value
WSBM participation coefficient	0.14 ± 0.04		
Modular participation coefficient	0.24 ± 0.06		
		$t(1128) = -34.10$	$p < 10^{-9}$
WSBM within-module z-score	0.17 ± 0.06		
Modular within-module z-score	0.14 ± 0.04		
		$t(1139) = 9.24$	$p < 10^{-9}$
WSBM assortativity	0.14 ± 0.05		
Modular assortativity	0.2 ± 0.07		
		$t(1107) = -20.61$	$p < 10^{-9}$
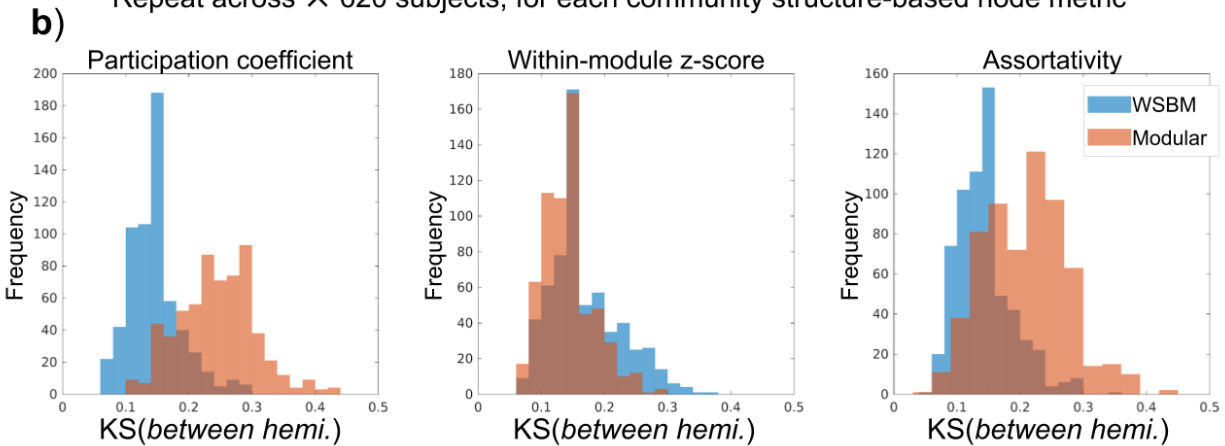
Figure 5 Evaluation of the laterality of the WSBM and modular community structures. **A)** We compute community-based network statistics on the subject network data, yielding node-wise statistics; we then calculate separate distributions of these statistics based on each node's laterality; we then measure the distance between these two distributions (note the shaded grey distribution illustrates the full, bilateral network statistic distribution) **b)** We compare the laterality of each community structure by illustrating the KS between hemispheric distributions of community-based network statistics. We observe that the WSBM partition balances the participation coefficient and node-wise assortativity distributions across hemispheres better than the modular partition. The modular partition preserves within-community z-score better than the WSBM partition.

Changes across the life span

We used multiple linear regression (MLR) to measure trends of block interaction strength across age. We observe strong quadratic relationships for within-community trends for both the WSBM and modularity models. We report the top 4 MLR trends for each model in Figure 6, and the top 12 trends for each model in Figure S3. The inverted-U shaped quadratic trend for block interaction *3-3* had the largest R^2 for both the WSBM and modular partitions (R^2: 0.25 and 0.20 respectively). Community *six* was involved in the second strongest trends for both the WSBM and modular partitions. Fewer on-diagonal MLR trends were significant for the WSBM partition than for the modular partition (4 and 6 block interactions respectively).
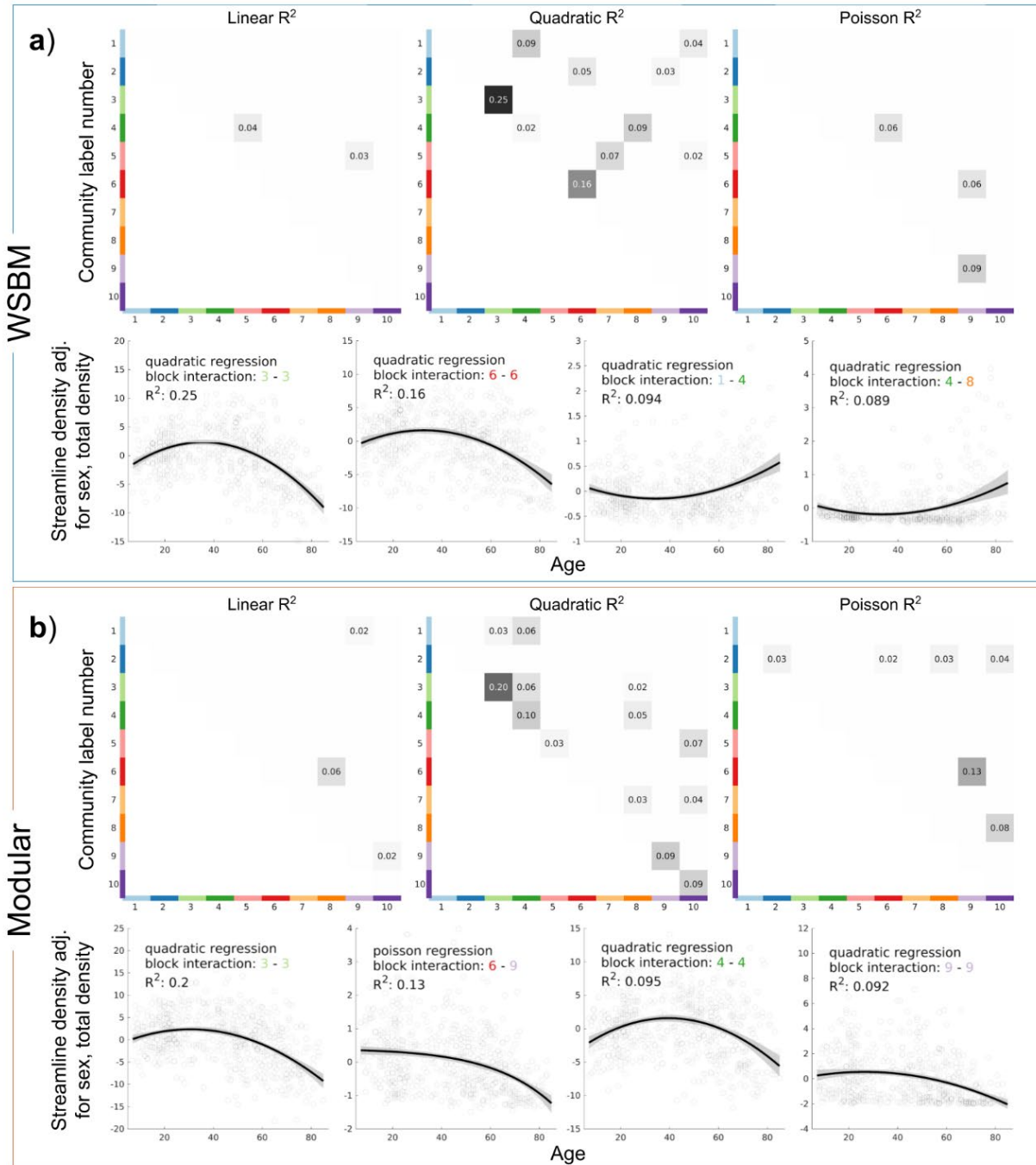
Figure 6 Results of multiple linear regression analysis on edge strengths of community interactions in the WSBM (**a**) and modular community (**b**) structures. The strongest quadratic relationship between age and community interaction edge strength is the 3-3 block interaction. All community interaction regressions that are statistically significant are shown. The top 4 MLR trends are visualized for each community structure model; the bootstrapped 95% confidence interval is shaded in grey.

When measuring community structure as a vector and computing vector similarity and distance from each subject to a consensus partition, we observed differences based on community partition used and observed strong MLR trends across age. Cosine similarity between subject and WSBM consensus vectors (M=0.96, SD=0.027) was significantly higher than the cosine similarity between subject and modular consensus vectors (M=0.92, SD=0.066; two-tailed paired t-test with unequal variances; $t(823.75)=20.46$, $p < 10^{-9}$). Using the city block distance measurement also displayed a significant overall difference ($t(960.89)=-24.44$, $p < 10^{-9}$) between using the WSBM (M=1.00, SD=0.19) or modular vectors (M=1.38, SD=0.34). These trends did not change substantially after regressing out covariates (sex, total network strength, movement; Figure 7b).
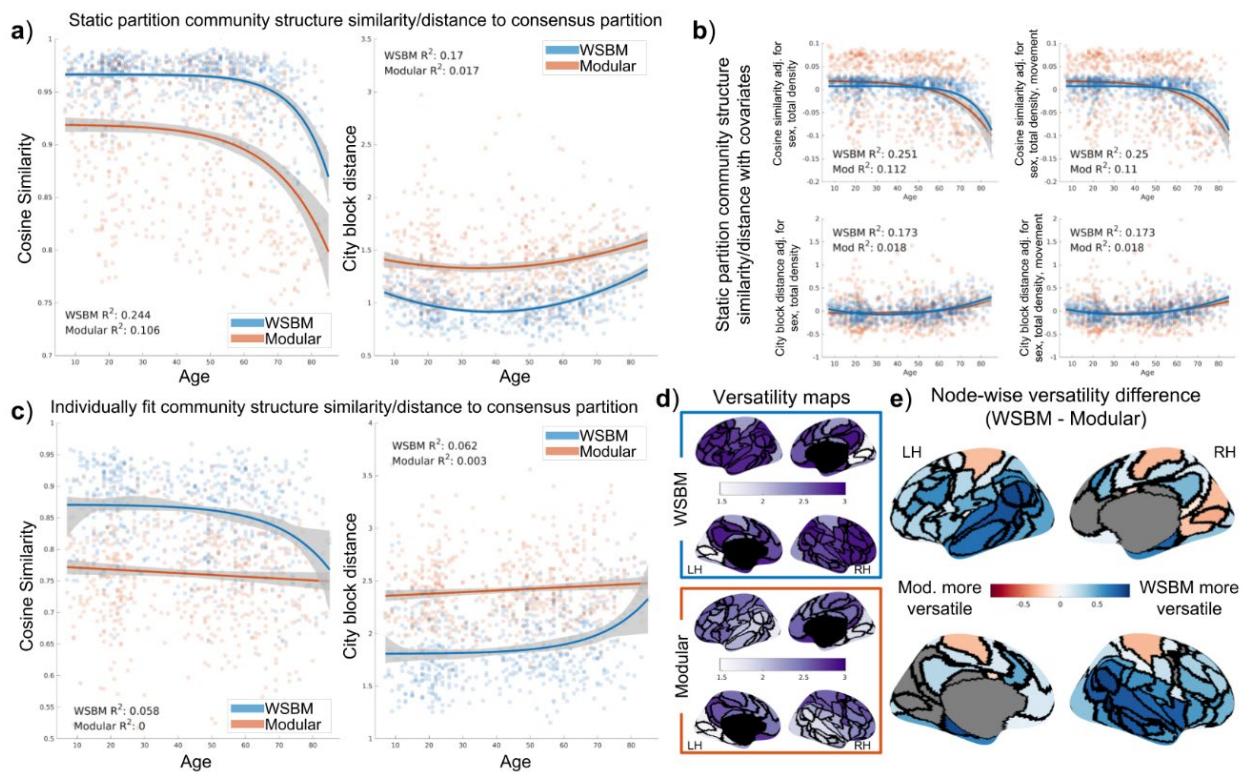
Figure 7 Measuring community structure vector similarity/distances. **a)** Regression of age versus vector measurements using the static community structure measured on subject-level data. Bootstrapped 95% confidence interval of trend shaded in grey. **b)** Regression of age versus vector distance adjusted for covariates. The trends do not change with the adjustment for covariates. **c)** Regression of age versus vector measurements of individually fit

community structure to the consensus partitions. **d)** Maps displaying across subject nodal versatility for WSBM and modular fit partitions **e)** Map of versatility differences between the two methods. In the difference map, only nodes with statistically significant differences are colored.

Individual vector similarity between subject and consensus partition varied strongly with age using the WSBM and modular consensus vectors. When measuring the similarity of subject to WSBM vector across age, we observed a Poisson curve with an R^2 of 0.24. For the analogous trend using the modular vector, we observed a Poisson curve with an R^2 of 0.11. The asymmetry of the Poisson curve allowed a fit to the data that suggested a pattern of high similarity between individual and consensus partition from childhood through approximately age 60, followed by a steep decline. When measuring the distance between subject and consensus vector across age, we observe in both the WSBM and modular cases a U-shaped trend (WSBM R^2: 0.17; modular R^2: 0.02).

When measuring individually fit community structure vectors each consensus vector, we again find that the WSBM derived community structure vectors are both more similar $(t(1.20\times10^3)=22.07, p < 10^{-9})$ and less distant $(t(1.12\times10^3)=-25.84, p < 10^{-9})$ than the modular consensus vectors. We find that using the WSBM fit explains more of the variance in vector similarity than using the modular fit. However, the MLR trend was weak for regressions of both vector distances versus age (R^2: 0.06 for both cosine similarity and city block distance). Using the modular fit, we observe that trends that do not, or negligibly, explain the variance in vector similarity or distance (R^2: 0 cosine similarity and R^2: 0.01 for city block distance).

We recorded the versatility at each node for each community detection method. We observed that nodal versatility across nodes is higher when using the WSBM method (M=2.66, SD=0.32) compared to modularity maximization (M=0.32, SD=0.31; two-tailed paired t-test with unequal variances; t(225.89)= 8.40, p < 10^{-9}). The pattern of node versatility differences (range: -

0.35 - 0.95) shows differential influence of spatial proximity between the community detection methods. We note that along the temporal lobe nodes reach the largest difference between the two methods (right temporal-occipital node), with a mean difference of 0.75 in "temporal" labeled lobe nodes.

Additional parcellation analyses

We also inferred WSBM and modular consensus community structures using an alternative parcellation scheme, based on an anatomical node definition (Hagmann, Cammoun et al. 2008). We report results of these evaluations in the Supplementary Information and show converging results with the analysis performed using the Yeo parcellation (Figures S4-S6). Additionally, we evaluated the degree of spatial similarity between community structures across parcellation selection. We find that both the WSBM and modular partitions across parcellation selection are statistically similar, compared to randomized community structures (Alexander-Bloch, Shou et al. 2018, Arslan, Ktena et al. 2018).

Discussion

Communities in brain networks have been hypothesized to form "building blocks" of the global network architecture and form functionally specialized systems that support specific subsets of cognitive tasks or information processing (Tononi, McIntosh et al. 1998, Stephan, Hilgetag et al. 2000, Bassett, Greenfield et al. 2010, Bullmore and Sporns 2012). It is important to understand that the methodological approaches and conceptual assumptions employed when running community detection on brain network data affect the community structure outcome. A community detection approach ideally suited for all applications does not exist (Von Luxburg, Williamson et al. 2012, Peel, Larremore et al. 2017) and the modular, internal density approach represents only

one plausible lens through which to view network communities (Rosvall, Delvenne et al. 2017, Schaub, Delvenne et al. 2017). The main contributions of the current study are to demonstrate the usage and utility of a statistical and generative modeling approach to community detection in brain network data, with a specific application to measuring changes in structural networks across the human life span.

Here we demonstrate an application of a block modeling approach to community detection in brain networks. The key advantage of this approach is the capacity to parse a brain network into a diverse set of communities (Betzel, Medaglia et al. 2018); with communities possibly exhibiting modular, core-periphery, or disassortative topologies. In the WSBM consensus partition, we see evidence of this mixed topology. Community *seven* in the model is an example of a disassortative community that modularity maximization would not be able to find. The community, consisting of nodes along the cingulate cortex, is weakly connected within-community and more strongly connected to communities *six* and *ten*. Three WSBM communities, *one*, *four*, and *ten*, have an off-diagonal average strength that exceeds the on-diagonal average strength. Importantly, we should note that using the WSBM does not preclude the identification of traditionally modular communities, such as the highly inter-connected nodes of community *seven*, containing nodes of the visual area. Additionally, interesting differences exist between the WSBM and modular partitions. WSBM community *one* contains bilateral prefrontal cortex nodes, whereas the prefrontal nodes of the modular partition are divided between communities *one* and *six*. Community *nine* of the WSBM partition indicated that the bilateral nodes of the PCC and precuneus connected in a stochastically equivalent manner, whereas in the modular partition the precuneus nodes form a small and segregated two-node community. The WSBM community *eight*

contained temporal nodes of both hemispheres, whereas the modular community *eight*, contains a large community spanning the right hemisphere.

We measured the extent to which each community structure captured patterns in our brain network data and demonstrated that the WSBM partition represented group averaged and group level data better than the modular partition. Using a generative modeling evaluation framework (Betzel, Avena-Koenigsberger et al. 2016) we demonstrate that parameters of the WSBM generate synthetic brain networks that deviate less from empirical data than do synthetic brain networks created with parameters estimated from the modular community structure. The WSBM model performed most poorly modeling the clustering coefficient distribution, which is expected given the design of both modular and SBM models and has been confirmed by previous work (Pavlovic, Vertes et al. 2014). In an additional evaluation of how these community structures align with the brain network data, we show that the WSBM partition modeled the symmetry of the brain better than the modular model. The statistical analysis confirms a visually obvious difference between the partitions: the WSBM partition is more symmetrically dispersed across the brain hemispheres than the modular partition.

When evaluating how these community structures change over the life span, we observe that the strength between communities follows inverted-U trends—patterns which align with previous life span studies (Westlye, Walhovd et al. 2010, Imperati, Colcombe et al. 2011, Betzel, Byrge et al. 2014, Yeatman, Wandell et al. 2014, Zhao, Cao et al. 2015). Here we show that these patterns extend to communities identified with a WSBM approach that covers a much wider space of possible network partitions. We found the strongest age-related change in strength between the nodes of community *three*, which cover the frontal cortex in modularity- as well as WSBM-derived partitions. This finding is in line with previous studies that have shown that ventromedial prefrontal

white matter connecting ventromedial prefrontal nodes was particularly vulnerable to aging processes (Salat, Tuch et al. 2005, Michielse, Coupland et al. 2010). Within-community connectivity of WSBM community *six*, containing bilateral nodes of somatomotor cortex and postcentral cortex, also displays a strong inverted-U quadratic trend (Figure 6a) that is likely due to age-related changes involving the integrity of corpus callosum connections (Lebel, Gee et al. 2012, Zhao, Cao et al. 2015, Ruddy, Leemans et al. 2017). In the modular partition, this trend, which appears at the connection between communities *six* and *ten*, is attenuated (Figure 6b).

To assess overall community structure changes, we employed vector similarity/distance comparisons. Employing the cosine similarity measure, we observe a pattern where individual subjects maintain similarity to the consensus partition until around the 6th decade of life, where a steep drop-off occurs. This trend could indicate a range of the life span with a stable community structure regardless of connectivity strength, since cosine similarity is a measure of vector orientation but not magnitude. When employing the city block distance, we can then observe a U-shaped trend in distances to the consensus partition, which is likely due in part to connectivity strengths modulated across age. Given that the WSBM partition results in MLR models in which age explains more of the variance in our outcome measures, the WSBM partition appears to be a representative group model for the brain network data across a large age range.

We also fit the WSBM and modular community structures to individual brain networks. This analysis rendered much weaker trends with age; indicating that individually fit community partitions vary substantially from our consensus model and data. We also used these individually fit community structures to analyze the variability of the fit partitions. In panel **d** of Figure 7, we report differences in nodal versatility measured across subjects. The difference in nodal versatility maps between the WSBM and modularity maximization methods demonstrates a difference in

flexibility between the methods. Recall that the WSBM aggregates nodes with similar connectivity patterns into a community, whereas modularity maximization parses the network into densely connected subnetworks. Unfortunately, the process of detecting modular communities is influenced by a distance-based bias in the structural brain network data (Betzel, Medaglia et al. 2017), which results in a spatially compact lateralized community structure. This bias most-likely affects the overall spatial layout of each community structure; we found smaller within-community distance between nodes of the modular than for the WSBM partition. To get closer to the biological reality would likely require several interconnected steps, including a systematic investigation of spatial and/or geometric bias in tractography, how these biases are expressed across age (Zhao, Cao et al. 2015), and how they affect the detection of streamlines and tracts that vary in length, curvature and trajectory (Sotiropoulos and Zalesky 2019). Future work is needed to fully address these challenges.

In the present study, we show how a statistical modeling approach to community detection in brain networks might differ (and confer some modeling advantages) compared to a modular approach. However, we would like to reinforce the notion that the choice of community detection algorithm should depend on factors related to the observed data and analytical goals (Fortunato and Hric 2016). These two community detection perspectives satisfy differing algorithmic criteria to define communities with different properties (Rosvall, Delvenne et al. 2017, Schaub, Delvenne et al. 2017). A nuanced, but crucial, point to consider is that community structures reflect a plausible grouping of nodes (Peel, Larremore et al. 2017). This organization, sometimes referred to as the *mesoscale* of a brain network (Betzel, Medaglia et al. 2018), in conjunction with community-based network statistics (such as participation coefficient) can elucidate patterns or trends in a brain network (Sohn, Choi et al. 2011, Baum, Ciric et al. 2017). To infer a community

structure from brain network data is to parse the data—which can always be trivially organized into some grouping. Whether that organization is biologically and functionally meaningful requires further experimental evidence or metadata (Newman and Clauset 2016). Thus, we would not assert that the WSBM perspective is 'better' at capturing the underlying anatomic organization than the modular perspective of communities in brain networks (Peel, Larremore et al. 2017). In fact, we present evidence in the supplemental materials that both algorithmic approaches capture non-random spatial configurations, across parcellation scheme (Figure S7). The modular approach is certainly valid for network neuroscience applications (Sporns and Betzel 2016), and has been employed, for example, to help explain how brain networks might be efficiently embedded in space (Bassett, Greenfield et al. 2010), to characterize functional MRI during learning (Bassett, Wymbs et al. 2011) and to differentiate between clinical groups (He, Lim et al. 2018). In the current study, the modular partition does as well as the WSBM partition to capture the block interaction (3-3, Figure 6) with the highest R^2 value. Additionally, while modularity maximization is designed to consider on-diagonal block interactions, some unmodeled off-diagonal interactions in our evaluation still display statistically significant trends. This considered, recent work has demonstrated a theoretic convergence of the statistical modeling and modularity maximization approaches in special cases of the SBM (Newman 2016, Young, St-Onge et al. 2018). Future advances along this line of research could better clarify the tradeoffs between inference of SBM and modular partitions.

In the current study, we applied new methods to resolve a consensus model from many community structure solutions of the WSBM inference. Although we measured the consistency of our method, we do note that stochasticity in the current framework still exists. We recognized that there are further parameters of the model that could be optimized, such as prior distribution

parameters and parameters governing the convergence criterion for the multiple loops of the variational-Bayes approximation approach. Additionally, we recognize that the WSBM inferred on our data has shortcomings. When using a normal distribution to model edge weights between communities, using the WSBM tools at our disposal we cannot assure that the model will completely avoid modeling negative weights. However, because there are no actual negative edges in our brain network data, we can assume that modeling too many negative edge weights would create lower likelihood, meaning such a model would not be retained by the WSBM inference. We note that because of this concern, we conducted our generative model analysis with binary network statistics based on edge-existence. Thus, the generative modeling validation could be improved upon by using non-negative weight distributions in future work.

Finally, we note that diffusion imaging and tractography perform computational inference rather than direct measurement of brain connectivity and thus must be interpreted with care (Sotiropoulos and Zalesky 2019). We made efforts in the current study to mitigate against certain biases. We used streamline density as an edge-weight to mitigate against the bias of large regions of interest and we seeded multiple streamlines randomly in each white matter voxel to obtain thorough streamline coverage across the brain. Additionally, we used anatomically-constrained streamline filtering process to recover only streamlines terminating in grey matter (Smith, Tournier et al. 2012). Despite these efforts, future work is needed to further improve the accuracy and sensitivity of structural connectivity measurements derived from noninvasive neuroimaging. In particular, objective quality control metrics can be used increase dMRI data fidelity, which could lead to more accurate associations between dMRI-derived data and age (Roalf, Quarmley et al. 2016).

In conclusion, we describe a method for applying the WSBM to brain networks, with an application across the life span. We hope to demonstrate the efficacy of using a generative model community structure when analyzing brain networks, by showing that brain networks are not exclusively modular. Our study opens new avenues for using the WSBM for brain network analysis as well as introduces frameworks through which WSBM partitions could be associated with phenotypic characteristics or variations in cognition/behavior (Newman and Clauset 2016, Betzel, Medaglia et al. 2018, Seghier and Price 2018). Future work should use this model to identify how community structure regimes, such as modular, core-periphery, or disassortative models (or a mix of these regimes), relate to aspects of behavior and cognition. Our study shows that the WSBM can provide a flexible and versatile model of brain network community structure and may offer new insights beyond those delivered by modularity analysis.

CHAPTER 2: MAPPING THE COMMUNITY STRUCTURE OF THE RAT CEREBRAL CORTEX WITH WEIGHTED STOCHASTIC BLOCK MODELING

Abstract

The anatomical architecture of the mammalian brain can be modeled as the connectivity between functionally distinct areas of cortex and sub-cortex, which we refer to as the *connectome*. The community structure of the connectome describes how the network can be parsed into meaningful groups of nodes. This process, called community detection, is commonly carried out to find internally densely connected communities—a modular topology. However, other community structure patterns are possible. Here, we employ the Weighted Stochastic Block Model (WSBM), which can identify a wide range of topologies. We apply the WSBM to the rat cerebral cortex connectome, to probe the network for evidence of modular, core, periphery, and disassortative organization, and compare to a modularity maximization approach. Despite its algorithmic flexibility, the WSBM identifies substantial modular and assortative topology throughout the rat cerebral cortex connectome, significantly aligning to the modular approach in some parts of the network. Significant deviations from modular partitions include the identification of communities that are highly enriched in core (rich club) areas. A comparison of the WSBM and modular models demonstrates that the former, when applied as a generative model, more closely captures several nodal network attributes. Leveraging an analysis of variations across an ensemble

of partitions provides a more complete understanding of the rat cortex connectome by revealing that certain parts of the network participate in multiple topological regimes. Overall, our findings demonstrate the potential benefits of adopting a broad definition of community structure that transcends the common approach based on cluster density.

Introduction

The mammalian brain is characterized by complex patterns of connectivity (Sporns 2011, Park and Friston 2013). This connectivity can be comprehensively described by creating a network model of the brain's wiring—an account of the patterns of connectivity between distinct regions, referred to as the *connectome* (Sporns, Tononi et al. 2005). Using the tools of network science, we can quantitatively analyze and model the connectome to characterize statistical properties of its organization (Bassett and Sporns 2017). A long series of prior studies of anatomical brain networks across several different species have revealed a consistent set of attributes, such as heavy-tailed degree distributions, a prevalence of specific classes of subgraphs or motifs, as well as the existence of densely connected network communities or modules (Sporns and Betzel 2016).

It is increasingly recognized that brain networks exhibit significant features of organization on multiple scales (Betzel and Bassett 2017). Of particular interest is the so-called mesoscale of organization, a level of analysis that describes network properties falling between node statistics (e.g. degree, clustering coefficient, or centrality) and global statistics (e.g. network density or efficiency) (Sporns 2013, Tunc and Verma 2015). A particularly important mesoscale organizational property of a connectome is the way in which its nodes can be grouped into distinct communities. Modular organization is of neurobiological interest as members of communities often share other common attributes, such as geometric placement and contiguity, functional specialization, and developmental and evolutionary origin (Sporns and Betzel 2016). In other

words, the community structure of a network is an organizational scale that can be used to identify meaningful groups of nodes based on patterns of connectivity or coactivation. Such node groups could function to support a specific cognitive domain (Crossley, Mechelli et al. 2013). Information about this community structure may also be used to classify brains into clinical groups (Kurmukov, Ananyeva et al. 2017, He, Lim et al. 2018). Brain network communities have been found in species as diverse as the nematode *C. elegans* (Sohn, Choi et al. 2011), the fruit fly *Drosophila melanogaster* (Shih, Sporns et al. 2015), mouse (Zingg, Hintiryan et al. 2014, Rubinov, Ypma et al. 2015), rat (Bota, Sporns et al. 2015, Swanson, Sporns et al. 2016, Swanson, Hahn et al. 2017, Swanson, Hahn et al. 2018), and rhesus monkey (Harriger, van den Heuvel et al. 2012).

Network communities can be detected by global maximization of a modularity metric (Newman 2006), which by design identifies collections of nodes densely connected within each community and sparsely connected between communities. This approach of *modularity maximization* has been widely applied to brain network data, across many species and anatomical subdivisions of the brain. For example, anatomical modules in the human brain have been mapped across development (Baum, Ciric et al. 2017) and the lifespan (Zhao, Cao et al. 2015), as well as in numerous clinical conditions such as degenerative (Contreras, Avena-Koenigsberger et al. 2019) and mental disorders (Alexander-Bloch, Lambiotte et al. 2012). Modular organization of brain networks has been theorized to conserve anatomical wiring cost (Bullmore and Sporns 2012, Betzel, Medaglia et al. 2017) and to promote efficient embedding in physical space (Bassett, Greenfield et al. 2010).

Despite its popularity, modularity maximization is subject to several important limitations. Recent work emphasizes that a single modular partition may represent only one solution to a problem with no universally optimal approach (Fortunato and Hric 2016, Peel, Larremore et al.

61

2017). Most complex networks have numerous plausible modular partitions that nearly maximize the modularity heuristic (Fortunato and Barthelemy 2007, Good, de Montjoye et al. 2010), and thus it is not guaranteed that any single modular partition of the data is truly representative of the data. Furthermore, one partition or scale might not adequately capture the richness of the network organization (Betzel and Bassett 2017). Recent methodological advances have allowed accessing modular organization at multiple scales, through implementing modularity maximization while varying a resolution parameter that renders the modularity metric sensitive to modules of different sizes (Jeub, Sporns et al. 2018).

To ascribe importance to any one partition without considering other 'just as plausible' partitions could lead to misinterpretations of a connectome's community structure. Two different analytical approaches address such concerns: 1) a representative community structure from a landscape of community structures, either using a representative partition (Meunier, Achard et al. 2009) or a consensus method (Lancichinetti and Fortunato 2012), can be chosen; or 2) analysis can be performed on a set of many plausible community structure realizations of an algorithm (Betzel, Medaglia et al. 2018).

Furthermore, communities need not necessarily or exclusively satisfy the condition of dense intra-community and sparse inter-community connectivity; groups of nodes can also be grouped into communities based on graph-cuts, states or types of dynamics, or statistical models (Schaub, Delvenne et al. 2017). Here, we are specifically interested in brain network communities identified within the framework of stochastic block models (SBM) (Holland, Laskey et al. 1983, Aicher, Jacobs et al. 2015, Moyer, Gutman et al. 2015, Faskowitz, Yan et al. 2018). The SBM is an edge-generative model that describes how communities connect to each other on average. An SBM community of nodes, referred to as a *block*, can be thought of as a group of nodes who

connect to other communities in a similar (i.e. stochastically equivalent) manner. By this design, the SBM is flexible; it can describe a range of community structure topologies, such as core-periphery (Pavlovic, Vertes et al. 2014, Noori, Schottler et al. 2017, Battiston, Guillon et al. 2018) or disassortative (Betzel, Medaglia et al. 2018), in addition to modular communities.

Spurred by recent advances in neuroinformatics, the anatomical wiring of the rat at the scale of areas and inter-areal connectivity has been assembled (Bota and Swanson 2007). Among the first anatomical subdivisions examined in the rat brain was the cerebral cortex (Bota, Sporns et al. 2015), which appears to share fundamental network properties with primate cerebral cortex, such as presence of a small-world, modular, and rich club organization (Bota, Sporns et al. 2015, van den Heuvel, Scholtens et al. 2016). The community structure of the rat cerebral cortex reveals modules that are spatially compact and have meaningful relationships with functionally and behaviorally specialized systems. An SBM approach could potentially complement the insights gained from standard modularity maximization by revealing partitions based on a different set of criteria for defining module membership.

Here, we identify community structure in the rat cerebral cortex connectome with a weighted variant of the stochastic blockmodel (WSBM) (Aicher, Jacobs et al. 2015, Peixoto 2018). The goal of the present work is to demonstrate how the blockmodeling approach can be applied to a singular brain network in a manner that reveals a range of plausible topologies. In conjunction, we compare the blockmodeling approach to a more standard approach, modularity maximization, in these analyses. We find that WSBM can recover a consensus community structure with non-modular elements, and we compare the resulting partitions to a classic modular community structure. We also show that this WSBM community structure is well-suited to generate synthetic data. We then use the range of plausible community structure partitions to assess the frequency at

which nodes and edges participate in certain community structure topologies. Overall, our approach provides a novel framework for inferring and utilizing the WSBM to analyze a range of community structure topologies in anatomical brain network data. We identify evidence that the community structure of the rat cerebral cortex connectome contains non-modular organizational elements, including brain regions that participate in core, periphery, or even disassortative relationships.

Methods
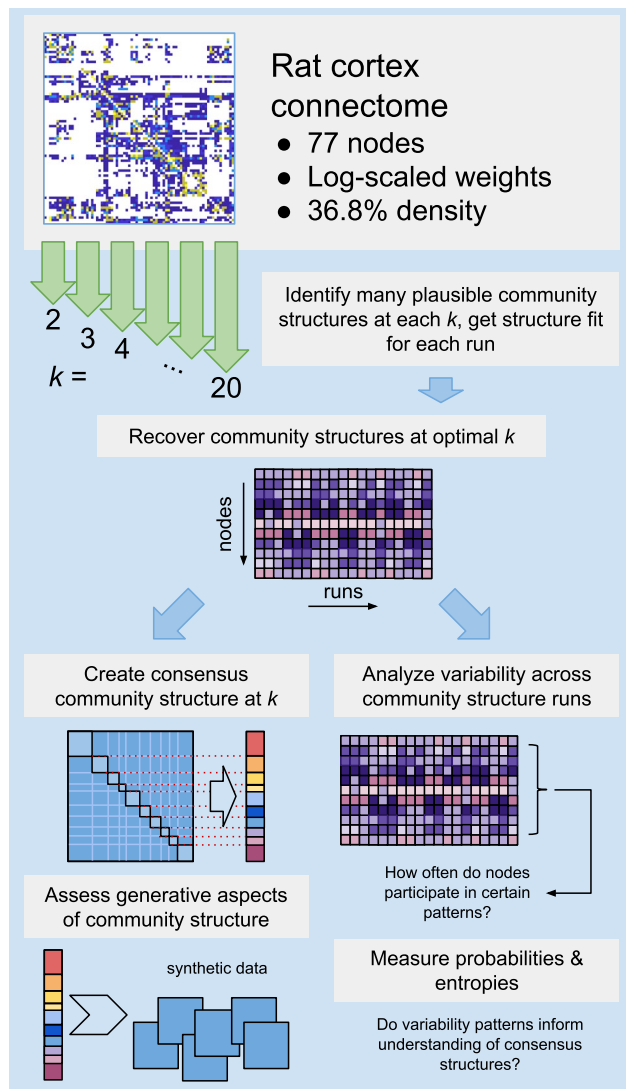
Figure 1 Diagrammatic overview of the methods and analyses employed in this study.

The data set used for our analysis is derived from (Swanson, Hahn et al. 2017), referred to as version *RCAMv2*. Directed and weighted connectivity was assembled between 77 distinct cortical grey matter regions of the rat cortex, delineated based on architecture, topography, and connectivity (Swanson, Sporns et al. 2016). Between these 77 regions there are 5,852 ($77^2 - 77$) potential edges to consider. Connection reports of monosynaptic anterograde and retrograde connections were recorded as an adjacency matrix. A total of 2155 nonzero edges were recorded, with weights assigned on an ordinal scale, from 0-7 in the following way: absent, very weak, weak, weak-moderate, moderate, moderate-strong, strong, and very strong. As in prior work (Bota, Sporns et al. 2015), this ordinal scale was transformed to a tapered log-weighted scale: $\{0, 0.0001, 0.001, 0.01, 0.075, 0.3, 0.75, 1.0\}$.

Stochastic blockmodel concepts

The stochastic blockmodel (SBM) is an edge-generative model for describing how groups of nodes interact with each other in a network. Importantly, a community as defined by an SBM is a group of nodes that connect to the rest of the network in a similar pattern. Specifically, nodes in the same community will, on average, have the same connectional profile to other communities (for an alternative analysis of node-level connectional similar, see Supplemental Information). This property is referred to as stochastic equivalence. The SBM can generate a network by assigning a probability of connection for all possible pairs of communities (including within-community [modular] interactions). In the classic SBM, this probability, Θ, is governed by a Bernoulli distribution. The collection of Θ that describe the probability of connection between each community is the affinity matrix, B. For an SBM describing k communities, B will be size $k \times k$.

This stochastic block modeling framework serves as a general model that can be extended for specialized purposes, such as blockmodels with mixed membership (Airoldi, Blei et al. 2008, Moyer, Gutman et al. 2015), degree correction (Karrer and Newman 2011, Xiaoran, Cosma et al. 2014), and weighted edges (Peixoto 2018). For the present study, we utilize the weighted variant of the SBM, known as the WSBM (Aicher, Jacobs et al. 2015). The MATLAB (The MathWorks, Inc., Natick, Massachusetts) code implementing this WSBM is available at *tuvalu.santafe.edu/~aaronc/wsbm/*. We provide wrapper scripts useful for the application of the WSBM to brain networks at *github.com/faskowit/blockmodeltools*.

We use a Bernoulli distribution to describe edge-existence between blocks and an exponential distribution to describe the weight distribution between blocks. The generative process of the WSBM can be summarized as follows:

- For each node, assign a community membership

- For each pair of communities, assign edge-existence and edge weight parameters

- For each edge, draw from a Bernoulli distribution with the corresponding edge-existence parameter

- For each existing edge, draw from an exponential distribution with the corresponding edge weight parameters

We use a variational Bayes algorithm (Aicher, Jacobs et al. 2015) to infer a block structure on the empirical network. This algorithm uses a maximum *a posteriori* approach to identify the WSBM model, which includes the community structure and the parameters for each community interaction (edge and weight) that is likely to have generated the observed data. The model likelihood (expressed as the log likelihood for mathematical convenience) is expressed as $P = (E \mid M, z)$, where E is the empirical data, M is a parameterized block model and z is the

community assignment vector. The number of communities k is a free parameter of the WSBM model. Therefore, picking a k value for the WSBM amounts to a model selection problem. In this project, we fit models from a range of $k = \{2, 3, ... 20\}$.

As with many community detection methods, the WSBM is stochastic, yielding many community structure configurations after multiple algorithmic trials. As such, we explore two analytical paths: 1) resolve a consensus model from various community structure realizations; or 2) analyze patterns across various community structure realizations. In what follows, we describe frameworks for both approaches.

Constructing consensus community structures

We designed a workflow to infer the WSBM in a consensus manner (Lancichinetti and Fortunato 2012, Faskowitz, Yan et al. 2018), in order to obtain a median solution from a landscape of plausible partitions. First, we select the optimal k-level to investigate, based on model likelihoods (Aicher, Jacobs et al. 2015). At this k level we identify an ensemble of N partitions, and we measure the pairwise variation of information (VI) (Meilă 2007) between them. We identify the N_q partitions that had less than median VI distance and greater than median model log evidence, to obtain well-fit and reasonably central partitions from the landscape of N solutions. Of N_q partitions, we identify the centroid (least distant) partition and align the other $N_q - 1$ partitions to it using Jaccard distance (Munkres 1957). We then create a prior for each node's community affiliation based on the frequency of community assignment for each node across the N_q aligned partitions. We then infer the WSBM community structure 100 more times, using the generated prior to initialize the inference. This process is iterated until the agreement across 100 inferred

partitions reaches a predefined level (Kwak, Choi et al. 2009). We retain the resultant model as the consensus WSBM community structure.

Modular model for comparison

We sought to compare the consensus WSBM community structure to a modular community structure at each scale k. We identify plausible modular community structures at multiple scales by sweeping across values of the γ parameter in the modularity equation. From a range of γ (from 0.01 to 4.0 in steps of 0.01, resulting in 400 γ values) we obtain communities using the Louvain method implemented in the Brain Connectivity Toolbox (Blondel, Guillaume et al. 2008, Rubinov and Sporns 2010). Then, for each level of k, we record the lowest and highest γ value that generates a partition with exactly k communities. Within this range, we then uniformly randomly sample an ensemble of γ values used to obtain N partitions, therefore matching the ensemble size obtained from WSBM runs at each level of k.

Generative modeling methods

We use a previously established framework to measure how a generative model could create synthetic networks that vary minimally across several distributions of network properties (Betzel, Avena-Koenigsberger et al. 2016). A WSBM models how each community connects to all other communities. We can sample from these distributions to create synthetic data adhering to the model parameters. For each synthetic network, we record five network statistic distributions: directed weighted degree (strength), directed binary degree, weighted directed clustering coefficient, weighted node betweenness centrality, and binary node betweenness centrality. We include binary network metrics in this evaluation because edge-existence (i.e. binary existence of edges between blocks, regardless of weight), is a network feature that the WSBM explicitly

models. We then use Kolmogorov–Smirnov (KS) to measure the histogram distance between the synthetic distributions and the empirical distributions for the five network statistics. The difference between the synthetic and empirical networks can be indexed by the average of these five KS statistics; a lower mean KS signifies a more accurate match between synthetic and empirical networks. For this evaluation, we also create null generative models to evaluate against. The null models are created by randomly permuting the parameters of the intact model's affinity matrix. This procedure therefore retains the parameters of the original model, but the specific configuration of block interactions is permuted.

Community motif analysis

We also measure the diversity of community motifs across the many inferred WSBM models at each k (Betzel, Medaglia et al. 2018). This analysis entails measuring patterns of between-community (block interaction) connectivity w_{rs}, where w is the matrix of average edge strength between blocks, and where r and s are communities contained within the total set of k total communities, $\{r, s\} \in \{1, \ldots, k\}$. Community motifs are defined in Table 1.

Table 1 Definitions for identifying community motif configurations for block matrix w.

Community motif	Description	Definition
On-diagonal	block represents within-community connectivity	w_{rs} when $r = s$
Assortative	minimum on-diagonal value is larger than the off-diagonal value	$\min(w_{rr}, w_{ss}) > w_{rs}$
Core/periphery	off-diagonal value is larger than one on-diagonal value; if the off-diagonal value is closer to the larger of the on-diagonal values, it is core; otherwise it is periphery	$(w_{rr} > w_{rs} > w_{ss})$ or $(w_{ss} > w_{rs} > w_{rr})$
Disassortative	off-diagonal value is larger than both on-diagonal values	$w_{rs} > \max(w_{rr}, w_{ss})$

For each community structure, we label each block interaction according to the above definitions. We then record which non-zero edges participate in each type of interaction, for each recovered partition. Measuring across partitions provides the frequency that an edge (a non-zero

entry in the adjacency matrix) participates in each community motif. We conceptualize this frequency as a probability. From this edge-wise probability, we calculate an entropy metric (referred to in (Betzel, Medaglia et al. 2018) as a *diversity index*) that measures the probability for an edge (e) to participate in one or more of the community motifs:

$$entropy_e = -\left(P_a \, log_2 \, P_a + P_c \, log_2 \, P_c + P_p \, log_2 \, P_p + P_d \, log_2 \, P_d + P_{od} \, log_2 \, P_{od}\right)$$

where P_a, P_c, P_p, P_d and P_{od} stand for the probability of participating in an assortative, core, periphery, disassortative or on-diagonal relationship, respectively. To compute node entropy, we sum each nodes' edge entropy (in- and out- connections) and divide by two.

Results

Consensus community structure results
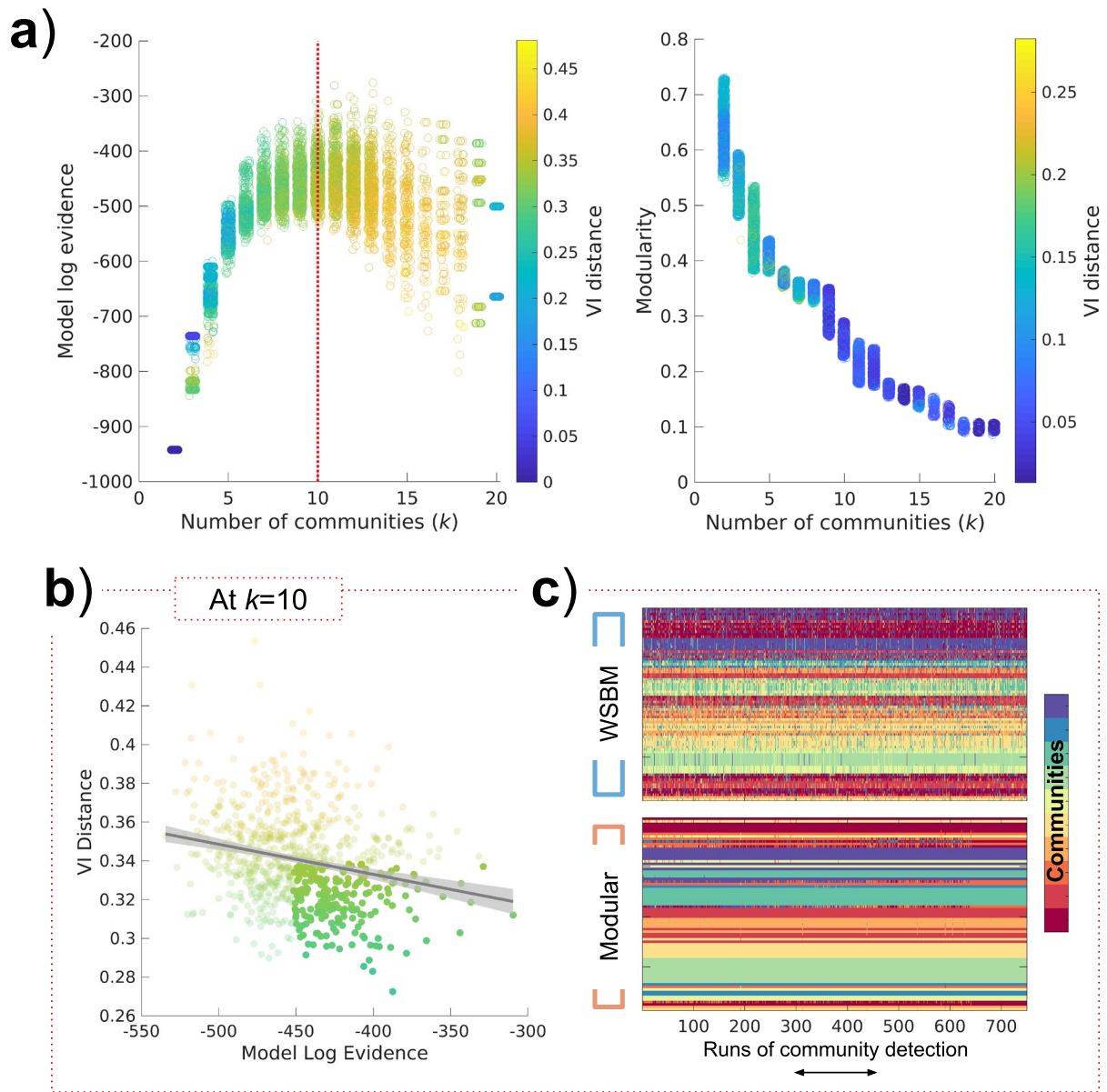
Figure 2 Community detection results across the number of communities, *k*, parameter; **a**) Scatter plots for WSBM (left) and modular (right) depicting the community recovered at each level of *k*; WSBM communities are plotted against model log evidence, modular communities are plotted against the Louvain algorithm's modularity metric; datapoints are colored by the average VI from one partition to all other partitions at *k*; the identified optimal $k = 10$ is denoted by a red vertical line in the WSBM plot; **b**) The relationship between model log evidence and average VI

distance, which explains 4.7% of the variance in model log evidence; points are colored by same scale as in **a**; opaque points indicate the models included in the construction of the consensus WSBM model; **c**) 750 communities recovered using each method, aligned using the Munkres algorithm to a common structure for visualization.

We fit the WSBM to the rat cortex connectome across a range of k and monitor when we reach a point of diminishing gains in model likelihood (Figure 2a). We recovered 750 models (the target N) for $k = \{2,3 \ldots 12\}$. Due to algorithm runtime, we recovered 500 models at $k = 13$, and 200 models at $k = \{14,15\}$. At $k = \{16, 17 \ldots 20\}$, the WSBM inference tools struggle to recover models with the specified k. At these levels, only 91, 32, 53, 7, and 2 valid models were recovered. We sampled with replacement 100 models from the available recovered models at $k = \{16,17 \ldots 20\}$.

To estimate the optimal k, we identified the scale at which model log evidence begins to decline as k grows. At each scale, we bootstrapped (10^4 iterations) the difference between mean model log evidence at k and $k + 1$. The transition at which the 99% confidence interval of these differences overlapped with 0 was taken to be a stopping criterion. This approach identified an optimum $k = 10$. At the $k = 10$ scale, we found that model log evidence relates to the mean VI distance (cross-validated $R^2 = 0.05$; Figure 2b).
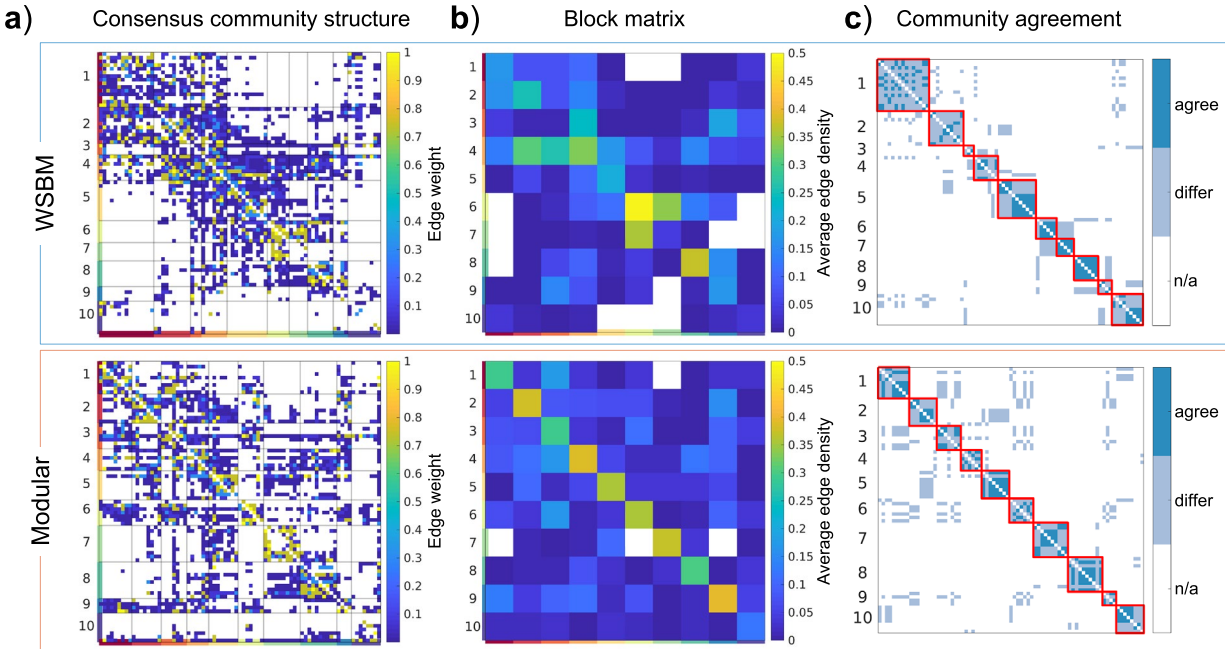
Figure 3 Consensus community structures; **a)** WSBM and modular consensus community structures at k=10; **b)** average block matrix for each community structure, depicting the average edge for each block interaction; areas in white indicate no edges present; **c)** Agreement matrix between community structures, permuted by the order of each structure; *agree*: classified in same community across structures; *differ*: not in same community; *n/a*: not applicable.

We obtained consensus community structures using two different approaches to community detection, each designed to parse a network based on different criteria: the WSBM and modularity maximization (Figure 3). Supplemental Table 1 provides complete listings of rat cerebral cortex brain areas, arranged by community, for approach. Differences in the resulting consensus partitions are apparent when visualizing the average between-block density (i.e. average edge weight). The WSBM, as a statistical description of network communities, identifies communities with strong (e.g. community 6) as well as weak (e.g. communities 3,7) on-diagonal density. The modular model, which optimizes the modularity metric, only identifies partitions with on-diagonal communities whose densities are, in all cases, stronger than any other off-diagonal interaction. Despite significant differences in the way communities are defined under the two approaches, the WSBM and modular consensus community structures are significantly less distant

73

from each other than expected by chance (VI: 0.359; randomization test, 10^4 iterations, $p <$

10^{-4}). We compared how each of these structures concentrate edge weight in a modular manner,

by evaluating the ratio of within on-diagonal blocks divided by edge weight between blocks:

$M_{ratio} = \frac{\sum_{r=s} w_{rs}}{\sum_{r \neq s} w_{rs}}$. The modular structure has a $M_{ratio} = 0.846$ and the WSBM structure has a

$M_{ratio} = 0.448$. The difference between these ratios was tested after randomizing the original rat

cortex connectome data (with BCT function *randmio_dir_connected*) at edge rewiring

probabilities of $p = \{0.25, 0.20, 0.15, 0.10, 0.05, 0.01\}$. For rewiring probabilities $0.25 - 0.05$,

the empirical difference in M_{ratio} was at least greater than 95% of synthetically generated M_{ratio}

values (10^4 iterations). We compared the modularity Q of the WSBM partition to synthetically

generated Q values (rewiring the network with 0.05 probability, keeping partition order intact) and

found that no synthetic values were greater than the empirical Q value (10^4 iterations).

Table 2 Node affiliations of WSBM and modular consensus community structures compared to a previously published community structure: *Swanson2017*.

	WSBM communities									
	1	2	3	4	5	6	7	8	9	10
Swanson2017 Module 1	15	10	1	3	1	0	0	0	2	9
Swanson2017 Module 2	0	0	0	1	10	5	5	0	0	0
Swanson2017 Module 3	0	0	2	3	0	1	0	7	2	0
	Modular communities									
	1	2	3	4	5	6	7	8	9	10
Swanson2017 Module 1	9	5	7	1	0	7	0	0	4	8
Swanson2017 Module 2	0	3	0	0	8	0	10	0	0	0
Swanson2017 Module 3	0	0	0	5	0	0	0	10	0	0

We compared these consensus community structures to a previously published modular

arrangement of these 77 nodes into three communities (Swanson, Hahn et al. 2017) (Table 2). We

find that for the WSBM model, five out of 10 communities are fully contained within one of the

Swanson2017 modules, while for the modular model, eight out of 10 communities are fully

contained within of one the *Swanson2017* modules. Divergence between the *Swanson2017* and

WSBM partitions is greatest for WSBM communities 3, 4, and 9, which are communities with no more than two thirds of the nodes co-classified to any one of the *Swanson2017* modules. These WSBM communities also maintain strong off-diagonal block interactions relative to their respective on-diagonal block interaction (Figure 3). Six out of seven previously (Swanson, Hahn et al. 2017) identified hub nodes (ENTl, AIp, PERI, ECT, BLAp, LA) are found in WSBM communities 2 and 4. All seven members of WSBM community 4 were previously identified as rich club areas (ENTl, ORBv, ORBm, MOs, PERI, ECT, CLA), with five more rich club areas found in community 2 (comprising half of its membership; CA1v, ILA, AIp, BLAp, LA), and the remaining three areas part of communities 3, 5 and 8. This high concentration of hubs/rich club areas in two WSBM communities indicates that the WSBM partition significantly captures the network's hub and rich club (or core-periphery) architecture.

Generative modeling results
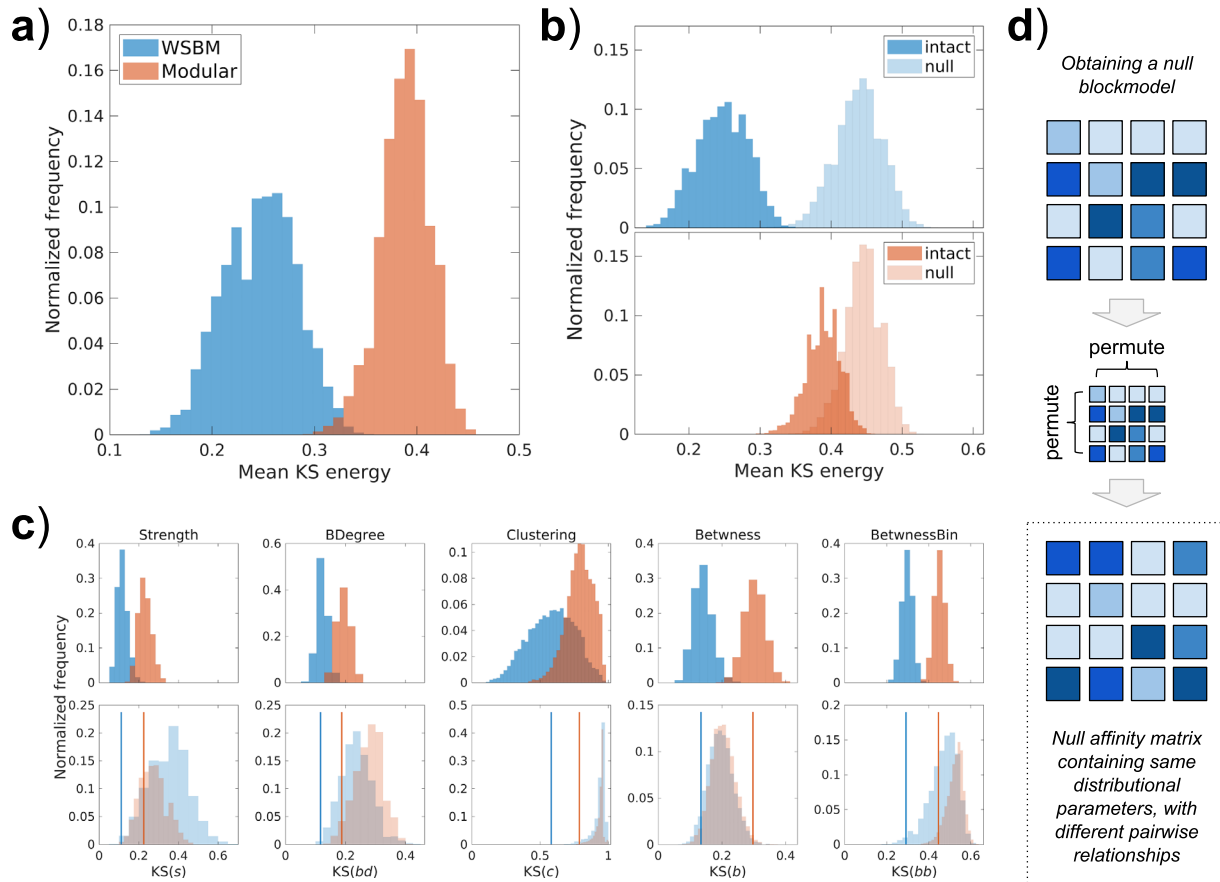
Figure 4 Evaluation framework for synthetically generated networks by measuring Kolmogorov–Smirnov (KS) energy from empirical network; **a)** Distribution of mean KS values of 10^4 generated networks from WSBM and modular community structures; **b)** KS energy values of intact generative model (emp) versus permuted model (null); **c)** Top: Individual KS distances for each network metric of the mean KS energy calculation; Bottom: Individual KS distances for each network metric of permuted model, with the median of the intact model distribution indicated with vertical line; **d)** Schematic of how the generative model affinity matrix is permuted to create a 'null' generative model; note that values of the inferred parameters are the same, but in new positions, introducing null community interactions.

When we fit a WSBM to network data, we obtain a generative model of the network based on the inferred community structure. We recorded the energy, computed as mean KS, between synthetic networks generated by the consensus WSBM and modular models. We find that the

WSBM created synthetic data that deviated less from the empirical data than the modular generative model (Figure 4a; bootstrapped difference of means, 10^4 iterations, $p < 10^{-4}$). Additionally, the difference between the WSBM energy distribution and its corresponding null distribution is greater than the difference between the modular counterparts (Figure 4b; bootstrapped difference of differences, 10^4 iterations, $p < 10^{-4}$). Observing the individual measures that comprise the overall energy, we see that the WSBM model produces less divergent strength, binary degree, and betweenness centrality distributions, while the modular model produces less divergent clustering coefficient and binary betweenness centrality distributions (Figure 4c).
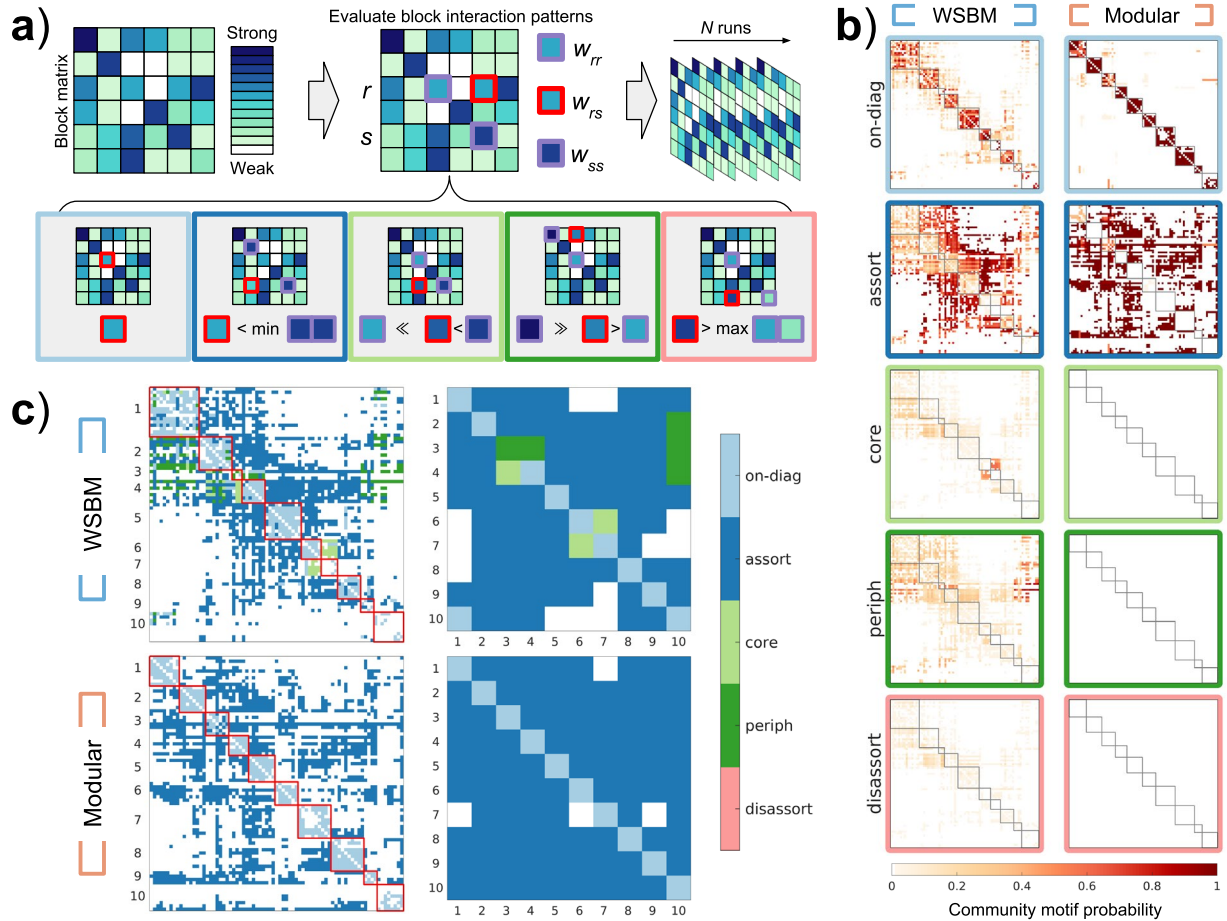
Figure 5 Quantification of edge-wise community motif participation; **a)** Diagram of steps used to evaluate community motif patterns; first, a matrix describing the average edge strength between blocks is obtained; second, the between-block relationships are labeled as either on-diagonal (light blue), assortative (dark blue), core (light green), periphery (dark green), or disassortative (salmon); third, these labels are assessed across multiple community structures; **b)** A visualization of the edge-wise probability of participating in each community motif at *k*=10; across modular communities at this scale, there are no core, periphery, nor disassortative community motifs identified; **c)** Left: each edge is colored according to the community motif it is more likely to participate in; Right: blocks are colored by the mode community motif for each block interaction; *on-diag*: on-diagonal, *assort*: assortative, *periph*: periphery, *disassort*: disassortative.

Unlike classic modularity, WSBM builds on a considerably broader definition of network community that goes beyond assortative partitions. We can assess the extent to which certain

community topology configurations occur by evaluating community motifs (Figure 5a). Across 750 WSBM community structures at $k = 10$, we find instances of each type of community motif, whereas across 750 modular community structures, we observe only on-diagonal and assortative configurations (Figure 5b). Concerning the motif probabilities derived from the WSBM model, 99.4% of edges participated in at least two community motifs across WSBM community structures. The top 10 highest probability edges for the core, periphery, and disassortative community motifs are shown in Table 3.

In contrast, considering the motif probabilities derived from the modular model, 79.1% percent of nonzero edges displayed no variation in community motif configuration (100% on-diagonal: 247 edges; 100% assortative: 1458 edges). 2 out of 10 modular communities were fully comprised of on-diagonal nonzero edges with 100% on-diagonal participation (communities 7 and 10). 6 out of 10 modular communities were comprised of nonzero edges with an average on-diagonal probability >98% (communities 2, 4, 5, 6, 8, and 9).

For each edge, we recorded the highest probability motif (Figure 5c, left). For each block interaction, we recorded the mode motif (Figure 5c, right). The block matrix of motif modes classifies 3 block interactions as core ($4 \rightarrow 3, 6 \rightarrow 7, 7 \rightarrow 6$), 5 block interactions as periphery ($2 \rightarrow 10, 3 \leftrightarrow 3, 3 \rightarrow 4, 3 \rightarrow 10, 4 \rightarrow 10$), and no block interactions as disassortative.

Table 3 Top 10 most probable edges for core, periphery, and disassortative community motif participation across WSBM community structures; i indicates row (source), and j indicates column (target) for entry in the rat cortex connectome adjacency matrix

|	Core			Periphery			Disassortative		
	i	j	Probability	i	j	Probability	i	j	Probability
1	VISp	VISlla	0.5827	ENTl	MOB	0.9307	ORBm	PL	0.2893
2	VISam	VISlla	0.5827	ENTl	AOB	0.9293	ORBv	ORBvl	0.284
3	VISp	VISll	0.5827	ENTm	IG	0.9133	MOs	ORBvl	0.2707
4	VISam	VISll	0.5827	ENTl	IG	0.9013	ECT	ORBvl	0.2707
5	VISp	VISli	0.5813	ENTl	FC	0.8973	CLA	ORBvl	0.2453
6	VISam	VISli	0.5813	ENTm	DG	0.868	ORBv	ORBl	0.2427
7	VISpm	VISli	0.5813	ENTl	DG	0.856	ORBm	ORBl	0.2427
8	VISal	VISlm	0.5813	ENTl	CA3	0.8427	MOs	ORBl	0.2387
9	VISp	VISlm	0.5813	ENTm	CA2	0.824	ECT	ORBl	0.2213
10	VISam	VISlm	0.5733	ENTl	CA2	0.8013	CLA	ORBl	0.216
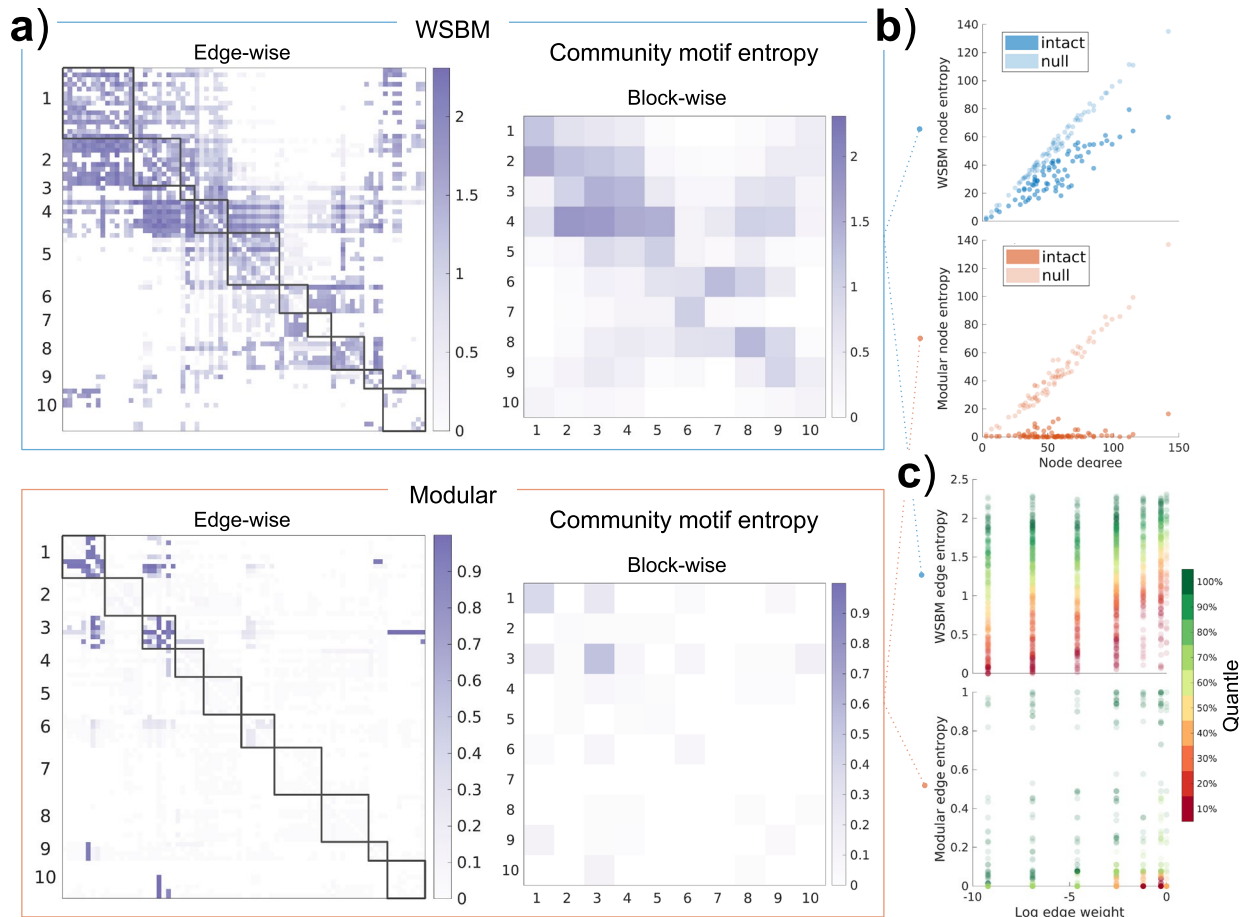
Figure 6 Visualization of community motif entropy measure, and its relationship to node strength and edge weight; **a**) Adjacency and block matrices of community motif entropy; **b**) Scatterplot of node strength versus node entropy for

both the WSBM and modular models; **c**) Scatterplot of log edge weight versus edge entropy measurement, colored by the edge weight quantile; *quantile computed within each unique edge weight.

We observe higher overall community motif entropy for the WSBM model than for the modular model (Figure 6a). For the WSBM model, the greatest average between-block entropies involve community 4 ($4 \rightarrow 2$, $4 \rightarrow 3$). For the modular model the greatest average between-block entropies concerned communities 1 and 3 ($3 \leftrightarrow 3$, $1 \leftrightarrow 1$, $1 \rightarrow 3$, and $3 \rightarrow 1$). Using a randomized block null model (like in Figure 4d), we show that at random, node entropy is highly correlated with node degree (Figure 6b; $\rho > 0.97$ for WSBM and modular). Community motif entropy measured across WSBM and modular partitions correlated with node degree substantially less than the entropy measured across random structure (WSBM $\rho = 0.85$, $p < 10^{-8}$; modular $\rho = 0.11$, not significant; for both models: difference between null and intact $p < 10^{-4}$). Further, we measured this change as a percentage change in entropy for each node (Supplemental Figure 2). These patterns in entropy change are not correlated with node degree (WSBM ρ 95% confidence interval: $[-0.14, 0.27]$; modular WSBM ρ 95% confidence interval: $[-0.02, 0.42]$). At an edge-wise scale, we observe that both WSBM ($\rho = 0.31$) and modular ($\rho = 0.21$) edge entropies correlate with log edge weight (Figure 6c); the WSBM correlation is reliably greater than the modular correlation across bootstrapped samples (bootstrapped difference of means, 10^4 iterations, $p < 10^{-4}$). All correlations reported are non-parametric Spearman's rank correlations.

Here we analyzed the one-hemisphere rat cerebral cortex brain. We also performed these analyses on a version of the data containing commissural connections and a second hemisphere. These analyses rendered analogous findings when comparing the WSBM and modular approaches (see Supplemental Information: *Analysis for two-hemisphere data*).

Discussion

This article describes a framework for fitting a blockmodel to the rat cortex connectome, represented as a weighted and directed connection matrix. First, we demonstrate how the blockmodel framework can be used to construct a consensus community structure from many plausible partitions. We compare the resulting consensus partition to another approach, more commonly used in the field, based on modularity maximization. We then compare the generative capabilities of these two different consensus community approaches. To gain a deeper understanding of the ensemble of partitions created by WSBM and modularity maximization we analyze the variation in community structure configurations across many runs of community detection. Overall, leveraging these analyses, we observe features specific to the way that the WSBM and modular algorithms parse the rat cortex connectome.

The consensus community structure derived by WSBM parses the rat cerebral cortex in a manner that, in some respects, significantly differs from the partition resulting from modularity maximization. The WSBM community structure captures non-modular aspects, such as block interactions classified as core and periphery (Figure 4c) in addition to strong off-diagonal block interactions (e.g. inter-modular interactions $4 \rightarrow 2$, $6 \rightarrow 7$, and $7 \rightarrow 6$). The $4 \rightarrow 2$ interaction links two communities that are highly enriched in putative hub and rich club areas, identified in previous work (Swanson, Hahn et al. 2017). The $6 \rightarrow 7$ and $7 \rightarrow 6$ interactions link two communities dominated by visual sensory areas, one containing areas that are mutually densely connected (community 6; VISrl, VISal, VISp, VISam, VISpm), the other containing areas that are mutually sparsely connected (community 7; VISlla, VISll, VISli, VISlm, VISpl).

Other aspects of the WSBM community structure are significantly modular, and node groupings resemble those detected by modularity maximization. In a previous report using

effectively the same data, a symmetric arrangement of three modules per hemisphere was identified using modularity maximization (Swanson, Hahn et al. 2017): a lateral module consisting of perceptive systems related to interactions with the environment such as visual, auditory, and somatosensory areas; a ventromedial module containing regions involved in visceral monitoring and memory; and a dorsomedial module containing regions that are mainly associated with executive function. In this paper, we used modularity maximization to identify a consensus partition with $k = 10$ modules (intended to serve as a point of comparison to the 'optimal' WSBM solution). Despite the much larger set of modules, the modular communities 1, 3, 6, 9, and 10 mostly recapitulate the *Swanson2017* module 1, 5 and 7 the *Swanson2017* module 2, and 4 and 8 the *Swanson2017* module 3. Indeed, as observed when applying multiresolution consensus clustering on rat sub-connectomes (Swanson, Hahn et al. 2018), finer-scale modular partitions generally represent hierarchical subdivisions of modules identified at coarser scales. Notably, even though the WSBM covers a much wider range of possible topologies than are accessed by modularity maximization, the overall WSBM partitioning scheme is less distant from modular community structure than chance, and it exhibits modularity, as indexed by the Q-metric, at levels far above those seen in random networks.

We demonstrate that a generative model based on the WSBM community structure produces synthetic networks with several network statistic properties that match the original network more closely than those obtained from modular synthetic networks. This implies that community structure formed by the WSBM can generate higher fidelity synthetic data. This capability could be explored further in future studies for creating surrogate brain networks that consider community structure information. The WSBM better matches the binary degree and weighted degree (strength) distributions, demonstrating its superior capability to model the

existence of connections and their weights. On the other hand, both methods perform worst at generating synthetic networks with accurate clustering coefficient distributions, a result that comports with previous blockmodeling studies (Pavlovic, Vertes et al. 2014, Faskowitz, Yan et al. 2018); this finding is likely due to the higher on-diagonal density of the modular model, which tends to produce more highly connected triplets (triangles). Both community structures are non-trivially organized with regards to their generative capacities, as randomly permuting the block-interaction significantly decreases their generative performance (Figure 3b).

When we fit the WSBM many times, we observe many ways in which the rat cortex connectome is parsed into plausible communities. To quantify this variation, we measure the proportion of times edges participate in specific community motifs (Betzel, Medaglia et al. 2018), across 750 runs of community detection. Across many runs of WSBM community detection, we find evidence of all five community motif configurations. More than 99% of the nonzero edges participate in at least two types of community motifs. In contrast, across many runs of modularity maximization, we observe only on-diagonal and assortative motifs. This analysis highlights complementary strengths of each community structure model: WSBM flexibly identifies communities based on various statistical patterns; modularity maximization reliably identifies communities with strong-within, and weak-between, topologies.

The probabilities of participating in community motifs demonstrate how connections of some brain areas might influence the structure of the communities that are formed. We observe how certain edges are repeatedly placed by the WSBM within the on-diagonal blocks, such as the edges within communities 5 and 6, communities composed of predominantly somatosensory, auditory, and visual areas. Numerous edges linking the visual community 6 to visual community 7 are classified as participating in core motifs. Edges between medial/lateral entorhinal areas and

areas of the olfactory bulb and hippocampus are most likely classified as participating in peripheral motifs; previously, the medial and lateral entorhinal areas were considered candidate hub and rich club nodes (Swanson, Hahn et al. 2017). While we do not find strong evidence of disassortative topologies across a majority of the WSBM, we note that the edges most likely to be disassortative all involve subdivisions of the orbital region of the rat cortex, as well as putative hub and rich club areas.

Across many recovered community structures, the WSBM partitions vary more than the modular partitions (Figure 2c). We quantify this variation with the community motif entropy and observe how this entropy is organized across the nodes and edges of the rat cortex connectome (Figure 6). Entropy is highly related to node degree when partitions are random. When the brain network is partitioned into a plausible community structure, we observe that entropy is systematically reduced relative to the random configuration. However, this reduction in entropy does not necessarily correlate with degree (Supplemental Figure 2); the entropy decreases the most for nodes of the visual areas for both methods. Across modular partitions, edge-wise entropy is mostly contained in connections between communities 1 and 3, which signal that node assignments between these communities are likely to exchange with one another; indeed, these two WSBM communities are placed within the same *Swanson2017* module, indicating their mutual affinity. This concurs with the modular agreement matrix, which also indicated this possibility (Supplemental Figure 1). A future direction of investigation would be to evaluate how such structural characteristics could relate to patterns of brain function. In a similar analysis, it was shown that the diversity community motif patterns correlated with individual difference in human task performance (Betzel, Medaglia et al. 2018). We note that variability of the identified partitions is in part based on input the network data and the stochasticity of the algorithm. Therefore, these

results should be interpreted as variability relative to the community detection methods employed. We repeated these analyses with an alternative modularity maximization algorithm to demonstrate this (Supplemental Figure 9).

The analyses reported in this paper add to a growing body of work indicating that a single community partition of brain data provides only an incomplete understanding of the brain's mesoscale organization. Instead, a more complete account of communities should consider multiple scales (Jeub, Sporns et al. 2018, Yeh, Panesar et al. 2018, Akiki and Abdallah 2019), the possible 'fuzziness' of partitions (Moyer, Gutman et al. 2015, Najafi, McMenamin et al. 2016), or build consensus structures from the data (Lancichinetti and Fortunato 2012, Faskowitz, Yan et al. 2018, Kurmukov, Musabaeva et al. 2018). Ensemble approaches to network communities take into account that (i) community structure can vary across multiple runs of the same community detection algorithm (Shinn, Romero-Garcia et al. 2017, Betzel, Bertolero et al. 2019); (ii) different annotations can afford different perspectives on the same data (Peel, Larremore et al. 2017); and (iii) different community detection algorithms maximize different criteria (Schaub, Delvenne et al. 2017). This idea carries over to the WSBM framework. Any single WSBM community structure is likely to be just one of many plausible partitions of the data, in a similar manner to the degeneracy of the modularity landscape (Fortunato and Barthelemy 2007, Good, de Montjoye et al. 2010). Here, we outline analytical approaches demonstrating that a brain network's community structure may be more than a grouping of nodes based on mutual density of connections. The identification of the community structure of a brain network reflects specific algorithmic goals and represents one of many plausible divisions of the network. By analyzing information across ensembles of network partitions, across scales and under varying definitions of what constitutes a 'community', we can achieve a fuller picture of the architecture of brain networks.

The understanding of mesoscale organization of the rat cerebral cortex will continue to develop as the connectivity data become more complete and the community detection algorithms grow more sophisticated. New connections continue to be added to the rat connectome dataset, including association fibers (Swanson, Hahn et al. 2017), connections to the endbrain (Swanson, Hahn et al. 2018), and thalamic nuclei connections (Swanson, Sporns et al. 2019). We provide further analyses of the two-hemisphere rat cerebral cortex connectome in Supplemental Information and report analogous results to the one-hemisphere findings. Notably, the two-hemisphere WSBM consensus community structure is symmetric across the hemispheres, reflecting a limitation of the underlying data. Future work on the organization of the rat connectome could focus on inferring mesoscale structure with added metadata (Hric, Peixoto et al. 2016) such as neurochemical relationships (Noori, Schottler et al. 2017) or using alternative node definitions or informatically collated data (Schmitt and Eipert 2012). Such added information could enhance our understanding of the potential functions identified communities might play. Further, algorithmic advances in community detection could aid in inferring the rat brain mesoscale organization. The WSBM algorithm recovered substantially less unique partitions at high values of k (i.e. $k >= 17$; Supplemental Figure 4), but future SBM algorithms could be more efficient for larger networks (Peixoto 2018). Alternatively, future work on the variability of plausible partitions could be conducted using different community detection criteria (Chen, Nguyen et al. 2013, Schaub, Delvenne et al. 2017).

CHAPTER 3: EDGE-CENTRIC FUNCTIONAL NETWORK REPRESENTATIONS OF HUMAN CEREBRAL CORTEX REVEAL OVERLAPPING SYSTEM-LEVEL ARCHITECTURE

Abstract

Network neuroscience has relied on a node-centric network model in which cells, populations, and regions are linked to one another via anatomical or functional connections. This model cannot account for interactions of edges with one another. Here, we develop an *edge*-centric network model, which generates the novel constructs of "edge time series" and "edge functional connectivity" (eFC). Using network analysis, we show that at rest eFC is consistent across datasets and reproducible within the same individual over multiple scan sessions. We demonstrate that clustering eFC yields communities of edges that naturally divide the brain into overlapping clusters, with regions in sensorimotor and attentional networks exhibiting the greatest levels of overlap. We show that eFC is systematically modulated by variation in sensory input. In future work, the edge-centric approach could be useful for identifying novel biomarkers of disease, characterizing individual variation, and for mapping the architecture of highly resolved neural circuits.

<u>Introduction</u>

Network science offers a promising framework for representing and modeling neural systems (Bassett and Sporns 2017). From interconnected cells (Schröter, Paulsen et al. 2017), to neuronal populations (Dann, Michaels et al. 2016), to large-scale brain areas (Park and Friston 2013), network analysis has contributed insight into the topological principles that govern nervous system organization and shape brain function. These include small-world architecture (Sporns and Zwi 2004), the emergence of integrative hubs and rich clubs (Power, Schlaggar et al. 2013), modular structure to promote specialized information processing (Sporns and Betzel 2016), and tradeoffs between topological features and the material and metabolic costs of wiring (Bullmore and Sporns 2012).

Central to these and other discoveries in network neuroscience is a simple representation of the brain in which neural elements and their pairwise interactions are treated as the nodes and edges of a network, respectively (Bullmore and Sporns 2009). This standard model is fundamentally node-centric in that it treats neural elements (nodes) as the irreducible units of brain structure and function. This emphasis on network nodes is further reinforced by the analyses carried out on brain networks, which tend to focus on properties of nodes or groups of nodes, e.g. their centralities or community affiliations (Rubinov and Sporns 2010).

A limitation of the node-centric approach is that it cannot capture potentially meaningful features or patterns of interrelationships among edges. In other scientific domains, prioritizing network edges, for example by modeling and analyzing edge-edge interactions as a graph, has provided important insights into the organization and function of complex systems (Evans and Lambiotte 2009, Ahn, Bagrow et al. 2010). Nonetheless, network neuroscience has remained largely focused on nodal features and partitions, paralleling a rich history of parceling, mapping,

and comparing cortical and subcortical gray matter regions (Eickhoff, Constable et al. 2018). On the other hand, several recent papers have begun modeling brain networks from the perspective of interacting edges, including one foundational paper that applied graph-theoretic measures to a "line graph" (Evans and Lambiotte 2009) of interrelated white matter tracts (de Reus, Saenger et al. 2014). Though highly novel, line graphs were never adopted widely, as their construction requires users to first specify and apply a sparsity threshold to a connectivity matrix.

Here, we present a novel modeling framework for investigating functional brain network data from an *edge*-centric perspective. Our approach can be viewed as a temporal "unwrapping" of the Pearson correlation measure – the metric commonly used for estimating the strength of functional connectivity between pairs of brain regions (Smith, Miller et al. 2011) – thereby generating interpretable time series for each edge that express fluctuations in its weight across time. Importantly, edge time series allow the estimation of edge correlation structure, a construct we refer to as edge functional connectivity (eFC). High eFC indexes strong similarity in the co-fluctuation of two edges across time, while low eFC indicates co-fluctuation patterns that are largely independent.

From a neuroscientific perspective, eFC can be viewed both as an extension of, and a complement to, traditional node-centric representations of brain networks. In node-centric network models, functional connections represent the temporal correlation of activity recorded from spatially distinct regions and often interpreted as a measure of inter-regional communication (Reid, Headley et al. 2019). That is, strong functional connections are thought to reflect the time-averaged strength of "communication" between brain regions. eFC, on the other hand, tracks how communication patterns evolve over time and ultimately assesses whether similar patterns are occurring in the brain simultaneously (See Supplementary Figure 1).

90

Here, we first demonstrate that eFC is highly replicable given sufficient amounts of data, stable within individuals across multiple scan sessions, and consistent across datasets. Next, we apply data-driven clustering algorithms to eFC, which result in partitions of the eFC network into communities of co-fluctuating edges. Each community can be mapped back to individual nodes, yielding overlapping regional community assignments. We find that brain regions associated with sensorimotor and attention networks participated in disproportionately many communities compared to other brain systems, but that, relative to one another, those same regions participate in similar sets of communities. Finally, we compare the organization of eFC at rest and during passive viewing of movies, and find that eFC is consistently and reliably modulated by changes in sensory input.

Results

In this section we analyze edge functional connectivity (eFC) estimated using neuroimaging data from three independently acquired datasets: 100 unrelated subjects from the Human Connectome Project (HCP) (Van Essen, Smith et al. 2013), ten subjects scanned ten times as part of the Midnight Scan Club (MSC) (Gordon, Laumann et al. 2017), and ten subjects scanned multiple times as part of the Healthy Brain Network Serial Scanning Initiative (HBN) (O'Connor, Potler et al. 2017).

Edge functional connectivity

Many studies have investigated networks whose nodes and edges represent brain regions and pairwise functional interactions, respectively (Park and Friston 2013). Here, we extend this framework to consider interactions not between pairs of brain regions, but pairs of *edges*.

Extant approaches for estimating edge-edge connectivity matrices include construction of line graphs (Evans and Lambiotte 2009) or calculating edge overlap indices (Ahn, Bagrow et al. 2010). While suitable for sparse networks with positively weighted edges, these approaches are less appropriate for functional neuroimaging data, where networks are typically fully weighted and signed. Here, we introduce a method that is well-suited for these types of data, operates directly on time series, and is closely related to the Pearson correlation coefficient (typically used to assess strength of interregional functional connections). We refer to the matrices obtained using this procedure as "edge functional connectivity" (eFC).

Beginning with regional time series, calculating eFC can be accomplished in three steps, starting by z-scoring the time series (Figure 1a,d). Next, for all pairs of brain regions, we calculate the element-wise product of their z-scored time series (Figure 1b,e). This results in a new set of time series, referred to as "edge time series," whose elements represent the instantaneous co-fluctuation magnitude between pairs of brain regions and whose average across time is exactly equal to the Pearson correlation coefficient (Figure 1c) (van Oort, Mennes et al. 2018). Co-fluctuation values are positive when activity of two regions deflects in the same direction at precisely the same moment in time, are negative when activity deflects in the opposite direction, and zero when activity is close to baseline. Importantly, the magnitude of these edge time series is not systematically related to in-scanner motion (Supplementary Figure 2). The third and final step involves calculating the element-wise product between pairs of edge time series. When repeated over all pairs of edges, the result is an edge-by-edge matrix, whose elements are normalized to the interval $[-1, 1]$ (Figure 1f and Figure 2a). See **Materials and Methods** for additional details on eFC construction.
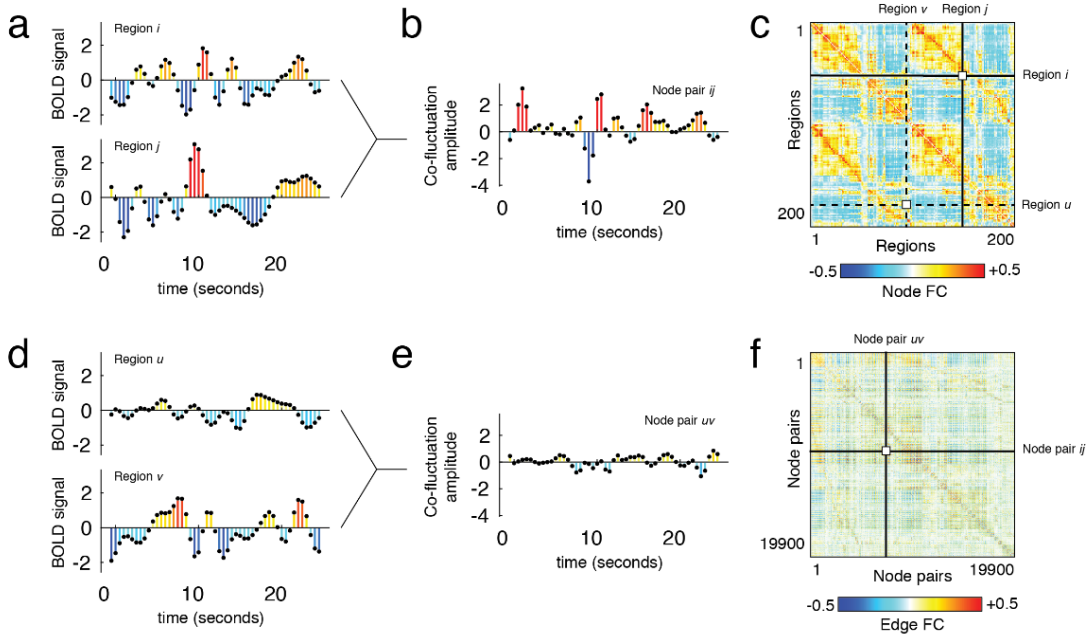
Figure 1 Derivation of edge functional connectivity (eFC) matrix. Each element of the eFC matrix is calculated based on the fMRI BOLD activity time series from four nodes (brain regions). In panels **a** and **d**, we show four representative times series from regions i, j, u, and v. Nodal FC (panel **c**; nFC) is typically calculated by standardizing (z-scoring) each time series, performing an element-wise product (dot product) of time series pairs, and calculating the average value of a product time series (actually the sum of each element divided by $T - 1$, where T is the number of observations). To calculate eFC, we retain the vectors of element-wise products for every pair of regions. In panels **b** and **e** we show product time series for the pairs $\{i, j\}$ and $\{u, v\}$, respectively. The elements of these product time series represent the magnitude of time-resolved co-fluctuation between region pairs (or edges in the nFC graph). We can calculate the magnitude of eFC by performing an element-wise multiplication of the product time series and normalizing the sum by the squared root standard deviations of both time series, ensuring that the magnitude of eFC is bounded to the interval $[-1,1]$. The resulting value is stored in the eFC matrix, shown in panel **f**.

While eFC is, to our knowledge, a novel construct, we note that the first two steps in calculating eFC are the same as those used to calculate nodal FC; the mean value of any co-fluctuation time series is simply the Pearson correlation coefficient. Given that eFC is mathematically related to nodal functional connectivity (nFC), we first asked whether it was

possible to approximate eFC using estimates of nFC. This is an important question; while the calculation of eFC can be implemented efficiently, performing certain operations on the eFC matrix can prove computationally expensive (it is a fully-weighted $[M \times M]$ matrix, where $M = \frac{N(N-1)}{2}$ and N is the number of nodes; Figure 2b). However, a direct comparison of eFC and nFC is not possible due to differences in dimensionality. Still, we can approximate eFC using nFC edge weights. Perhaps the simplest approach is to model the edge connection between region pairs $\{i, j\}$ and $\{u, v\}$ as a linear combination of the six edges that can be formed from those regions (see **Materials and Methods**). Although this model performs poorly (correlation of observed and approximated eFC; $r = 0.21$; $n = 197{,}995{,}050$ edge-edge pairs;), we can improve upon its performance by including interaction terms based on node connectivity, i.e. $nFC_{ij} \times nFC_{uv}$ ($r = 0.73$; $p < 10^{-15}$; $n = 197{,}995{,}050$ edge-edge pairs; Figure 2c). Collectively, these observations suggest that eFC is not well approximated using linear combinations of nFC, but with non-linear transformations and inclusion of interaction terms, nFC can approximate eFC. However, these transformations are unintuitive, and the approximation still fails to fully explain variance in eFC.
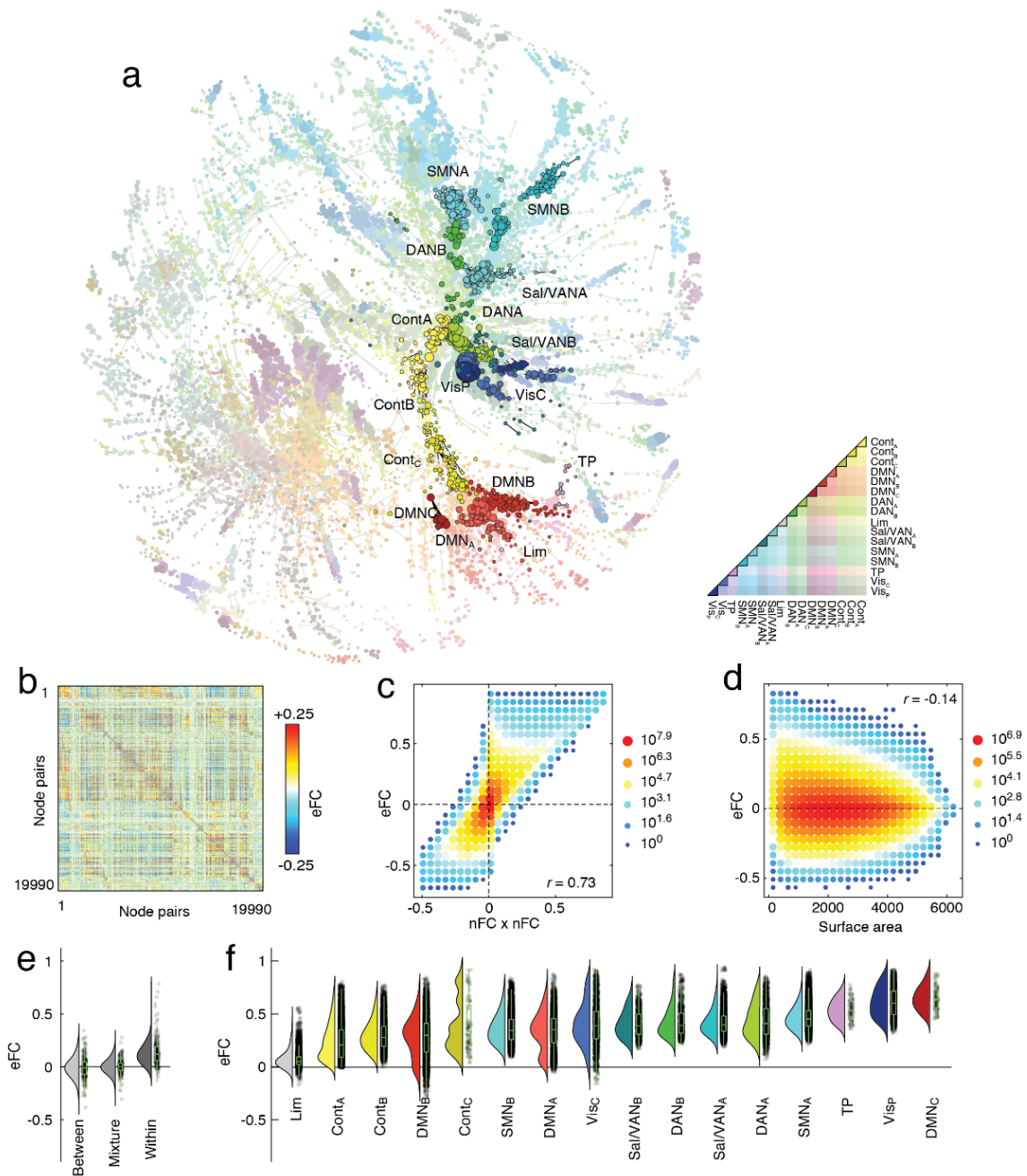
Figure 2 Organization of edge functional connectivity (eFC). (**a**) Force-directed layout of eFC matrix (largest

connected component). Nodes in this graph represent edges in the traditional nodal functional connectivity (nFC)

matrix. Here, nodes are colored according to whether the corresponding edge fell within or between cognitive systems.

Within-system edges are encircled in black. (**b**) eFC matrix in which rows and columns correspond to pairs of brain

regions. (**c**) Two-dimensional histogram of relationship between eFC and the product of edges' respective nFC

weights. (**d**) Two-dimensional histogram of relationship between eFC and the surface area of the quadrilateral defined by the four nodes. (**e**) Mean eFC among edges where both edges fall between systems (between; $n = 2.3 \times 10^8$), where one edge falls within and the other between systems (mixture; $n = 1.7 \times 10^8$), and where both edges fall within systems (within; $n = 8.1 \times 10^5$). (**f**) Mean eFC among edges within sixteen cognitive systems ($n = 6.5 \times 10^4$). All results presented in this figure derived from Human Connectome Project data. Boxplots, shown in green and overlaid on data points in panels **e** and **f**, depict the interquartile range (IQR) and median value of the distribution. Whiskers extend to the nearest points $\pm 1.5 \times$ IQR above and below 25th and 75th percentiles. Note that in panel **e**, not all points can be displayed due to the large number of edge-edge connections.

Next, we explored variation of eFC across acquisitions and processing decisions. We found that eFC weights are similar across three independently acquired datasets (Supplementary Figure 3), and that the omission of global signal regression from our preprocessing pipeline induced a consistent upwards shift of eFC weights, analogous to its effect on nFC (Supplementary Figure 4). Additionally, we found that the overall pattern of eFC calculated using edge time series estimated from observed data was uncorrelated with the pattern of eFC calculated using edge time series estimated from phase-randomized surrogate time series (Supplementary Figure 5).

Next, we asked whether eFC exhibits any clear spatial dependence, as nFC is known to decay as a function of Euclidean distance (Esfahlani, Bertolero et al. 2020). We assessed the spatial dispersion of eFC with the surface area of the quadrilateral formed by the centroids of the brain region pairs (we explore an alternative edge-level distance metric in Supplementary Figure 6). We found evidence of a weak negative relationship between surface area and eFC ($r = -0.14, p < 10^{-15}; n = 197,995,050$ edge-edge pairs; Figure 2d), suggesting that unlike traditional nFC, whose connection weights are more strongly influenced by spatial relationships of brain areas to one another, eFC is less constrained by the brain's geometry.

Finally, we asked whether eFC bears the imprint of nFC communities – brain regions whose activity is highly correlated with members of its own community, but weakly or anti-correlated with members of other communities (Sporns and Betzel 2016). To address this question we classified every edge in the nFC network according to whether it fell within or between communities (Schaefer, Kong et al. 2018), resulting in three possible combinations of connections in the eFC graph: eFC could link edges that both fell within a community, edges that both fell between communities, or an edge that fell within and an edge that fell between communities. In general, we found that eFC was significantly stronger for within-community edges compared to the other two categories (Figure 2e). Interestingly, we found eFC could be distinguished further by dividing within-community edges by cognitive system (Schaefer, Kong et al. 2018) (one-way ANOVA; $F(15, 65819) = 2667.4, p < 10^{-15}$; Figure 2f).

Edge functional connectivity is stable within individuals

In this section, we test the robustness of eFC to scan duration, i.e. how much data is required before eFC stabilizes, and whether eFC is consistent across repeated scans of the same individual. To address these questions, we leveraged the within-subject design of the MSC dataset. For each subject, we aggregated their fMRI data across all scan sessions and estimated a single eFC matrix. Then, we sampled smaller amounts of temporally contiguous data, thus approximately preserving the auto-correlation structure, and estimated eFC, which we compared against the aggregated eFC matrix (this procedure was repeated 25 times). Similar to other studies (Laumann, Gordon et al. 2015), we found that with small amounts of data eFC was highly variable (Figure 3a). However, we observed a monotonic increase in similarity as a function of time, so that with 30 minutes of data, the similarity was much greater ($r = 0.78; p < 10^{-15}; n = 197,995,050$ edge-edge pairs). This is of practical significance; like traditional nFC, it implies that eFC

estimated using data from short scan sessions may not deliver accurate representations of an individual's edge network organization. We note that this relationship is strengthened when data are subsampled randomly and uniformly ($r = 0.90$; $p < 10^{-15}$; $n = 197,995,050$ edge-edge pairs; See Supplementary Figure 7).
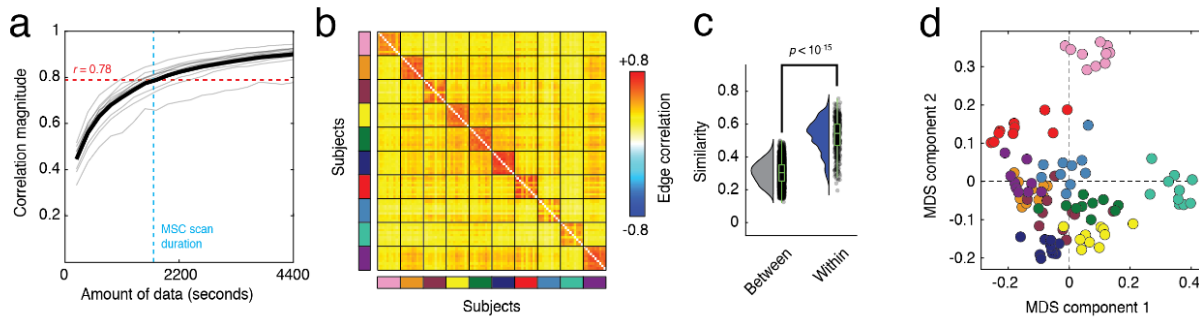
Figure 3 Intra- and inter-subject similarity of eFC across scan sessions. (**a**) Correlation of session-averaged eFC matrices with eFC estimated using different amounts of data; mean value shown as black line. (**b**) Similarity of eFC within and between subjects. Each block corresponds to data from a single subject; subjects are also identifiable by the color of the rectangle alongside each bock. (**c**) Violin plots of within- and between-subject similarity values from the matrix shown in panel **b**; $n_w = 450$ and $n_b = 4500$ within- and between-subject comparisons (two-sample t-test; $t(4948) = 62.98$; $p < 10^{-15}$). Boxplots, shown in green and overlaid on data points in panel **c**, depict the interquartile range (box) and median value of the distribution. Whiskers extend to the nearest points $\pm 1.5\times$ IQR above and below 25th and 75th percentiles. (**d**) Scan sessions plotted according to coordinates generated by performing a two-dimensional multi-dimensional scaling analysis of the matrix in panel **b**. Note that scans from the same subject (shown here with the same color) are located near each other. All panels from this figure were generated using data from the Midnight Scan Club.

Next, we examined the reliability of eFC over multiple scan sessions. That is, if we imaged an individual on separate days, would their eFC on those days be more similar to each other than to that of a different individual?. We estimated eFC and calculated the pairwise similarity (Pearson correlation) between all pairs of MSC subjects and scans. We found eFC to be highly reliable in the MSC dataset, where the mean within-subject similarity was $r = 0.53 \pm 0.10$ compared to

$r = 0.30 \pm 0.07$ between subjects (two-sample t-test; $t(4948) = 62.98$; $p < 10^{-15}$; Figure 3b,c). Indeed, we found that for each eFC matrix, the matrix to which it was most similar belonged to the same subject (100% accuracy). Additionally, eFC exhibited slightly greater differential identifiability compared to nFC (0.224 to 0.210) – calculated as the difference between mean within- and between-subject similarity (Amico and Goni 2018). In Figure 3d, we show the results of applying multi-dimensional scaling to the similarity matrix from Figure 3b. We found similar results in the HBN and HCP datasets (see Supplementary Figure 8).

Collectively, these findings suggest that eFC exhibits a high level of subject specificity and captures idiosyncratic features of an individual, provided that eFC was estimated over a sufficiently long time period. This observation serves as an important validation of eFC, and suggests that eFC may be useful in future applications as substrate for biomarker generation and "fingerprinting" (Finn, Shen et al. 2015).

The overlapping community structure of human cerebral cortex

While many studies have investigated the brain's community structure (Sporns and Betzel 2016), most have relied on methodology that forces each brain region into one and only one community. However, partitioning brain regions into non-overlapping communities clashes with evidence suggesting that cognition and behavior requires contributions from regions that span multiple node-defined communities and systems (Anderson, Kinnison et al. 2013). Accordingly, a definition of communities is needed that more closely matches the brain's multifunctional nature and the pervasive overlap of its community structure (Pessoa 2014).

While deriving overlapping communities of brain regions can be challenging when using nFC, overlap is inherent (indeed, pervasive (Ahn, Bagrow et al. 2010)) within the eFC construct. Clustering the eFC graph assigns each edge to a community. Each edge is associated with two

brain regions (the nodes it connects). Thus edge community assignments can be mapped back onto individual brain regions and, because every region is associated with $N - 1$ edges, allow regions to simultaneously maintain a plurality of community assignments.

In this section, we cluster eFC matrices to discover overlapping communities in human cerebral cortex. More specifically, we use a modified *k*-means algorithm to partition the eFC graph into non-overlapping communities and map the edge assignments back to individual nodes.
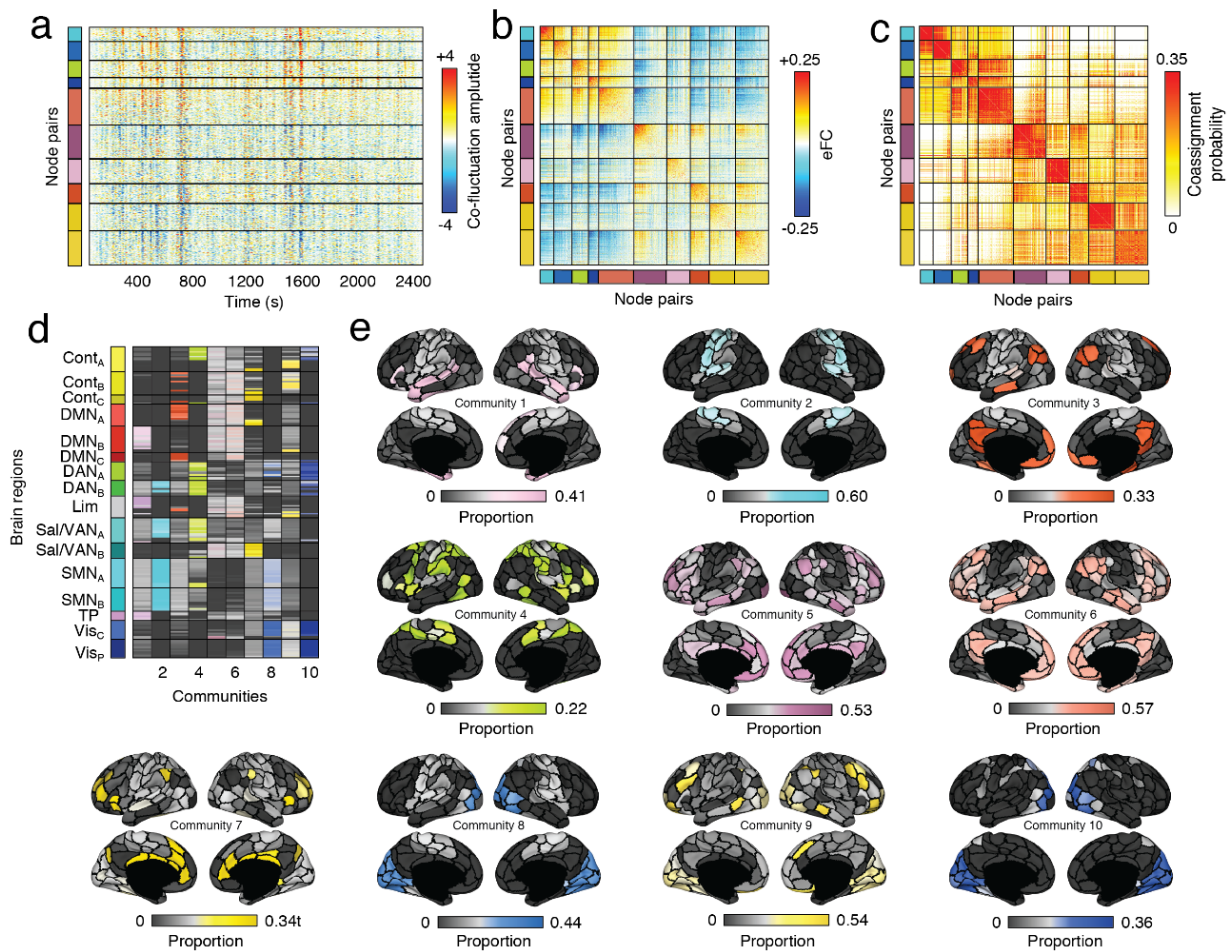
Figure 4 Edge communities. We applied similarity-based clustering to eFC from the HCP dataset. Here, we show results with the number of clusters fixed at k $= 10$. (**a**) Here, we reordered edge time series according to the detected community assignments. In this panel, horizontal lines divide communities from each other. The colors to the left of the time series plots identify each of the ten communities. (**b**) We also reordered the rows and columns of the eFC

matrix to highlight the same ten communities. Note that, on average, within-community eFC is greater than between-community eFC. (**c**) We calculated the probability that pairs of edges (node pairs) were co-assigned to the same community. Here, we show the co-assignment matrix with rows and columned reordered according to community assignments. Note that, in general, the range of co-assignment probabilities goes to 1. Here, we truncate the color limits to emphasize the 10-community partition (In Supplementary Figure 9 we show the same co-assignment matrix at different values of k and with non-truncated color limits). We present two visualizations of the edge communities projected back to brain regions (nodes). In **d**, we depict overlapping communities in matrix form. Each column in this matrix represents one of ten communities. For each community and for each node, we calculated the proportion of all edges assigned to the community that included that node as one of its endpoints ("stubs"), indicated by the color and brightness of each cell. Dark colors indicate few edges; bright colors indicate many (**e**) Topographic distribution of communities. Note that many of the communities resemble known intrinsic connectivity networks. However, because the communities here can overlap, it is possible for nodes associated with a particular intrinsic connectivity network to participate in multiple edge communities.

In Figure 4 we show representative communities obtained with $k = 10$ (See Supplementary Figure 9 and Supplementary Figure 10 for examples with different numbers of communities). To demonstrate that the communities capture meaningful variance in our data, we show the edge co-fluctuation time series, the eFC matrix, and the community co-assignment matrix reordered according to the derived communities (Figure 4a,b,c). Here, the elements of the co-assignment matrix represent the probability that two edges were assigned to the same community across partitions as we varied the number of communities from $k = 2$ to $k = 20$.

While the communities detected here are defined at the level of edges rather than nodes, we can project edge communities back onto brain regions. This was accomplished by extracting the edges associated with each community, determining which nodes were at the endpoints of each edge (the "stubs"), and counting the number of times that each node was represented in this stub

list. We show these results in matrix form in Figure 4d. In this panel, rows and columns represent nodes ordered according to the canonical system labels described in Schaefer, Kong et al. (2018).

The overlapping nature of communities is made clearer in Figure 4e, in which communities are represented topographically. The edges associated with the same visual nodes are all involved in communities 7, 8, 9, and 10 to some extent, thereby linking the visual system to multiple other brain systems. In community 8, for example, edges incident upon nodes in the visual and somatomotor systems are clustered together, whereas in community 9, edges incident upon visual and control network nodes are assigned to the same community.

Community overlap and functional diversity of cognitive systems

In the previous section, we showed that the human cerebral cortex could be partitioned into overlapping communities based on its edge correlation structure. This observation leads to a series of additional questions. For instance, which brain areas participate in many communities? Which participate in few? If we changed the scale of inquiry – the number of detected communities – do the answers to these questions change? Do the answers depend on which dataset we analyze? In this section we explore these questions in detail.
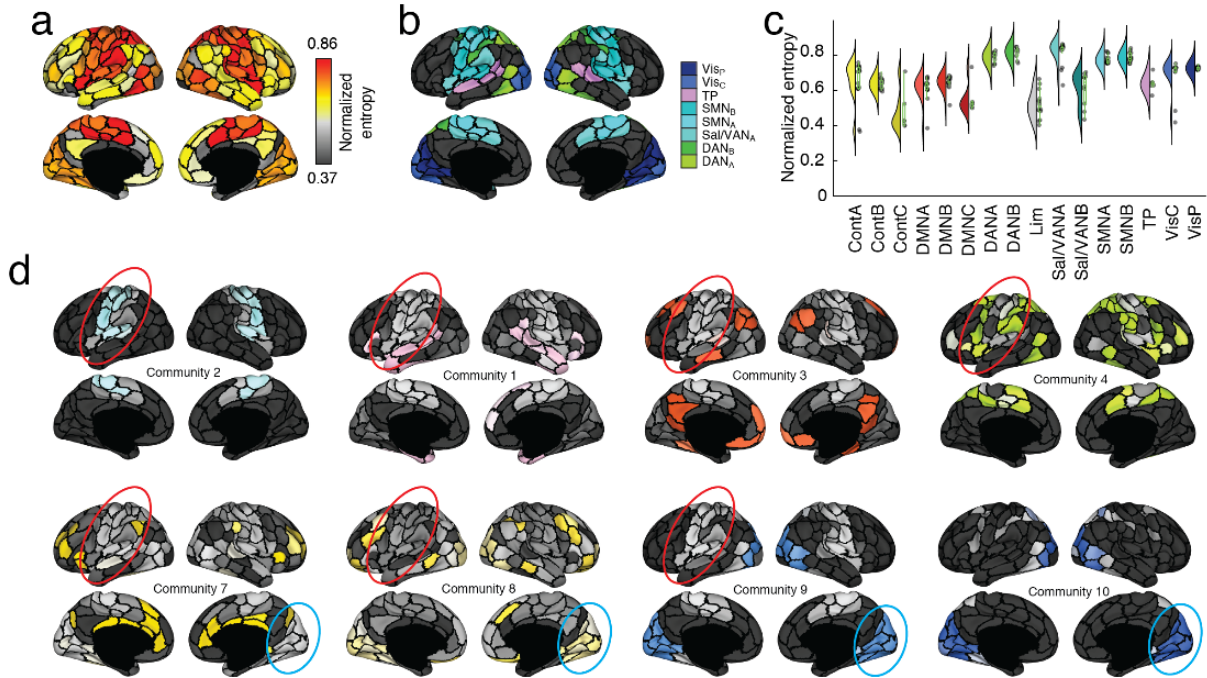
Figure 5 Edge community entropy and overlap. (a) Topographic distribution of normalized entropies. Normalized entropy, in this case, measures the uniformity of a node's community assignments across all communities and serves as a measure of overlap. In general, higher entropy corresponds to greater levels of overlap. **(b)** Brain systems associated with the highest levels of normalized entropy. These include visual, attentional, somatomotor, and temporo-parietal systems. **(c)** Entropy values for all brain systems; n = 200 brain regions. Boxplots, shown in green and overlaid on data points in panel **c**, depict the interquartile range (box) and median value of the distribution. Whiskers extend to the nearest points $\pm 1.5\times$ IQR above and below 25th and 75th percentiles. **(d)** Here, we highlight communities in which somatomotor (red) and visual (blue) systems are represented.

One strategy for assessing community overlap is to simply count the number of different communities to which each nodes' edges are assigned (Yeo, Krienen et al. 2014). A more nuanced measure that accounts for the distribution of edge community assignments is the normalized entropy, which indexes the uniformity of a distribution. We therefore calculated normalized entropy for every brain region while varying the number of communities from $k = 2$ to $k = 20$. In this section we focus on results with $k = 10$.

We found that normalized community entropy was greatest within sensorimotor and attentional systems and lowest within regions traditionally associated with control and default mode networks (Figure 5a,b,c). Importantly, we obtained similar results from the MSC and HBN datasets (Supplementary Figure 11), at the level of individual subjects (Supplementary Figure 12), as we varied the number of clusters (Supplementary Figure 13), and using different parcellation schemes (Supplementary Figure 14). These observations seemingly contradict previous reports in which functional overlap was greatest in control networks and lowest in primary sensory systems (Figure 5d)[6,28].

Is it possible to reconcile these seemingly opposed viewpoints? To address this question, we calculated a second measure of functional diversity. Whereas normalized entropy was defined at the level of individual brain regions based on the edge communities in which they participated, this second measure was defined at the level of brain systems as a whole, and assessed the average similarity of edge community assignments among the system regions (Figure 6a,b; see **Materials and Methods**). Intuitively, functionally diverse systems are comprised of brain regions whose edge community assignments are unique and dissimilar from one another. We find that regions within sensorimotor networks, which exhibited among the highest levels of entropy, exhibited the greatest levels of within-system similarity (Figure 6c). In contrast, sub-networks that make up the control network exhibit the lowest levels of within-system similarity, while their constituent nodes have among the lowest entropy (Figure 6c).
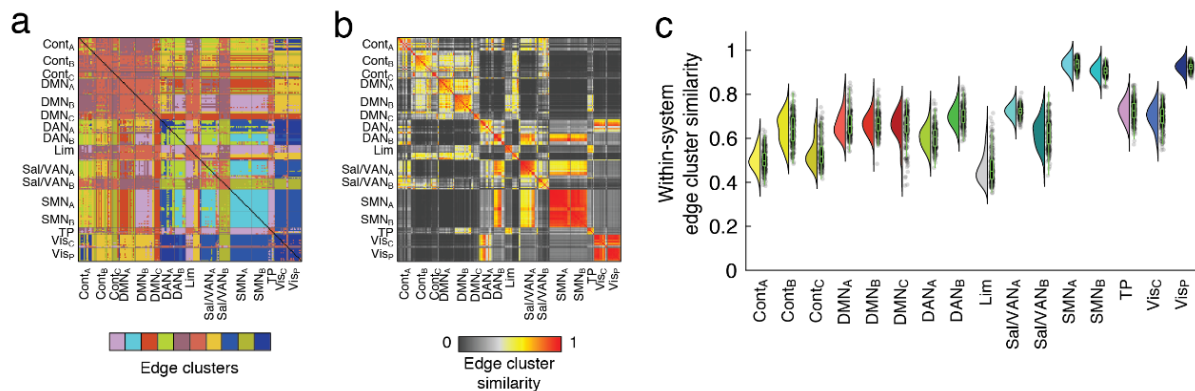
Figure 6 System-level similarity of edge communities. (**a**) Edge communities can be mapped into a [N × N] matrix. The element at row i and column j of the edge community matrix denotes the community label of edge {i, j}. (**b**) We can then calculate the similarity of edge communities involving nodes i and j by comparing the values of columns i and j. This matrix depicts the similarity for all pairs of nodes. (**c**) Within-system similarity values for each of the 16 pre-defined brain systems; n = 1,272 within-system similarity values. Boxplots, shown in green and overlaid on data points in panel **c**, depict the interquartile range (box) and median value of the distribution. Whiskers extend to the nearest points ±1.5× IQR above and below 25th and 75th percentiles.

In the supplementary material, we explore the relationship of normalized entropy with more familiar measures of overlap derived from nFC, including participation coefficient, dynamic flexibility, and versatility (see Supplementary Figure 15 and Supplementary Figure 16). We also compare patterns of normalized entropy derived from eFC community structure with entropy patterns obtained using alternative methods, including line graphs, the affiliation graph model, Bayesian non-negative matrix factorization, and mixed-membership stochastic blockmodels (see Supplementary Figure 17).

Edge functional connectivity is modulated by changes in sensory input

In the previous sections, we demonstrated that eFC is a reliable marker of an individual and that by clustering eFC we naturally obtain overlapping communities. We leveraged this final

observation to demonstrate that primary sensory and attentional systems participate in disproportionately more communities than association cortices. Analogous to previous studies documenting the effect of task on nodal FC, we expect that eFC is also modulated by task.

To address this question, we analyzed fMRI data from the Healthy Brain Network Serial Scanning Initiative recorded during rest and while subjects passively viewed the movie "Raiders of the Lost Ark." We estimated group-averaged eFC separately for each of the movie and rest scans.

In general, we found that eFC during movie-watching was highly correlated with eFC estimated during rest (Figure 7a). Across six movie scans, the mean correlation with resting eFC was $r = 0.55 \pm 0.02$ (all $p < 10^{-15}$; $n = 197,995,050$ edge-edge pairs). When we compared the pairwise similarity of all movie-watching scans with rest, we found that similarity of eFC was greater within a given task than between tasks ($p < 10^{-4}$, uniform and random permutation of movie and rest conditions; Figure 7b). To better understand what was driving this effect, we generated representative matrices for rest and movie conditions and computed the element-wise difference between these matrices. We contrasted these differences with those estimated after randomly permuting scan (condition) labels, and found that 8.63% of all edge connections exhibited significant changes between conditions (permutation test; $p < 10^{-4}$; uncorrected). While eFC differences were widespread, the most pronounced effects were associated with two specific communities (Figure 7c), one of which exhibited a decrease in its within-module eFC, while both decreased eFC with respect to each other. These communities, consisted of edges associated with somatomotor and visual systems (Figure 7d). To confirm that these system-level effects were statistically significant, we compared the mean within- and between-system eFC differences against a constrained null model in which edge communities were randomly permuted

(1000 repetitions; see Supplementary Figure 18 for a detailed schematic illustrating this procedure). As expected, the eFC involving systems 5 and 6 was significantly decreased from rest-to-movie (permutation test; false discovery rate fixed at 5%; $p_{adjusted} = 3.7 \times 10^{-5}$). See Supplementary Figure 19a for the complete list of condition differences.
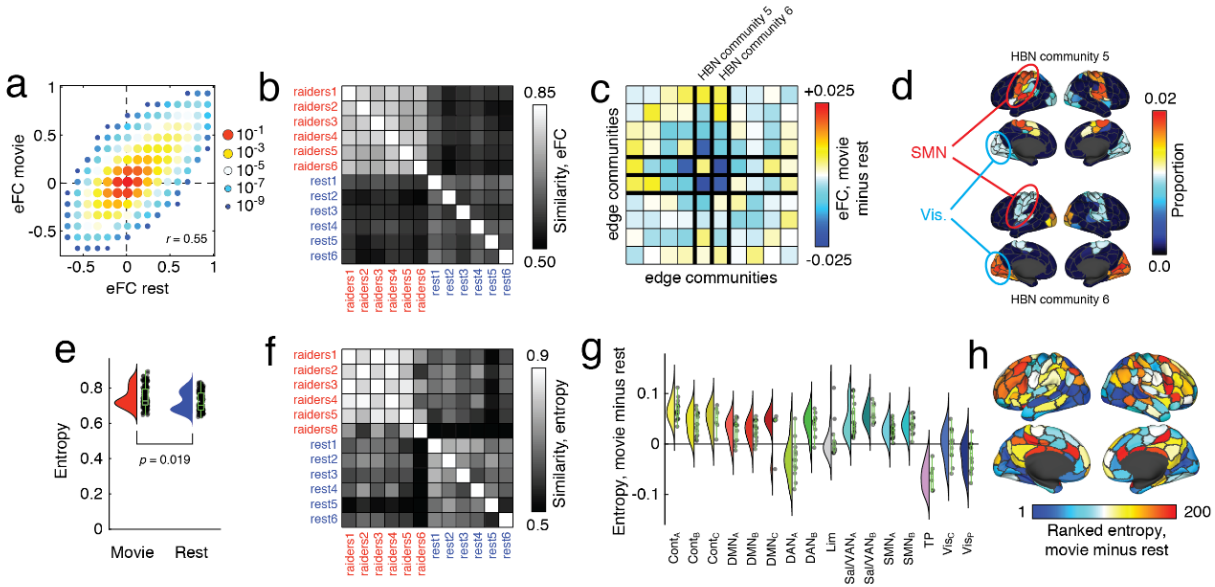
Figure 7 Effect of passive movie-watching on eFC. (**a**) Two-dimensional histogram of eFC estimated at rest with eFC estimated during movie-watching. (**b**) Similarity of whole-brain eFC estimated at rest with movie-watching. Note that within-condition similarity is greater for both conditions. (**c**) Community-averaged differences in eFC. Communities 5 and 6 are associated with the largest magnitude differences, on average. Note: these are communities estimated from HBN data and are not identical to those shown in Figure 4, which were estimated from HCP data. (**d**) Topographic distribution of communities 5 and 6. Note that these communities involve edges associated with visual and somatomotor systems. (**e**) Averaged differences in community overlap (normalized entropy); n = 200 brain regions whose entropy scores were compared across rest and movie-watching conditions (permutation test; mean difference in paired sample; p = 0.019). (**f**) Similarity of whole-brain normalized entropy estimated at rest with movie-watching. (**g**) Violin plot showing system-specific differences in normalized entropy. Note that some of the greatest increases in entropy are concentrated with control and default mode networks; n = 200 brain regions. (**h**) Topographic distribution of differences in entropy. Boxplots, shown in green and overlaid on data points in panels **e**

and **g**, depict the interquartile range (box) and median value of the distribution. Whiskers extend to the nearest points $\pm 1.5\times$ IQR above and below 25th and 75th percentiles.

The differences in the connection weights of eFC between movie-watching and rest strongly suggested that the locations of high and low cluster overlap might also differ between conditions. To test this, we used the same clustering algorithm described earlier to partition node pairs into non-overlapping clusters and, based on these clusters, calculated each node's cluster overlap as a normalized entropy. We found that compared to rest, entropy increased during movie-watching (permutation test; mean difference in paired samples; $p = 0.019$), indicating increased overlap between communities (Figure 7e), and that the brain-wide pattern of entropy also differed (permutation test; $p < 10^{-4}$; Figure 7f). We performed analogous tests at the level of individual brain regions, and found that 28% of brain regions passed statistical testing (permutation test; false discovery rate fixed at 5%; $p_{adjusted} = 0.014$; Supplementary Figure 19b). We further tested whether these differences exhibited system-specific effects by calculating the mean change in entropy for each system and comparing it against mean changes after randomly and uniformly permuting system labels. We found that seven systems exhibited such effects, with increases concentrated within control and salience/ventral attention networks and decreases in dorsal attention temporal-parietal, and visual systems (permutation of system labels; false discovery rate fixed at 5%; $p_{adjusted} = 0.012$; Figure 7,g,h; Supplementary Figure 19c).

Collectively, these results suggest that, like nFC, eFC is reconfigurable and can be modulated by sensory inputs. The observed changes in eFC, which implicated two clusters associated both with somatomotor and visual systems, is in close agreement with past studies of passive movie-watching that documented changes in activity and nFC in similar areas (Wilf, Strappini et al. 2017). We also found increased overlap in areas associated with control and default

mode networks, which agrees with evidence that activity throughout these areas is sensitive to movie narrative structure (Baldassano, Hasson et al. 2018). An important area of future research involves systematically assessing the effect of different cognitively demanding tasks on eFC.

Discussion

Here, we presented a network model of human cerebral cortex that focused on edge-edge interactions. The network formed by these interactions, a construct we referred to as edge functional connectivity (eFC), was similar across datasets and more similar within subjects than between. When clustered, eFC provided a natural estimate of pervasively overlapping community structure. We found that the amount of overlap varied across the cortex but peaked in sensorimotor and attention networks. We found that brain regions associated with sensorimotor and attention networks participated in disproportionately many communities compared to other brain systems, but that, relative to one another, those same regions participated in similar sets of communities. Lastly, we showed that eFC and community overlap varied systematically during passive viewing of movies.

Edge-centric perspective on functional network organization

Node-centric representations have dominated the field of network neuroscience and have served as the basis for nearly every discovery within that field (Bassett and Sporns 2017). The edge-centric representation shifts focus away from dyadic relationships between nodal activations and onto the interactions between edges (similarity in patterns of co-fluctuation, a potential hallmark of communication), instead. While related models have been explored in other scientific domains (Evans and Lambiotte 2009, Ahn, Bagrow et al. 2010) including neuroscience, where they were first used in a study to represent interacting white matter tracts (de Reus, Saenger et al.

2014), they require as input sparse node-node connectivity matrices and are poorly suited for continuous-valued time series data.

Here, we developed a novel edge-centric representation of functional neuroimaging data that operates directly on observed time series. Our method for estimating connection weights between edges can be viewed as a temporal "unwrapping" of the familiar Pearson correlation – the measure frequently used to estimate the magnitude of nFC between pairs of brain regions. Whereas the Pearson correlation coefficient calculates the time-averaged co-fluctuation magnitude for node pairs, we simply omit the averaging step, yielding "edge time series," which represent the co-fluctuation magnitude between two nodes at every instant in time. This simple step enables us to track fluctuations in edge weight across time and, critically, allow for dyadic relationships between edges, creating an edge-centric representation of nervous system architecture (Figure 1).If we interpret edge time series as a temporal unwrapping of nFC, which is thought to reflect the aggregate effect of communication processes between neural elements (Avena-Koenigsberger, Misic et al. 2018), then edge times series track, with high temporal resolution, the communication patterns between distributed neural elements.

We note that our edge-centric approach is conceptually similar to several existing methods. For instance, "multiplication of temporal derivatives" (MTDs) (Shine, Koyejo et al. 2015) calculates the element-wise products using differenced activity time series for all pairs of nodes. These time series are then convolved with a kernel to generate smooth estimates of time-varying nFC. Though similar, our approach relies on untransformed activity to estimate edge time series, thereby preserving the relationship between static nFC and the mean value of each edge time series. Another related method is "Co-activation Patterns" (CAPs) (Liu and Duyn 2013), which extracts and clusters voxel- or vertex-level activity during high-activity frames. Because a voxel can be co-

active under different contexts, the cluster centroids spatially overlap with one another. Though both CAPs and eFC result in overlapping structures, they operate on distinct substrates, with CAPs focusing on activity and eFC focusing on similarity of co-activity. While CAPs requires the specification of additional parameters compared to eFC, e.g. the threshold for a high-activity frame, CAPs may scale better due to the focus on activity rather than connectivity.

Finally, we note that nFC and eFC are both frameworks for investigating pairwise relationships from neural time series. Critically, however, nFC and eFC differ in terms of what elements are being related to one another and how we interpret those relationships. In the case of nFC, correlations refer to similarities in the activity of individual neural elements, often interpreted as two parts of the brain "talking" to one another. In the case of eFC, on the other hand, correlations express similarities in co-fluctuations along edges, which may loosely be interpreted as "conversations" between node pairs (Supplementary Figure 1). In other words, nFC focuses on co-activation between nodes while eFC focuses on co-fluctuation along edges. In this way, nFC and eFC should be viewed as complementary approaches that can reveal unique organizational features of nervous systems.

Overlapping communities extend our understanding of system-level cortical organization

Here, we demonstrated that clustering eFC using community detection methods naturally leads to communities that overlap when mapped back to the level of brain regions and nodes. Past investigations of cortical organization have focused almost exclusively on non-overlapping communities. The decision to define communities in this way is partially motivated by interpretability but also by limitations of the methods used to detect communities, which assign nodes to one community, only (Newman and Girvan 2004, Rosvall and Bergstrom 2008). This current view of communities has been profoundly successful (Sporns and Betzel 2016). It provides

111

a low-dimensional description of the brain, it can be used to define node roles and to detect hubs (Bertolero, Yeo et al. 2015), and can be applied to both anatomical and functional networks with equal success.

The dominant non-overlapping perspective of communities has strongly influenced how we think about brain function. Because functional communities exhibit reliable correspondence with patterns of task-evoked activity (Smith, Fox et al. 2009), we have come to associate individual communities with specific cognitive domains. For instance, it is not uncommon to refer to communities as primarily processing visual information, enacting cognitive control, or performing attentional functions. This localization of brain function to communities, though likely a reasonable first-order approximation, perpetuates a view of brain function in which brain areas, systems, and communities are fundamentally unifunctional. Such a view, however, disagrees with observations that many aspects of cognition and behavior transcend these traditional community labels.

Another perspective is that overlap arises from time-varying fluctuations in community structure (Bassett, Wymbs et al. 2011). That is, at any given instant communities are non-overlapping, but appear "fuzzy" due to nodes changing their community allegiances over time. The approach developed here is closely aligned with the perspective that brain areas and communities are dynamic and exhibit highly degenerate functionality. Other studies have investigated overlapping and dynamic communities by studying overlap in co-activation or through the use of sliding window analysis and multilayer models to detect flexible regions that change their community assignment over time. Our approach, however, is distinct, emphasizing a state of pervasive overlap (Ahn, Bagrow et al. 2010) in which nodes belong to several communities instantaneously.

112

Limitations

One of the most important limitations concerns the estimation of edge time series from functional imaging data. To calculate edge time series, we first z-score regional time series. Here, the z-score is only appropriate if the time series has a temporally invariant mean and standard deviation. If there is a sustained increase or decrease in activity, e.g. the effect of a blocked task, then the z-scoring procedure can result in a biased mean and standard deviation, resulting in poor estimates of fluctuations in activity. In future work, investigation of task-evoked changes in eFC could be investigated with already common preprocessing steps, e.g. constructing task regressors to remove the first-order effect of tasks on activity (Cole, Ito et al. 2019).

Another limitation concerns the scalability of eFC. Calculating eFC given for a brain divided into N parcels results in an eFC matrix of dimensions $\frac{N(N-1)}{2}$. This means that an increase in the number of parcels results in a squared increase in the dimensionality of eFC; if the number of parcels is large, then this can result in large, fully-weighted matrices that require large amounts of memory to store and manipulate. In the future, however, it may be necessary to explore dimension reduction methods to retain the most relevant subgraphs for a given task or set of behaviors.

Future directions

While eFC characterizes interactions between edges rather than nodes, it can still be analyzed using the same methods previously applied to nFC. We can use graph theory to detect its hubs and communities (Power, Schlaggar et al. 2013) (see Supplementary Figure 20 for examples), estimate edge gradients (Margulies, Ghosh et al. 2016), and compare eFC connection weights across individuals (Finn, Shen et al. 2015) and conditions (Cole, Ito et al. 2019). On the other hand,

eFC affords many new opportunities, beginning with the edge time series used to estimate eFC. Essentially, edge time series offer a moment-to-moment assessment of how strongly two nodes (brain regions) co-fluctuate with one another, providing an estimate of time-varying nFC without the requirement that we specify a window (Zamani Esfahlani, Jo et al. 2020). This overcomes one of the main limitations of sliding window estimates of time-varying nFC, namely that the use of a window leads to a "blurring" of events across time (Lurie, Kessler et al. 2020). Other directions for future work include developing whole-brain functional atlases with overlapping system labels and applications to specific brain areas and sub-systems for constructing fine-grained overlapping atlases (King, Hernandez-Castillo et al. 2019). We note, also, that because the derivation of eFC is based on Pearson correlations, it would be straightforward to estimate analogs of eFC based on lagged and partial relationships.

eFC might be useful in applications of machine learning and classification of neuroimaging data (Pereira, Mitchell et al. 2009). The dimensionality of the eFC matrix is much greater than that of a typical nFC matrix. We speculate that some of the added dimensions may be useful for studying brain-behavior relationships, for example by identifying manifolds along which subjects, clinical cohorts, or behaviors naturally separate, enhancing classification accuracy (Huys, Maia et al. 2016) (we show results of exploratory analyses of brain-behavior relationships based on eFC in Figs. S21, S22, S23). On the other hand, the increased dimensionality of eFC requires special considerations, as it presents statistical and interpretational challenges. Multivariate methods (McIntosh and Misic 2013) like canonical correlation analysis or partial least squares, both of which can help circumvent multiple comparison issues, may prove useful and should be investigated in future brain-behavior analysis involving eFC.

Additionally, future studies should investigate appropriate null models for eFC. Like nFC, eFC is correlation-based and the weights of edge-edge connections are not independent of one another (Zalesky, Fornito et al. 2012). This means that rewiring-based null models (which treat connections as independent) are not appropriate. Consideration should be given to other classes of null models, including time-series based surrogates. Appropriate null models may help clarify brain-behavior relationships in future studies.

The framework proposed here for investigating interactions between pairs of nodes can be generalized to study mutual interactions between many more nodes by simply calculating the element-wise product of nodes triplets, quartets, quintets (Owen, Chang et al. 2019). This extension is, in some respects, analogous to recent applications of algebraic topology (Sizemore, Phillips-Cremins et al. 2019), which can uncover higher-order relationships in a network (through graph simplices). We note, however, that while generating higher-order time series is straightforward, it is necessarily accompanied by an increase in dimensionality, potentially making the approach computationally intractable for whole-brain networks. On the other hand, higher-order time series (and their corresponding eFC analogs) may be useful for investigating the organization of predefined circuits composed of relatively few brain regions or nuclei.

Lastly, the edge-centric framework developed here is not limited to functional MRI and can be easily extended to different recording modalities, including scalp/intracranial EEG or MEG, which makes it possible to track seizure propagation at the level of edges (Khambhati, Davis et al. 2015). Similarly, the application of this approach to datasets resolving single neuron activity could uncover important connection-level insight into circuit organization (Dann, Michaels et al. 2016).

Materials and Methods

In this study, we utilized data from three independently acquired, openly available neuroimaging datasets (Van Essen, Smith et al. 2013, Gordon, Laumann et al. 2017, O'Connor, Potler et al. 2017) and therefore, did not collect any data for this study. No statistical methods were used to pre-determine sample sizes, but our sample sizes are similar to those reported in previous publications (Power, Schlaggar et al. 2013, de Reus, Saenger et al. 2014, Davison, Schlesinger et al. 2015, Finn, Shen et al. 2015, Gordon, Laumann et al. 2017, Shine, Breakspear et al. 2019) and represent either all usable data (MSC, HBN) or a subset preselected by the study coordinators (HCP). We did not perform any randomization of subjects into experimental groups, and we opted to analyze each dataset separately. Appropriate counterbalancing of task conditions was performed by the authors of the original studies (Van Essen, Smith et al. 2013, Gordon, Laumann et al. 2017, O'Connor, Potler et al. 2017). Data analysis was not performed blind to the conditions of the experiments. Blinding was not relevant because subjects were not evaluated based on group membership and blinding is not applicable to the whole-group analyses reported in this study. All analyses were performed with MATLAB (The MathWorks Inc.) version 2019a. Further study design and statistical details can be found in the Life Sciences Reporting Summary available online.

Datasets

The Human Connectome Project (HCP) dataset (Van Essen, Smith et al. 2013) included resting state functional data (rsfMRI) from 100 unrelated adult subjects (54% female, mean age = 29.11 ± 3.67, age range = 22-36). These subjects were selected as they comprised the "100 Unrelated Subjects" (U100) released by the Human Connectome Project. The study was approved

by the Washington University Institutional Review Board and informed consent was obtained from all subjects. Subjects underwent four 15-minute rsfMRI scans over a two-day span. A full description of the imaging parameters and image preprocessing can be found in Glasser, Sotiropoulos et al. (2013). The rsfMRI data was acquired with a gradient-echo EPI sequence (run duration = 14:33 min, TR = 720 ms, TE = 33.1 ms, flip angle = 52∘, 2 mm isotropic voxel resolution, multiband factor = 8) with eyes open and instructions to fixate on a cross. Images were collected on a 3T Siemens Connectome Skyra with a 32-channel head coil.

The Midnight Scan Club (MSC) dataset (Gordon, Laumann et al. 2017) included rsfMRI from 10 adults (50% female, mean age = 29.1± 3.3, age range = 24-34). The study was approved by the Washington University School of Medicine Human Studies Committee and Institutional Review Board and informed consent was obtained from all subjects. Subjects underwent 12 scanning sessions on separate days, each session beginning at midnight. 10 rsfMRI scans per subject were collected with a gradient-echo EPI sequence (run duration = 30 min, TR = 2200 ms, TE = 27 ms, flip angle = 90∘, 4 mm isotropic voxel resolution) with eyes open and with eye tracking recording to monitor for prolonged eye closure (to assess drowsiness). Images were collected on a 3T Siemens Trio.

The Healthy Brain Network Serial Scanning Initiative (HBN) dataset (O'Connor, Potler et al. 2017) included rsfMRI and movie watching (mvfMRI) data from 13 adults (54% female, mean age = 30.3 ± 6.4, age range = 21-42). Three subjects of the HBN dataset did not have enough non-outlier functional scans (see quality control criteria below) to be meaningfully analyzed (non-outlier scan percentage = 7%, 0%, and 0%), and were excluded entirely from the current study. This rendered the HBN dataset as 10 subjects (50% female, mean age = 29.8 ± 5.3, age range = 23-37). The study was approved by the Chesapeake Institutional Review Board and informed

117

consent was obtained from all subjects. Subjects underwent 14 scanning sessions over a 1-2 month period, in which 13 rsfMRI runs were acquired per subject. On the 8th session, subjects viewed the movie "Raiders of the Lost Ark" (Lucasfilm Ltd., 1981) in six approximately 20-minute scans. The rsfMRI and mvfMRI were acquired with a gradient-echo EPI sequence (run duration rsfMRI = 10:18 min, mvfMRI = 20 min per segment, TR = 1450 ms, TE = 40 ms, flip angle = 55∘, 2.46x2.46x2.5 mm voxel resolution, multiband factor = 3) with subjects instructed to keep their eyes open and gazed directed towards a cross during the fsMRI scan. Images were collected on a 1.5T Siemens Avanto with a 32-channel head coil. The mvfMRI was divided into six successive scan sessions, which we further truncated by retaining the first 420 samples so that the duration matched that of the HBN rsfMRI, of which we retained the first six for the sake of balance.

Image preprocessing

HCP functional preprocessing

Functional images in the HCP dataset were minimally preprocessed according to the description provided in Glasser, Sotiropoulos et al. (2013). Briefly, these data were corrected for gradient distortion, susceptibility distortion, and motion, and then aligned to a corresponding T1-weighted (T1w) image with one spline interpolation step. This volume was further corrected for intensity bias and normalized to a mean of 10000. This volume was then projected to the *32k_fs_LR* mesh, excluding outliers, and aligned to a common space using a multimodal surface registration (Robinson, Jbabdi et al. 2014). The resultant cifti file for each HCP subject used in this study followed the file naming pattern: *REST{1,2}_{LR,RL}_Atlas_MSMAll.dtseries.nii.

MSC and HBN functional preprocessing

Functional images in the MSC and HBN datasets were preprocessed using *fMRIPrep* 1.3.2 (Esteban, Markiewicz et al. 2019) which is based on Nipype 1.1.9 (Gorgolewski, Burns et al.

2011). The following description of *fMRIPrep*'s preprocessing is based on boilerplate distributed with the software covered by a "no rights reserved" (CC0) license. Internal operations of *fMRIPrep* use Nilearn 0.5.0 (Abraham, Pedregosa et al. 2014), ANTs 2.2.0 , FreeSurfer 6.0.1 , FSL 5.0.9, and AFNI v16.2.07. For more details about the pipeline, see the section corresponding to workflows in *fMRIPrep*'s documentation.

The T1-weighted (T1w) image was corrected for intensity non-uniformity with N4BiasFieldCorrection (Avants, Epstein et al. 2008, Tustison, Avants et al. 2010), distributed with ANTs, and used as T1w-reference throughout the workflow. The T1w-reference was then skull-stripped with a Nipype implementation of the antsBrainExtraction.sh workflow, using NKI as the target template. Brain surfaces were reconstructed using recon-all (Dale, Fischl et al. 1999), and the brain mask estimated previously was refined with a custom variation of the method to reconcile ANTs-derived and FreeSurfer-derived segmentations of the cortical gray matter using Mindboggle (Klein, Ghosh et al. 2017). Spatial normalization to the ICBM 152 Nonlinear Asymmetrical template version 2009c (Fonov, Evans et al. 2009) was performed through nonlinear registration with antsRegistration, using brain extracted versions of both T1w volume and template. Brain tissue segmentation of cerebrospinal fluid (CSF), white-matter (WM) and gray matter (GM) was performed on the brain-extracted T1w using FSL's fast (Zhang, Brady et al. 2001).

Functional data was slice time corrected using AFNI's 3dTshift and motion corrected using FSL's mcflirt (Jenkinson, Bannister et al. 2002). *Fieldmap-less* distortion correction was performed by co-registering the functional image to the same-subject T1w image with intensity inverted (Wang, Peterson et al. 2017) constrained with an average fieldmap template (Treiber, White et al. 2016), implemented with antsRegistration. This was followed by co-registration to the corresponding T1w using boundary-based registration (Greve and Fischl 2009) with 9 degrees of

freedom. Motion correcting transformations, field distortion correcting warp, BOLD-to-T1w transformation and T1w-to-template (MNI) warp were concatenated and applied in a single step using antsApplyTransforms using Lanczos interpolation. Several confounding timeseries were calculated based on this preprocessed BOLD: framewise displacement (FD), DVARS and three region-wise global signals. FD and DVARS are calculated for each functional run, both using their implementations in Nipype (Power, Mitra et al. 2014). The three global signals are extracted within the CSF, the WM, and the whole-brain masks. The resultant nifti file for each MSC and HBN subject used in this study followed the file naming pattern: *space-T1w_desc-preproc_bold.nii.gz.

Image quality control

All functional images in the HCP and MSC datasets were retained. The quality of functional images in the MSC and HBN were assessed using *fMRIPrep*'s visual reports and MRIQC 0.15.1 (Esteban, Birman et al. 2017). Data was visually inspected for whole brain field of view coverage, signal artifacts, and proper alignment to the corresponding anatomical image. Functional data were excluded if greater than 25% of the frames exceeded 0.2 mm framewise displacement (Parkes, Fulcher et al. 2018). Furthermore, HBN functional data were excluded if marked as an outlier (exceeding 1.5x inter-quartile range in the adverse direction) in more than half of the following image quality metrics (calculated within-dataset, across all functional acquisitions): dvars, tsnr, fd mean, aor, aqi, snr, and efc. Information about these image quality metrics can be found within MRIQC 's documentation.

Functional and structural networks preprocessing

Parcellation preprocessing

A functional parcellation designed to optimize both local gradient and global similarity measures of the fMRI signal (Schaefer, Kong et al. 2018) (Schaefer200) was used to define 200 areas on the cerebral cortex. These nodes are also mapped to the Yeo canonical functional networks (Yeo, Krienen et al. 2011). For the HCP dataset, the Schaefer200 is openly available in 32k fs LR space as a cifti file. For the MSC and HBN datasets, a Schaefer200 parcellation was obtained for each subject using a Gaussian classifier surface atlas (Fischl, van der Kouwe et al. 2004) (trained on 100 unrelated HCP subjects) and FreeSurfer's mris_ca_label function. These tools utilize the surface registrations computed in the recon-all pipeline to transfer a group average atlas to subject space based on individual surface curvature and sulcal patterns. This method rendered a T1w space volume for each subject. For use with functional data, the parcellation was resampled to 2mm T1w space. This process could be repeated for other resolutions of the parcellation (i.e. Schaefer100).

Functional network preprocessing

Each preprocessed BOLD image was linearly detrended, band-pass filtered (0.008-0.08 Hz) (Parkes, Fulcher et al. 2018), confound regressed and standardized using Nilearn signal.clean, which removes confounds orthogonally to the temporal filters (Lindquist, Geuter et al. 2019). The confound regression employed (Satterthwaite, Elliott et al. 2013) included 6 motion estimates, time series of the mean CSF, mean WM, and mean global signal, the derivatives of these nine regressors, and the squares these 18 terms. Furthermore, a spike regressor was added for each fMRI frame exceeding a motion threshold (HCP = 0.25 mm root mean squared displacement; MSC, HBN = 0.5 mm framewise displacement). This confound strategy has been shown to be relatively effective option for reducing motion-related artifacts (Parkes, Fulcher et al. 2018).

Following preprocessing and nuisance regression, residual mean BOLD time series at each node were recovered. eFC matrices for each subject were computed and then averaged across subjects, to obtain a representative eFC matrix for each dataset. This processing was performed for both resting state and movie watching data.

Edge graph construction

Constructing networks from fMRI data (or any neural time series data) requires estimating the statistical dependency between every pair of time series. The magnitude of that dependency is usually interpreted as a measure of how strongly (or weakly) those voxels or parcels are functionally connected to each other. By far the most common measure of statistic dependence is the Pearson correlation coefficient. Let $x_i = [x_i(1), \ldots, x_i(T)]$ and $x_j = [x_j(1), \ldots, x_j(T)]$ be the time series recorded from voxels or parcels i and j, respectively. We can calculate the correlation of i and j by first z-scoring each time series, such that at $z_i = \frac{x_i - \mu_i}{\sigma_i}$ where $\mu_i = \frac{1}{T} \sum_t x_i(t)$ and $\sigma_i = \sqrt{\frac{1}{T-1} \sum_t (x_i(t) - \mu_i)^2}$ are the time-averaged mean and standard deviation. Then, the correlation of i and j can be calculated as: $r_{ij} = \frac{1}{T-1} \sum_t [z_i(t) \cdot z_j(t)]$. Repeating this this procedure for all pairs of parcels results in a node-by-node correlation matrix, i.e. an estimate of FC. If there are N nodes, this matrix has dimensions $[N \times N]$.

To estimate edge-centric networks, we need to modify the above approach in one small but crucial way. Suppose we have two z-scored parcel time series, z_i and z_j. To estimate their correlation we calculate the mean their element-wise product (not exactly the average, because we divide by $T - 1$ rather than T). Suppose, instead, that we never calculate the mean and simply stop after calculating the element-wise product. This operation would result in a vector of length

T whose elements encode the moment-by-moment co-fluctuations magnitude of parcels i and j.

For instance, suppose at time t, parcels i and j simultaneously increased their activity relative to baseline. These increases are encoded in z_i and z_j as positive entries in the tth position, so their product is also positive. The same would be true if i and j decreased their activity simultaneously (because the product of negatives is a positive). On the other hand, if i increased while j decreased (or *vice versa*), this would manifest as a negative entry. Similarly, if either i or j increased or decreased while the activity of the other was close to baseline, the corresponding entry would be close to zero.

Accordingly, the vector resulting from the element-wise product of z_i and z_j can be viewed as encoding the magnitude of moment-to-moment co-fluctuations between i and j. An analogous vector can easily be calculated for every pair of parcels (network nodes), resulting in a set of co-fluctuation (edge) time series. With N parcels, this results in $\frac{N(N-1)}{2}$ pairs, each of length T. From these time series we can estimate the statistical dependency for every pair of edges. We refer to this construct as edge functional connectivity (eFC). Let $c_{ij} = \left[z_i(1) \cdot z_j(1), \ldots, z_i(T) \cdot z_j(T) \right]$ and $c_{uv} = \left[z_u(1) \cdot z_v(1), \ldots, z_u(T) \cdot z_v(T) \right]$ be the time series for edges $\{i, j\}$ and $\{u, v\}$, respectively. Then we can calculate eFC as:

$$eFC_{ij,uv} = \frac{\sum_t c_{ij}(t) \cdot c_{uv}(t)}{\sqrt{\sum_t c_{ij}(t)^2} \sqrt{\sum_t c_{uv}(t)^2}}$$

Here, the denominator is necessary to bound eFC to the interval $[-1, 1]$.

Clustering algorithm

In general, eFC matrices are much larger than traditional nodal FC matrices. While most clustering algorithms can be applied to hundreds or even thousands of observations, estimating

123

clusters for eFC (which consists of tens of thousands of observations, each paired with at least as many features), presents a computational challenge, especially if the aim is to explore the space of possible partitions. To address this issue and to cluster eFC, we developed a simple two-step clustering procedure that operates on a low-dimensional representation of the eFC matrix.

First, we performed an eigen decomposition of the eFC matrix, retaining the top 50 eigenvectors. These eigen-vectors were rescaled to the interval $[-1, 1]$ by dividing each eigenvector by its largest magnitude element. Then simply clustered the rescaled eigenvectors using a standard k-means algorithm with Euclidean distance. We varied the number of communities, k, from $k = 2$ to $k = 20$, repeating the clustering algorithm 250 at each value. We retained as a representative partition the one with the greatest overall similarity to all other partitions. We note that the edge time series can be clustered directly and that, in general, the results were highly similar (Supplementary Figure 12).

We note that, in general, other community detection algorithms could be used in place of k-means; our decision to use this algorithm was practically motivated, as k-means exhibited significantly faster runtimes than other algorithms, e.g. modularity maximization (Newman and Girvan 2004) and Infomap (Rosvall and Bergstrom 2008), which have been used extensively in previous work to derive communities in both functional and structural brain networks.

Community overlap metrics

The clustering algorithm partitioned edges into non-overlapping clusters. That is, every edge $\{i, j\}$, where $i, j \in \{1, \ldots, N\}$, was assigned to one of k clusters. In this list of edges, each node appeared $N - 1$ times (we excluded self-connections). Region i's participation in cluster c was calculated as:

$$p_{ic} = \frac{1}{N-1} \sum_{j \neq i} \delta(g_{ij}, c)$$

where $g_{ij} \in \{1, \ldots, k\}$ was the cluster assignment of the edge linking nodes i and j and $\delta(x, y)$ is the Kronecker delta, whose value is 1 if $x = y$ and 0 otherwise. By definition, $\sum_c p_{ic} = 1$, and we can treat the vector $p_i = [p_{i1}, \ldots, p_{ik}]$ as a probability distribution. The entropy of this distribution measures the extent to which region i's community affiliations are distributed evenly across all communities (high entropy and high overlap) or concentrated within a small number of communities (low entropy and low overlap). We calculate this entropy as:

$$h_i = -\sum_c p_{ic} \log_2 p_{ic}$$

To normalize this measure and bound it to the interval $[0,1]$, we divided by $\log_2 k$. We refer to this measure as community entropy and interpret this value as an index of overlap. Intuitively, as the distribution of edge community assignments approaches uniformity its normalized entropy is close to 1; when edges are assigned to a single community normalized entropy is closer to 0.

Edge community similarity

When we cluster an eFC matrix, we assign each edge to a single community. These edge communities can be rearranged into the upper triangle of a $N \times N$ matrix, **X**, whose element x_{ij} denotes the edge community assignment of the edge between nodes i and j. The ith column of **X**, which we denote as $x_i = [x_{1i}, \ldots, x_{Ni}]$, encodes the community labels of all edges in which node i participates. Note that we do not consider self-edges, so the element x_{ii} is left empty.

From this matrix, we can compare the edge communities of nodes i and j by calculating the similarity of vectors x_i and x_j. Here, we measure that similarity as the fraction of elements in both vectors with the same community label. That is:

$$s_{ij} = \frac{1}{N-2} \sum_{u \neq i,j} \delta(x_{iu}, x_{ju})$$

Here, $\delta(x, y)$ is the Kronecker delta and takes on a value of 1 when x and y have the same value, but is zero otherwise. Note that the normalization of over $N - 2$ because we ignore the self-connections x_{ii} and x_{jj}. Repeating this comparison for all pairs of nodes generates the similarity matrix, $S = \{s_{ij}\}$.

Estimating overlapping community structure from nFC

In this paper we applied a clustering algorithm to eFC, which generates overlapping nodal communities. In contrast, field-standard community detection algorithms like Infomap (Rosvall and Bergstrom 2008) and modularity maximization (Newman and Girvan 2004) partition nFC into non-overlapping communities. However, there are non-standard methods that can be applied directly to nFC that generate overlapping communities. These include but are not limited to stochastic variational inference for the mixed-membership stochastic block model (Gopalan and Blei 2013) (SVINET), the Affiliation Graph Model (Yang and Leskovec 2014) (AGMFIT), Bayesian non-negative matrix factorization (Psorakis, Roberts et al. 2011) (NMF), and thresholded weighted link clustering (Ahn, Bagrow et al. 2010, de Reus, Saenger et al. 2014) (ThrLink).

We applied these methods to group-representative nFC data from the HCP dataset (with the number of communities fixed at $k = 10$) and compared their patterns of overlap with those obtained from clustering eFC. In general, each of these alternative methods require that the input connectivity matrix contain only positively weighted or binary edges, necessitating that it be thresholded. To do this, we computed the maximum spanning tree of the nFC matrix (to ensure that all nodes form a single connected component) and added edges to this backbone to reach a desired network density. We repeated the following comparisons across densities of 10%, 20%,

30% and 40% (a range in which negative edges were not retained). For each method, 250 overlapping community structures were recovered. We describe each method in more detail, below, and summarize the results in Supplementary Figure 17.

The SVINET method employs a mixed-membership stochastic block model algorithm, which is a generative model of network communities based on grouping nodes with similar connectivity patterns (Gopalan and Blei 2013). This method has been previously used to demonstrate the areas of the brain that participate in many cognitive functions also participate in proportionally more communities (Najafi, McMenamin et al. 2016). This method operates on binary connections; thus, edge weights were discarded. Each run was seeded with a random integer and run for 250 iterations with link-sampling. Resulting community assignments with at least 5% membership likelihood were recorded as a membership affiliation.

The AGMFIT method employs a generative model of communities based on a bipartite graph structure, linking nodes to communities (Yang and Leskovec 2014). The central concept of the AGMFIT algorithm is that communities overlap in a "tiled" manner, meaning that nodes with overlapping community membership are more densely interconnected than non-overlapping nodes. This model of overlapping structure has been shown to accurately capture core-periphery structure in large-scale social networks. This method operates on binary connections; thus, edge weights were discarded. Each run was seeded with a random integer.

The NMF method employs a probabilistic data reduction model that results in a soft partitioning of the network (Psorakis, Roberts et al. 2011). This method has been shown to avoid over-fitting communities in synthetic random graph data where no real communities exist. Edge weights were retained for this method and diagonal entries of the adjacency matrix were set to the nodal degree (as suggested in the documentation). Each run was randomly initialized. Runs that

did not produce the desired number of communities were rejected and sampling continued until 250 partitions were obtained. Resulting community assignments with at least 5% membership likelihood were recorded as membership affiliation.

For the ThrLink method, we created a weighted line graph from the thresholded adjacency matrix (Evans and Lambiotte 2009). This matrix was clustered using the generalized Louvain algorithm with the resolution parameter, γ, tuned to produce the desired number of communities. To tune this parameter, a range of values were used to recover communities of varying sizes. The minimum and maximum values producing the desired number of communities were recorded. Uniformly randomly sampled γ values within this range were used to recover communities of the weighted line graph. Runs that did not produce the desired number of communities were rejected and sampling continued until 250 partitions were obtained. Community memberships of the weighted line graph were projected to the nodes to gather the overlapping structure.

We compare community entropy against a series of related statistics that can be easily derived from nFC as opposed to eFC. These include static measures of participation coefficient (Guimera and Nunes Amaral 2005) and versatility (Shinn, Romero-Garcia et al. 2017) and the "dynamic" measure of flexibility (Bassett, Wymbs et al. 2011, Pedersen, Zalesky et al. 2018). We calculated static measures using a group-representative nFC matrix that was the average nFC data from all scans and subjects. Flexibility was calculated first at the single subject level where time series were divided into 10 non-overlapping windows containing $L = 120$ samples each (approximately 86 seconds) and subsequently averaged across individuals. Details of how each measure was calculated are presented below.

Participation coefficient measures the uniformity with which a node's connections are distributed across (non-overlapping) communities. Values closer to 1 indicate that connections are distributed evenly. Participation coefficient is calculated as:

$$pc_i = 1 - \sum \left(\frac{k_{is}}{k_i}\right)^2$$

Here, k_i is the total strength of node i and k_{is} is the strength of node i to community s. We calculated several variants of participation coefficient in which we varied how communities were defined. First, we treated the system labels from Schaefer, Kong et al. (2018) as a communities and calculated participation coefficient with respect to these labels. We also tested a more data-driven procedure in which we used multiscale modularity maximization (Reichardt and Bornholdt 2006) to detect the communities of the nFC matrix. In doing so, we used a uniform null model (Traag, Van Dooren et al. 2011, Bazzi, Porter et al. 2016), which is appropriate for correlation matrices and has been used extensively in the neuroimaging community (see Betzel, Bertolero et al. (2019) as just one example), and systematically varied the resolution parameter, γ over the interval $[0, 0.5]$ (repeating a Louvain-like algorithm 1000 times). In all cases, we separately calculated participation coefficient using for positive and negative connection weights.

We also used the detected communities to estimate regional versatility (Shinn, Romero-Garcia et al. 2017), which measures the variability of a node's community assignment across repeated runs of a community detection algorithm. We calculated versatility as:

$$v_i = \frac{\sum_j \sin(\pi \cdot p_{ij})}{\sum_j p_{ij}}$$

For a given value of γ, p_{ij} denotes the fraction of times that nodes i and j were co-assigned to the same community. We calculated versatility with respect to communities detected using the same values of γ.

Lastly, we calculated network flexibility, which measures how frequently a brain region changes communities across time. We modeled FC estimated within each non-overlapping window as a layer in a multilayer network, and a used multilayer modularity maximization algorithm (Mucha, Richardson et al. 2010) to cluster all layers simultaneously. The result is a node-by-layer matrix of communities, whose element $g_{i,s}$ indicates the community assignment of node i in layer s. From this matrix, we calculate flexibility as:

$$f_i = 1 - \frac{1}{T-1} \sum_{s=1}^{T-1} \delta\big(g_{i,s}, g_{i,s+1}\big)$$

Here, $T = 10$ is the number of layers and $\delta\big(g_{i,s}, g_{i,s+1}\big)$ is the Kronecker delta function and is equal to 1 when $g_{i,s} = g_{i,s+1}$ and is zero otherwise. In essence, flexibility measures the fraction of times that a node's community assignment changes in successive layers (time points). In addition to the γ resolution parameter, the output of the multilayer modularity maximization algorithm depends upon a second parameter, ω, that controls the consistency of communities across layers. We systematically varied these parameters over the ranges $\gamma = [0, 0.25, 0.5]$ and $\omega = [0.1, 0.5, 1]$ and calculated flexibility for all possible $\{\gamma, \omega\}$ pairs.

Graph-theoretic analysis of eFC

We applied graph-theoretic measures to the eFC matrix to characterize its topological features (Rubinov and Sporns 2010). We focused on local measures that characterize features at the level of a network's nodes (in the case of eFC, nodes represent pairs of brain regions). To visualize these measures, we reshaped their values into the upper triangle of a region-by-region matrix (Supplementary Figure 20). We focused on several different measures:

1. Degree (±) measures separately the total number of positive and negative connections incident upon a given node in the eFC network.

2. Strength (±) is the weighted analog of degree and measures separately the total weight of positive and negative connections incident upon a given node in the eFC network. Both degree and strength tell us, on average, how strongly or weakly a given node in the eFC network interacts with other nodes in the eFC network.

3. Participation coefficient (±) measures the extent to which a node's connections in the eFC network are concentrated within or distributed across edge communities. Values close to zero mean that a given node in the eFC network interacts primarily with other nodes in its own edge community; values close to one mean that given node in the eFC network interactions uniformly with all edge communities.

4. Betweenness centrality measures the number of shortest paths between pairs of nodes in the eFC network that pass through a given node. In general, betweenness centrality implies that a particular node in the eFC network may occupy a position of importance in the network.

5. Clustering coefficient measures the extent to which node's neighbors in the eFC network are also connected to one another.

Exploratory analyses of brain-behavior relationships using eFC

Correlations of eFC weights with behavior

We also used eFC data to explore brain-behavior relationships (Smith, Nichols et al. 2015). The overall pipeline begins by calculating each subjects edge-by-edge eFC matrix (Supplementary Figure 21a) and representing its upper triangle elements as a vector (Supplementary Figure 21b). This procedure is repeated for all subjects in the HCP 100 unrelated subjects cohort so that the

vectorized eFC is stored in a single matrix (Supplementary Figure 21c). In parallel, we z-scored subjects' behavioral data and performed principal components analysis, resulting in a set of scores that characterize orthogonal modes of behavioral variability (Supplementary Figure 21d; see Supplementary Table 1 for more details). We the compute the correlation of scores with rows from the matrix of vectorized eFC matrices (each row represents the eFC for a particular edge-edge interaction; (Supplementary Figure 21e)). Repeating this procedure for all rows results in a vector of correlation coefficients that can be reshaped to fit into the upper triangle of an edge-by-edge matrix, resulting in a correlation map (Supplementary Figure 21f). This entire process is repeated separately for principal components 1-10 and for scans REST1 and REST2.

We compare the correlation maps from REST1 and REST2 and find good correspondence (Supplementary Figure 21,h,i). To better interpret these maps, we adopted a community-level analysis (see Supplementary Figure 22 for a short schematic). Briefly, this involves aggregating and averaging correlation coefficients by edge communities (Supplementary Figure 22b), comparing the average correlation coefficients against a null distribution obtained using a constrained permutation test (Supplementary Figure 22c), and performing statistical evaluation, controlling for false-discovery rate at the level of communities (Supplementary Figure 22d). Further details of the permutation test can be found in Supplementary Figure 18.

Using this community-level approach, we investigated the relationship between eFC and PC1 in greater detail. We note that PC1 explains approximately 17% of the variance in behavioral data (almost three times as much as PC2) and defines a task accuracy/reaction time axis of behavior (Supplementary Figure 21j,k). We include brief descriptions of the other PCs in Table. S1. We show the correlation map for PC1 with eFC in Supplementary Figure 21l. To illustrate how the community-level analysis facilitates a clearer interpretation of brain-behavior correlations,

consider eFC of edges in communities 7 and 9 (the block highlighted in Supplementary Figure 21l). Community 7 links higher order cognitive areas in the control and default mode networks with visual cortex, forming an "executive-visual" complex, while community 9 links control and default mode to the salience/ventral attention network as part of an "executive-insular" complex (Supplementary Figure 21m,n). Accordingly, the positive correlation eFC between community 7 and 9 with PC1 means that as the edges within those communities become more synchronized across time (stronger eFC) the value of PC1 increases proportionally (Supplementary Figure 21o,p).

In addition to modeling brain-behavior relationships using the original eFC data, we repeated this same analysis with residual eFC after regressing out the effect of nFC. Specifically, we used the procedure described in Figure 2c to generate an approximation of eFC using only nFC data. We then regressed out the approximated eFC from the actual eFC and assessed brain-behavior relationships using the residual values. As with the previous analysis, we found that brain-behavior correlation maps were reproducible across scan sessions (Supplementary Figure 23).

Correlations of regional statistics with behavior

We also compared eFC and nFC brain-behavior relationships by deriving a series of regional (local) network statistics from each and calculating the correlations of behavioral measures with these statistics (Supplementary Figure 24). We note that the measures derived from both nFC and eFC have identical dimensionality, effectively accounting for any differences in the dimensionality of the original nFC and eFC matrices. In general, we found that the correlation patterns estimated using nFC-derived statistics were highly similar to one another, while the correlation pattern derived from the eFC statistic was dissimilar (Supplementary Figure 24f).

133

These findings demonstrate that eFC has the potential to uniquely explain patterns of inter-individual variability not currently explainable by nFC, opening new opportunities for studying individual differences in subjects' cognitive, developmental, and clinical states.

Modeling eFC in terms of nFC

eFC and nFC are both derived from the same substrate: regional fMRI BOLD time series. Can the eFC between edges $\{i, j\}$ and $\{u, v\}$ be easily modeled in terms of nFC? We tested whether this was the case using linear regression to explain the eFC between pairs of edges $\{i, j\}$ and $\{u, v\}$ using information about the pairwise nFC among the same set of nodes: $\{i, j\}, \{i, u\}, \{i, v\}, \{j, u\}, \{j, v\}$, and $\{u, v\}$. We considered two classes of models. The first modeled eFC in terms of the six nFC weights:

$$eFC_{ij,uv} = \beta_1 nFC_{ij} + \beta_2 nFC_{iu} + \beta_3 nFC_{iv} + \beta_4 nFC_{ju} + \beta_5 nFC_{jv} + \beta_6 nFC_{uv} + \beta_0 + \varepsilon$$

The second modeled eFC in terms of nFC interactions:

$$eFC_{ij,uv} = \beta_1 [nFC_{ij} \times nFC_{uv}] + \beta_0 + \varepsilon$$

In this model, we systematically varied the interaction term, $nFC_{ij} \times nFC_{uv}$, so that we tested all possible pairs of edges.

In general, we found that neither model 1 nor model 2 could fully reproduce eFC. Model 1 performed particularly poorly ($r = 0.21$). The results of model 2 were more varied. When all nodes were represented in the interaction term, e.g. $nFC_{ij} \times nFC_{uv}$, the model performed well ($r = 0.72 \pm 0.05$), consistent with what we reported in Figure 2c. When any node is repeated, e.g. $nFC_{ij} \times nFC_{iv}$, the model performed poorly ($r = 0.06 \pm 0.04$).

Collectively, these observations suggest that eFC is not well approximated using linear combinations of nFC, but with non-linear transformations and inclusion of interaction terms, nFC

can approximate eFC. However, these transformations are unintuitive and the approximation still

fails to fully explain variance in eFC.

CHAPTER 4: EDGY BRAINS: A REVIEW OF EDGES FOR NETWORK NEUROSCIENCE

Abstract

Network models describe the brain as sets of nodes and edges that represent its distributed organization. So far, nearly all discoveries in network neuroscience have prioritized insights that highlight distinct groupings and specialized functional contributions of the network's nodes. However, between the nodes exists a web of relationships, formed by the network's edges, that crucially document how the nodes relate to each other. Here, we underscore the importance of brain network edges for understanding distributed brain organization. Edges can represent different types of relationships, which can fundamentally alter how we comprehend and analyze a brain network. By focusing on the edges, and the higher-order or dynamic information they can chracterize, we bring attention to how brain organization can be found beyond the nodes.

Introduction

Modern neuroscience has come to appreciate the complexity of the brain's wiring structure and functional dynamics. Increasingly, neuroscientists employ the tools of network science to model the brain as a network, a mathematical representation of data well suited to investigate complex systems (Bullmore and Sporns 2009, Bassett and Sporns 2017). Brain networks can reveal many aspects of brain structure and function, including hierarchical organization (Zamora-Lopez, Zhou et al. 2010), clusters and modules (Betzel, Medaglia et al. 2018), or information flow and communication (Avena-Koenigsberger, Misic et al. 2018). Approaching the brain as a network, a connectome (Sporns, Tononi et al. 2005) composed of distinct elements and their interrelationships, naturally integrates local and global perspectives, linking the roles of individual

network elements to distributed function. In essence, networks map neuronal architecture from neurons, neural populations, and large-scale regions, to their mutual relationships (Park and Friston 2013).

There are many ways to map and represent connectomes. For a select few "model" organisms the micro-scale, single neuron networks of the compete nervous system have been meticulously documented via electron microscopy (White, Southgate et al. 1986, Ryan, Lu et al. 2016). Other approaches, using techniques that afford less spatial resolution while offering broader coverage, have yielded meso and macroscale connectomes across many species, including humans. For example, noninvasive imaging allows the brain to be represented as a network of inferred paths of axonal tracts through the white matter (Hagmann, Cammoun et al. 2008), of morphometric similarity between parts of the cortex (Alexander-Bloch, Raznahan et al. 2013, Seidlitz, Vasa et al. 2018), or of functional correlation of intrinsic hemodynamic fluctuations across time (Biswal, Mennes et al. 2010, Gratton, Laumann et al. 2018). Brain networks provide a common modeling framework enabling comparisons across data modality, scale, and species.

The nodes are generally taken to represent distinct neural elements, such as neurons, neural populations, or regions, and the edges record the relationships between these elements. Fundamentally, these two parts of the network model are inseparable. Nodes would not connect without edges, and edges would be nonsensical without nodes. Yet, when applied to the brain, networks are often used as a vehicle to describe and differentiate the nodes. Key concepts are hubs or "important nodes", which integrate information, or dense clusters or coherent communities of nodes, that serve specialized functional roles. Furthermore, we obtain distributions of measures like clustering or participation coefficient, to associate with certain traits or characteristics. Less heralded are the edges, which provide crucial information to make these nodal network

assessments. The focus on the nodal characteristics extends prevailing trends in the long history of brain mapping, which has been dominated by the search for localized neural elements that relate to specific functions (Raichle 2009).

Even though edges are half of the network model, many issues concerning the brain's interrelationships have so far been underappreciated. The edges of the brain, and the topology they collectively form, are the information that elevate static maps of the brain, into wiring diagrams capable of supporting the functional dynamics of the system (Sporns 2012). Here we shine a spotlight on brain network edges, surveying the ways in which information located between the nodes can be used to understand brain network organization. We begin by clarifying that the type of edge, supported by underlying neural data, is consequential for the downstream network analyses. Then, we review the various constructs that edges can jointly form, which are useful because they can capture relationships that extend beyond pairwise interactions. We cover the importance of edges for studying brain communication and briefly review ways in which communication dynamics evolve over time at the edge level. Finally, we look to the future, at a few new developments for interpreting information at the edge level. Overall, we endeavor to bring attention to the importance of brain network edges, and to demonstrate the value in carefully considering the information that can be resolved at the edges.

Network Primer

Network definition and construction

Networks offer a universal language to describe complex systems with many interacting parts. The basic ingredients for any network are its nodes and edges. The set of N nodes describes the discrete units of a system, whereas the E edges express the relationships that can be measured

between the nodes. While the definition of networks as sets of nodes and edges is universal, which real-world constructs are taken to be nodes and which as edges depends on assumptions and interpretations that guide the construction of the network model (Butts 2009). Depending on the system being modeled, edges may be binary or may carry a weight. Weights may be both positive and negative, and they may express directed or undirected relations. In many real-world networks, like a social network, the subway map, or a power grid, these basic network ingredients are generally well-defined and accessible to data collection. In contrast, defining the nodes and edges of a brain network is less straightforward.

Aside from the micro-scale, where it could be argued that nodes and edges can unambiguously be represented as neurons and synaptic contacts, representing brain data as a network requires choosing from a range of reasonable node definitions and picking a valid metric for their interrelationships. As such, it has been demonstrated that definition of nodes and nodal parcellations can significantly influence the results of downstream network analyses (Wang, Wang et al. 2009, Zalesky, Fornito et al. 2010, Arslan, Ktena et al. 2018, Messe 2020). Edge definition is just as consequential. Neuroscientists can choose from a wide range of instruments and techniques to collect neural data. These choices determine how the constructed network model relates to the brain (Bassett, Zurn et al. 2018). Focusing on the brain's interrelationships, we can broadly classify edges as documenting connectivity or similarity between the brain's nodes.

Connectivity

Edges of connectivity quantify the notion of a material linkage or contact, supporting flow, spread, or communication. Depending on data modality, connectivity can be resolved from the micro- (White, Southgate et al. 1986) to the macroscale (Hagmann, Cammoun et al. 2008), providing varying levels of evidence of a true connection at each scale. At the microscale, edges

represent biophysically effective connections such as a synapse or gap junction, resolved with techniques such as electron microscopy or through light-microscopic labeling and imaging (Motta, Berning et al. 2019). At increasing scales, neural data can document coarser patterns of connectivity, which traverse the brain's white matter. For example, tract tracing can resolve distant interregional synaptic connectivity (Markov, Ercsey-Ravasz et al. 2014, Gamanut, Kennedy et al. 2018). By informatically collating the literature of tract tracing experiments, ordinal edges of connection evidence can be formed (Kotter 2004, Bota, Sporns et al. 2015). At the scale of millimeters, bundles of topographically organized axonal paths through the white matter, commonly referred to as tracts, can be estimated via tractography (Jbabdi, Sotiropoulos et al. 2015) and can serve to quantify connectivity (Sotiropoulos and Zalesky 2019, Yeh, Jones et al. 2020). Common to these edge definitions is a notion of anatomical substrate enabling between-node communication. Using functional data, the effective connectivity can be estimated, via methods that establish statistical or model-based causality between the dynamic nodal signals (Valdes-Sosa, Roebroeck et al. 2011, Reid, Headley et al. 2019). Ultimately, edges of connectivity document the potential for one node to influence another, made possible by estimated anatomical linkage.

Similarity

Edges of similarity quantify the association between features relating to nodes. Computing the statistical similarity (or distance) between each pair of nodal feature sets forms a dense similarity matrix, which may be interpreted as a network. Notably, the feature sets at each node can reflect datapoints collected across space or time, which modulates the interpretation of such edges. Using imaging or histological observations, neuroanatomical features can be sampled at each node, including for example cortical thickness (Carmon, Heege et al. 2020), layer intensity profile (Paquola, Vos De Wael et al. 2019), or a collection of morphometric features (Seidlitz,

Vasa et al. 2018). These features can then be statistically compared to create edges that represent the similarity of feature sets. The strength of such anatomical similarity edges could point to shared developmental or genetic influence (Alexander-Bloch, Giedd et al. 2013). Structural similarity between regions, which can reflect cytoarchitectonic similarity, is thought to relate to underlying connectivity (Goulas, Majka et al. 2019). Another similarity-based approach quantifies the correlated gene expression between areas of cortex (Richiardi, Altmann et al. 2015), made possible by extensive brain atlases documenting genetic profiles in stereotaxic space (Ng, Bernard et al. 2009, Hawrylycz, Lein et al. 2012). Edges based on correlated gene expression from a set of genes known to be enriched in supra-granular cortex align with canonical system organization (Krienen, Yeo et al. 2016) and show an increased association with edges of structural covariance (Romero-Garcia, Whitaker et al. 2018). The informatic collation of functional activation experiments provides across-study evidence that certain region pairs co-activate more readily than others, forming meta-analytic co-activation edges (Crossley, Mechelli et al. 2013).

Extracting timeseries at neural elements and comparing the similarity of these sequential feature sets is a widely employed approach to interrogate brain organization. Neural activity can be recorded across a range of resolutions and frequencies, and in turn, can serve as the basis of many types of bivariate similarity calculations (Smith, Miller et al. 2011, see also Basti, Nili et al. 2020). Neural recordings with high temporal precision, such as electrical potentials or magnetic fields (Hari and Puce 2017), provide data allowing the resolution of directed, non-linear, and/or information theoretic edge weights (Astolfi, Cincotti et al. 2007, Ince, Giordano et al. 2017). Brain signals recorded a lower temporal resolution, such as the bold oxygen level dependent (BOLD) signal or Ca^{2+} recordings, can be compared using Pearson correlation or wavelet coherence. Such edges have been referred to as functional connectivity, but this nomenclature has recently become

controversial given the lack of causal evidence that correlation provides (c.f. Reid, Headley et al. 2019). A looming question in the realm of time series comparison is that of the dynamics of such relationships, and if these edges represent stationary relationships (Lurie, Kessler et al. 2020). Relatedly, the similarity of dynamics could be influenced by cognitive state, raising the question whether the recorded edge represents a trait or state measurement (Geerligs, Rubinov et al. 2015). Dynamics at each node can also be used to collect large feature sets of time series properties (Fulcher and Jones 2017), which can be used to compare temporal profile similarity (Shafiei, Markello et al. 2020); an edge measure that is distinct from correlation and well-suited to study dynamical hierarchies (Ito, Hearne et al. 2020).

Measurements of attributes that annotate existing edges can also be taken between neural elements. Whereas edges of similarity and connectivity provide a quantification of the relationship between two nodes, already-existing edges can be associated with metrics representing additional features, possibly from another modality. This approach allows for network edges to carry annotated layers of data derived from sources not directly related to the network construction process. Attributes such as Euclidean distance (Cherniak 1994), connection cost (Kaiser and Hilgetag 2006), or indices of myelination status (Mancini, Giulietti et al. 2018, Boshkovski, Kocarev et al. 2020) are all examples of attributes that can be ascribed to already existing edges.

Edgy network analysis

Once a brain network is constructed, common practice is to use the tools of network science and graph theory to describe the organizational patterns of the data (Rubinov and Sporns 2010). In many instances, network analyses are used to obtain information per node, asking questions like: Which nodes are highly connected? Or how can these nodes be meaningfully grouped? Such approaches use information rendered at the node level to differentiate parts of the network.

Often underappreciated are network analyses that result in information at the edge level. Paths that are taken on the network, such as a shortest path or random walk, can be analyzed based on the sequence of edges the path traverses. For example, the edge betweenness centrality describes the percentage of shortest paths that take a specific node. Paths can also be classified based on the type of edges traversed, such as edges within the putative rich-club, to form path motifs (van den Heuvel, Kahn et al. 2012). Other types of network paths, such as random walks or biased random walks, can be used to estimate the potential for communication between nodes, annotating each edge with a valuation of this potential (Goni, van den Heuvel et al. 2014, Seguin, Tian et al. 2020). Edge measures can also be obtained by removing select edges and measuring the effect on global network statistics (de Reus, Saenger et al. 2014, Ardesch, Scholtens et al. 2019). This "edge-lesioning" approach can be applied to a range of common network measures, even if they produce measurements per node like clustering coefficient, since the global effect of edge removal is assessed.

Network science also offers approaches to represent a *network of edges*, to focus on how the edges relate to each other. One approach is to construct a line graph which documents how edges share nodes. Whereas a traditional network documents adjacency, or how nodes are linked via edges, a line graph documents incidence, or how edges are linked via common nodes (Evans and Lambiotte 2009). For the line graph network representation, the nodes consist of edges from the original network. In practice, the line graph has matrix dimensions of *E*-by-*E*, where *E* is the number of unique edges of the original network. A notable property of line graphs is that high degree nodes in the original network become dense cliques in the line graph. Apart from line graphs, the similarity of edge connection patterns can be obtained using a Jaccard index applied to edge connection patterns (Ahn, Bagrow et al. 2010). This also results in a *E*-by-*E* matrix.

143

Clustering link similarity matrices, or any E-by-E matrix, results in overlapping community structure at the level of nodes, where each node is affiliated with the communities assigned to its emanating edges. Clustering an E-by-E line graph of the brain reveals bilateral spatially coherent link communities, with differential connectivity scores per community, and community overlap that converged on nodes that are traditionally considered hubs (de Reus, Saenger et al. 2014).

Some edgy brain network considerations

Not all edges in the brain are alike. Accordingly, information about how an edge was constructed and the underlying relationship that the edge is intended to represent affects how the network should be analyzed. Take for example path-based measurements applied to brain networks. Paths over structural edges are intuitive, given that the path could represent hypothetical signal propagation over a physical substrate (Misic, Betzel et al. 2015, Avena-Koenigsberger, Mišić et al. 2017). For each path, its constituent edges and edge weights should reflect the cost of communication between nodes, such as distance, capacity, volume, or bandwidth. Often this is not the case, with structural edges commonly representing the magnitude of connectivity (i.e., large values are more connected). Therefore, prior to path analysis, such edge weights, like those estimated from tract-tracing or tractography, should be transformed with a logarithmic or inverse function to convert large weights into short distances.

Paths over functional edges that denote the statistical similarity of time series are less intuitive than paths over edges of connectivity. What does a path over functional similarity measurements mean? One interpretation is that structural and functional edge weights are indeed positively associated (Honey, Sporns et al. 2009), so that paths over functional similarities are likely associated with underlying connectivity. However, given that measures such as Pearson's correlation can be confounded by direct and indirect sources of variance in a networked setting

(Zalesky, Fornito et al. 2012, Sanchez-Romero and Cole 2021), this interpretation could be considered too charitable. Another approach for using functional edges to construct paths is to study the transient routes that appear along the underlying structural graph (Griffa, Ricaud et al. 2017). Network paths and their derived measures should be interpreted differently based on edge type, as they likely capture different organizational features of a brain network.

Another instance in which the edge definition influences network analysis is the case of surrogate data modeling, when an empirical network measurement needs to be compared to hypothetical, yet plausible, network topologies. Null or generative models should be able to create surrogate data that recapitulates certain network characteristics, but with a different pattern of edges (Vertes, Alexander-Bloch et al. 2012, Betzel, Avena-Koenigsberger et al. 2016, Faskowitz and Sporns 2020). Such null models are important, for example, for community detection. Within the modularity maximization formulation is a term for the expected number of connections under a null model. Commonly, the default option operates with the assumption that edges can be swapped, preserving the node degree (Maslov and Sneppen 2002, Betzel 2020). However, for brain networks constructed from statistical comparisons, there exist more suitable null models that account for signed edges (Rubinov and Sporns 2011, Almog, Buijink et al. 2019), or additionally, spatial information (Esfahlani, Bertolero et al. 2020). Even for structural networks, the degree-preserving null model will alter the distribution of edges distances (Betzel, Medaglia et al. 2017). In applications of community detection and beyond, null models that account for the physical distance distribution of edges are a more accurate model of the brain, which is a spatially embedded network (Bassett, Greenfield et al. 2010, Roberts, Perry et al. 2016, Gollo, Roberts et al. 2018). Surrogate data that does not account for the distance distribution of edges will be less efficiently embedded, with longer connections than expected. Network science offers a range of null and

generative models which neuroscientists can choose from or modify, to better align with edge definition.

Many observable real-world networks are sparse, in that relatively few edges exist out of all the possible pairwise node combinations (Barabási 2016). Estimates of connectivity between nodes is also observed to be sparse, a likely evolutionary outcome of wiring constraints (Bullmore and Sporns 2012, Bassett and Bullmore 2017). However, similarity assessments can be made between each pair of nodes, resulting in fully dense networks that are often also signed. Fully dense (and signed) networks present practical and conceptual challenges for network tools like community detection or shortest path estimation. Some practitioners may opt to selectively remove edges below a certain threshold to achieve a certain sparsity (Garrison, Scheinost et al. 2015, Fallani, Latora et al. 2017), across-group consensus (van den Heuvel, de Lange et al. 2017, Betzel, Griffa et al. 2019) or to retain a network feature such as a connected component or minimum spanning tree (Tewarie, van Dellen et al. 2015, Nicolini, Forcellini et al. 2020). Thresholding can induce biases and confounds (Zalesky, Fornito et al. 2012, Cantwell, Liu et al. 2020) in the overall network topology and therefore must be performed with justification. Applying a thresholding reflects a practitioner's determination that certain edges should not be part of a network's topology. Minimally, if a threshold is employed, the effect of thresholds with similar magnitude on the main findings should be understood. Given that methods to estimate connectivity or similarity are subject to noise (Yamashita, Yahata et al. 2019, Rheault, Poulin et al. 2020), the removal of some edges is within reason. Alternatively, a network model that incorporates noisy edges or imperfect graph observation could a fruitful future direction for network neuroscientists (Newman 2018, Young, Cantwell et al. 2020).

Networks are a universal phenomenon, and generally, the algorithms we apply to networks to uncover clustered, community, or scale-free organization are data agnostic. This means that network measures like the clustering coefficient are easy to compute on a power grid, a brain network, or any other sort of network in hand with a minimal set of assumptions (fulfilling the requirements of a *simple graph*, a network without self-loops and hyperedges). However, while it is possible to run the gambit of network tools on brain data, doing so without considering the neural data source and its relationship to the edges is unwise. As covered here, there are many ways to define interrelationships in the brain, and these different edge definitions possibly necessitate different analytic approaches. Therefore, incorporation of domain-specific neuroscience expertise—knowledge about the neural data source, and an understanding of how a network measure relates to the brain organization being modeled—is a key factor for studying brain networks.

Edgy Constructs: From Motifs to Higher-Order Relations

Edges on their own report a straightforward relational quantity. These quantities can be treated as independent features, to be associated with traits and behaviors through mass univariate testing, in what is sometimes referred to as a bag-of-edges approach or brain-wide association (Marek, Tervo-Clemmens et al. 2020, Chung, Bridgeford et al. 2021). However, edges may also be grouped together to form richer constructs that capture distributed patterns of brain organization. Small groups of edges form constructs that can be analyzed as building blocks or primitives of the complete network (Navlakha, Bar-Joseph et al. 2018). Mass univariate methods could fail to uncover these higher-order relationships, and even prove to be underpowered (Zalesky, Fornito et al. 2010), because they focus on edges as independent entities. Here we

147

describe edge-based constructs moving from more localized patterns such as motifs or connectivity fingerprints to more global patterns of brain network topology.

Motifs

Network motifs are subgraphs with a fixed number of nodes and differentiated by the pattern of edges falling between these nodes. For example, between three connected nodes, there are 13 topologically unique ways that edges (directed and unweighted) can be placed, forming 13 motifs. The frequency of that each motif's expression tells us about the network's local building blocks (Song, Sjostrom et al. 2005, Sporns, Honey et al. 2007, Dechery and MacLean 2018). Motif frequencies are assessed using surrogate networks, to gauge the under- or over-expression of certain motifs (Horvat, Gamanut et al. 2016) or can be related to principal dimensions of network organization (Morgan, Achard et al. 2018). The edge configurations of specific motifs logically constrain the possibility for dynamics (Sporns and Kotter 2004). For example, motif configurations containing bi-directional connections, termed resonance pairs, can induce zero-lag synchrony in a variety of neuronal spiking models (Gollo, Mirasso et al. 2014). Taken together, we see that even a pattern of just three edges can be informative for investigating how the wider network might support functional activity.

Fingerprints

In most brain networks, the pattern of edges attached to each node is unique to individual brain regions. These edge patterns, known as connectional fingerprints, were proposed as fundamental structural profiles that shape the functional specialization of a given region (Passingham, Stephan et al. 2002, Mars, Passingham et al. 2018). This concept was originally illustrated with radial plots of connectivity magnitudes with various regions, making it clear that

brain areas, even in the same circuit, can be differentially connected to the rest of the brain. The fingerprinting approach can help to clarify the functional roles regions might play, based on their differential weights to other areas (Tang, Jbabdi et al. 2019, Voets, Jones et al. 2019) or even be used to predict functional activation patterns (Osher, Saxe et al. 2016, Saygin, Osher et al. 2016). A key concept of the fingerprinting approach is the embedding of areas within an abstract connectivity space, as opposed to a geometric space, through which to understand where brain activity occurs (Mars, Passingham et al. 2018). The connectivity space can be used, in conjunction with common structures, to help identify homologies between species (Mars, Sotiropoulos et al. 2018, Balsters, Zerbi et al. 2020). Furthermore, this connectivity space can be used to demarcate distinct areas, in a procedure known as connectivity-based parcellation (Behrens, Johansen-Berg et al. 2003).

From a network perspective, a connectivity fingerprint is a row or column of the adjacency matrix which records a vector of edge weights attached to each node. Relatedly, this row of edge weights is a discrete analogue of traditional seed-based connectivity. Whereas seed-based approaches focus on maps, connectivity fingerprinting utilizes sets of edges. The similarity of edge patterns can be measured using the normalized matching index (Zamora-Lopez, Zhou et al. 2010, Fornito, Zalesky et al. 2016) or cosine similarity (Song, Kennedy et al. 2014, Betzel and Bassett 2018), to gauge connectional homophily between nodes, which is a critical ingredient for generative models of brain networks (Betzel, Avena-Koenigsberger et al. 2016, Goulas, Betzel et al. 2019). Ultimately, the pattern of edges emanating from each node describe the context of the node given the larger network architecture. The connectivity fingerprinting approach demonstrates the utility at assessing a pattern of connections to each node, rather than looking at one or two eminent connections.

Community structure

Although network communities are often interpreted from a node-perspective—defined as coherent groupings of nodes—it is the edges that inform which nodes should be grouped together, whether by strength of connection (Sporns and Betzel 2016) or by similarity of edge connectivity patterns (Moyer, Gutman et al. 2015, Betzel, Medaglia et al. 2018, Faskowitz, Yan et al. 2018). Given an established or inferred community structure, the edges that fall between communities are used to characterize the integrative hub-like roles of select nodes. For example, edge information is used to identify nodes whose edges are highly dispersed amongst functional areas (Bertolero, Yeo et al. 2015) or to classify hub areas associated with different cognitive domains (Gordon, Lynch et al. 2018). Furthermore, the community structure can be used to reduce the network to its block structure, by recording the summed or averaged edge strength between communities. This block structure can be used to characterize meso-scale between-community connection patterns, such as modular, core-periphery, or disassortative configurations (Betzel, Medaglia et al. 2018, Faskowitz and Sporns 2020).

Higher-order relationships

Thus far, we have reviewed the ways groups of edges form constructs that can be used to probe the organization of a brain network. Groups of edges can capture patterns beyond the pairwise relationship reported by a single edge. Another avenue for uncovering such patterns is to employ the tools of algebraic topology (Patania, Vaccarino et al. 2017, Battiston, Cencetti et al. 2020), which provides a formal mathematical framework for analyzing the higher-order relational content of a network using concepts such as cliques and cavities (Sizemore, Phillips-Cremins et al. 2019). Applied to brain data, such tools can show how all-to-all components of a network can

serve to localize hub-like roles that some brain areas might play (Sizemore, Giusti et al. 2018) or help to elucidate spiking activity progression in large neuronal microcircuit simulations (Reimann, Nolte et al. 2017, Nolte, Gal et al. 2020). An advantage of these approaches is the ability to describe how components of the ordinary network of pairwise relationships take part in higher-order mesoscale organization, observable by applying mathematical reformulations like filtrations. Such exercises can highlight the increase in integrative organization under psilocybin by identifying edges that support topological cycles (Petri, Expert et al. 2014). Algebraic topology also offers new ways to draw relationships between nodes based on clustering in a low-dimensional embedding space (Patania, Selvaggi et al. 2019).

Networks can capture organizational information at many scales. In particular, we see that the relational content of a network extends beyond simple edge relationships. That is not to say that the study of a single relationship in isolation is invalid. Whereas a single edge is merely a single datum, there are ways to extract rich information describing the relationships between neural elements outside of a network context. For example, psychophysiological interaction analysis (O'Reilly, Woolrich et al. 2012) allows for the functional coactivation of regions to assessed during specific tasks and the structural relationships between areas can be annotated with sequential measurements of white matter integrity (Chandio, Risacher et al. 2020).

From a network perspective, edges are the raw datapoints of the topology. Without edges, a network would merely be a set of nodes with no relational content. All network assessments, even the ones that produce node-wise measurements like clustering coefficient, need edge data. Evidently, edges are trivially important for network analysis. Here, we have highlighted the further utility of edge grouping to understand levels or organization in brain networks. The features that form from groups of edges, from motifs to fingerprints to cliques can capture local relationships

that implicate certain functional capabilities or can place nodes within a global connectivity context.

Edges in Communication and Brain Dynamics

The history of neuroscience provides us with vast cumulative knowledge about the localization of structural and functional features across the cortex and subcortex, from the micro to the macro scale, resulting in comprehensive maps of the brain (Amunts and Zilles 2015, Poldrack and Yarkoni 2016, Eickhoff, Constable et al. 2018). Through extensive brain mapping studies, specific areas can be associated with specialized function, tuned to a behavior or cognitive processes. Such maps document the spatial layout of areas, but not necessarily how these areas interact. The addition of edges to a map provides information about how the elements of a map collectively form an integrative system, supportive of both local and distributed activity (Friston 2002, Sporns, Tononi et al. 2005). Edges are key ingredients for documenting brain communication. They can represent the structural scaffold on which community unfolds or document the ongoing dynamic activity between neural elements (Zamora-Lopez, Zhou et al. 2009, Wang, Chen et al. 2013, Avena-Koenigsberger, Misic et al. 2018). Here we examine the role that edges, and information at the edges, for understanding how the brain forms an integrative communicating system.

Structure-function relationships

A profitable starting point for investigating brain communication is to assess the relationship between structural and functional network organization (Bansal, Nakuci et al. 2018, Suarez, Markello et al. 2020), to observe the extent to which structural edge weights estimated *in vivo* possibly constrain the resultant functional topology. Focusing on edge weights, we can find a

moderate positive association between structure and function at the group level (Honey, Sporns et al. 2009), across node sets (Messe 2020), and even at the individual level (Zimmermann, Griffiths et al. 2018). However, the structure function relationship is more complex than this bivariate comparison, which can also be confounded by transitive correlation issues (Zalesky, Fornito et al. 2012) and biased by distance (Honey, Sporns et al. 2009). Notably, the communication that takes place between regions likely is a mix between direct and indirect routes (Avena-Koenigsberger, Mišić et al. 2017). The implication is that the observed co-activation activity of any one edge is a result of communication from direct connections and a mix of intermediate and global contexts. Thus, it is conceivable that evaluating structure function relationships could be better modeled with by utilizing information beyond the pairwise connectivity. Take for example, the comparison of structural and functional connectivity fingerprint coupling at each node (Vazquez-Rodriguez, Suarez et al. 2019, Baum, Cui et al. 2020), which follow an established hierarchical cortical gradient topography (Margulies, Ghosh et al. 2016). Other sorts of higher order contexts, such as embedding vectors generated from biased random walks of the network (Rosenthal, Váša et al. 2018, Levakov, Faskowitz et al. 2021), can predict the functional topology with greater accuracy and can even make out-of-sample predictions about intelligence and age, based on the information from these embeddings.

As we understand that the structural edges provide a scaffold on which communication takes place, it makes sense that network communication modeling has been taken up by neuroscientists to explain structural function relationships. Many communication models are based on network paths over a topology that is assumed to be efficiently wired, based on metabolic and volumetric constraints (Bullmore and Sporns 2012). Communication models based on paths taken over the structural topology produce edgewise information about the ease of communication

153

between nodes, e.g., diffusion (Abdelnour, Voss et al. 2014), search information (Goni, van den Heuvel et al. 2014), communicability (Seguin, van den Heuvel et al. 2018, Vezquez-Rodriguez, Liu et al. 2020). These values, or combinations thereof, are used to predict (or correlate with) the functional topology. The incorporation of higher order information, or poly-synaptic signaling, not only improves alignment with the empirical functional topology, but also can increase the predictive utility of structural connectivity, allowing for better prediction of broad behavioral dimensions (Seguin, Tian et al. 2020).

Understanding the mapping from structure to function has been scrutinized using frameworks ranging from communication modeling (Avena-Koenigsberger, Misic et al. 2018) to deep learning (Sarwar, Tian et al. 2021) to neural mass modeling (Sanz-Leon, Knock et al. 2015). In this pursuit, we concede that the target goal of mapping to the functional topology, commonly defined by a collection of pairwise correlation or coherence measures, is made more difficult by the fact these pairwise estimates are averaged over time. Time-averaged estimates of functional similarity could be insensitive to important dynamics at the edge level that reflect communication processes. Therein lies a motivation for observing time-resolved functional activity.

Dynamic functional connectivity

We expect that communication between brain regions would ebb and flow over short time scales, reflected in a sequence of correlation or coupling values at each edge. These dynamics could be in response to varying cognitive demands and environmental cues or simply reflect a dynamic repertoire of intrinsic functionality. Recent emphasis has been placed on tracking and quantifying how functional coactivation changes moment-by-moment between nodes, termed dynamic or time-varying functional connectivity (Preti, Bolton et al. 2017, Heitmann and Breakspear 2018, Lurie, Kessler et al. 2020). In practice, time-varying connectivity resolves the

transient relationships between regions, which can signal different internal states that the brain is occupying or passing through (Fukushima, Betzel et al. 2018, Fong, Yoo et al. 2019). These dynamics can even be synchronized by external stimuli (Simony, Honey et al. 2016) or associated with clinical grouping or outcome (Douw, van Dellen et al. 2019, Fiorenzato, Strafella et al. 2019). Circling back to structure-function relationships, it is the case that the structural topology also influences the range of observable dynamic fluctuations that arise (Shen, Hutchison et al. 2015, Zamora-Lopez, Chen et al. 2016, Fukushima and Sporns 2020).

There are two main approaches for studying the time-varying connectivity, using either model-based dynamical systems that simulate the activity of neural populations, or data-driven statistical evaluations that operate on the observed timeseries (Lurie, Kessler et al. 2020). A common data-driven method for rendering dynamic correlation values is by subdividing the empirical timeseries into T overlapping windows. For each window, a correlation matrix is calculated, rendering T values at each edge representing changing co-activity from window to window. Such an approach is subject to key parameter choices, like window length and offset (Shakil, Lee et al. 2016) that can affect the detection of potentially blur sharp or instantaneous periods of synchrony.

Time series at the edges

Recently, a new approach has been proposed that obviates the need for sliding windows, while still recovering a frame-by-frame account of an edge's activity (Faskowitz, Esfahlani et al. 2020, Zamani Esfahlani, Jo et al. 2020). An edge time series is constructed by multiplying the z-scored signals of two nodes, which also happens to be an intermediate step of calculating Pearson's correlation (van Oort, Mennes et al. 2018). These time series track each edge's functional fluctuations at the same temporal resolution as the original signal. Applying this construct to fMRI

time series, we can observe high magnitude "events" of fluctuation activity that can account for a large portion of the time-averaged functional similarity. This finding implies that the time-averaged correlation, which can be thought of as the summary of communication processes over time, could be driven by brief "event"-like activity (Tagliazucchi, Balenzuela et al. 2012, Liu and Duyn 2013, Betzel, Fukushima et al. 2016, Thompson and Fransson 2016). Interestingly, high amplitude frames map to a shared functional organization, and yet, also exhibit deviations to reliably distinguish subjects from each other (Betzel, Cutts et al. 2021). A mathematical necessity of edge time series also shows that at any given frame, the instantaneous co-fluctuation pattern can be broken into two communities (Sporns, Faskowitz et al. 2021). This decomposition has implications for dynamic interplay between stable functional systems, suggesting transient communication patterns overlay across time to form the canonical node-based systems as we know them (Yeo, Krienen et al. 2011).

By recovering temporally resolved time series for each edge, the communication dynamics can be studied with high precision. The simple Pearson correlation "unwrapping" procedures can easily be extended to domains beyond fMRI such as electrophysiological recordings. Such recordings with higher sampling rates could be analyzed with a variant of the edge time series that adds lag terms that could possibly establish directionality of the edge dynamics. In a further extension, at the neuronal level models of spike transmission at the edge (synapse) level can be built (McKenzie, Huszar et al. 2021). Additionally, mutual information can be "unwrapped" into pointwise mutual information (Lizier 2014) that can also record time-resolved edge fluctuations (Martínez-Cancino, Heng et al. 2019). Findings based on edge time series compliments previous map-based approaches (Liu and Duyn 2013), which also focus on the co-fluctuating activity at single frames. There remains much to be explored regarding the networked edge dynamics,

including the ongoing topology these dynamics form (Betzel, Cutts et al. 2021), the cascading dynamics observable at the edge level (Rabuffo, Fousek et al. 2020), as well as the co-fluctuation patterns that might evolve in response to external stimuli (Rosenthal, Sporns et al. 2017).

Future directions

Relationships between edges

The common conceptualization of brain networks follows a familiar formula, which we have reviewed here, with *N* nodes describing the physical neural elements and the *E* edges describing the web of various types of interrelationships between these elements. In this approach, we take the neural elements to be the fundamental units, to be compared in a pairwise manner. An alternative approach would be to take the *edges* as the units to be compared (Ahn, Bagrow et al. 2010), to construct edge-edge matrices that index the similarity between edge information, particularly over time (Bassett, Wymbs et al. 2014, Davison, Schlesinger et al. 2015, see also Iraji, Calhoun et al. 2016, Faskowitz, Esfahlani et al. 2020, Uddin 2020).

Comparing the pairwise temporal co-fluctuation profiles of edges enables the creation of hyperedges, to reveal temporally similar edge bundles that evolved in a task-specific manner (Davison, Schlesinger et al. 2015). These profiles can also serve as the basis of inter-subject dynamic similarity evaluated during a movie watching task, which can flow between integrated and segregated topologies related to stimulus properties (Betzel, Byrge et al. 2020) or serve as the basis to investigate higher-order correlations related to narrative content (Owen, Chang et al. 2019). Comparing edge time series in a pairwise fashion results in an edge functional connectivity (eFC) matrix (Faskowitz, Esfahlani et al. 2020). Clustering this matrix exposes a pervasively overlapping community structure at the node level that not only bridges canonical systems, but

also reveals nested edge-level structure for diverse canonical systems like the control and default mode network (Jo, Esfahlani et al. 2020). Comparing the edges—taking the edges as the fundamental units to interrelate—provides a new perspective through which to interrogate brain organization.

White matter matters

The white matter is the anatomical tissue that, by volume, comprises over half of the human brain. In terms of inter-areal connectivity, the *white matter matters* (Fields 2008). The dogma that the white matter is 'passive wiring' is being challenged by evidence that the myelin plays a role in how action potentials are propagated through the brain, which in turn could affect oscillatory activity in the cortex (Fields, Woo et al. 2015). At a macroscopic level, lesions in the white matter have been linked to specific object-naming deficits, suggesting a role for white matter tracts in semantic knowledge (Fang, Wang et al. 2018, Pestilli 2018). New methods are emerging to uncover functional activation of white matter tracts (Nozais, Forkel et al. 2021), which could serve to further map cognitive phenomena to information flow in these tracts. Furthermore, indices of white matter integrity have long been linked with clinical deficits, suggesting a possible role for white matter in disease models (Karlsgodt 2020, Kochunov, Zavaliangos-Petropulu et al. 2021). Ultimately, the white matter has the potential to shape dynamics and affect cognitive processing.

The brain network model is in part useful because it abstracts the complex physical biology of the brain into a simple mathematical representation. When visualizing networks, often edges are represented as straight lines through space, with thicknesses or transparency that denotes edge strength. However, we should not lose sight that this representation is divergent from the anatomical reality of the brain, which is embedded in space (Bassett, Greenfield et al. 2010), has contains topographically organized white matter connections (Jbabdi, Sotiropoulos et al. 2015).

The relationships indexed by edges could be shaped by physical paths taken through the white matter—paths of a physical substrate occupying space and demanding metabolic resources. Similarity of functional activity could be influenced by activity-dependent myelination (Fields, Woo et al. 2015), or possible ephaptic coupling of sheets of axons within white matter tracts (Sheheitli and Jirsa 2020). Thus, future work along these lines could focus on better understanding how the white matter plays a role in differentially shaping the relational content of brain networks.

Subject-specific edge information

Recent emphasis has been placed on extracting information from fMRI functional connectivity data, to characterize organizational features that robustly associate with a specific trait, like intelligence or attention (Finn, Shen et al. 2015, Rosenberg, Finn et al. 2016, Shen, Finn et al. 2017, Scheinost, Noble et al. 2019). This *connectome predictive modeling* approach involves filtering edges based on statistical criteria (such as correlation with a phenotype) and summing the edge weights for each subject. These sums are then used to create a statistical prediction model, in left-out subject data. The resultant cross-validated model outlines a set of edges important for predicting a desired phenotype. Notably, the networked characteristics of these edges can be analyzed to reveal system-level organization, such as the number of between system edges that participate in a high-attention predictive model (Rosenberg, Finn et al. 2016). This approach demonstrates the potential for mapping brain-behavior correlations at the level of brain edges. It remains to be seen how these predictive models could be extended to utilize edge constructs that capture higher-order relationships, which could be a productive future direction in tandem with the growing interest in applications of algebraic topology to brain network data.

Conclusion

In contrast to brain network nodes, whose definition and differentiation have been the focus of brain mapping studies for years, issues and concepts relating to brain network edges have been underappreciated to date. Here we have reviewed ways in which the edges matter, in terms of construction approaches that influence network analysis or in settings where groups of edges form higher-order relational information available for analysis. Furthermore, edges are a prime candidate through which to explore how communication processes unfold within the brain. Regardless of data modality, across neural data that spans spatial and time scales, we advocate for careful consideration of the information at the edge level. Brain network analyses conducted with regard for edge information not only makes our science better, but also enhance our exploration of the brain's distributed organization.

A greater focus on the information contained at the edges, otherwise known as an edge-centric perspective (de Reus, Saenger et al. 2014, de Reus 2015, Faskowitz, Esfahlani et al. 2020), can potentially stimulate novel exploration of brain organization. However, it is worth mentioning that a focus on edge information does not preclude exploration of networked information as it pertains to nodes. It is not a one or the other choice between what is important. Nodes are an equally important half of the brain network model, and analyses of how the distributed organization converges on certain nodes will remain a fruitful endeavor going forward. Furthermore, both nodes and edges are fundamentally intertwined as the basic ingredients of a network model. Network neuroscience explorations can evidently benefit from both edge-centric and node-centric perspectives.

DISCUSSION

Summary

The four chapters of this thesis highlight the importance of edges for understanding and analyzing brain network organization, particularly in the setting of community detection. The three empirical studies presented (Chapters 1-3) demonstrate how edge information can be used to uncover unconventional community structure—mesoscale organization that deviates from the common modular view of brain network communities. The scholarly review (Chapter 4) covers the many ways in which edges can represent relational information, and how edges, and edge groupings, can be used to uncover different aspects of brain organization. Although this review does not directly address the application of community detection, it does examine the importance of finely considering edge information. To this end, the review provides motivation for why edges should be clustered via community detection methods, especially in an edge-edge relationship framework. Here, we will summarize key takeaways from these chapters and build up to the next section which will provide a definition of the edge-centric approach.

Block models across the lifespan

The study provided in Chapter 1 demonstrates potential advantages of using a block modeling framework to analyze the structure of a network. Unlike modularity maximization, which can only find communities that are densely connected, the stochastic block model can find other sorts of communities, due to an alternative definition of community structure. The main contributions of the chapter are as follows:

- Development of a methodological framework for fitting the WSBM, at the group and individual level; the WSBM consensus community structure generalizes to the cross-sectional data, including the characterization of bilateral organization.

- We demonstrate ways in which the consensus WSBM community structure provides an alternate reference frame for evaluating cross-sectional lifespan regression trends.

In this chapter, we devised a method for fitting the WSBM in a consensus manner, which is illustrated in Figure 2. This method addresses two complications when fitting the block model: that the number of communities must be prespecified; and that community structures are variable across runs. Based on recommendations from the WSBM authors (Aicher, Jacobs et al. 2013, Aicher, Jacobs et al. 2015), the Bayes Factor was used to select the k number of communities on a young-adult consensus matrix. Then, the partitions across multiple fits were integrated using a novel iterative method (Chapter 1, Figure 2d). As a result of these steps, we could identify a *consensus* WSBM community structure to be used to probe the network structure across the life span. Additionally, the inferred parameters of the WSBM were shown to better generate synthetic data (Chapter 1, Figure 4) (using a framework from Betzel, Avena-Koenigsberger et al. (2016)) and the resultant community structure better captured topological bilaterality (Chapter 1, Figure 5).

A key impetus for this project was to understand how our view of lifespan brain changes would differ if using an alternative approach for characterizing brain network communities. Modularity has become the *de facto* standard for brain network community detection, including applications measuring brain changes in human samples (Lim, Han et al. 2015, Baum, Ciric et al. 2017). This approach is not inherently wrong, as modularity is a plausible organizational regime for all sorts of networks, including brain networks (Sporns and Betzel 2016). However, it is a

limited approach with a narrow definition of communities. Using the non-modular community structure of the WSBM inferred on young adults as a reference frame, we measured between-community edge strengths over time (Chapter 1, Figure 6 and 7). The regressions using the WSBM communities consistently resulted in higher cross validated R^2, indicating the creation of communities that are possibly better suited to capture lifespan (development, adulthood, and senescence) processes. It remains to be seen if the WSBM's specific consideration of off-diagonal edge patterns is the reason for these better fitting cross-sectional trends.

The chapter demonstrates that a block model community structure can be used to evaluate cross-sectional structural changes in edge density, as measured by diffusion tractography. Interestingly, the WSBM model, which is sensitive to a range of community structure topologies, identified non-modular as well as modular communities. The study overall offers a demonstration of an alternative community detection approach and shows how the resultant community structure consolidates edge weights in a manner that is slightly different than the analogous modular structure.

Block models of the rat cortex

The study provided in Chapter 2 demonstrates a block modeling approach used to probe for organizational features of a singular canonical matrix. Here, we fit the WSBM to the informatically-collated rat brain, representing connectivity information gathered from hundreds of tract-tracing experiments, and follows a line of studies examining these data (Bota, Sporns et al. 2015, Swanson, Hahn et al. 2017, Swanson, Sporns et al. 2019, Swanson, Hahn et al. 2020). A challenge that this family of studies addresses is the quantification of network organization in one canonical network. Any distributed organization identified on this network cannot be reassessed using a resampling procedure (de Reus, Saenger et al. 2014) nor validated using a held-out sample.

Here, given the context of community detection, we illustrated ways to fit communities repeatedly to show consensus WSBM community structure. The main contributions of the chapter are as follows:

- Using a block modeling framework, we demonstrate that various nodes and edges of a single network can participate in different community motif topologies.

As noted previously, the WSBM has the unique capability of identifying non-modular community configurations, such as core-periphery or disassortative structure. In any one run of community detection, each between-community interaction can be sorted following an analysis proposed in Betzel, Medaglia et al. (2018) (Chapter 2, Figure 5a). Information from each run can then be mapped to the edges that participate in configuration. By averaging across many repetitions of either WSBM inference or modularity maximization, we can get an idea of how likely edges are to engage in different configurations (Chapter 2, Figure 5b). This analysis was taken a step further, by converting these multiple probability values into an entropy at each edge, demonstrating the propensity for edges to participate in many or few configurations (Chapter 2, Figure 6). This analysis shows how the WSBM can be used to uncover a range of topologies, across algorithmic iterations. In one realized community structure, a large-magnitude edge might be contained within an on-diagonal block, whereas in another iteration, this same edge could be off the diagonal, connecting blocks in a core-periphery manner. This finding is only possible due to the flexibility of the WSBM, as the modular model does not show any evidence of non-modular organization (which it is not designed to find). Collectively, this analysis demonstrates that no one community structure is sufficient for describing the mesoscale organization of a brain network. Methods that analyze the structural variability from iteration to iteration, or even across a parameter sweep (Jeub,

164

Sporns et al. 2018, Betzel, Bertolero et al. 2019), capture a more complete view mesoscale organization.

Overlapping functional organization

The study provided in Chapter 3 provides a new method for analyzing functional connectivity through a simple mathematical reframing that exposes time-resolved information. In this study, we show how classic Pearson's correlation can be 'unwrapped' (van Oort, Mennes et al. 2018) by not completing the final summation and division steps of the formula (i.e., the averaging), thus exposing a time series of co-fluctuation magnitudes. We call these sequences of magnitudes *edge time series*. These sequences can then be compared in a pairwise manner, creating a second-order functional connectivity matrix of co-fluctuation similarity, which we call the edge functional connectivity matrix (eFC). We then go on to perform analyses on eFC matrices, which reveal overlapping community structure for functional brain networks. The main contributions of the chapter are as follows:

- Demonstrating how dynamic information can be resolved at a framewise level, using the edge time series approach. These time series can then be compared to form eFC.

- Clustering of the eFC, which indexes the similarity of edges, results in overlapping community structure at the level of nodes. The level of community overlap at the node level can be measured as an entropy, creating a cortex-wide map of overlap extent.

Using edge time series, we can produce a matrix of size edge-by-edge, that can be submitted to analyses, such as community detection. We first demonstrated that the eFC matrix is not merely the same as an analogous FC×FC multiplication (Chapter 3, Figure 2c). We also showed that eFC values generally align with system-level information at the nodes (Chapter 3, Figure 2f). We clustered a group average eFC matrix using simple *k-means* clustering to obtain

communities of edges with similar co-fluctuation patterns. Therefore, at the level of edge-edge relationships, we intended to find modular communities. However, when the resultant edge communities are mapped into node space, they create an unconventional overlapping structure (Chapter 3, Figure 4d-e) in which a node can belong to many communities. The entropy of community affiliations at each node creates a map that indicates high overlap at dorsal attention, somatomotor, and visual nodes (Chapter 3, Figure 5c). We further discovered that high entropy can be explained by a 'banding' pattern evident when the edge communities are mapped to node-by-node space (Chapter 3, Figure 6a; Supplementary Figure 16d-e); indicating how stub edges of high entropy nodes tend to be assigned to many communities, but in a non-diverse manner (Chapter 3, Figure 6b). Finally, these entropy patterns were shown to be modulated by movie data, indicating that overlap is sensitive to the different mesoscale patterns presents between rest and a passive task.

This study lays out a new way in which to recover temporal information at the edges. The first application of this new approach was community detection, which resulted in clusters of edges, as opposed to clusters of nodes. Like previous methods that cluster edges (Ahn, Bagrow et al. 2010, de Reus, Saenger et al. 2014), the edge community structure naturally results in overlap at the node level. Although neuroscientists likely believe that brain regions can be associated with multiple systems (i.e., polyfunctionality), community detection applied to traditional node-by-node functional connectivity rarely captures such overlap (but see Najafi, McMenamin et al. 2016). Collectively, this study shows how new edge information can be used to obtain a non-traditional community structure.

Edges are important

The final chapter of this thesis consists of a scholarly review of brain network edges. Even though nodes and edges are the two fundamental ingredients of a network, in network neuroscience, most attention is paid to the nodes. We surmise this from the type of questions we ask, the network tools we employ, and the papers we write (e.g. Zalesky, Fornito et al. 2010). Therefore, with this review we aim to fill a literature gap by explaining how different edges can be constructed, what types of higher order relationships edges can form, and how edges are important for studying brain communication. In the context of the present thesis, this review establishes the importance of focusing on the edges. Also, this review could stimulate further exploration of edges and the organization they form.

Synthesis of the edge-centric perspective

Edge-centric-ism

What ties the chapters of this thesis together? In the previous section, we have summarized the key contributions of these chapters and quickly covered ways in which the edges proved useful for investigating brain organization. Here we will further explain what we call the edge-centric perspective. All brain network studies implicitly employ *nodes* and *edges* as part of the standard network model. Therefore, we pose the question: What makes a network neuroscience study specifically edge-centric—more so than a normally conducted study? Here, we contend that an edge-centric approach is an investigation into brain network organization that either *reads in* or *writes out* information at the *edge level*. Edge-centric approaches are not employed merely in service of differentiating nodes. Rather, such approaches also promote the exploration of organization of the edges.

167

What makes the SBM approach edge-centric? With the SBM (and WSBM), the interpretation of a community is a group of nodes that have statistically the same connectivity patterns, which is documented by the affinity matrix (Chapter 1, Figure 1). In contrast, for modularity maximization, the interpretation of a community is a group of nodes that is densely intra-connected and sparsely inter-connected. Interestingly, it can be shown that modularity maximization is a special form of the SBM model, but with reduced consideration for the off-diagonal connectivity patterns (Newman 2016). In this special 'modular' SBM, called the planted partition model, the probabilities for on-diagonal and off-diagonal connectivity are described by two values, rather than the k-by-k matrix of values for an SBM. These extra parameters endow the SBM with the ability to capture a variety of mesoscopic patterns (i.e., modular, core-periphery, and disassortative structure) (Young, St-Onge et al. 2018).

As a community detection method, the SBM does indeed parse the nodes into groupings; but the way it does so, which is based on between-community edge probabilities, makes it a more edge-centric approach than modularity maximization. An empirical example of how the SBM detects edge patterns is evidenced by the bilaterality of the WSBM consensus community structure. Notably, tractography has a difficult time rendering inter-hemispheric tracts, due to the compression of directional information at the corpus callosum (Jbabdi and Johansen-Berg 2011), making stronger inter-hemispheric edges rare. The WSBM community structure contains exclusively bilateral communities, whereas the modular partition does not. This is likely because the SBM assigns homotopic regions with similar edge connectivity patterns to the same community.

When commencing the study described in Chapter 1, an initial goal was to see if the WSBM would model between-community patterns that would result in interesting life span trends missed

by the commonly used modular approach. None of the top significant trends identified (Chapter 1, Figure 6) were noted as being non-modular. In fact, our data show that the most significant trend (inverted u-shape) in our structural data is within a modular community (3-3). Thus, even with a model that is flexible to find non-modular organization, we still find modular structure. This was also the case when we applied the WSBM to the rat cortex, as we found evidence that many edges did indeed participate in on-diagonal or assortative configurations (Chapter 2, Figure 5b). Even with methods that use edge information to flexibly model a range of community topologies, evidence for modularity community structure is still widespread.

In Chapter 3, we shift gears to functional data, and outline a method for shifting the analytic focus to the edges. Normally, we gather time series information from discrete nodes from implanted arrays, electrodes on the scalp, or computationally defined volumetric regions of cortex or subcortex. In this chapter, we show how nodal time series can be used to additionally make edge time series, which exposes more information at the edge level. This led to a series of findings, including the overlapping community structure at the node level (Chapter 3, Figure 4d-e), and the characterization of node-level overlap entropy (Chapter 3, Figure 5a). This new community structure challenges aspects of the traditional modular view of brain network communities. For example, in Figure 4 and 5, we show how visual regions, which are commonly partitioned as highly modular communities (Moussa, Steen et al. 2012), are linked with other systems, such as the somatomotor system, via edge community structure. The constructs of edge time series and eFC present many possibilities to characterize edge-centric brain organization, which we will describe in upcoming sections of this thesis.

Both-centric analyses

Overall, through these three empirical studies we show how information at the edges can be read in, or written out, in pursuit of discovering new aspects of brain network organization. This contrasts with the node-centric network analysis, where the main analytic outcome is to differentiate the nodes through maps of network measures such as participation coefficient or clustering coefficient. However, as we see in Chapter 3, in the pursuit of an edge-centric analysis we can also glean information at the node level. In this case, the edge community structure serves as the basis for node-level entropy measures.

An edge centric approach does not exclude nodes, or node-level organization. In fact, node-centric and edge-centric analyses can be conducted concurrently. For example, Betzel and Bassett (2018) investigate the length distributions of weighted edges, to assess the impact of long connections on the shortest-path statistics. They use edge information—the edges' distances and weights—to better understand the connectivity profiles of specific nodes. By removing certain edges and simulating functional covariance on the lesioned matrix, they could show through changes in the participation coefficient, that distant edges are important for functional diversity. Here, we see an example of edge organizational information (the distance "fingerprints") being used to characterize node-level organization (the functional covariance structure). Another brief example of the integration of edge and node-level organization is the analysis of path motifs (van den Heuvel, Kahn et al. 2012), in which nodes are differentiated based on hub-like properties, and the sequences of shortest paths on the network are differentiated based on contact with the specialized nodes along each route. A suggestion for incorporating more edge-centric analyses into traditional network neuroscience studies would be to 'utilize' the edges as a conduit for simulated processes like network paths. Overall, we take the position that network neuroscience has plenty

to gain by expanding the traditional set of analysis tools, which mostly focus on differentiating nodes. In the next section, we will further detail an edge-centric approach that fundamentally 'flips' our perspective on brain networks.

Edges as fundamental units

One of the fundamental tenets of neuroscience is the 'neuron doctrine' (Swanson and Lichtman 2016), simply stated as the notion that individual neurons are the basic anatomical and functional units of the nervous system. The primacy of neurons has left an imprint, pervasive and yet not often made explicit, on most extant studies of brain networks. Most network approaches treat neural elements—neurons, neural populations, or brain regions —as the fundamental units from which brain networks are constructed. The primacy of nodes reflects long-standing research agendas in brain mapping, for example efforts to parcel cortex into cytoarchitectonic or functionally specialized areas (Amunts and Zilles 2015, Glasser, Coalson et al. 2016), as well as fundamental assumptions about brain function as computation carried out primarily in ensembles of neurons or neuronal populations (Mountcastle 1997). Under this view, edges simply relay the outputs of the local computations. From a theoretical perspective, nothing dictates that nodes *must* be taken as the fundamental units, through which to understand brain organization.

Here, we explore the idea of taking the edges as the fundamental units of a brain, to create a new representation where edges are compared in a pairwise manner. By creating an edge-edge representation, we can probe a network of second-order similarities for signs of non-random organization. In Chapter 3 of this thesis, we introduced edge functional connectivity (eFC), which is an edge-by-edge representation of co-fluctuation similarity. In Chapter 4 of this thesis, we briefly covered eFC and related concepts that compare edges in a pairwise manner. Here, we will

further explore the implications of framing the edges as the fundamental units of brain organization.

Overlap and diversity

The eFC construct introduced in Chapter 3 records the similarity of edge activity and takes the form of a square matrix of size edge-by-edge. Our first exploration of eFC organization focused on the mesoscale organization of the eFC matrix, via *k-means* community detection (Chapter 3, Figure 4), to uncover dense clusters that contain similarly co-fluctuating edges. The relationship between these clusters and canonical system-level organization is multifaceted. Edge-edge comparisons within a system are consistently above zero (Chapter 3, Figure 2e-f), providing evidence that eFC conforms to canonical functional systems. However, this finding merely reflects a special case of edge-edge comparisons for edge pairs that fall entirely within a system. We can further ask how the edge community pattern, or profile, of any one node compares to other profiles. Grouping nodal profile similarities by system reveals the heterogeneity of edge-community mixtures within each system (Chapter 3, Figure 6c). What we find is that some canonical systems are more diverse than others, which could be related to the polyfunctionality of higher-order systems, or even an indicator that some systems can be further partitioned into specialized subcomponents (Andrews-Hanna, Reidler et al. 2010, Braga and Buckner 2017, Gordon, Laumann et al. 2020). It remains to be seen how this diversity could also relate to the hierarchical maps that document gradients from unimodal to multimodal cortex (Margulies, Ghosh et al. 2016). Further, we can ask if edge communities emerge from the links between specific systems, or do they span many systems? Initial evidence in both recent work (Jo, Esfahlani et al. 2020) and from Chapter 3 suggests that edge communities create pervasive overlap (Ahn, Bagrow et al. 2010), where each node is associated with many communities. Only in rare instances, such as the edges involving

172

unimodal processing systems (like somatomotor cortex), do we see evidence that nodes of a canonical functional system correspond to less than half of the k edge communities.

Identifiability

An emerging trend for neuroimaging analysis is the discovery of individual-specific features or feature sets, that differentiate one brain from another (Finn, Shen et al. 2015, Byrge and Kennedy 2019). In this line of work, frontoparietal nodes have been recognized as nodes with connectivity patterns that are unique to individual datasets (Finn, Shen et al. 2015, Pena-Gomez, Avena-Koenigsberger et al. 2018). Further work has focused on using dimension reduction techniques to amplify the individual uniqueness, or identifiability, of each dataset (Amico and Goni 2018). So far, these approaches have focused on the organization between the nodes. It could be the case that edge-edge relationships contain identifiable information (Jo, Faskowitz et al. 2020). One argument for using eFC as a substrate for studying identifiability is that the eFC matrix exposes more datapoints per subject (but note, eFC is built from the same input as traditional FC). Thus, with the larger eFC matrix, there could be a greater opportunity for subject-specific features (or features groupings) to be exposed and extracted. An initial study supports the idea that eFC can potentially increase identifiability of fMRI data, and similarly points to frontoparietal (i.e., control network) nodes as areas for unique subject information (Jo, Faskowitz et al. 2020). It remains to be seen if this increase in identifiability is due in part to the increased dimensionality of eFC.

Alternative edge-edge comparisons

The eFC construction as laid out in Chapter 3 compares the similarity of co-fluctuation patterns across time. As reviewed in Chapter 4, time series are merely one type of feature set that

can be compared in a pairwise manner. Different types of edge-by-edge matrices can be constructed if multiple features at each edge can be gathered and compared (Seidlitz, Vasa et al. 2018). One such idea is to collect multiple values per edge, from variable task contexts or differently parameterized tractography algorithms (Zhan, Jahanshad et al. 2015, Petrov, Ivanov et al. 2017, Faskowitz, Tanner et al. 2021). Using multi-task fMRI data (Van Essen, Smith et al. 2013, Salehi, Greene et al. 2020), we can compute the Pearson correlation in different tasks to create a feature set at each edge. Edge-edge comparisons then assess how pairs of edges covary when measured across contexts. Doing this creates an edge-edge measure somewhat analogous to general FC at the node level (Elliott, Knodt et al. 2019). The edge-by-edge representation formed by this approach contains mesoscale organization that share properties with the eFC communities of Chapter 3, such as a single community largely consisting of somatomotor edges and pervasive overlap at the node level. Notably, from this data we can compute the loading of each task onto each community, to observe how some communities appear to consolidate edge magnitudes for specific tasks. Using a more constrained set of tasks (i.e., more nuanced than the HCP task battery), the edge covariance method could help to identify cognitively relevant edge communities.

A considerable next step in the development of analyzing edge-edge organization would be to ascertain the cognitive or behavioral relevance of edge communities. In Chapter 3, we demonstrated how the constitution of edge communities, and in turn, nodal entropy, was modulated during a passive movie watching task (Chapter 3, Figure 7). Although this provides evidence of a changing mesoscale organization, we cannot finely resolve the task relevance of the changes as we averaged over a complex stimulus (*Raiders of the Lost Ark*, Lucasfilm) that could have induced a range of cognitive processes. To uncover edge communities with cognitive/behavioral relevance, we could turn to metanalytic neuroimaging data. In Crossley,

Mechelli et al. (2013), the authors devised a way to create a node-by-node network of metanalytic co-activation from the BrainMap database (Laird, Lancaster et al. 2005). The key to their methodology was to treat peak-activation information as "frames" in a "time series" of experiments (Smith, Fox et al. 2009). The metanalytic network structure was similar to FC in terms of degree distribution and community structure. Furthermore, these communities were differentiated based on edge loadings related to the behavioral domain associated with certain experiments.

Here, we envision the construction of metanalytic eFC and in turn, metanalytic edge communities, using the BrainMap database. In the original Crossley paper, edges were drawn between co-activating nodes via the Jaccard index, marking the propensity for two nodes to be considered *peak coordinates* within the same experiment. To compare the binary co-fluctuation patterns of co-activating pairs of nodes, we can turn to pointwise mutual information (Lizier 2014), which is an 'unwrapping' of mutual information. Comparing pointwise mutual information time series in a pairwise manner would create an edge-by-edge representation of the metanalytic data (meta-eFC). As a first assessment of this new representation, community detection should be applied to this meta-eFC matrix. Doing so would assess whether groups of co-fluctuating edges over a short timescale (the course of an fMRI session) would also co-fluctuate across experiments performed by the collective neuroimaging community. Furthermore, we can breakdown experiments (frames) based on BrainMap's annotation of behavioral domain for each experiment (action, cognition, emotion, perception, and introspection). Behavioral domain subsets of the data could be used to form behavioral specific edge communities or could be used to compute a loading onto already existing edge communities computed with eFC or meta-eFC (as in Faskowitz, Tanner et al. (2021)). Establishing the task-relevance of edge communities is imperative. As soon as edge

communities can be linked with task-relevance, opportunities will arise to study their modulation in different contexts.

More edgy time series

The edge time series introduced in Chapter 3 provide the material for the edge-edge comparisons that constitute eFC. However, edge time series on their own also hold vast potential for future edge-centric studies. The key feature of edge time series is that they represent sequences of co-fluctuation values at each edge, at the same sampling rate of the collected data. This is unlike sliding window FC, which also recovers sequences of correlation values at each edge, but must be parameterized in multiple ways, including window size, taper, and offset (Shakil, Lee et al. 2016). The collection of edge time series from a single functional session exhibits interesting properties that underly traditional FC (which falls out of the time-collapsed average of edge time series).

For example, the topographic pattern of FC can be recapitulated with a select few frames of high co-fluctuation amplitude, suggesting that the traditional FC network topography is driven by transient co-fluctuation "events" (Zamani Esfahlani, Jo et al. 2020). Furthermore, based on the construction of edge time series, any one frame of the scan can be exactly partitioned into two communities (Sporns, Faskowitz et al. 2020). One implication of these bipartitions is that mesoscale organization is the result of transient bipartitions that overlay across time. The bipartitions at the single frame level also bring into question how the presence of imbalanced triangles emerges in the final FC topology (Teixeira, Santos et al. 2017). An open question remains about how the variability at the edge time series level could relate to the dynamic range of the neural system (Uddin 2020). Edge time series are appealing because they open the door to many new dynamic analyses of synchronization and co-fluctuation, without having to compromise temporal resolution of the input signal.

Here we have covered applications primarily involving fMRI. However, the edge time series methodology can be applied or adapted to many other contexts. For example, the mutual information-based edge time series could be applied to spiking data (Varley, Sporns et al. 2020), to characterize neuronal cascading processes (Rabuffo, Fousek et al. 2020). Based on the large and instantaneous nature of cascades, the advantage of employing edge time series might not rely on precise temporal timing; rather, co-fluctuation cascades could be used define a network topology of these events, using the methods of Zamani Esfahlani, Jo et al. (2020). The edge time series construction could also be adapted for application to signals with much higher temporal resolution, like EEG or MEG, and could involve the addition of a lag parameter. Finally, based on the mathematical simplicity of this approach makes it applicable to non-neural contexts, and could be employed with general time series data.

Opportunities for edgy work

It is out hope that the edge-centric ideas expressed in this thesis will be adopted to new context and new data. A key motivation for pursuing the edge-centric perspective and developing methods to assess edge information is that there is potentially more organization at the edge level to uncover. Previously, we briefly reviewed new ways to perform edge-edge comparisons using edge covariance and metanalytic analyses. Here, we briefly highlight a couple more contexts where edge-centric analyses could be fruitful.

Recent focus has been paid to recording brain activity during the presentation of complex stimuli, such as movies or other narrative-based content (Betzel, Byrge et al. 2020, van der Meer, Breakspear et al. 2020, Willems, Nastase et al. 2020, Finn and Bandettini 2021). One motivation for this line of work is the increased ecological validity of the stimulus presentation. However, complex stimuli unfolding over time are also challenging to analyze with traditional neuroimaging

analysis methods. Over the course of a movie, it could be difficult to isolate a block or event that

corresponding to a precise feature of interest to the experimenter. This challenge has led to new

analytical methods such as inter-subject correlation, which can model subject signal and noise, as

well as the shared response across subjects (Nastase, Gazzola et al. 2019). This paradigm has been

employed show that the default-mode network connectivity tracks with intact narrative content,

revealing an active pattern of co-fluctuation for a group of areas typically associated with task

deactivation (Simony, Honey et al. 2016). We believe edge time series could have increased

sensitivity to capture brief moments of inter-subject synchronization at the edge level, without the

need for windows. This feature alone could help to differentiate rapid cognitive processes that

might unfold in stimuli not necessarily designed for scientific inquiry (e.g., blockbuster movies).

Also, the higher sampling rate of edge time series could potentially be better suited for the

incorporation of data from additional modalities, such as eye-tracking or heart-rate monitoring. By

probing which edges transiently co-fluctuate, we could potentially build a better understanding of

brain network communication in response to varied cognitive processes.

To this point, applications of edge-centric approaches have been discussed here implicitly

in terms of understanding healthy or normative functioning. A large focus of neuroimaging

research is on the extraction of features that pertain to pathology or maladaptive functioning. We

think that the edge-centric methodologies describe in this thesis could also be employed in clinical

research settings. To begin, modularity has been employed as an organizational regime that is

disrupted in diseases such as schizophrenia (Bordier, Nicolini et al. 2018, Gollo, Roberts et al.

2018). We have shown in this thesis that the SBM approach captures both modular and non-

modular topological organization. If a consensus WSBM were to be applied to data from

schizophrenia patients, would the off-diagonal community interactions recapitulate the modular

disruption evidenced previously? Additionally, would a block models inferred from control brains make for better generative models than analogously trained models from clinical cohort brains (Zhang, Braun et al. 2021)? The dynamics of disease brains could also be an area of interest for differentiating clinical from control cohorts. Using edge time series, dynamic features of diseased brains can be assessed. However, in its current state, the dynamic functional connectivity literature is crowded with findings of differences in dynamic features (e.g., states, transition times) under task-free conditions. Perhaps a more profitable approach would be to employ edge time series to trace instantaneous changes in the presence of rich, complex stimuli, as mentioned in the previous paragraph.

Conclusion

The current thesis has reviewed the importance of edges for understanding the distributed organization of the brain—what we call the edge-centric perspective. Additionally, this perspective has allowed for the characterization of novel mesoscale organization, revealed through alternative community detection techniques. Brain networks are inherently constructed of nodes and edges. Yet the edges figure less prominently than the nodes when analyzing and assessing brain organization. Perhaps this is because the edges are sometimes harder to mentally grasp and visualize. Edges represent the physical connections tangled up within white matter topography. Edges also represent mathematical notions of co-activation or co-fluctuation or co-variance. Edges can take many forms and can form complex higher order relationships. In this way, it can be hard to grasp what an edge is, particularly because edges can be so many things. However, we see this as an opportunity. Edges provide abundant fodder for sustained exploration of brain network organization, *and beyond*.

REFERENCES

Abdelnour, F., H. U. Voss and A. Raj (2014). "Network diffusion accurately models the relationship between structural and functional brain connectivity networks." Neuroimage **90**: 335-347. https://doi.org/10.1016/j.neuroimage.2013.12.039

Abraham, A., F. Pedregosa, M. Eickenberg, P. Gervais, A. Mueller, J. Kossaifi, . . . G. Varoquaux (2014). "Machine learning for neuroimaging with scikit-learn." Front Neuroinform **8**: 14. https://doi.org/10.3389/fninf.2014.00014

Achard, S. and E. Bullmore (2007). "Efficiency and cost of economical brain functional networks." PLoS Comput Biol **3**(2): e17. https://doi.org/10.1371/journal.pcbi.0030017

Aggarwal, C. C., A. Hinneburg and D. A. Keim (2001). On the Surprising Behavior of Distance Metrics in High Dimensional Space. Database Theory — ICDT 2001. J. Van den Bussche and V. Vianu. Berlin, Heidelberg, Springer Berlin Heidelberg**:** 420-434. https://doi.org/10.1007/3-540-44503-x_27

Ahn, Y. Y., J. P. Bagrow and S. Lehmann (2010). "Link communities reveal multiscale complexity in networks." Nature **466**(7307): 761-764. https://doi.org/10.1038/nature09182

Aicher, C., A. Z. Jacobs and A. Clauset (2013). "Adapting the stochastic block model to edge-weighted networks." arXiv preprint arXiv:1305.5782.

Aicher, C., A. Z. Jacobs and A. Clauset (2015). "Learning latent block structure in weighted networks." Journal of Complex Networks **3**(2): 221-248. https://doi.org/10.1093/comnet/cnu026

Airoldi, E. M., D. M. Blei, S. E. Fienberg and E. P. Xing (2008). "Mixed Membership Stochastic Blockmodels." J Mach Learn Res **9**(Sep): 1981-2014.

Akiki, T. J. and C. G. Abdallah (2019). "Determining the hierarchical architecture of the human brain using subject-level clustering of functional networks." BioRxiv: 350462.

Alavash, M., S. Tune and J. Obleser (2019). "Modular reconfiguration of an auditory control brain network supports adaptive listening behavior." Proc Natl Acad Sci U S A **116**(2): 660-669. https://doi.org/10.1073/pnas.1815321116

Alexander-Bloch, A., J. N. Giedd and E. Bullmore (2013). "Imaging structural co-variance between human brain regions." Nature Reviews Neuroscience **14**(5): 322-336. https://doi.org/10.1038/nrn3465

Alexander-Bloch, A., R. Lambiotte, B. Roberts, J. Giedd, N. Gogtay and E. Bullmore (2012). "The discovery of population differences in network community structure: new methods

and applications to brain functional networks in schizophrenia." Neuroimage **59**(4): 3889-3900. https://doi.org/10.1016/j.neuroimage.2011.11.035

Alexander-Bloch, A., A. Raznahan, E. Bullmore and J. Giedd (2013). "The convergence of maturational change and structural covariance in human cortical networks." J Neurosci **33**(7): 2889-2899. https://doi.org/10.1523/JNEUROSCI.3554-12.2013

Alexander-Bloch, A. F., H. Shou, S. Liu, T. D. Satterthwaite, D. C. Glahn, R. T. Shinohara, . . . A. Raznahan (2018). "On testing for spatial correspondence between maps of human brain structure and function." Neuroimage **178**: 540-551. https://doi.org/10.1016/j.neuroimage.2018.05.070

Almog, A., M. R. Buijink, O. Roethler, S. Michel, J. H. Meijer, J. H. T. Rohling and D. Garlaschelli (2019). "Uncovering functional signature in neural systems via random matrix theory." PLoS Comput Biol **15**(5): e1006934. https://doi.org/10.1371/journal.pcbi.1006934

Amico, E. and J. Goni (2018). "The quest for identifiability in human functional connectomes." Sci Rep **8**(1): 8254. https://doi.org/10.1038/s41598-018-25089-1

Amunts, K. and K. Zilles (2015). "Architectonic Mapping of the Human Brain beyond Brodmann." Neuron **88**(6): 1086-1107. https://doi.org/10.1016/j.neuron.2015.12.001

Anderson, M. L., J. Kinnison and L. Pessoa (2013). "Describing functional diversity of brain regions and brain networks." Neuroimage **73**: 50-58. https://doi.org/10.1016/j.neuroimage.2013.01.071

Andrews-Hanna, J. R., J. S. Reidler, J. Sepulcre, R. Poulin and R. L. Buckner (2010). "Functional-anatomic fractionation of the brain's default network." Neuron **65**(4): 550-562.

Ardesch, D. J., L. H. Scholtens, L. Li, T. M. Preuss, J. K. Rilling and M. P. van den Heuvel (2019). "Evolutionary expansion of connectivity between multimodal association areas in the human brain compared with chimpanzees." Proceedings of the National Academy of Sciences **116**(14): 7101-7106. https://doi.org/10.1073/pnas.1818512116

Arnatkeviciute, A., B. D. Fulcher, R. Pocock and A. Fornito (2018). "Hub connectivity, neuronal diversity, and gene expression in the Caenorhabditis elegans connectome." PLoS Comput Biol **14**(2): e1005989. https://doi.org/10.1371/journal.pcbi.1005989

Arslan, S., S. I. Ktena, A. Makropoulos, E. C. Robinson, D. Rueckert and S. Parisot (2018). "Human brain mapping: A systematic comparison of parcellation methods for the human cerebral cortex." Neuroimage **170**: 5-30. https://doi.org/10.1016/j.neuroimage.2017.04.014

Astolfi, L., F. Cincotti, D. Mattia, M. G. Marciani, L. A. Baccala, F. de Vico Fallani, . . . F. Babiloni (2007). "Comparison of different cortical connectivity estimators for high-resolution EEG recordings." Hum Brain Mapp **28**(2): 143-157. https://doi.org/10.1002/hbm.20263

Avants, B. B., C. L. Epstein, M. Grossman and J. C. Gee (2008). "Symmetric diffeomorphic image registration with cross-correlation: evaluating automated labeling of elderly and neurodegenerative brain." Med Image Anal **12**(1): 26-41. https://doi.org/10.1016/j.media.2007.06.004

Avants, B. B., N. J. Tustison, G. Song, P. A. Cook, A. Klein and J. C. Gee (2011). "A reproducible evaluation of ANTs similarity metric performance in brain image registration." Neuroimage **54**(3): 2033-2044. https://doi.org/10.1016/j.neuroimage.2010.09.025

Avena-Koenigsberger, A., B. Mišić, R. X. Hawkins, A. Griffa, P. Hagmann, J. Goñi and O. Sporns (2017). "Path ensembles and a tradeoff between communication efficiency and resilience in the human connectome." Brain Structure and Function **222**(1): 603-618. https://doi.org/10.1007/s00429-016-1238-5

Avena-Koenigsberger, A., B. Misic and O. Sporns (2018). "Communication dynamics in complex brain networks." Nature Reviews Neuroscience **19**(1): 17. https://doi.org/10.1038/nrn.2017.149

Baldassano, C., U. Hasson and K. A. Norman (2018). "Representation of Real-World Event Schemas during Narrative Perception." J Neurosci **38**(45): 9689-9699. https://doi.org/10.1523/JNEUROSCI.0251-18.2018

Balsters, J. H., V. Zerbi, J. Sallet, N. Wenderoth and R. B. Mars (2020). "Primate homologs of mouse cortico-striatal circuits." Elife **9**: e53680. https://doi.org/10.7554/eLife.53680

Bandettini, P. A. (2020). Fmri.

Bansal, K., J. Nakuci and S. F. Muldoon (2018). "Personalized brain network models for assessing structure-function relationships." Curr Opin Neurobiol **52**: 42-47. https://doi.org/10.1016/j.conb.2018.04.014

Barabási, A.-L. (2016). Network science, Cambridge university press.

Barabasi, A. L. (2009). "Scale-free networks: a decade and beyond." Science **325**(5939): 412-413. https://doi.org/10.1126/science.1173299

Bassett, D. S. and E. T. Bullmore (2017). "Small-World Brain Networks Revisited." Neuroscientist **23**(5): 499-516. https://doi.org/10.1177/1073858416667720

Bassett, D. S., D. L. Greenfield, A. Meyer-Lindenberg, D. R. Weinberger, S. W. Moore and E. T. Bullmore (2010). "Efficient physical embedding of topologically complex information processing networks in brains and computer circuits." PLoS Comput Biol **6**(4): e1000748. https://doi.org/10.1371/journal.pcbi.1000748

Bassett, D. S. and O. Sporns (2017). "Network neuroscience." Nat Neurosci **20**(3): 353-364. https://doi.org/10.1038/nn.4502

Bassett, D. S., N. F. Wymbs, M. A. Porter, P. J. Mucha, J. M. Carlson and S. T. Grafton (2011). "Dynamic reconfiguration of human brain networks during learning." Proc Natl Acad Sci U S A **108**(18): 7641-7646. https://doi.org/10.1073/pnas.1018985108

Bassett, D. S., N. F. Wymbs, M. A. Porter, P. J. Mucha and S. T. Grafton (2014). "Cross-linked structure of network evolution." Chaos **24**(1): 013112. https://doi.org/10.1063/1.4858457

Bassett, D. S., P. Zurn and J. I. Gold (2018). "On the nature and use of models in network neuroscience." Nature Reviews Neuroscience **19**(9): 566-578. https://doi.org/10.1038/s41583-018-0038-8

Basti, A., H. Nili, O. Hauk, L. Marzetti and R. N. Henson (2020). "Multi-dimensional connectivity: a conceptual and mathematical review." Neuroimage **221**: 117179. https://doi.org/10.1016/j.neuroimage.2020.117179

Battiston, F., G. Cencetti, I. Iacopini, V. Latora, M. Lucas, A. Patania, . . . G. Petri (2020). "Networks beyond pairwise interactions: structure and dynamics." Physics Reports. https://doi.org/10.1016/j.physrep.2020.05.004

Battiston, F., J. Guillon, M. Chavez, V. Latora and F. De Vico Fallani (2018). "Multiplex core-periphery organization of the human connectome." J R Soc Interface **15**(146): 20180514. https://doi.org/10.1098/rsif.2018.0514

Baum, G. L., R. Ciric, D. R. Roalf, R. F. Betzel, T. M. Moore, R. T. Shinohara, . . . T. D. Satterthwaite (2017). "Modular Segregation of Structural Brain Networks Supports the Development of Executive Function in Youth." Curr Biol **27**(11): 1561-1572 e1568. https://doi.org/10.1016/j.cub.2017.04.051

Baum, G. L., Z. Cui, D. R. Roalf, R. Ciric, R. F. Betzel, B. Larsen, . . . T. D. Satterthwaite (2020). "Development of structure-function coupling in human brain networks during youth." Proc Natl Acad Sci U S A **117**(1): 771-778. https://doi.org/10.1073/pnas.1912034117

Bazzi, M., M. A. Porter, S. Williams, M. McDonald, D. J. Fenn and S. D. Howison (2016). "Community detection in temporal multilayer networks, with an application to correlation networks." Multiscale Modeling & Simulation **14**(1): 1-41. https://doi.org/10.1137/15M1009615

Behrens, T. E. J., H. Johansen-Berg, M. W. Woolrich, S. M. Smith, C. A. M. Wheeler-Kingshott, P. A. Boulby, . . . P. M. Matthews (2003). "Non-invasive mapping of connections between human thalamus and cortex using diffusion imaging." Nat Neurosci **6**(7): 750-757. https://doi.org/10.1038/nn1075

Bertolero, M. A., B. T. Yeo and M. D'Esposito (2015). "The modular and integrative functional architecture of the human brain." Proc Natl Acad Sci U S A **112**(49): E6798-6807. https://doi.org/10.1073/pnas.1510619112

Bertolero, M. A., B. T. T. Yeo, D. S. Bassett and M. D'Esposito (2018). "A mechanistic model of connector hubs, modularity and cognition." Nat Hum Behav **2**(10): 765-777. https://doi.org/10.1038/s41562-018-0420-6

Betzel, R., S. Cutts, S. Greenwell and O. Sporns (2021). "Individualized event structure drives individual differences in whole-brain functional connectivity." bioRxiv. https://doi.org/10.1101/2021.03.12.435168

Betzel, R. F. (2020). "Community detection in network neuroscience." arXiv preprint arXiv:2011.06723.

Betzel, R. F., A. Avena-Koenigsberger, J. Goni, Y. He, M. A. de Reus, A. Griffa, . . . O. Sporns (2016). "Generative models of the human connectome." Neuroimage **124**(Pt A): 1054-1064. https://doi.org/10.1016/j.neuroimage.2015.09.041

Betzel, R. F. and D. S. Bassett (2017). "Multi-scale brain networks." Neuroimage **160**: 73-83. https://doi.org/10.1016/j.neuroimage.2016.11.006

Betzel, R. F. and D. S. Bassett (2018). "Specificity and robustness of long-distance connections in weighted, interareal connectomes." Proc Natl Acad Sci U S A **115**(21): E4880-E4889. https://doi.org/10.1073/pnas.1720186115

Betzel, R. F., M. A. Bertolero, E. M. Gordon, C. Gratton, N. U. F. Dosenbach and D. S. Bassett (2019). "The community structure of functional brain networks exhibits scale-specific patterns of inter- and intra-subject variability." Neuroimage **202**: 115990. https://doi.org/10.1016/j.neuroimage.2019.07.003

Betzel, R. F., L. Byrge, F. Z. Esfahlani and D. P. Kennedy (2020). "Temporal fluctuations in the brain's modular architecture during movie-watching." Neuroimage **213**: 116687. https://doi.org/10.1016/j.neuroimage.2020.116687

Betzel, R. F., L. Byrge, Y. He, J. Goni, X. N. Zuo and O. Sporns (2014). "Changes in structural and functional connectivity among resting-state networks across the human lifespan." Neuroimage **102 Pt 2**: 345-357. https://doi.org/10.1016/j.neuroimage.2014.07.067

Betzel, R. F., M. Fukushima, Y. He, X. N. Zuo and O. Sporns (2016). "Dynamic fluctuations coincide with periods of high and low modularity in resting-state functional brain networks." Neuroimage **127**: 287-297. https://doi.org/10.1016/j.neuroimage.2015.12.001

Betzel, R. F., A. Griffa, P. Hagmann and B. Misic (2019). "Distance-dependent consensus thresholds for generating group-representative structural brain networks." Netw Neurosci **3**(2): 475-496. https://doi.org/10.1162/netn_a_00075

Betzel, R. F., J. D. Medaglia and D. S. Bassett (2018). "Diversity of meso-scale architecture in human and non-human connectomes." Nat Commun **9**(1): 346. https://doi.org/10.1038/s41467-017-02681-z

Betzel, R. F., J. D. Medaglia, L. Papadopoulos, G. L. Baum, R. Gur, R. Gur, . . . D. S. Bassett (2017). "The modular organization of human anatomical brain networks: Accounting for the cost of wiring." Network Neuroscience **1**(1): 42-68. https://doi.org/10.1162/NETN_a_00002

Biswal, B., F. Zerrin Yetkin, V. M. Haughton and J. S. Hyde (1995). "Functional connectivity in the motor cortex of resting human brain using echo-planar MRI." Magnetic resonance in medicine **34**(4): 537-541. https://doi.org/10.1002/mrm.1910340409

Biswal, B. B., M. Mennes, X. N. Zuo, S. Gohel, C. Kelly, S. M. Smith, . . . M. P. Milham (2010). "Toward discovery science of human brain function." Proc Natl Acad Sci U S A **107**(10): 4734-4739. https://doi.org/10.1073/pnas.0911855107

Blondel, V. D., J.-L. Guillaume, R. Lambiotte and E. Lefebvre (2008). "Fast unfolding of communities in large networks." Journal of statistical mechanics: theory and experiment **2008**(10): P10008.

Blondel, V. D., J.-L. Guillaume, R. Lambiotte, E. J. J. o. s. m. t. Lefebvre and experiment (2008). "Fast unfolding of communities in large networks." **2008**(10): P10008.

Bordier, C., C. Nicolini, G. Forcellini and A. Bifone (2018). "Disrupted modular organization of primary sensory brain areas in schizophrenia." NeuroImage: Clinical **18**: 682-693.

Boshkovski, T., L. Kocarev, J. Cohen-Adad, B. Mišić, S. Lehéricy, N. Stikov and M. Mancini (2020). "The R1-weighted connectome: complementing brain networks with a myelin-sensitive measure." Network Neuroscience(Just Accepted): 1-34. https://doi.org/10.1162/netn_a_00179

Bota, M., O. Sporns and L. W. Swanson (2015). "Architecture of the cerebral cortical association connectome underlying cognition." Proc Natl Acad Sci U S A **112**(16): E2093-2101. https://doi.org/10.1073/pnas.1504394112

Bota, M. and L. W. Swanson (2007). "Online workbenches for neural network connections." J Comp Neurol **500**(5): 807-814. https://doi.org/10.1002/cne.21209

Braga, R. M. and R. L. Buckner (2017). "Parallel interdigitated distributed networks within the individual estimated by intrinsic functional connectivity." Neuron **95**(2): 457-471. e455.

Brett, M., I. S. Johnsrude and A. M. Owen (2002). "The problem of functional localization in the human brain." Nat Rev Neurosci **3**(3): 243-249. https://doi.org/10.1038/nrn756

Bryant, C., H. Zhu, M. Ahn and J. Ibrahim (2017). "LCN: a random graph mixture model for community detection in functional brain networks." Stat Interface **10**(3): 369-378. https://doi.org/10.4310/SII.2017.v10.n3.a1

Buckner, R. L., P. A. Bandettini, K. M. O'Craven, R. L. Savoy, S. E. Petersen, M. E. Raichle and B. R. Rosen (1996). "Detection of cortical activation during averaged single trials of a cognitive task using functional magnetic resonance imaging." Proceedings of the National Academy of Sciences **93**(25): 14878-14883.

Bullmore, E. and O. Sporns (2009). "Complex brain networks: graph theoretical analysis of structural and functional systems." Nat Rev Neurosci **10**(3): 186-198. https://doi.org/10.1038/nrn2575

Bullmore, E. and O. Sporns (2012). "The economy of brain network organization." Nat Rev Neurosci **13**(5): 336-349. https://doi.org/10.1038/nrn3214

Bullock, D., H. Takemura, C. F. Caiafa, L. Kitchell, B. McPherson, B. Caron and F. Pestilli (2019). "Associative white matter connecting the dorsal and ventral posterior human cortex." Brain structure and Function **224**(8): 2631-2660. https://doi.org/10.1007/s00429-019-01907-8

Butts, C. T. (2009). "Revisiting the foundations of network analysis." Science **325**(5939): 414-416. https://doi.org/10.1126/science.1171022

Byrge, L. and D. P. Kennedy (2019). "High-accuracy individual identification using a "thin slice" of the functional connectome." Network Neuroscience **3**(2): 363-383.

Cantwell, G. T., Y. Liu, B. F. Maier, A. C. Schwarze, C. A. Servan, J. Snyder and G. St-Onge (2020). "Thresholding normally distributed data creates complex networks." Phys Rev E **101**(6-1): 062302. https://doi.org/10.1103/PhysRevE.101.062302

Cao, M., J. H. Wang, Z. J. Dai, X. Y. Cao, L. L. Jiang, F. M. Fan, . . . Y. He (2014). "Topological organization of the human brain functional connectome across the lifespan." Dev Cogn Neurosci **7**: 76-93. https://doi.org/10.1016/j.dcn.2013.11.004

Carmon, J., J. Heege, J. H. Necus, T. W. Owen, G. Pipa, M. Kaiser, . . . Y. Wang (2020). "Reliability and comparability of human brain structural covariance networks." Neuroimage **220**: 117104. https://doi.org/10.1016/j.neuroimage.2020.117104

Catani, M., M. T. de Schotten, D. Slater and F. Dell'Acqua (2013). "Connectomic approaches before the connectome." Neuroimage **80**: 2-13. https://doi.org/10.1016/j.neuroimage.2013.05.109

Catani, M. (2017). "A little man of some importance." Brain **140**(11): 3055-3061. https://doi.org/10.1093/brain/awx270

Chan, M. Y., D. C. Park, N. K. Savalia, S. E. Petersen and G. S. Wig (2014). "Decreased segregation of brain systems across the healthy adult lifespan." Proc Natl Acad Sci U S A **111**(46): E4997-5006. https://doi.org/10.1073/pnas.1415122111

Chandio, B. Q., S. L. Risacher, F. Pestilli, D. Bullock, F. C. Yeh, S. Koudoro, . . . E. Garyfallidis (2020). "Bundle analytics, a computational framework for investigating the shapes and profiles of brain pathways across populations." Sci Rep **10**(1): 17149. https://doi.org/10.1038/s41598-020-74054-4

Chen, M., T. Nguyen and B. K. Szymanski (2013). On measuring the quality of a network community structure. 2013 International Conference on Social Computing, IEEE. https://doi.org/10.1109/SocialCom.2013.25

Chen, Z. J., Y. He, P. Rosa-Neto, J. Germann and A. C. Evans (2008). "Revealing modular architecture of human brain structural networks by using cortical thickness from MRI." Cerebral cortex **18**(10): 2374-2381. https://doi.org/10.1093/cercor/bhn003

Cherniak, C. (1994). "Component placement optimization in the brain." J Neurosci **14**(4): 2418-2427.

Chung, J., E. Bridgeford, J. Arroyo, B. D. Pedigo, A. Saad-Eldin, V. Gopalakrishnan, . . . J. T. Vogelstein (2021). "Statistical Connectomics." Annual Review of Statistics and Its Application **8**: 463-492. https://doi.org/10.1146/annurev-statistics-042720-023234

Cole, M. W., T. Ito, D. Schultz, R. Mill, R. Chen and C. Cocuzza (2019). "Task activations produce spurious but systematic inflation of task functional connectivity estimates." Neuroimage **189**: 1-18. https://doi.org/10.1016/j.neuroimage.2018.12.054

Collin, G., E. Turk and M. P. van den Heuvel (2016). "Connectomics in Schizophrenia: From Early Pioneers to Recent Brain Network Findings." Biol Psychiatry Cogn Neurosci Neuroimaging **1**(3): 199-208. https://doi.org/10.1016/j.bpsc.2016.01.002

Contreras, J. A., A. Avena-Koenigsberger, S. L. Risacher, J. D. West, E. Tallman, B. C. McDonald, . . . M. Dzemidzic (2019). "Resting state network modularity along the prodromal late onset Alzheimer's disease continuum." NeuroImage: Clinical: 101687.

Conturo, T. E., N. F. Lori, T. S. Cull, E. Akbudak, A. Z. Snyder, J. S. Shimony, . . . M. E. Raichle (1999). "Tracking neuronal fiber pathways in the living human brain." Proc Natl Acad Sci U S A **96**(18): 10422-10427. https://doi.org/10.1073/pnas.96.18.10422

Cook, S. J., T. A. Jarrell, C. A. Brittin, Y. Wang, A. E. Bloniarz, M. A. Yakovlev, . . . J. S. Duerr (2019). "Whole-animal connectomes of both Caenorhabditis elegans sexes." <u>Nature</u> **571**(7763): 63-71. https://doi.org/10.1038/s41586-019-1352-7

Crossley, N. A., A. Mechelli, P. E. Vertes, T. T. Winton-Brown, A. X. Patel, C. E. Ginestet, . . . E. T. Bullmore (2013). "Cognitive relevance of the community structure of the human brain functional coactivation network." <u>Proc Natl Acad Sci U S A</u> **110**(28): 11583-11588. https://doi.org/10.1073/pnas.1220826110

Dale, A. M., B. Fischl and M. I. Sereno (1999). "Cortical surface-based analysis. I. Segmentation and surface reconstruction." <u>Neuroimage</u> **9**(2): 179-194. https://doi.org/10.1006/nimg.1998.0395

Dann, B., J. A. Michaels, S. Schaffelhofer and H. Scherberger (2016). "Uniting functional network topology and oscillations in the fronto-parietal single unit network of behaving primates." <u>Elife</u> **5**: e15719. https://doi.org/10.7554/eLife.15719

Davison, E. N., K. J. Schlesinger, D. S. Bassett, M. E. Lynall, M. B. Miller, S. T. Grafton and J. M. Carlson (2015). "Brain network adaptability across task states." <u>PLoS Comput Biol</u> **11**(1): e1004029. https://doi.org/10.1371/journal.pcbi.1004029

de Reus, M. A. (2015). <u>An eccentric perspective on brain networks</u>, Uitgeverij BOXPress.

de Reus, M. A., V. M. Saenger, R. S. Kahn and M. P. van den Heuvel (2014). "An edge-centric perspective on the human connectome: link communities in the brain." <u>Philos Trans R Soc Lond B Biol Sci</u> **369**(1653): 20130527. https://doi.org/10.1098/rstb.2013.0527

Dechery, J. B. and J. N. MacLean (2018). "Functional triplet motifs underlie accurate predictions of single-trial responses in populations of tuned and untuned V1 neurons." <u>PLoS Comput Biol</u> **14**(5): e1006153. https://doi.org/10.1371/journal.pcbi.1006153

Desikan, R. S., F. Ségonne, B. Fischl, B. T. Quinn, B. C. Dickerson, D. Blacker, . . . B. T. Hyman (2006). "An automated labeling system for subdividing the human cerebral cortex on MRI scans into gyral based regions of interest." <u>Neuroimage</u> **31**(3): 968-980. https://doi.org/10.1016/j.neuroimage.2006.01.021

Douw, L., E. van Dellen, A. A. Gouw, A. Griffa, W. de Haan, M. van den Heuvel, . . . C. J. Stam (2019). "The road ahead in clinical network neuroscience." <u>Netw Neurosci</u> **3**(4): 969-993. https://doi.org/10.1162/netn_a_00103

Dunne, J. A., R. J. Williams and N. D. Martinez (2002). "Network structure and biodiversity loss in food webs: robustness increases with connectance." <u>Ecology letters</u> **5**(4): 558-567. https://doi.org/10.1046/j.1461-0248.2002.00354.x

Eickhoff, S. B., R. T. Constable and B. T. T. Yeo (2018). "Topographic organization of the cerebral cortex and brain cartography." Neuroimage **170**: 332-347. https://doi.org/10.1016/j.neuroimage.2017.02.018

Elliott, M. L., A. R. Knodt, M. Cooke, M. J. Kim, T. R. Melzer, R. Keenan, . . . A. R. Hariri (2019). "General functional connectivity: Shared features of resting-state and task fMRI drive reliable and heritable individual differences in functional brain networks." Neuroimage **189**: 516-532. https://doi.org/10.1016/j.neuroimage.2019.01.068

Engel, S. A., G. H. Glover and B. A. Wandell (1997). "Retinotopic organization in human visual cortex and the spatial precision of functional MRI." Cereb Cortex **7**(2): 181-192. https://doi.org/10.1093/cercor/7.2.181

Esfahlani, F. Z., M. A. Bertolero, D. S. Bassett and R. F. Betzel (2020). "Space-independent community and hub structure of functional brain networks." NeuroImage **211**: 116612. https://doi.org/10.1016/j.neuroimage.2020.116612

Esteban, O., D. Birman, M. Schaer, O. O. Koyejo, R. A. Poldrack and K. J. Gorgolewski (2017). "MRIQC: Advancing the automatic prediction of image quality in MRI from unseen sites." PLoS One **12**(9): e0184661. https://doi.org/10.1371/journal.pone.0184661

Esteban, O., C. J. Markiewicz, R. W. Blair, C. A. Moodie, A. I. Isik, A. Erramuzpe, . . . K. J. Gorgolewski (2019). "fMRIPrep: a robust preprocessing pipeline for functional MRI." Nat Methods **16**(1): 111-116. https://doi.org/10.1038/s41592-018-0235-4

Evans, T. S. and R. Lambiotte (2009). "Line graphs, link partitions, and overlapping communities." Phys Rev E Stat Nonlin Soft Matter Phys **80**(1 Pt 2): 016105. https://doi.org/10.1103/PhysRevE.80.016105

Fallani, F. D. V., V. Latora and M. Chavez (2017). "A topological criterion for filtering information in complex brain networks." PLoS computational biology **13**(1): e1005305. https://doi.org/10.1371/journal.pcbi.1005305

Fang, Y., X. Wang, S. Zhong, L. Song, Z. Han, G. Gong and Y. Bi (2018). "Semantic representation in the white matter pathway." PLoS Biol **16**(4): e2003993. https://doi.org/10.1371/journal.pbio.2003993

Faskowitz, J., G. I. de Zubicaray, K. L. McMahon, M. J. Wright, P. M. Thompson and N. Jahanshad (2016). Comparison of template registration methods for multi-site meta-analysis of brain morphometry. Medical Imaging 2016: Biomedical Applications in Molecular, Structural, and Functional Imaging, International Society for Optics and Photonics. https://doi.org/10.1117/12.2217370

Faskowitz, J., F. Z. Esfahlani, Y. Jo, O. Sporns and R. F. Betzel (2020). "Edge-centric functional network representations of human cerebral cortex reveal overlapping system-level

architecture." <u>Nat Neurosci</u> **23**(12): 1644-1654. https://doi.org/10.1038/s41593-020-00719-y

Faskowitz, J. and O. Sporns (2020). "Mapping the community structure of the rat cerebral cortex with weighted stochastic block modeling." <u>Brain Struct Funct</u> **225**(1): 71-84. https://doi.org/10.1007/s00429-019-01984-9

Faskowitz, J., J. Tanner, B. Misic and R. Betzel (2021). "An edge-centric model for harmonizing multi-relational network datasets." <u>bioRxiv</u>. https://doi.org/10.1101/2021.01.07.425450

Faskowitz, J., X. Yan, X.-N. Zuo and O. Sporns (2018). "Weighted Stochastic Block Models of the Human Connectome across the Life Span." <u>Scientific Reports</u> **8**(1): 12997. https://doi.org/10.1038/s41598-018-31202-1

Felleman, D. J. and D. E. Van (1991). "Distributed hierarchical processing in the primate cerebral cortex." <u>Cerebral cortex (New York, NY: 1991)</u> **1**(1): 1-47.

ffytche, D. H. and M. Catani (2005). "Beyond localization: from hodology to function." <u>Philos Trans R Soc Lond B Biol Sci</u> **360**(1456): 767-779. https://doi.org/10.1098/rstb.2005.1621

Fields, R. D. (2008). "White matter matters." <u>Sci Am</u> **298**(3): 42-49.

Fields, R. D., D. H. Woo and P. J. Basser (2015). "Glial regulation of the neuronal connectome through local and long-distant communication." <u>Neuron</u> **86**(2): 374-386. https://doi.org/10.1016/j.neuron.2015.01.014

Finc, K., K. Bonna, X. He, D. M. Lydon-Staley, S. Kühn, W. Duch and D. S. Bassett (2020). "Dynamic reconfiguration of functional brain networks during working memory training." <u>Nature communications</u> **11**(1): 1-15. https://doi.org/10.1038/s41467-020-15631-z

Finn, E. S. and P. A. Bandettini (2021). "Movie-watching outperforms rest for functional connectivity-based prediction of behavior." <u>NeuroImage</u>: 117963.

Finn, E. S., X. Shen, D. Scheinost, M. D. Rosenberg, J. Huang, M. M. Chun, . . . R. T. Constable (2015). "Functional connectome fingerprinting: identifying individuals using patterns of brain connectivity." <u>Nature neuroscience</u> **18**(11): 1664-1671. https://doi.org/10.1038/nn.4135

Fiorenzato, E., A. P. Strafella, J. Kim, R. Schifano, L. Weis, A. Antonini and R. Biundo (2019). "Dynamic functional connectivity changes associated with dementia in Parkinson's disease." <u>Brain</u> **142**(9): 2860-2872. https://doi.org/10.1093/brain/awz192

Fischl, B. (2012). "FreeSurfer." <u>Neuroimage</u> **62**(2): 774-781. https://doi.org/10.1016/j.neuroimage.2012.01.021

Fischl, B., A. van der Kouwe, C. Destrieux, E. Halgren, F. Segonne, D. H. Salat, . . . A. M. Dale (2004). "Automatically parcellating the human cerebral cortex." Cereb Cortex **14**(1): 11-22. https://doi.org/10.1093/cercor/bhg087

Fong, A. H. C., K. Yoo, M. D. Rosenberg, S. Zhang, C. R. Li, D. Scheinost, . . . M. M. Chun (2019). "Dynamic functional connectivity during task performance and rest predicts individual differences in attention across studies." Neuroimage **188**: 14-25. https://doi.org/10.1016/j.neuroimage.2018.11.057

Fonov, V. S., A. C. Evans, R. C. McKinstry, C. Almli and D. Collins (2009). "Unbiased nonlinear average age-appropriate brain templates from birth to adulthood." NeuroImage(47): S102.

Fornito, A., A. Zalesky and E. Bullmore (2016). Fundamentals of brain network analysis, Academic Press.

Fortunato, S. and M. Barthelemy (2007). "Resolution limit in community detection." Proc Natl Acad Sci U S A **104**(1): 36-41. https://doi.org/10.1073/pnas.0605965104

Fortunato, S. and D. Hric (2016). "Community detection in networks: A user guide." Physics reports **659**: 1-44. https://doi.org/10.1016/j.physrep.2016.09.002

Fox, P. T. and J. L. Lancaster (2002). "Opinion: Mapping context and content: the BrainMap model." Nat Rev Neurosci **3**(4): 319-321. https://doi.org/10.1038/nrn789

Friston, K. (2002). "Beyond phrenology: what can neuroimaging tell us about distributed circuitry?" Annual review of neuroscience **25**(1): 221-250. https://doi.org/10.1146/annurev.neuro.25.112701.142846

Friston, K. J. (2011). "Functional and effective connectivity: a review." Brain Connect **1**(1): 13-36. https://doi.org/10.1089/brain.2011.0008

Fruchterman, T. M. J. and E. M. Reingold (1991). "Graph drawing by force-directed placement." Software: Practice and Experience **21**(11): 1129-1164. https://doi.org/10.1002/spe.4380211102

Fukushima, M., R. F. Betzel, Y. He, M. A. de Reus, M. P. van den Heuvel, X.-N. Zuo and O. Sporns (2018). "Fluctuations between high-and low-modularity topology in time-resolved functional connectivity." NeuroImage **180**: 406-416. https://doi.org/10.1016/j.neuroimage.2017.08.044

Fukushima, M. and O. Sporns (2020). "Structural determinants of dynamic fluctuations between segregation and integration on the human connectome." Communications biology **3**(1): 1-11. https://doi.org/10.1038/s42003-020-01331-3

Fulcher, B. D. and N. S. Jones (2017). "hctsa: A computational framework for automated time-series phenotyping using massive feature extraction." Cell systems **5**(5): 527-531. e523. https://doi.org/10.1016/j.cels.2017.10.001

Gamanut, R., H. Kennedy, Z. Toroczkai, M. Ercsey-Ravasz, D. C. Van Essen, K. Knoblauch and A. Burkhalter (2018). "The Mouse Cortical Connectome, Characterized by an Ultra-Dense Cortical Graph, Maintains Specificity by Distinct Connectivity Profiles." Neuron **97**(3): 698-715 e610. https://doi.org/10.1016/j.neuron.2017.12.037

Garrison, K. A., D. Scheinost, E. S. Finn, X. Shen and R. T. Constable (2015). "The (in)stability of functional brain network measures across thresholds." Neuroimage **118**: 651-661. https://doi.org/10.1016/j.neuroimage.2015.05.046

Garyfallidis, E., M. Brett, B. Amirbekian, A. Rokem, S. van der Walt, M. Descoteaux, . . . C. Dipy (2014). "Dipy, a library for the analysis of diffusion MRI data." Front Neuroinform **8**(8): 8. https://doi.org/10.3389/fninf.2014.00008

Geerligs, L., M. Rubinov, C. Cam and R. N. Henson (2015). "State and Trait Components of Functional Connectivity: Individual Differences Vary with Mental State." J Neurosci **35**(41): 13949-13961. https://doi.org/10.1523/JNEUROSCI.1324-15.2015

Gennatas, E. D., B. B. Avants, D. H. Wolf, T. D. Satterthwaite, K. Ruparel, R. Ciric, . . . R. C. Gur (2017). "Age-Related Effects and Sex Differences in Gray Matter Density, Volume, Mass, and Cortical Thickness from Childhood to Young Adulthood." J Neurosci **37**(20): 5065-5073. https://doi.org/10.1523/JNEUROSCI.3550-16.2017

Glasser, M. F., T. S. Coalson, E. C. Robinson, C. D. Hacker, J. Harwell, E. Yacoub, . . . D. C. Van Essen (2016). "A multi-modal parcellation of human cerebral cortex." Nature **536**(7615): 171-178. https://doi.org/10.1038/nature18933

Glasser, M. F., S. N. Sotiropoulos, J. A. Wilson, T. S. Coalson, B. Fischl, J. L. Andersson, . . . W. U.-M. H. Consortium (2013). "The minimal preprocessing pipelines for the Human Connectome Project." Neuroimage **80**: 105-124. https://doi.org/10.1016/j.neuroimage.2013.04.127

Gollo, L. L., C. Mirasso, O. Sporns and M. Breakspear (2014). "Mechanisms of zero-lag synchronization in cortical motifs." PLoS Comput Biol **10**(4): e1003548. https://doi.org/10.1371/journal.pcbi.1003548

Gollo, L. L., J. A. Roberts, V. L. Cropley, M. A. Di Biase, C. Pantelis, A. Zalesky and M. Breakspear (2018). "Fragility and volatility of structural hubs in the human connectome." Nat Neurosci **21**(8): 1107-1116. https://doi.org/10.1038/s41593-018-0188-z

Goni, J., M. P. van den Heuvel, A. Avena-Koenigsberger, N. Velez de Mendizabal, R. F. Betzel, A. Griffa, . . . O. Sporns (2014). "Resting-brain functional connectivity predicted by

analytic measures of network communication." Proc Natl Acad Sci U S A **111**(2): 833-838. https://doi.org/10.1073/pnas.1315529111

Good, B. H., Y. A. de Montjoye and A. Clauset (2010). "Performance of modularity maximization in practical contexts." Phys Rev E Stat Nonlin Soft Matter Phys **81**(4 Pt 2): 046106. https://doi.org/10.1103/PhysRevE.81.046106

Gopalan, P. K. and D. M. Blei (2013). "Efficient discovery of overlapping communities in massive networks." Proc Natl Acad Sci U S A **110**(36): 14534-14539. https://doi.org/10.1073/pnas.1221839110

Gordon, E. M., T. O. Laumann, A. W. Gilmore, D. J. Newbold, D. J. Greene, J. J. Berg, . . . N. U. F. Dosenbach (2017). "Precision Functional Mapping of Individual Human Brains." Neuron **95**(4): 791-807 e797. https://doi.org/10.1016/j.neuron.2017.07.011

Gordon, E. M., T. O. Laumann, S. Marek, R. V. Raut, C. Gratton, D. J. Newbold, . . . S. M. Nelson (2020). "Default-mode network streams for coupling to language and control systems." Proc Natl Acad Sci U S A **117**(29): 17308-17319. https://doi.org/10.1073/pnas.2005238117

Gordon, E. M., C. J. Lynch, C. Gratton, T. O. Laumann, A. W. Gilmore, D. J. Greene, . . . S. M. Nelson (2018). "Three Distinct Sets of Connector Hubs Integrate Human Brain Function." Cell Rep **24**(7): 1687-1695 e1684. https://doi.org/10.1016/j.celrep.2018.07.050

Gorgolewski, K., C. D. Burns, C. Madison, D. Clark, Y. O. Halchenko, M. L. Waskom and S. S. Ghosh (2011). "Nipype: a flexible, lightweight and extensible neuroimaging data processing framework in python." Front Neuroinform **5**: 13. https://doi.org/10.3389/fninf.2011.00013

Goulas, A., R. F. Betzel and C. C. Hilgetag (2019). "Spatiotemporal ontogeny of brain wiring." Sci Adv **5**(6): eaav9694. https://doi.org/10.1126/sciadv.aav9694

Goulas, A., P. Majka, M. G. P. Rosa and C. C. Hilgetag (2019). "A blueprint of mammalian cortical connectomes." PLoS Biol **17**(3): e2005346. https://doi.org/10.1371/journal.pbio.2005346

Goulas, A., K. Zilles and C. C. Hilgetag (2018). "Cortical Gradients and Laminar Projections in Mammals." Trends Neurosci **41**(11): 775-788. https://doi.org/10.1016/j.tins.2018.06.003

Grasby, K. L., N. Jahanshad, J. N. Painter, L. Colodro-Conde, J. Bralten, D. P. Hibar, . . . g. Enhancing NeuroImaging Genetics through Meta-Analysis Consortium -Genetics working (2020). "The genetic architecture of the human cerebral cortex." Science **367**(6484). https://doi.org/10.1126/science.aay6690

Gratton, C., T. O. Laumann, A. N. Nielsen, D. J. Greene, E. M. Gordon, A. W. Gilmore, . . . B. L. Schlaggar (2018). "Functional brain networks are dominated by stable group and individual factors, not cognitive or daily variation." Neuron **98**(2): 439-452. e435. https://doi.org/10.1016/j.neuron.2018.03.035

Greicius, M. D., B. Krasnow, A. L. Reiss and V. Menon (2003). "Functional connectivity in the resting brain: a network analysis of the default mode hypothesis." Proc Natl Acad Sci U S A **100**(1): 253-258. https://doi.org/10.1073/pnas.0135058100

Greve, D. N. and B. Fischl (2009). "Accurate and robust brain image alignment using boundary-based registration." Neuroimage **48**(1): 63-72. https://doi.org/10.1016/j.neuroimage.2009.06.060

Griffa, A., B. Ricaud, K. Benzi, X. Bresson, A. Daducci, P. Vandergheynst, . . . P. Hagmann (2017). "Transient networks of spatio-temporal connectivity map communication pathways in brain functional systems." Neuroimage **155**: 490-502. https://doi.org/10.1016/j.neuroimage.2017.04.015

Guimera, R. and L. A. Nunes Amaral (2005). "Functional cartography of complex metabolic networks." Nature **433**(7028): 895-900. https://doi.org/10.1038/nature03288

Haber, S. N. and B. Knutson (2010). "The reward circuit: linking primate anatomy and human imaging." Neuropsychopharmacology **35**(1): 4-26. https://doi.org/10.1038/npp.2009.129

Hagmann, P., L. Cammoun, X. Gigandet, R. Meuli, C. J. Honey, V. J. Wedeen and O. Sporns (2008). "Mapping the structural core of human cerebral cortex." PLoS Biol **6**(7): e159. https://doi.org/10.1371/journal.pbio.0060159

Hagmann, P., O. Sporns, N. Madan, L. Cammoun, R. Pienaar, V. J. Wedeen, . . . P. E. Grant (2010). "White matter maturation reshapes structural connectivity in the late developing human brain." Proc Natl Acad Sci U S A **107**(44): 19067-19072. https://doi.org/10.1073/pnas.1009073107

Hari, R. and A. Puce (2017). MEG-EEG Primer, Oxford University Press.

Harriger, L., M. P. van den Heuvel and O. Sporns (2012). "Rich club organization of macaque cerebral cortex and its role in network communication." PLoS One **7**(9): e46497. https://doi.org/10.1371/journal.pone.0046497

Hawrylycz, M. J., E. S. Lein, A. L. Guillozet-Bongaarts, E. H. Shen, L. Ng, J. A. Miller, . . . A. R. Jones (2012). "An anatomically comprehensive atlas of the adult human brain transcriptome." Nature **489**(7416): 391-399. https://doi.org/10.1038/nature11405

Haxby, J. V., A. C. Connolly and J. S. Guntupalli (2014). "Decoding neural representational spaces using multivariate pattern analysis." Annual review of neuroscience **37**: 435-456. https://doi.org/10.1146/annurev-neuro-062012-170325

He, Y., S. Lim, S. Fortunato, O. Sporns, L. Zhang, J. Qiu, . . . X. N. Zuo (2018). "Reconfiguration of Cortical Networks in MDD Uncovered by Multiscale Community Detection with fMRI." Cereb Cortex **28**(4): 1383-1395. https://doi.org/10.1093/cercor/bhx335

He, Y., J. Wang, L. Wang, Z. J. Chen, C. Yan, H. Yang, . . . A. C. Evans (2009). "Uncovering intrinsic modular organization of spontaneous brain activity in humans." PLoS One **4**(4): e5226. https://doi.org/10.1371/journal.pone.0005226

Heitmann, S. and M. Breakspear (2018). "Putting the "dynamic" back into dynamic functional connectivity." Network Neuroscience **2**(02): 150-174. https://doi.org/10.1162/netn_a_00041

Hibar, D. P., L. T. Westlye, T. G. van Erp, J. Rasmussen, C. D. Leonardo, J. Faskowitz, . . . O. A. Andreassen (2016). "Subcortical volumetric abnormalities in bipolar disorder." Mol Psychiatry **21**(12): 1710-1716. https://doi.org/10.1038/mp.2015.227

Hilgetag, C. C., S. F. Beul, S. J. van Albada and A. Goulas (2019). "An architectonic type principle integrates macroscopic cortico-cortical connections with intrinsic cortical circuits of the primate brain." Netw Neurosci **3**(4): 905-923. https://doi.org/10.1162/netn_a_00100

Hilgetag, C. C., G. A. Burns, M. A. O'Neill, J. W. Scannell and M. P. Young (2000). "Anatomical connectivity defines the organization of clusters of cortical areas in the macaque monkey and the cat." Philos Trans R Soc Lond B Biol Sci **355**(1393): 91-110. https://doi.org/10.1098/rstb.2000.0551

Holland, P. W., K. B. Laskey and S. Leinhardt (1983). "Stochastic blockmodels: First steps." Social networks **5**(2): 109-137.

Honey, C. J., O. Sporns, L. Cammoun, X. Gigandet, J. P. Thiran, R. Meuli and P. Hagmann (2009). "Predicting human resting-state functional connectivity from structural connectivity." Proc Natl Acad Sci U S A **106**(6): 2035-2040. https://doi.org/10.1073/pnas.0811168106

Horvat, S., R. Gamanut, M. Ercsey-Ravasz, L. Magrou, B. Gamanut, D. C. Van Essen, . . . H. Kennedy (2016). "Spatial Embedding and Wiring Cost Constrain the Functional Layout of the Cortical Network of Rodents and Primates." PLoS Biol **14**(7): e1002512. https://doi.org/10.1371/journal.pbio.1002512

Hric, D., T. P. Peixoto and S. Fortunato (2016). "Network structure, metadata, and the prediction of missing nodes and annotations." Physical Review X **6**(3): 031038. https://doi.org/10.1103/PhysRevX.6.031038

Huang, L., J. M. Kebschull, D. Fürth, S. Musall, M. T. Kaufman, A. K. Churchland and A. M. Zador (2020). "BRICseq bridges brain-wide interregional connectivity to neural activity and gene expression in single animals." Cell **182**(1): 177-188. e127. https://doi.org/10.1016/j.cell.2020.05.029

Hughes, C., B. S. Cassidy, J. Faskowitz, A. Avena-Koenigsberger, O. Sporns and A. C. Krendl (2019). "Age differences in specific neural connections within the default mode network underlie theory of mind." NeuroImage **191**: 269-277. https://doi.org/10.1016/j.neuroimage.2019.02.024

Hughes, C., J. Faskowitz, B. S. Cassidy, O. Sporns and A. C. Krendl (2020). "Aging relates to a disproportionately weaker functional architecture of brain networks during rest and task states." NeuroImage **209**: 116521. https://doi.org/10.1016/j.neuroimage.2020.116521

Huth, A. G., W. A. De Heer, T. L. Griffiths, F. E. Theunissen and J. L. Gallant (2016). "Natural speech reveals the semantic maps that tile human cerebral cortex." Nature **532**(7600): 453-458. https://doi.org/10.1038/nature17637

Huys, Q. J., T. V. Maia and M. J. Frank (2016). "Computational psychiatry as a bridge from neuroscience to clinical applications." Nature neuroscience **19**(3): 404. https://doi.org/10.1038/nn.4238

Imperati, D., S. Colcombe, C. Kelly, A. Di Martino, J. Zhou, F. X. Castellanos and M. P. Milham (2011). "Differential development of human brain white matter tracts." PLoS One **6**(8): e23437. https://doi.org/10.1371/journal.pone.0023437

Ince, R. A., B. L. Giordano, C. Kayser, G. A. Rousselet, J. Gross and P. G. Schyns (2017). "A statistical framework for neuroimaging data analysis based on mutual information estimated via a gaussian copula." Hum Brain Mapp **38**(3): 1541-1573. https://doi.org/10.1002/hbm.23471

Iñiguez, G., F. Battiston and M. Karsai (2020). "Bridging the gap between graphs and networks." Communications Physics **3**(1): 1-5. https://doi.org/10.1038/s42005-020-0359-6

Iraji, A., V. D. Calhoun, N. M. Wiseman, E. Davoodi-Bojd, M. R. Avanaki, E. M. Haacke and Z. Kou (2016). "The connectivity domain: Analyzing resting state fMRI data using feature-based data-driven and model-based methods." Neuroimage **134**: 494-507. https://doi.org/10.1016/j.neuroimage.2016.04.006

Ito, T., L. J. Hearne and M. W. Cole (2020). "A cortical hierarchy of localized and distributed processes revealed via dissociation of task activations, connectivity changes, and intrinsic timescales." Neuroimage **221**: 117141. https://doi.org/10.1016/j.neuroimage.2020.117141

Jahanshad, N., G. Roshchupkin, J. Faskowitz, D. P. Hibar, B. A. Gutman, H. H. Adams, . . . M. P. Zwiers (2018). Multisite Metaanalysis of Image-Wide Genome-Wide Associations

With Morphometry. <u>Imaging Genetics</u>, Elsevier**:** 1-23. https://doi.org/10.1016/B978-0-12-813968-4.00001-8

Jarrell, T. A., Y. Wang, A. E. Bloniarz, C. A. Brittin, M. Xu, J. N. Thomson, . . . S. W. Emmons (2012). "The connectome of a decision-making neural network." <u>Science</u> **337**(6093): 437-444. https://doi.org/10.1126/science.1221762

Jbabdi, S. and H. Johansen-Berg (2011). "Tractography: where do we go from here?" <u>Brain connectivity</u> **1**(3): 169-183. https://doi.org/10.1089/brain.2011.0033

Jbabdi, S., S. N. Sotiropoulos, S. N. Haber, D. C. Van Essen and T. E. Behrens (2015). "Measuring macroscopic brain connections in vivo." <u>Nat Neurosci</u> **18**(11): 1546-1555. https://doi.org/10.1038/nn.4134

Jenkinson, M., P. Bannister, M. Brady and S. Smith (2002). "Improved optimization for the robust and accurate linear registration and motion correction of brain images." <u>Neuroimage</u> **17**(2): 825-841. https://doi.org/10.1016/s1053-8119(02)91132-8

Jenkinson, M., C. F. Beckmann, T. E. Behrens, M. W. Woolrich and S. M. Smith (2012). "Fsl." <u>Neuroimage</u> **62**(2): 782-790. https://doi.org/10.1016/j.neuroimage.2011.09.015

Jeub, L. G., O. Sporns and S. Fortunato (2018). "Multiresolution consensus clustering in networks." <u>Scientific reports</u> **8**(1): 3259. https://doi.org/10.1038/s41598-018-21352-7

Jo, Y., F. Z. Esfahlani, J. Faskowitz, E. Chumin, O. Sporns and R. Betzel (2020). "The diversity and multiplexity of edge communities within and between brain systems." <u>bioRxiv</u>. https://doi.org/10.1101/2020.05.05.067777

Jo, Y., J. Faskowitz, F. Z. Esfahlani, O. Sporns and R. F. Betzel (2020). "Subject identification using edge-centric functional connectivity." <u>bioRxiv</u>. https://doi.org/10.1101/2020.09.13.291898

Kaiser, M. and C. C. Hilgetag (2006). "Nonoptimal component placement, but short processing paths, due to long-distance projections in neural systems." <u>PLoS Comput Biol</u> **2**(7): e95. https://doi.org/10.1371/journal.pcbi.0020095

Karlsgodt, K. H. (2020). "White Matter Microstructure across the Psychosis Spectrum." <u>Trends Neurosci</u> **43**(6): 406-416. https://doi.org/10.1016/j.tins.2020.03.014

Karrer, B. and M. E. Newman (2011). "Stochastic blockmodels and community structure in networks." <u>Phys Rev E Stat Nonlin Soft Matter Phys</u> **83**(1 Pt 2): 016107. https://doi.org/10.1103/PhysRevE.83.016107

Kashtan, N. and U. Alon (2005). "Spontaneous evolution of modularity and network motifs." <u>Proc Natl Acad Sci U S A</u> **102**(39): 13773-13778. https://doi.org/10.1073/pnas.0503610102

Khambhati, A. N., K. A. Davis, B. S. Oommen, S. H. Chen, T. H. Lucas, B. Litt and D. S. Bassett (2015). "Dynamic Network Drivers of Seizure Generation, Propagation and Termination in Human Neocortical Epilepsy." PLoS Comput Biol **11**(12): e1004608. https://doi.org/10.1371/journal.pcbi.1004608

King, M., C. R. Hernandez-Castillo, R. A. Poldrack, R. B. Ivry and J. Diedrichsen (2019). "Functional boundaries in the human cerebellum revealed by a multi-domain task battery." Nat Neurosci **22**(8): 1371-1378. https://doi.org/10.1038/s41593-019-0436-x

Klein, A., S. S. Ghosh, F. S. Bao, J. Giard, Y. Hame, E. Stavsky, . . . A. Keshavan (2017). "Mindboggling morphometry of human brains." PLoS Comput Biol **13**(2): e1005350. https://doi.org/10.1371/journal.pcbi.1005350

Knox, J. E., K. D. Harris, N. Graddis, J. D. Whitesell, H. Zeng, J. A. Harris, . . . S. Mihalas (2019). "High-resolution data-driven model of the mouse connectome." Netw Neurosci **3**(1): 217-236. https://doi.org/10.1162/netn_a_00066

Kochunov, P., A. Zavaliangos-Petropulu, N. Jahanshad, P. M. Thompson, M. C. Ryan, J. Chiappelli, . . . L. E. Hong (2021). "A White Matter Connection of Schizophrenia and Alzheimer's Disease." Schizophr Bull **47**(1): 197-206. https://doi.org/10.1093/schbul/sbaa078

Kotter, R. (2004). "Online retrieval, processing, and visualization of primate connectivity data from the CoCoMac database." Neuroinformatics **2**(2): 127-144. https://doi.org/10.1385/NI:2:2:127

Krienen, F. M., B. T. Yeo, T. Ge, R. L. Buckner and C. C. Sherwood (2016). "Transcriptional profiles of supragranular-enriched genes associate with corticocortical network architecture in the human brain." Proc Natl Acad Sci U S A **113**(4): E469-478. https://doi.org/10.1073/pnas.1510903113

Kurmukov, A., M. Ananyeva, Y. Dodonova, B. Gutman, J. Faskowitz, N. Jahanshad, . . . L. Zhukov (2017). Classifying Phenotypes Based on the Community Structure of Human Brain Networks, Cham, Springer International Publishing. https://doi.org/10.1007/978-3-319-67675-3_1

Kurmukov, A., A. Musabaeva, Y. Denisova, D. Moyer and B. Gutman (2018). Connectivity-Driven Brain Parcellation via Consensus Clustering, Cham, Springer International Publishing. https://doi.org/10.1007/978-3-030-00755-3_13

Kwak, H., Y. Choi, Y.-H. Eom, H. Jeong and S. Moon (2009). Mining communities in networks: a solution for consistency and its evaluation. Proceedings of the 9th ACM SIGCOMM conference on Internet measurement conference, ACM. https://doi.org/10.1145/1644893.1644930

Ladino, L. D., S. Rizvi and J. F. Tellez-Zenteno (2018). "The Montreal procedure: The legacy of the great Wilder Penfield." Epilepsy Behav **83**: 151-161. https://doi.org/10.1016/j.yebeh.2018.04.001

Laird, A. R., J. L. Lancaster and P. T. Fox (2005). "BrainMap: the social evolution of a human brain mapping database." Neuroinformatics **3**(1): 65-78. https://doi.org/10.1385/ni:3:1:065

Lancichinetti, A. and S. Fortunato (2012). "Consensus clustering in complex networks." Sci Rep **2**: 336. https://doi.org/10.1038/srep00336

Laughlin, S. B. and T. J. Sejnowski (2003). "Communication in neuronal networks." Science **301**(5641): 1870-1874. https://doi.org/10.1126/science.1089662

Laumann, T. O., E. M. Gordon, B. Adeyemo, A. Z. Snyder, S. J. Joo, M. Y. Chen, . . . S. E. Petersen (2015). "Functional System and Areal Organization of a Highly Sampled Individual Human Brain." Neuron **87**(3): 657-670. https://doi.org/10.1016/j.neuron.2015.06.037

Lebel, C., M. Gee, R. Camicioli, M. Wieler, W. Martin and C. Beaulieu (2012). "Diffusion tensor imaging of white matter tract evolution over the lifespan." Neuroimage **60**(1): 340-352. https://doi.org/10.1016/j.neuroimage.2011.11.094

Levakov, G., J. Faskowitz, G. Avidan and O. Sporns (2021). "Mapping individual differences across brain network structure to function and behavior with connectome embedding." bioRxiv: 2021.2001.2013.426513. https://doi.org/10.1101/2021.01.13.426513

Lim, S., C. E. Han, P. J. Uhlhaas and M. Kaiser (2015). "Preferential detachment during human brain development: age- and sex-specific structural connectivity in diffusion tensor imaging (DTI) data." Cereb Cortex **25**(6): 1477-1489. https://doi.org/10.1093/cercor/bht333

Lindquist, M. A., S. Geuter, T. D. Wager and B. S. Caffo (2019). "Modular preprocessing pipelines can reintroduce artifacts into fMRI data." Human brain mapping **40**(8): 2358-2376. https://doi.org/10.1002/hbm.24528

Liu, X. and J. H. Duyn (2013). "Time-varying functional network information extracted from brief instances of spontaneous brain activity." Proc Natl Acad Sci U S A **110**(11): 4392-4397. https://doi.org/10.1073/pnas.1216856110

Lizier, J. T. (2014). "JIDT: An information-theoretic toolkit for studying the dynamics of complex systems." Frontiers in Robotics and AI **1**: 11. https://doi.org/10.3389/frobt.2014.00011

Logothetis, N. K., J. Pauls, M. Augath, T. Trinath and A. Oeltermann (2001). "Neurophysiological investigation of the basis of the fMRI signal." Nature **412**(6843): 150-157. https://doi.org/10.1038/35084005

Lurie, D. J., D. Kessler, D. S. Bassett, R. F. Betzel, M. Breakspear, S. Kheilholz, . . . V. D. Calhoun (2020). "Questions and controversies in the study of time-varying functional connectivity in resting fMRI." Netw Neurosci **4**(1): 30-69. https://doi.org/10.1162/netn_a_00116

Mancini, M., G. Giulietti, N. Dowell, B. Spano, N. Harrison, M. Bozzali and M. Cercignani (2018). "Introducing axonal myelination in connectomics: A preliminary analysis of g-ratio distribution in healthy subjects." Neuroimage **182**: 351-359. https://doi.org/10.1016/j.neuroimage.2017.09.018

Marek, S., B. Tervo-Clemmens, F. J. Calabro, D. F. Montez, B. P. Kay, A. S. Hatoum, . . . E. Feczko (2020). "Towards reproducible brain-wide association studies." BioRxiv. https://doi.org/10.1101/2020.08.21.257758

Margulies, D. S., S. S. Ghosh, A. Goulas, M. Falkiewicz, J. M. Huntenburg, G. Langs, . . . J. Smallwood (2016). "Situating the default-mode network along a principal gradient of macroscale cortical organization." Proc Natl Acad Sci U S A **113**(44): 12574-12579. https://doi.org/10.1073/pnas.1608282113

Markov, N. T., M. M. Ercsey-Ravasz, A. R. Ribeiro Gomes, C. Lamy, L. Magrou, J. Vezoli, . . . H. Kennedy (2014). "A weighted and directed interareal connectivity matrix for macaque cerebral cortex." Cereb Cortex **24**(1): 17-36. https://doi.org/10.1093/cercor/bhs270

Mars, R. B., R. E. Passingham and S. Jbabdi (2018). "Connectivity Fingerprints: From Areal Descriptions to Abstract Spaces." Trends Cogn Sci **22**(11): 1026-1037. https://doi.org/10.1016/j.tics.2018.08.009

Mars, R. B., S. N. Sotiropoulos, R. E. Passingham, J. Sallet, L. Verhagen, A. A. Khrapitchev, . . . S. Jbabdi (2018). "Whole brain comparative anatomy using connectivity blueprints." Elife **7**: e35237. https://doi.org/10.7554/eLife.35237

Martínez-Cancino, R., J. Heng, A. Delorme, K. Kreutz-Delgado, R. C. Sotero and S. Makeig (2019). "Measuring transient phase-amplitude coupling using local mutual information." NeuroImage **185**: 361-378. https://doi.org/10.1016/j.neuroimage.2018.10.034

Maslov, S. and K. Sneppen (2002). "Specificity and stability in topology of protein networks." Science **296**(5569): 910-913. https://doi.org/10.1126/science.1065103

McIntosh, A. R. and B. Misic (2013). "Multivariate statistical analyses for neuroimaging data." Annu Rev Psychol **64**: 499-525. https://doi.org/10.1146/annurev-psych-113011-143804

McKenzie, S., R. Huszar, D. F. English, K. Kim, F. Christensen, E. Yoon and G. Buzsaki (2021). "Preexisting hippocampal network dynamics constrain optogenetically induced place fields." Neuron **109**(6): 1040-1054 e1047. https://doi.org/10.1016/j.neuron.2021.01.011

Meilă, M. (2007). "Comparing clusterings—an information based distance." Journal of Multivariate Analysis **98**(5): 873-895. https://doi.org/10.1016/j.jmva.2006.11.013

Messe, A. (2020). "Parcellation influence on the connectivity-based structure-function relationship in the human brain." Hum Brain Mapp **41**(5): 1167-1180. https://doi.org/10.1002/hbm.24866

Meunier, D., S. Achard, A. Morcom and E. Bullmore (2009). "Age-related changes in modular organization of human brain functional networks." Neuroimage **44**(3): 715-723. https://doi.org/10.1016/j.neuroimage.2008.09.062

Meunier, D., R. Lambiotte, A. Fornito, K. D. Ersche and E. T. Bullmore (2009). "Hierarchical modularity in human brain functional networks." Front Neuroinform **3**: 37. https://doi.org/10.3389/neuro.11.037.2009

Michielse, S., N. Coupland, R. Camicioli, R. Carter, P. Seres, J. Sabino and N. Malykhin (2010). "Selective effects of aging on brain white matter microstructure: a diffusion tensor imaging tractography study." Neuroimage **52**(4): 1190-1201. https://doi.org/10.1016/j.neuroimage.2010.05.019

Misic, B., R. F. Betzel, A. Nematzadeh, J. Goni, A. Griffa, P. Hagmann, . . . O. Sporns (2015). "Cooperative and Competitive Spreading Dynamics on the Human Connectome." Neuron **86**(6): 1518-1529. https://doi.org/10.1016/j.neuron.2015.05.035

Morgan, S. E., S. Achard, M. Termenon, E. T. Bullmore and P. E. Vertes (2018). "Low-dimensional morphospace of topological motifs in human fMRI brain networks." Netw Neurosci **2**(2): 285-302. https://doi.org/10.1162/netn_a_00038

Motta, A., M. Berning, K. M. Boergens, B. Staffler, M. Beining, S. Loomba, . . . M. Helmstaedter (2019). "Dense connectomic reconstruction in layer 4 of the somatosensory cortex." Science **366**(6469). https://doi.org/10.1126/science.aay3134

Mountcastle, V. B. (1997). "The columnar organization of the neocortex." Brain **120 (Pt 4)**(4): 701-722. https://doi.org/10.1093/brain/120.4.701

Moussa, M. N., M. R. Steen, P. J. Laurienti and S. Hayasaka (2012). "Consistency of network modules in resting-state FMRI connectome data." PLoS One **7**(8): e44428. https://doi.org/10.1371/journal.pone.0044428

Moyer, D., B. Gutman, G. Prasad, J. Faskowitz, G. Ver Steeg and P. Thompson (2015). Blockmodels for connectome analysis. 11th International Symposium on Medical

Information Processing and Analysis, International Society for Optics and Photonics. https://doi.org/10.1117/12.2211519

Moyer, D., B. Gutman, G. Prasad, G. Ver Steeg and P. Thompson (2015). Mixed Membership Stochastic Blockmodels for the Human Connectome. MICCAI-BAMBI: Workshop on Bayesian And Graphical Models.

Mucha, P. J., T. Richardson, K. Macon, M. A. Porter and J. P. Onnela (2010). "Community structure in time-dependent, multiscale, and multiplex networks." Science **328**(5980): 876-878. https://doi.org/10.1126/science.1184819

Munkres, J. (1957). "Algorithms for the Assignment and Transportation Problems." Journal of the Society for Industrial and Applied Mathematics **5**(1): 32-38. https://doi.org/10.1137/0105003

Najafi, M., B. W. McMenamin, J. Z. Simon and L. Pessoa (2016). "Overlapping communities reveal rich structure in large-scale brain networks during rest and task conditions." Neuroimage **135**: 92-106. https://doi.org/10.1016/j.neuroimage.2016.04.054

Nastase, S. A., V. Gazzola, U. Hasson and C. Keysers (2019). Measuring shared responses across subjects using intersubject correlation, Oxford University Press.

Navlakha, S., Z. Bar-Joseph and A. L. Barth (2018). "Network Design and the Brain." Trends Cogn Sci **22**(1): 64-78. https://doi.org/10.1016/j.tics.2017.09.012

Newman, M. E. (2006). "Modularity and community structure in networks." Proc Natl Acad Sci U S A **103**(23): 8577-8582. https://doi.org/10.1073/pnas.0601602103

Newman, M. E. (2016). "Equivalence between modularity optimization and maximum likelihood methods for community detection." Phys Rev E **94**(5-1): 052315. https://doi.org/10.1103/PhysRevE.94.052315

Newman, M. E. (2018). "Estimating network structure from unreliable measurements." Physical Review E **98**(6): 062321. https://doi.org/10.1103/PhysRevE.98.062321

Newman, M. E. and A. Clauset (2016). "Structure and inference in annotated networks." Nat Commun **7**: 11863. https://doi.org/10.1038/ncomms11863

Newman, M. E. and M. Girvan (2004). "Finding and evaluating community structure in networks." Phys Rev E Stat Nonlin Soft Matter Phys **69**(2 Pt 2): 026113. https://doi.org/10.1103/PhysRevE.69.026113

Ng, L., A. Bernard, C. Lau, C. C. Overly, H. W. Dong, C. Kuan, . . . M. Hawrylycz (2009). "An anatomic gene expression atlas of the adult mouse brain." Nat Neurosci **12**(3): 356-362. https://doi.org/10.1038/nn.2281

Nicolini, C., G. Forcellini, L. Minati and A. Bifone (2020). "Scale-resolved analysis of brain functional connectivity networks with spectral entropy." Neuroimage **211**: 116603. https://doi.org/10.1016/j.neuroimage.2020.116603

Nieuwenhuys, R. (2013). "The myeloarchitectonic studies on the human cerebral cortex of the Vogt–Vogt school, and their significance for the interpretation of functional neuroimaging data." Brain Structure and Function **218**(2): 303-352. https://doi.org/10.1007/s00429-012-0460-z

Nolte, M., E. Gal, H. Markram and M. W. Reimann (2020). "Impact of higher order network structure on emergent cortical activity." Netw Neurosci **4**(1): 292-314. https://doi.org/10.1162/netn_a_00124

Nooner, K. B., S. J. Colcombe, R. H. Tobe, M. Mennes, M. M. Benedict, A. L. Moreno, . . . M. P. Milham (2012). "The NKI-Rockland Sample: A Model for Accelerating the Pace of Discovery Science in Psychiatry." Front Neurosci **6**: 152. https://doi.org/10.3389/fnins.2012.00152

Noori, H. R., J. Schottler, M. Ercsey-Ravasz, A. Cosa-Linan, M. Varga, Z. Toroczkai and R. Spanagel (2017). "A multiscale cerebral neurochemical connectome of the rat brain." PLoS Biol **15**(7): e2002612. https://doi.org/10.1371/journal.pbio.2002612

Nozais, V., S. J. Forkel, C. Foulon, L. Petit and M. Thiebaut de Schotten (2021). "Functionnectome: a framework to analyse the contribution of brain circuits to fMRI." bioRxiv: 2021.2001.2006.425574. https://doi.org/10.1101/2021.01.06.425574

O'Reilly, J. X., M. W. Woolrich, T. E. Behrens, S. M. Smith and H. Johansen-Berg (2012). "Tools of the trade: psychophysiological interactions and functional connectivity." Soc Cogn Affect Neurosci **7**(5): 604-609. https://doi.org/10.1093/scan/nss055

O'Connor, D., N. V. Potler, M. Kovacs, T. Xu, L. Ai, J. Pellman, . . . S. Ghosh (2017). "The Healthy Brain Network Serial Scanning Initiative: a resource for evaluating inter-individual differences and their reliabilities across scan conditions and sessions." Gigascience **6**(2): giw011. https://doi.org/10.1093/gigascience/giw011

Ogawa, S., T. M. Lee, A. R. Kay and D. W. Tank (1990). "Brain magnetic resonance imaging with contrast dependent on blood oxygenation." Proc Natl Acad Sci U S A **87**(24): 9868-9872. https://doi.org/10.1073/pnas.87.24.9868

Osher, D. E., R. R. Saxe, K. Koldewyn, J. D. Gabrieli, N. Kanwisher and Z. M. Saygin (2016). "Structural Connectivity Fingerprints Predict Cortical Selectivity for Multiple Visual Categories across Cortex." Cereb Cortex **26**(4): 1668-1683. https://doi.org/10.1093/cercor/bhu303

Owen, L. L., T. H. Chang and J. R. Manning (2019). "High-level cognition during story listening is reflected in high-order dynamic correlations in neural activity patterns." bioRxiv: 763821. https://doi.org/10.1101/763821

Paquola, C., R. Vos De Wael, K. Wagstyl, R. A. I. Bethlehem, S. J. Hong, J. Seidlitz, . . . B. C. Bernhardt (2019). "Microstructural and functional gradients are increasingly dissociated in transmodal cortices." PLoS Biol **17**(5): e3000284. https://doi.org/10.1371/journal.pbio.3000284

Park, H. J. and K. Friston (2013). "Structural and functional brain networks: from connections to cognition." Science **342**(6158): 1238411. https://doi.org/10.1126/science.1238411

Parkes, L., B. Fulcher, M. Yucel and A. Fornito (2018). "An evaluation of the efficacy, reliability, and sensitivity of motion correction strategies for resting-state functional MRI." Neuroimage **171**: 415-436. https://doi.org/10.1016/j.neuroimage.2017.12.073

Passingham, R. E., K. E. Stephan and R. Kotter (2002). "The anatomical basis of functional localization in the cortex." Nat Rev Neurosci **3**(8): 606-616. https://doi.org/10.1038/nrn893

Patania, A., P. Selvaggi, M. Veronese, O. Dipasquale, P. Expert and G. Petri (2019). "Topological gene expression networks recapitulate brain anatomy and function." Netw Neurosci **3**(3): 744-762. https://doi.org/10.1162/netn_a_00094

Patania, A., F. Vaccarino and G. Petri (2017). "Topological analysis of data." EPJ Data Science **6**(1): 1-6. https://doi.org/10.1140/epjds/s13688-017-0104-x

Pavlovic, D. M., P. E. Vertes, E. T. Bullmore, W. R. Schafer and T. E. Nichols (2014). "Stochastic blockmodeling of the modules and core of the Caenorhabditis elegans connectome." PLoS One **9**(7): e97584. https://doi.org/10.1371/journal.pone.0097584

Pedersen, M., A. Zalesky, A. Omidvarnia and G. D. Jackson (2018). "Multilayer network switching rate predicts brain performance." Proc Natl Acad Sci U S A **115**(52): 13376-13381. https://doi.org/10.1073/pnas.1814785115

Peel, L., D. B. Larremore and A. Clauset (2017). "The ground truth about metadata and community detection in networks." Sci Adv **3**(5): e1602548. https://doi.org/10.1126/sciadv.1602548

Peixoto, T. P. (2018). "Nonparametric weighted stochastic block models." Phys Rev E **97**(1-1): 012306. https://doi.org/10.1103/PhysRevE.97.012306

Pena-Gomez, C., A. Avena-Koenigsberger, J. Sepulcre and O. Sporns (2018). "Spatiotemporal Network Markers of Individual Variability in the Human Functional Connectome." Cereb Cortex **28**(8): 2922-2934. https://doi.org/10.1093/cercor/bhx170

Pereira, F., T. Mitchell and M. Botvinick (2009). "Machine learning classifiers and fMRI: a tutorial overview." Neuroimage **45**(1 Suppl): S199-209. https://doi.org/10.1016/j.neuroimage.2008.11.007

Pessoa, L. (2014). "Understanding brain networks and brain organization." Physics of life reviews **11**(3): 400-435. https://doi.org/10.1016/j.plrev.2014.03.005

Pestilli, F. (2018). "Human white matter and knowledge representation." PLoS Biol **16**(4): e2005758. https://doi.org/10.1371/journal.pbio.2005758

Petri, G., P. Expert, F. Turkheimer, R. Carhart-Harris, D. Nutt, P. J. Hellyer and F. Vaccarino (2014). "Homological scaffolds of brain functional networks." J R Soc Interface **11**(101): 20140873. https://doi.org/10.1098/rsif.2014.0873

Petrov, D., A. Ivanov, J. Faskowitz, B. Gutman, D. Moyer, J. Villalon, . . . P. Thompson (2017). Evaluating 35 methods to generate structural connectomes using pairwise classification. International Conference on medical Image Computing and Computer-Assisted Intervention, Springer.

Pizzagalli, F., G. Auzias, P. Kochunov, J. I. Faskowitz, P. M. Thompson and N. Jahanshad (2017). The core genetic network underlying sulcal morphometry. 12th international symposium on medical information processing and analysis, International Society for Optics and Photonics. https://doi.org/10.1117/12.2256959

Pizzagalli, F., G. Auzias, Q. Yang, S. R. Mathias, J. Faskowitz, J. D. Boyd, . . . G. I. de Zubicaray (2020). "The reliability and heritability of cortical folds and their genetic correlations across hemispheres." Communications biology **3**(1): 1-12. https://doi.org/10.1038/s42003-020-01163-1

Poldrack, R. A. (2006). "Can cognitive processes be inferred from neuroimaging data?" Trends in cognitive sciences **10**(2): 59-63. https://doi.org/10.1016/j.tics.2005.12.004

Poldrack, R. A. and T. Yarkoni (2016). "From Brain Maps to Cognitive Ontologies: Informatics and the Search for Mental Structure." Annu Rev Psychol **67**: 587-612. https://doi.org/10.1146/annurev-psych-122414-033729

Power, J. D., A. L. Cohen, S. M. Nelson, G. S. Wig, K. A. Barnes, J. A. Church, . . . S. E. Petersen (2011). "Functional network organization of the human brain." Neuron **72**(4): 665-678. https://doi.org/10.1016/j.neuron.2011.09.006

Power, J. D., A. Mitra, T. O. Laumann, A. Z. Snyder, B. L. Schlaggar and S. E. Petersen (2014). "Methods to detect, characterize, and remove motion artifact in resting state fMRI." Neuroimage **84**: 320-341. https://doi.org/10.1016/j.neuroimage.2013.08.048

Power, J. D., B. L. Schlaggar, C. N. Lessov-Schlaggar and S. E. Petersen (2013). "Evidence for hubs in human functional brain networks." Neuron **79**(4): 798-813. https://doi.org/10.1016/j.neuron.2013.07.035

Preti, M. G., T. A. Bolton and D. Van De Ville (2017). "The dynamic functional connectome: State-of-the-art and perspectives." Neuroimage **160**: 41-54. https://doi.org/10.1016/j.neuroimage.2016.12.061

Psorakis, I., S. Roberts, M. Ebden and B. Sheldon (2011). "Overlapping community detection using bayesian non-negative matrix factorization." Physical Review E **83**(6): 066114. https://doi.org/10.1103/PhysRevE.83.066114

Puxeddu, M. G., J. Faskowitz, R. F. Betzel, M. Petti, L. Astolfi and O. Sporns (2020). "The modular organization of brain cortical connectivity across the human lifespan." Neuroimage **218**: 116974. https://doi.org/10.1016/j.neuroimage.2020.116974

Rabuffo, G., J. Fousek, C. Bernard and V. Jirsa (2020). "Neuronal cascades shape whole-brain functional dynamics at rest." bioRxiv. https://doi.org/10.1101/2020.12.25.424385

Raichle, M. E., A. M. MacLeod, A. Z. Snyder, W. J. Powers, D. A. Gusnard and G. L. Shulman (2001). "A default mode of brain function." Proc Natl Acad Sci U S A **98**(2): 676-682. https://doi.org/10.1073/pnas.98.2.676

Raichle, M. E. (2009). "A brief history of human brain mapping." Trends Neurosci **32**(2): 118-126. https://doi.org/10.1016/j.tins.2008.11.001

Reichardt, J. and S. Bornholdt (2006). "Statistical mechanics of community detection." Phys Rev E Stat Nonlin Soft Matter Phys **74**(1 Pt 2): 016110. https://doi.org/10.1103/PhysRevE.74.016110

Reid, A. T., D. B. Headley, R. D. Mill, R. Sanchez-Romero, L. Q. Uddin, D. Marinazzo, . . . M. W. Cole (2019). "Advancing functional connectivity research from association to causation." Nat Neurosci **22**(11): 1751-1760. https://doi.org/10.1038/s41593-019-0510-4

Reimann, M. W., M. Nolte, M. Scolamiero, K. Turner, R. Perin, G. Chindemi, . . . H. Markram (2017). "Cliques of neurons bound into cavities provide a missing link between structure and function." Frontiers in computational neuroscience **11**: 48. https://doi.org/10.3389/fncom.2017.00048

Rheault, F., P. Poulin, A. Valcourt Caron, E. St-Onge and M. Descoteaux (2020). "Common misconceptions, hidden biases and modern challenges of dMRI tractography." J Neural Eng **17**(1): 011001. https://doi.org/10.1088/1741-2552/ab6aad

Richiardi, J., A. Altmann, A. C. Milazzo, C. Chang, M. M. Chakravarty, T. Banaschewski, . . . I. consortium (2015). "BRAIN NETWORKS. Correlated gene expression supports

synchronous activity in brain networks." Science **348**(6240): 1241-1244. https://doi.org/10.1126/science.1255905

Roalf, D. R., M. Quarmley, M. A. Elliott, T. D. Satterthwaite, S. N. Vandekar, K. Ruparel, . . . R. E. Gur (2016). "The impact of quality assurance assessment on diffusion tensor imaging outcomes in a large-scale population-based cohort." Neuroimage **125**: 903-919. https://doi.org/10.1016/j.neuroimage.2015.10.068

Roberts, J. A., A. Perry, A. R. Lord, G. Roberts, P. B. Mitchell, R. E. Smith, . . . M. Breakspear (2016). "The contribution of geometry to the human connectome." Neuroimage **124**(Pt A): 379-393. https://doi.org/10.1016/j.neuroimage.2015.09.009

Roberts, J. A., A. Perry, G. Roberts, P. B. Mitchell and M. Breakspear (2017). "Consistency-based thresholding of the human connectome." Neuroimage **145**(Pt A): 118-129. https://doi.org/10.1016/j.neuroimage.2016.09.053

Robinson, E. C., S. Jbabdi, M. F. Glasser, J. Andersson, G. C. Burgess, M. P. Harms, . . . M. Jenkinson (2014). "MSM: a new flexible framework for Multimodal Surface Matching." Neuroimage **100**: 414-426. https://doi.org/10.1016/j.neuroimage.2014.05.069

Romero-Garcia, R., K. J. Whitaker, F. Vasa, J. Seidlitz, M. Shinn, P. Fonagy, . . . P. E. Vertes (2018). "Structural covariance networks are coupled to expression of genes enriched in supragranular layers of the human cortex." Neuroimage **171**: 256-267. https://doi.org/10.1016/j.neuroimage.2017.12.060

Rosenberg, M. D., E. S. Finn, D. Scheinost, X. Papademetris, X. Shen, R. T. Constable and M. M. Chun (2016). "A neuromarker of sustained attention from whole-brain functional connectivity." Nat Neurosci **19**(1): 165-171. https://doi.org/10.1038/nn.4179

Rosenthal, G., O. Sporns and G. Avidan (2017). "Stimulus Dependent Dynamic Reorganization of the Human Face Processing Network." Cereb Cortex **27**(10): 4823-4834. https://doi.org/10.1093/cercor/bhw279

Rosenthal, G., F. Váša, A. Griffa, P. Hagmann, E. Amico, J. Goñi, . . . O. Sporns (2018). "Mapping higher-order relations between brain structure and function with embedded vector representations of connectomes." Nature communications **9**(1): 1-12. https://doi.org/10.1038/s41467-018-04614-w

Rosvall, M. and C. T. Bergstrom (2008). "Maps of random walks on complex networks reveal community structure." Proc Natl Acad Sci U S A **105**(4): 1118-1123. https://doi.org/10.1073/pnas.0706851105

Rosvall, M., J.-C. Delvenne, M. T. Schaub and R. Lambiotte (2017). "Different approaches to community detection." arXiv preprint arXiv:1712.06468.

Rubinov, M. and O. Sporns (2010). "Complex network measures of brain connectivity: uses and interpretations." Neuroimage **52**(3): 1059-1069. https://doi.org/10.1016/j.neuroimage.2009.10.003

Rubinov, M. and O. Sporns (2011). "Weight-conserving characterization of complex functional brain networks." Neuroimage **56**(4): 2068-2079. https://doi.org/10.1016/j.neuroimage.2011.03.069

Rubinov, M., R. J. Ypma, C. Watson and E. T. Bullmore (2015). "Wiring cost and topological participation of the mouse brain connectome." Proc Natl Acad Sci U S A **112**(32): 10032-10037. https://doi.org/10.1073/pnas.1420315112

Ruddy, K. L., A. Leemans and R. G. Carson (2017). "Transcallosal connectivity of the human cortical motor network." Brain Struct Funct **222**(3): 1243-1252. https://doi.org/10.1007/s00429-016-1274-1

Ryan, K., Z. Lu and I. A. Meinertzhagen (2016). "The CNS connectome of a tadpole larva of Ciona intestinalis (L.) highlights sidedness in the brain of a chordate sibling." Elife **5**: e16962. https://doi.org/10.7554/eLife.16962

Sachs, H., M. Stiebitz and R. J. Wilson (1988). "An historical note: Euler's Königsberg letters." Journal of Graph Theory **12**(1): 133-139. https://doi.org/10.1002/jgt.3190120114

Salat, D. H., D. S. Tuch, N. D. Hevelone, B. Fischl, S. Corkin, H. D. Rosas and A. M. Dale (2005). "Age-related changes in prefrontal white matter measured by diffusion tensor imaging." Ann N Y Acad Sci **1064**(1): 37-49. https://doi.org/10.1196/annals.1340.009

Saleeba, C., B. Dempsey, S. Le, A. Goodchild and S. McMullan (2019). "A Student's Guide to Neural Circuit Tracing." Front Neurosci **13**: 897. https://doi.org/10.3389/fnins.2019.00897

Salehi, M., A. S. Greene, A. Karbasi, X. Shen, D. Scheinost and R. T. Constable (2020). "There is no single functional atlas even for a single individual: Functional parcel definitions change with task." NeuroImage **208**: 116366.

Sanchez-Romero, R. and M. W. Cole (2021). "Combining Multiple Functional Connectivity Methods to Improve Causal Inferences." J Cogn Neurosci **33**(2): 180-194. https://doi.org/10.1162/jocn_a_01580

Sanz-Leon, P., S. A. Knock, A. Spiegler and V. K. Jirsa (2015). "Mathematical framework for large-scale brain network modeling in The Virtual Brain." Neuroimage **111**: 385-430. https://doi.org/10.1016/j.neuroimage.2015.01.002

Sarwar, T., Y. Tian, B. T. T. Yeo, K. Ramamohanarao and A. Zalesky (2021). "Structure-function coupling in the human connectome: A machine learning approach." Neuroimage **226**: 117609. https://doi.org/10.1016/j.neuroimage.2020.117609

Satterthwaite, T. D., M. A. Elliott, R. T. Gerraty, K. Ruparel, J. Loughead, M. E. Calkins, . . . D. H. Wolf (2013). "An improved framework for confound regression and filtering for control of motion artifact in the preprocessing of resting-state functional connectivity data." Neuroimage **64**: 240-256. https://doi.org/10.1016/j.neuroimage.2012.08.052

Saygin, Z. M., D. E. Osher, E. S. Norton, D. A. Youssoufian, S. D. Beach, J. Feather, . . . N. Kanwisher (2016). "Connectivity precedes function in the development of the visual word form area." Nat Neurosci **19**(9): 1250-1255. https://doi.org/10.1038/nn.4354

Scannell, J. W., C. Blakemore and M. P. Young (1995). "Analysis of connectivity in the cat cerebral cortex." J Neurosci **15**(2): 1463-1483.

Scannell, J. W. and M. P. Young (1993). "The connectional organization of neural systems in the cat cerebral cortex." Curr Biol **3**(4): 191-200. https://doi.org/10.1016/0960-9822(93)90331-h

Schaefer, A., R. Kong, E. M. Gordon, T. O. Laumann, X. N. Zuo, A. J. Holmes, . . . B. T. T. Yeo (2018). "Local-Global Parcellation of the Human Cerebral Cortex from Intrinsic Functional Connectivity MRI." Cereb Cortex **28**(9): 3095-3114. https://doi.org/10.1093/cercor/bhx179

Schafer, W. R. (2018). "The Worm Connectome: Back to the Future." Trends Neurosci **41**(11): 763-765. https://doi.org/10.1016/j.tins.2018.09.002

Schaub, M. T., J.-C. Delvenne, M. Rosvall and R. Lambiotte (2017). "The many facets of community detection in complex networks." Applied Network Science **2**(1): 4. https://doi.org/10.1007/s41109-017-0023-6

Schaub, M. T., J. C. Delvenne, M. Rosvall and R. Lambiotte (2017). "The many facets of community detection in complex networks." Appl Netw Sci **2**(1): 4. https://doi.org/10.1007/s41109-017-0023-6

Scheinost, D., S. Noble, C. Horien, A. S. Greene, E. M. Lake, M. Salehi, . . . R. T. Constable (2019). "Ten simple rules for predictive modeling of individual differences in neuroimaging." Neuroimage **193**: 35-45. https://doi.org/10.1016/j.neuroimage.2019.02.057

Schmitt, O. and P. Eipert (2012). "neuroVIISAS: approaching multiscale simulation of the rat connectome." Neuroinformatics **10**(3): 243-267. https://doi.org/10.1007/s12021-012-9141-6

Schröter, M., O. Paulsen and E. T. Bullmore (2017). "Micro-connectomics: probing the organization of neuronal networks at the cellular scale." Nature Reviews Neuroscience **18**(3): 131-146. https://doi.org/10.1038/nrn.2016.182

Seghier, M. L. and C. J. Price (2018). "Interpreting and Utilising Intersubject Variability in Brain Function." Trends Cogn Sci **22**(6): 517-530. https://doi.org/10.1016/j.tics.2018.03.003

Seguin, C., Y. Tian and A. Zalesky (2020). "Network communication models improve the behavioral and functional predictive utility of the human structural connectome." Netw Neurosci **4**(4): 980-1006. https://doi.org/10.1162/netn_a_00161

Seguin, C., M. P. van den Heuvel and A. Zalesky (2018). "Navigation of brain networks." Proc Natl Acad Sci U S A **115**(24): 6297-6302. https://doi.org/10.1073/pnas.1801351115

Seidlitz, J., F. Vasa, M. Shinn, R. Romero-Garcia, K. J. Whitaker, P. E. Vertes, . . . E. T. Bullmore (2018). "Morphometric Similarity Networks Detect Microscale Cortical Organization and Predict Inter-Individual Cognitive Variation." Neuron **97**(1): 231-247 e237. https://doi.org/10.1016/j.neuron.2017.11.039

Shafiei, G., R. D. Markello, R. Vos de Wael, B. C. Bernhardt, B. D. Fulcher and B. Misic (2020). "Topographic gradients of intrinsic dynamics across neocortex." Elife **9**: e62116. https://doi.org/10.7554/eLife.62116

Shakil, S., C. H. Lee and S. D. Keilholz (2016). "Evaluation of sliding window correlation performance for characterizing dynamic functional connectivity and brain states." Neuroimage **133**: 111-128. https://doi.org/10.1016/j.neuroimage.2016.02.074

Sheheitli, H. and V. K. Jirsa (2020). "A mathematical model of ephaptic interactions in neuronal fiber pathways: Could there be more than transmission along the tracts?" Network Neuroscience **4**(3): 595-610. https://doi.org/10.1162/netn_a_00134

Shen, K., R. M. Hutchison, G. Bezgin, S. Everling and A. R. McIntosh (2015). "Network structure shapes spontaneous functional connectivity dynamics." J Neurosci **35**(14): 5579-5588. https://doi.org/10.1523/JNEUROSCI.4903-14.2015

Shen, X., E. S. Finn, D. Scheinost, M. D. Rosenberg, M. M. Chun, X. Papademetris and R. T. Constable (2017). "Using connectome-based predictive modeling to predict individual behavior from brain connectivity." nature protocols **12**(3): 506-518. https://doi.org/10.1038/nprot.2016.178

Shih, C. T., O. Sporns, S. L. Yuan, T. S. Su, Y. J. Lin, C. C. Chuang, . . . A. S. Chiang (2015). "Connectomics-based analysis of information flow in the Drosophila brain." Curr Biol **25**(10): 1249-1258. https://doi.org/10.1016/j.cub.2015.03.021

Shine, J. M. (2019). "Neuromodulatory Influences on Integration and Segregation in the Brain." Trends Cogn Sci **23**(7): 572-583. https://doi.org/10.1016/j.tics.2019.04.002

Shine, J. M., M. Breakspear, P. T. Bell, K. A. E. Martens, R. Shine, O. Koyejo, . . . R. A. Poldrack (2019). "Human cognition involves the dynamic integration of neural activity

and neuromodulatory systems." Nature neuroscience **22**(2): 289-296. https://doi.org/10.1038/s41593-018-0312-0

Shine, J. M., O. Koyejo, P. T. Bell, K. J. Gorgolewski, M. Gilat and R. A. Poldrack (2015). "Estimation of dynamic functional connectivity using Multiplication of Temporal Derivatives." NeuroImage **122**: 399-407. https://doi.org/10.1016/j.neuroimage.2015.07.064

Shinn, M., R. Romero-Garcia, J. Seidlitz, F. Vasa, P. E. Vertes and E. Bullmore (2017). "Versatility of nodal affiliation to communities." Sci Rep **7**(1): 4273. https://doi.org/10.1038/s41598-017-03394-5

Shrout, P. E. and J. L. Fleiss (1979). "Intraclass correlations: uses in assessing rater reliability." Psychol Bull **86**(2): 420-428. https://doi.org/10.1037//0033-2909.86.2.420

Simony, E., C. J. Honey, J. Chen, O. Lositsky, Y. Yeshurun, A. Wiesel and U. Hasson (2016). "Dynamic reconfiguration of the default mode network during narrative comprehension." Nat Commun **7**: 12141. https://doi.org/10.1038/ncomms12141

Sizemore, A. E., C. Giusti, A. Kahn, J. M. Vettel, R. F. Betzel and D. S. Bassett (2018). "Cliques and cavities in the human connectome." J Comput Neurosci **44**(1): 115-145. https://doi.org/10.1007/s10827-017-0672-6

Sizemore, A. E., J. E. Phillips-Cremins, R. Ghrist and D. S. Bassett (2019). "The importance of the whole: Topological data analysis for the network neuroscientist." Netw Neurosci **3**(3): 656-673. https://doi.org/10.1162/netn_a_00073

Smith, R. E., J. D. Tournier, F. Calamante and A. Connelly (2012). "Anatomically-constrained tractography: improved diffusion MRI streamlines tractography through effective use of anatomical information." Neuroimage **62**(3): 1924-1938. https://doi.org/10.1016/j.neuroimage.2012.06.005

Smith, S. M., P. T. Fox, K. L. Miller, D. C. Glahn, P. M. Fox, C. E. Mackay, . . . C. F. Beckmann (2009). "Correspondence of the brain's functional architecture during activation and rest." Proc Natl Acad Sci U S A **106**(31): 13040-13045. https://doi.org/10.1073/pnas.0905267106

Smith, S. M., K. L. Miller, G. Salimi-Khorshidi, M. Webster, C. F. Beckmann, T. E. Nichols, . . . M. W. Woolrich (2011). "Network modelling methods for FMRI." Neuroimage **54**(2): 875-891. https://doi.org/10.1016/j.neuroimage.2010.08.063

Smith, S. M., T. E. Nichols, D. Vidaurre, A. M. Winkler, T. E. Behrens, M. F. Glasser, . . . K. L. Miller (2015). "A positive-negative mode of population covariation links brain connectivity, demographics and behavior." Nat Neurosci **18**(11): 1565-1567. https://doi.org/10.1038/nn.4125

Snijders, T. A. and K. Nowicki (1997). "Estimation and prediction for stochastic blockmodels for graphs with latent block structure." Journal of classification **14**(1): 75-100.

Sohn, Y., M. K. Choi, Y. Y. Ahn, J. Lee and J. Jeong (2011). "Topological cluster analysis reveals the systemic organization of the Caenorhabditis elegans connectome." PLoS Comput Biol **7**(5): e1001139. https://doi.org/10.1371/journal.pcbi.1001139

Song, H. F., H. Kennedy and X. J. Wang (2014). "Spatial embedding of structural similarity in the cerebral cortex." Proc Natl Acad Sci U S A **111**(46): 16580-16585. https://doi.org/10.1073/pnas.1414153111

Song, S., P. J. Sjostrom, M. Reigl, S. Nelson and D. B. Chklovskii (2005). "Highly nonrandom features of synaptic connectivity in local cortical circuits." PLoS Biol **3**(3): e68. https://doi.org/10.1371/journal.pbio.0030068

Sotiropoulos, S. N. and A. Zalesky (2019). "Building connectomes using diffusion MRI: why, how and but." NMR Biomed **32**(4): e3752. https://doi.org/10.1002/nbm.3752

Sowell, E. R., P. M. Thompson and A. W. Toga (2004). "Mapping changes in the human cortex throughout the span of life." Neuroscientist **10**(4): 372-392. https://doi.org/10.1177/1073858404263960

Sporns, O. (2011). "The human connectome: a complex network." Ann N Y Acad Sci **1224**(1): 109-125. https://doi.org/10.1111/j.1749-6632.2010.05888.x

Sporns, O. (2011). "The non-random brain: efficiency, economy, and complex dynamics." Front Comput Neurosci **5**: 5. https://doi.org/10.3389/fncom.2011.00005

Sporns, O. (2012). Discovering the human connectome, MIT press.

Sporns, O. (2013). "Making sense of brain network data." Nat Methods **10**(6): 491-493. https://doi.org/10.1038/nmeth.2485

Sporns, O. (2013). "Network attributes for segregation and integration in the human brain." Curr Opin Neurobiol **23**(2): 162-171. https://doi.org/10.1016/j.conb.2012.11.015

Sporns, O. (2015). "Cerebral cartography and connectomics." Philos Trans R Soc Lond B Biol Sci **370**(1668). https://doi.org/10.1098/rstb.2014.0173

Sporns, O. (2017). "The future of network neuroscience." Netw Neurosci **1**(2): 1-2. https://doi.org/10.1162/NETN_e_00005

Sporns, O. and R. F. Betzel (2016). "Modular Brain Networks." Annu Rev Psychol **67**: 613-640. https://doi.org/10.1146/annurev-psych-122414-033634

Sporns, O., J. Faskowitz, A. S. Teixeira, S. A. Cutts and R. F. Betzel (2021). "Dynamic expression of brain functional systems disclosed by fine-scale analysis of edge time series." Network Neuroscience: 1-29. https://doi.org/10.1162/netn_a_00182

Sporns, O., C. J. Honey and R. Kotter (2007). "Identification and classification of hubs in brain networks." PLoS One 2(10): e1049. https://doi.org/10.1371/journal.pone.0001049

Sporns, O. and R. Kotter (2004). "Motifs in brain networks." PLoS Biol 2(11): e369. https://doi.org/10.1371/journal.pbio.0020369

Sporns, O., G. Tononi and R. Kotter (2005). "The human connectome: A structural description of the human brain." PLoS Comput Biol 1(4): e42. https://doi.org/10.1371/journal.pcbi.0010042

Sporns, O. and J. D. Zwi (2004). "The small world of the cerebral cortex." Neuroinformatics 2(2): 145-162. https://doi.org/10.1385/NI:2:2:145

St-Jean, S., P. Coupe and M. Descoteaux (2016). "Non Local Spatial and Angular Matching: Enabling higher spatial resolution diffusion MRI datasets through adaptive denoising." Med Image Anal 32: 115-130. https://doi.org/10.1016/j.media.2016.02.010

Stephan, K. E., C. C. Hilgetag, G. A. Burns, M. A. O'Neill, M. P. Young and R. Kotter (2000). "Computational analysis of functional connectivity between areas of primate cerebral cortex." Philos Trans R Soc Lond B Biol Sci 355(1393): 111-126. https://doi.org/10.1098/rstb.2000.0552

Stiso, J. and D. S. Bassett (2018). "Spatial Embedding Imposes Constraints on Neuronal Network Architectures." Trends Cogn Sci 22(12): 1127-1142. https://doi.org/10.1016/j.tics.2018.09.007

Stopczynski, A., V. Sekara, P. Sapiezynski, A. Cuttone, M. M. Madsen, J. E. Larsen and S. Lehmann (2014). "Measuring large-scale social networks with high resolution." PLoS One 9(4): e95978. https://doi.org/10.1371/journal.pone.0095978

Storsve, A. B., A. M. Fjell, C. K. Tamnes, L. T. Westlye, K. Overbye, H. W. Aasland and K. B. Walhovd (2014). "Differential longitudinal changes in cortical thickness, surface area and volume across the adult life span: regions of accelerating and decelerating change." J Neurosci 34(25): 8488-8498. https://doi.org/10.1523/JNEUROSCI.0391-14.2014

Suarez, L. E., R. D. Markello, R. F. Betzel and B. Misic (2020). "Linking Structure and Function in Macroscale Brain Networks." Trends Cogn Sci 24(4): 302-315. https://doi.org/10.1016/j.tics.2020.01.008

Swanson, L. W. (2000). "What is the brain?" Trends in neurosciences 23(11): 519-527. https://doi.org/10.1016/S0166-2236(00)01639-8

Swanson, L. W., J. D. Hahn, L. G. S. Jeub, S. Fortunato and O. Sporns (2018). "Subsystem organization of axonal connections within and between the right and left cerebral cortex and cerebral nuclei (endbrain)." Proc Natl Acad Sci U S A **115**(29): E6910-E6919. https://doi.org/10.1073/pnas.1807255115

Swanson, L. W., J. D. Hahn and O. Sporns (2017). "Organizing principles for the cerebral cortex network of commissural and association connections." Proc Natl Acad Sci U S A **114**(45): E9692-E9701. https://doi.org/10.1073/pnas.1712928114

Swanson, L. W., J. D. Hahn and O. Sporns (2020). "Structure-function subsystem models of female and male forebrain networks integrating cognition, affect, behavior, and bodily functions." Proc Natl Acad Sci U S A **117**(49): 31470-31481. https://doi.org/10.1073/pnas.2017733117

Swanson, L. W. and J. W. Lichtman (2016). "From Cajal to Connectome and Beyond." Annu Rev Neurosci **39**: 197-216. https://doi.org/10.1146/annurev-neuro-071714-033954

Swanson, L. W., O. Sporns and J. D. Hahn (2016). "Network architecture of the cerebral nuclei (basal ganglia) association and commissural connectome." Proc Natl Acad Sci U S A **113**(40): E5972-E5981. https://doi.org/10.1073/pnas.1613184113

Swanson, L. W., O. Sporns and J. D. Hahn (2019). "The network architecture of rat intrinsic interbrain (diencephalic) macroconnections." Proc Natl Acad Sci U S A **116**(52): 26991-27000. https://doi.org/10.1073/pnas.1915446116

Swanson, L. W., O. Sporns and J. D. Hahn (2019). "The network organization of rat intrathalamic macroconnections and a comparison with other forebrain divisions." Proc Natl Acad Sci U S A **116**(27): 13661-13669. https://doi.org/10.1073/pnas.1905961116

Tagliazucchi, E., P. Balenzuela, D. Fraiman and D. R. Chialvo (2012). "Criticality in large-scale brain FMRI dynamics unveiled by a novel point process analysis." Front Physiol **3**: 15. https://doi.org/10.3389/fphys.2012.00015

Tang, W., S. Jbabdi, Z. Zhu, M. Cottaar, G. Grisot, J. F. Lehman, . . . S. N. Haber (2019). "A connectional hub in the rostral anterior cingulate cortex links areas of emotion and cognitive control." Elife **8**: e43761. https://doi.org/10.7554/eLife.43761

Tax, C. M., B. Jeurissen, S. B. Vos, M. A. Viergever and A. Leemans (2014). "Recursive calibration of the fiber response function for spherical deconvolution of diffusion MRI data." Neuroimage **86**: 67-80. https://doi.org/10.1016/j.neuroimage.2013.07.067

Teixeira, A. S., F. C. Santos and A. P. Francisco (2017). Emergence of social balance in signed networks. International Workshop on Complex Networks, Springer.

Telesford, Q. K., S. L. Simpson, J. H. Burdette, S. Hayasaka and P. J. Laurienti (2011). "The brain as a complex system: using network science as a tool for understanding the brain." Brain connectivity **1**(4): 295-308. https://doi.org/10.1089/brain.2011.0055

Tewarie, P., E. van Dellen, A. Hillebrand and C. J. Stam (2015). "The minimum spanning tree: an unbiased method for brain network analysis." Neuroimage **104**: 177-188. https://doi.org/10.1016/j.neuroimage.2014.10.015

Thompson, P. and A. W. Toga (1996). "A surface-based technique for warping three-dimensional images of the brain." IEEE Trans Med Imaging **15**(4): 402-417. https://doi.org/10.1109/42.511745

Thompson, W. H. and P. Fransson (2016). "Bursty properties revealed in large-scale brain networks with a point-based method for dynamic functional connectivity." Sci Rep **6**(1): 39156. https://doi.org/10.1038/srep39156

Toga, A. W., P. M. Thompson, S. Mori, K. Amunts and K. Zilles (2006). "Towards multimodal atlases of the human brain." Nat Rev Neurosci **7**(12): 952-966. https://doi.org/10.1038/nrn2012

Tononi, G., A. R. McIntosh, D. P. Russell and G. M. Edelman (1998). "Functional clustering: identifying strongly interactive brain regions in neuroimaging data." Neuroimage **7**(2): 133-149. https://doi.org/10.1006/nimg.1997.0313

Tononi, G., O. Sporns and G. M. Edelman (1994). "A measure for brain complexity: relating functional segregation and integration in the nervous system." Proc Natl Acad Sci U S A **91**(11): 5033-5037. https://doi.org/10.1073/pnas.91.11.5033

Tournier, J. D., F. Calamante and A. Connelly (2007). "Robust determination of the fibre orientation distribution in diffusion MRI: non-negativity constrained super-resolved spherical deconvolution." Neuroimage **35**(4): 1459-1472. https://doi.org/10.1016/j.neuroimage.2007.02.016

Traag, V. A., P. Van Dooren and Y. Nesterov (2011). "Narrow scope for resolution-limit-free community detection." Phys Rev E Stat Nonlin Soft Matter Phys **84**(1 Pt 2): 016114. https://doi.org/10.1103/PhysRevE.84.016114

Treiber, J. M., N. S. White, T. C. Steed, H. Bartsch, D. Holland, N. Farid, . . . C. C. Chen (2016). "Characterization and Correction of Geometric Distortions in 814 Diffusion Weighted Images." PLoS One **11**(3): e0152472. https://doi.org/10.1371/journal.pone.0152472

Tunc, B. and R. Verma (2015). "Unifying Inference of Meso-Scale Structures in Networks." PLoS One **10**(11): e0143133. https://doi.org/10.1371/journal.pone.0143133

Tustison, N. J., B. B. Avants, P. A. Cook, Y. Zheng, A. Egan, P. A. Yushkevich and J. C. Gee (2010). "N4ITK: improved N3 bias correction." IEEE Trans Med Imaging **29**(6): 1310-1320. https://doi.org/10.1109/TMI.2010.2046908

Uddin, L. Q. (2020). "Bring the Noise: Reconceptualizing Spontaneous Neural Activity." Trends Cogn Sci **24**(9): 734-746. https://doi.org/10.1016/j.tics.2020.06.003

Uddin, L. Q. (2020). "An 'edgy'new look." Nature Neuroscience **23**(12): 1471-1472. https://doi.org/10.1038/s41593-020-00741-0

Valdes-Sosa, P. A., A. Roebroeck, J. Daunizeau and K. Friston (2011). "Effective connectivity: influence, causality and biophysical modeling." Neuroimage **58**(2): 339-361. https://doi.org/10.1016/j.neuroimage.2011.03.058

van den Heuvel, M. P., S. C. de Lange, A. Zalesky, C. Seguin, B. T. T. Yeo and R. Schmidt (2017). "Proportional thresholding in resting-state fMRI functional connectivity networks and consequences for patient-control connectome studies: Issues and recommendations." Neuroimage **152**: 437-449. https://doi.org/10.1016/j.neuroimage.2017.02.005

van den Heuvel, M. P., R. S. Kahn, J. Goni and O. Sporns (2012). "High-cost, high-capacity backbone for global brain communication." Proc Natl Acad Sci U S A **109**(28): 11372-11377. https://doi.org/10.1073/pnas.1203593109

van den Heuvel, M. P., L. H. Scholtens and M. A. de Reus (2016). "Topological organization of connectivity strength in the rat connectome." Brain Struct Funct **221**(3): 1719-1736. https://doi.org/10.1007/s00429-015-0999-6

van den Heuvel, M. P., L. H. Scholtens, L. Feldman Barrett, C. C. Hilgetag and M. A. de Reus (2015). "Bridging Cytoarchitectonics and Connectomics in Human Cerebral Cortex." J Neurosci **35**(41): 13943-13948. https://doi.org/10.1523/JNEUROSCI.2630-15.2015

van den Heuvel, M. P. and O. Sporns (2011). "Rich-club organization of the human connectome." J Neurosci **31**(44): 15775-15786. https://doi.org/10.1523/JNEUROSCI.3539-11.2011

van den Heuvel, M. P. and O. Sporns (2013). "Network hubs in the human brain." Trends Cogn Sci **17**(12): 683-696. https://doi.org/10.1016/j.tics.2013.09.012

van der Meer, J. N., M. Breakspear, L. J. Chang, S. Sonkusare and L. Cocchi (2020). "Movie viewing elicits rich and reliable brain state dynamics." Nature communications **11**(1): 1-14.

Van Erp, T. G., E. Walton, D. P. Hibar, L. Schmaal, W. Jiang, D. C. Glahn, . . . R. Hashimoto (2018). "Cortical brain abnormalities in 4474 individuals with schizophrenia and 5098 control subjects via the Enhancing Neuro Imaging Genetics Through Meta Analysis

(ENIGMA) Consortium." Biological psychiatry **84**(9): 644-654. https://doi.org/10.1016/j.biopsych.2018.04.023

Van Essen, D. C., S. M. Smith, D. M. Barch, T. E. Behrens, E. Yacoub, K. Ugurbil and W. U.-M. H. Consortium (2013). "The WU-Minn Human Connectome Project: an overview." Neuroimage **80**: 62-79. https://doi.org/10.1016/j.neuroimage.2013.05.041

van Oort, E. S., M. Mennes, T. N. Schröder, V. J. Kumar, N. I. Z. Jimenez, W. Grodd, . . . C. F. Beckmann (2018). "Functional parcellation using time courses of instantaneous connectivity." Neuroimage **170**: 31-40. https://doi.org/10.1016/j.neuroimage.2017.07.027

Varley, T. F., O. Sporns, A. Puce and J. Beggs (2020). "Differential effects of propofol and ketamine on critical brain dynamics." PLOS Computational Biology **16**(12): e1008418.

Vazquez-Rodriguez, B., L. E. Suarez, R. D. Markello, G. Shafiei, C. Paquola, P. Hagmann, . . . B. Misic (2019). "Gradients of structure-function tethering across neocortex." Proc Natl Acad Sci U S A **116**(42): 21219-21227. https://doi.org/10.1073/pnas.1903403116

Vertes, P. E., A. F. Alexander-Bloch, N. Gogtay, J. N. Giedd, J. L. Rapoport and E. T. Bullmore (2012). "Simple models of human brain functional networks." Proc Natl Acad Sci U S A **109**(15): 5868-5873. https://doi.org/10.1073/pnas.1111738109

Vezquez-Rodriguez, B., Z. Q. Liu, P. Hagmann and B. Misic (2020). "Signal propagation via cortical hierarchies." Netw Neurosci **4**(4): 1072-1090. https://doi.org/10.1162/netn_a_00153

Vincent, J. L., G. H. Patel, M. D. Fox, A. Z. Snyder, J. T. Baker, D. C. Van Essen, . . . M. E. Raichle (2007). "Intrinsic functional architecture in the anaesthetized monkey brain." Nature **447**(7140): 83-86. https://doi.org/10.1038/nature05758

Voets, N. L., O. P. Jones, R. B. Mars, J. E. Adcock, R. Stacey, V. Apostolopoulos and P. Plaha (2019). "Characterising neural plasticity at the single patient level using connectivity fingerprints." NeuroImage: Clinical **24**: 101952. https://doi.org/10.1016/j.nicl.2019.101952

Voevodskaya, O., J. B. Pereira, G. Volpe, O. Lindberg, E. Stomrud, D. van Westen, . . . O. Hansson (2018). "Altered structural network organization in cognitively normal individuals with amyloid pathology." Neurobiol Aging **64**: 15-24. https://doi.org/10.1016/j.neurobiolaging.2017.11.014

Von Luxburg, U., R. C. Williamson and I. Guyon (2012). Clustering: Science or art? Proceedings of ICML Workshop on Unsupervised and Transfer Learning.

Wang, J., L. Wang, Y. Zang, H. Yang, H. Tang, Q. Gong, . . . Y. He (2009). "Parcellation-dependent small-world brain functional networks: a resting-state fMRI study." Hum Brain Mapp **30**(5): 1511-1523. https://doi.org/10.1002/hbm.20623

Wang, S., D. J. Peterson, J. C. Gatenby, W. Li, T. J. Grabowski and T. M. Madhyastha (2017). "Evaluation of Field Map and Nonlinear Registration Methods for Correction of Susceptibility Artifacts in Diffusion MRI." Front Neuroinform **11**: 17. https://doi.org/10.3389/fninf.2017.00017

Wang, Y. J. and G. Y. Wong (1987). "Stochastic Blockmodels for Directed Graphs." Journal of the American Statistical Association **82**(397): 8-19. https://doi.org/10.2307/2289119

Wang, Z., L. M. Chen, L. Negyessy, R. M. Friedman, A. Mishra, J. C. Gore and A. W. Roe (2013). "The relationship of anatomical and functional connectivity to resting-state connectivity in primate somatosensory cortex." Neuron **78**(6): 1116-1126. https://doi.org/10.1016/j.neuron.2013.04.023

Wasserman, S. and K. Faust (1994). Social network analysis: Methods and applications, Cambridge university press.

Watts, D. J. and S. H. Strogatz (1998). "Collective dynamics of 'small-world'networks." nature **393**(6684): 440-442. https://doi.org/10.1038/30918

Westlye, L. T., K. B. Walhovd, A. M. Dale, A. Bjornerud, P. Due-Tonnessen, A. Engvig, . . . A. M. Fjell (2010). "Differentiating maturational and aging-related changes of the cerebral cortex by use of thickness and signal intensity." Neuroimage **52**(1): 172-185. https://doi.org/10.1016/j.neuroimage.2010.03.056

Whelan, C. D., D. P. Hibar, L. S. van Velzen, A. S. Zannas, T. Carrillo-Roa, K. McMahon, . . . I. Alzheimer's Disease Neuroimaging (2016). "Heritability and reliability of automatically segmented human hippocampal formation subregions." Neuroimage **128**: 125-137. https://doi.org/10.1016/j.neuroimage.2015.12.039

White, J. G., E. Southgate, J. N. Thomson and S. Brenner (1986). "The structure of the nervous system of the nematode Caenorhabditis elegans." Philos Trans R Soc Lond B Biol Sci **314**(1165): 1-340. https://doi.org/10.1098/rstb.1986.0056

Wig, G. S. (2017). "Segregated Systems of Human Brain Networks." Trends Cogn Sci **21**(12): 981-996. https://doi.org/10.1016/j.tics.2017.09.006

Wilf, M., F. Strappini, T. Golan, A. Hahamy, M. Harel and R. Malach (2017). "Spontaneously Emerging Patterns in Human Visual Cortex Reflect Responses to Naturalistic Sensory Stimuli." Cereb Cortex **27**(1): 750-763. https://doi.org/10.1093/cercor/bhv275

Willems, R. M., S. A. Nastase and B. Milivojevic (2020). "Narratives for Neuroscience." Trends Neurosci **43**(5): 271-273. https://doi.org/10.1016/j.tins.2020.03.003

Xiaoran, Y., S. Cosma, E. J. Jacob, K. Florent, M. Cristopher, Z. Lenka, . . . Z. Yaojia (2014). "Model selection for degree-corrected block models." Journal of Statistical Mechanics: Theory and Experiment **2014**(5): P05007.

Yamashita, A., N. Yahata, T. Itahashi, G. Lisi, T. Yamada, N. Ichikawa, . . . N. Okada (2019). "Harmonization of resting-state functional MRI data across multiple imaging sites via the separation of site differences into sampling bias and measurement bias." PLoS biology **17**(4): e3000042. https://doi.org/10.1371/journal.pbio.3000042

Yan, X. (2016). Bayesian model selection of stochastic block models. 2016 IEEE/ACM International Conference on Advances in Social Networks Analysis and Mining (ASONAM). https://doi.org/10.1109/ASONAM.2016.7752253

Yang, J. and J. Leskovec (2014). "Overlapping communities explain core–periphery organization of networks." Proceedings of the IEEE **102**(12): 1892-1902. https://doi.org/10.1109/JPROC.2014.2364018

Yarkoni, T., R. A. Poldrack, T. E. Nichols, D. C. Van Essen and T. D. Wager (2011). "Large-scale automated synthesis of human functional neuroimaging data." Nat Methods **8**(8): 665-670. https://doi.org/10.1038/nmeth.1635

Yeatman, J. D., B. A. Wandell and A. A. Mezer (2014). "Lifespan maturation and degeneration of human brain white matter." Nat Commun **5**: 4932. https://doi.org/10.1038/ncomms5932

Yeh, C. H., D. K. Jones, X. Liang, M. Descoteaux and A. Connelly (2020). "Mapping structural connectivity using diffusion MRI: Challenges and opportunities." Journal of Magnetic Resonance Imaging. https://doi.org/10.1002/jmri.27188

Yeh, F. C., S. Panesar, D. Fernandes, A. Meola, M. Yoshino, J. C. Fernandez-Miranda, . . . T. Verstynen (2018). "Population-averaged atlas of the macroscale human structural connectome and its network topology." Neuroimage **178**: 57-68. https://doi.org/10.1016/j.neuroimage.2018.05.027

Yeo, B. T., F. M. Krienen, M. W. Chee and R. L. Buckner (2014). "Estimates of segregation and overlap of functional connectivity networks in the human cerebral cortex." Neuroimage **88**: 212-227. https://doi.org/10.1016/j.neuroimage.2013.10.046

Yeo, B. T., F. M. Krienen, J. Sepulcre, M. R. Sabuncu, D. Lashkari, M. Hollinshead, . . . R. L. Buckner (2011). "The organization of the human cerebral cortex estimated by intrinsic functional connectivity." J Neurophysiol **106**(3): 1125-1165. https://doi.org/10.1152/jn.00338.2011

Young, J.-G., G. T. Cantwell, M. E. J. Newman and T. P. Peixoto (2020). "Bayesian inference of network structure from unreliable data." Journal of Complex Networks **8**(6). https://doi.org/10.1093/comnet/cnaa046

Young, J.-G., G. St-Onge, P. Desrosiers and L. J. Dubé (2018). "Universality of the stochastic block model." Physical Review E **98**(3). https://doi.org/10.1103/PhysRevE.98.032309

Young, M. P. (1993). "The organization of neural systems in the primate cerebral cortex." Proc Biol Sci **252**(1333): 13-18. https://doi.org/10.1098/rspb.1993.0040

Zalesky, A., A. Fornito and E. Bullmore (2012). "On the use of correlation as a measure of network connectivity." Neuroimage **60**(4): 2096-2106. https://doi.org/10.1016/j.neuroimage.2012.02.001

Zalesky, A., A. Fornito and E. T. Bullmore (2010). "Network-based statistic: identifying differences in brain networks." Neuroimage **53**(4): 1197-1207. https://doi.org/10.1016/j.neuroimage.2010.06.041

Zalesky, A., A. Fornito, I. H. Harding, L. Cocchi, M. Yücel, C. Pantelis and E. T. Bullmore (2010). "Whole-brain anatomical networks: does the choice of nodes matter?" Neuroimage **50**(3): 970-983. https://doi.org/10.1016/j.neuroimage.2009.12.027

Zamani Esfahlani, F., Y. Jo, J. Faskowitz, L. Byrge, D. P. Kennedy, O. Sporns and R. F. Betzel (2020). "High-amplitude cofluctuations in cortical activity drive functional connectivity." Proc Natl Acad Sci U S A **117**(45): 28393-28401. https://doi.org/10.1073/pnas.2005531117

Zamora-Lopez, G., Y. Chen, G. Deco, M. L. Kringelbach and C. Zhou (2016). "Functional complexity emerging from anatomical constraints in the brain: the significance of network modularity and rich-clubs." Sci Rep **6**(1): 38424. https://doi.org/10.1038/srep38424

Zamora-Lopez, G., C. Zhou and J. Kurths (2009). "Graph analysis of cortical networks reveals complex anatomical communication substrate." Chaos **19**(1): 015117. https://doi.org/10.1063/1.3089559

Zamora-Lopez, G., C. Zhou and J. Kurths (2010). "Cortical hubs form a module for multisensory integration on top of the hierarchy of cortical networks." Front Neuroinform **4**: 1. https://doi.org/10.3389/neuro.11.001.2010

Zhan, L., N. Jahanshad, J. Faskowitz, D. Zhu, G. Prasad, N. G. Martin, . . . P. M. Thompson (2015). Heritability of brain network topology in 853 twins and siblings. 2015 IEEE 12th International Symposium on Biomedical Imaging (ISBI), IEEE. https://doi.org/10.1109/ISBI.2015.7164080

Zhang, T., Q. Huang, C. Jiao, H. Liu, B. Nie, S. Liang, . . . B. Shan (2019). "Modular architecture of metabolic brain network and its effects on the spread of perturbation impact." Neuroimage **186**: 146-154. https://doi.org/10.1016/j.neuroimage.2018.11.003

Zhang, X., U. Braun, A. Harneit, Z. Zang, L. S. Geiger, R. F. Betzel, . . . J. R. Reinwald (2021). "Generative network models of altered structural brain connectivity in schizophrenia." Neuroimage **225**: 117510.

Zhang, Y., M. Brady and S. Smith (2001). "Segmentation of brain MR images through a hidden Markov random field model and the expectation-maximization algorithm." IEEE Trans Med Imaging **20**(1): 45-57. https://doi.org/10.1109/42.906424

Zhao, T., M. Cao, H. Niu, X. N. Zuo, A. Evans, Y. He, . . . N. Shu (2015). "Age-related changes in the topological organization of the white matter structural connectome across the human lifespan." Hum Brain Mapp **36**(10): 3777-3792. https://doi.org/10.1002/hbm.22877

Zhu, D., N. Jahanshad, B. C. Riedel, L. Zhan, J. Faskowitz, G. Prasad and P. M. Thompson (2016). Population learning of structural connectivity by white matter encoding and decoding. 2016 IEEE 13th International Symposium on Biomedical Imaging (ISBI), IEEE. https://doi.org/10.1109/ISBI.2016.7493329

Zimmermann, J., J. Griffiths, M. Schirner, P. Ritter and A. R. McIntosh (2018). "Subject specificity of the correlation between large-scale structural and functional connectivity." Network Neuroscience **3**(1): 90-106. https://doi.org/10.1162/netn_a_00055

Zingg, B., H. Hintiryan, L. Gou, M. Y. Song, M. Bay, M. S. Bienkowski, . . . H. W. Dong (2014). "Neural networks of the mouse neocortex." Cell **156**(5): 1096-1111. https://doi.org/10.1016/j.cell.2014.02.023

Zuo, X. N., Y. He, R. F. Betzel, S. Colcombe, O. Sporns and M. P. Milham (2017). "Human Connectomics across the Life Span." Trends Cogn Sci **21**(1): 32-45. https://doi.org/10.1016/j.tics.2016.10.005

Zuo, X. N., C. Kelly, A. Di Martino, M. Mennes, D. S. Margulies, S. Bangaru, . . . M. P. Milham (2010). "Growing together and growing apart: regional and sex differences in the lifespan developmental trajectories of functional homotopy." J Neurosci **30**(45): 15034-15043. https://doi.org/10.1523/JNEUROSCI.2612-10.2010

CURRICULUM VITAE
Joshua Ian Faskowitz

Education

2016-2021   Indiana University (IU), Bloomington, IN
Ph.D. Dual major in Neuroscience and Psychology, conferred May 2021
Advisor: Olaf Sporns, Ph.D.
Research Committee: Olaf Sporns, Ph.D. (co-chair), Aina Puce, Ph.D. (co-chair), Amanda Mejia, Ph.D., Richard F. Betzel, Ph.D.

2010-2014   University of Southern California (USC), Los Angeles, CA
B.A. Neuroscience and Cognitive Science, May 2014
Minor Marketing

Honors, Awards, Fellowships

2021   IU Department of Psychological and Brain Sciences J.R. Kantor Graduate Award (outstanding advanced graduate student)
2020-2021   IU College of Arts and Sciences Dissertation Research Fellowship
2019   Program in Neuroscience Travel Award
2016-2021   National Science Foundation Graduate Research Fellowship Program
2016, 2019   Advanced Computational Neuroscience Network Workshop Travel Award
2016   IU Department of Psychological and Brain Sciences Rebec Fellow
2014   USC Order of Troy
2014   USC Renaissance Scholar, Discovery Scholar
2014   Undergraduate Student Government Academic Research Fund Award
2013   USC Dornsife Student Opportunities for Undergraduate Research Award
2013   USC Dornsife Summer Undergraduate Research Fund Grant
2013   USC Davis Travel Undergraduate Research Fund Grant
2010-2014   USC Trustee Scholarship (full tuition)

Research and Training Experience

2016-2021   Graduate Research Assistant, Computational Cognitive Neuroscience Laboratory, Indiana University
Principal Investigator, Olaf Sporns Ph.D.
Researching and studying how to model the brain as a complex network using the tools of network science and graph theory; writing algorithms, functions, and scripts to analyze brain network data.

2014-2016	Project Assistant, Imaging Genetics Center, University of Southern California
	Principal Investigator, Paul Thompson Ph.D.
	Under Supervision of Neda Jahanshad Ph.D.
	Professional position in charge of processing raw scanner data to normalized, pre-processed, and analysis-ready neuroimages by writing workflows in Bash and Python.
2012-2014	Undergraduate Research Assistant, Emotion & Cognition Lab, University of Southern California
	Principal Investigator, Mara Mather, Ph.D.
	Under Supervision of Allison Ponzio Ph.D.
	Ran participants through experimental protocols, including electrical stimulation, physiological monitoring, and assisted setup for fMRI study

Academic Activities

Teaching

| 2018 | P211: Methods of Experimental Psychology (instructor of record) |
| 2018 | P303: Health Psychology (teaching assistant) |

Departmental Activities

2020-2021	Program in Neuroscience student representative
2018-2020	Student organizer of Grey Matters graduate student colloquium
2018-2021	SfN graduate student booth for Program in Neuroscience

Departmental Talks

2020	Decoding Neural Representational Spaces Using Multivariate Pattern Analysis, guest lecture for neuroscience seminar
2019	Networks and Brain Networks, graduate student colloquium
2019	Human Connectomics: Structural networks + community detection, guest lecture for P457: The Connected Brain
2019	The Stochastic Blockmodel, (SBM & WSBM), departmental meeting for Emerging Areas of Research grant
2017	Bag o DICOMS or: How I learned to love the Spaghetti, open lab meeting
2017	Connectomes, Weighted Stochastic Blockmodels, and the Life Span, graduate student colloquium

Schools, Workshops, Hackathons

2019	OHBM Hackathon, Rome, IT
2019	Brainhack-Networks, Pre-Netsci, University of Vermont
2018	Brainhack Global, Indiana University
2017	5th Indiana Neuroimaging Symposium and Hackathon, Purdue University
2017	Neurohackweek, University of Washington
2016	4th Indiana Neuroimaging Symposium and Hackathon, Indiana University
2015	OHBM Hackathon, Honolulu, USA

Publications

Preprints

1. **Faskowitz**, *, Tanner, *, Misic, B., Betzel, R., "An edge-centric model for harmonizing multi-relational network datasets," bioRxiv, 2021.
2. Levakov, G., **Faskowitz, J.**, Avidan, G., Sporns, O., "Mapping structure to function and behavior with individual-level connectome embedding," bioRxiv, 2021.
3. Milardi, D., Basile, G. A., **Faskowitz, J.**, Bertino, S., Quartarone, A., Anastasi, G., Bramanti, A., Cacciola, A., "Effects of diffusion signal modeling and segmentation approaches on subthalamic nucleus parcellation," bioRxiv, 2021.
4. Jo, Y., Esfahlani, F. Z., **Faskowitz, J.**, Chumin, E., Sporns, O., Betzel, R., "The diversity and multiplexity of edge communities within and between brain systems," bioRxiv, 2020.
5. Jo, Y., **Faskowitz, J.**, Esfahlani, F. Z., Sporns, O., Betzel, R. F., "Subject identification using edge-centric functional connectivity," bioRxiv, 2020.
6. Jahanshad, N., Ganjgahi, H., Bralten, J., Den Braber, A., **Faskowitz, J.**, Knodt, A., Lemaitre, H., Nir, T., Patel, B., Richie, S., "Do candidate genes affect the brain's white matter microstructure? large-scale evaluation of 6,165 diffusion mri scans," BioRxiv, 2017.
7. Moyer, D., Gutman, B. A., **Faskowitz, J.**, Jahanshad, N., Thompson, P. M., "An empirical study of continuous connectivity degree sequence equivalents," arXiv, 2016.

Scientific Journal Articles

1. Sporns, O., **Faskowitz, J.**, Teixeira, A. S., Cutts, S. A., Betzel, R. F., "Dynamic expression of brain functional systems disclosed by fine-scale analysis of edge time series," Network Neuroscience, no. Just Accepted, pp. 1–34,
2. Caron, B., Stuck, R., McPherson, B., Bullock, D., Kitchell, L., **Faskowitz, J.**, Kellar, D., Cheng, H., Newman, S., Port, N., "Collegiate athlete brain data for white matter mapping and network neuroscience," Scientific Data, vol. 8, no. 1, pp. 1–17, 2021.
3. Nir, T. M., Fouche, J.-P., Ananworanich, J., Ances, B. M., Boban, J., Brew, B. J., Chang, L., Chaganti, J. R., Ching, C. R., ... **Faskowitz, J.**, ... Jahanshad, N., "Association of immunosuppression and viral load with subcortical brain volume in an international sample of people living with hiv," JAMA network open, vol. 4, no. 1, e2031190–e2031190, 2021.
4. Esfahlani, F. Z., Jo, Y., **Faskowitz, J.**, Byrge, L., Kennedy, D. P., Sporns, O., Betzel, R. F., "High-amplitude cofluctuations in cortical activity drive functional connectivity," Proceedings of the National Academy of Sciences, vol. 117, no. 45, pp. 28 393–28 401, 2020.

5. **Faskowitz, J.**, Esfahlani, F. Z., Jo, Y., Sporns, O., Betzel, R. F., "Edge-centric functional network representations of human cerebral cortex reveal overlapping system-level architecture," Nature Neuroscience, 2020.
6. **Faskowitz, J.**, Sporns, O., "Mapping the community structure of the rat cerebral cortex with weighted stochastic block modeling," Brain Structure and Function, vol. 225, no. 1, pp. 71–84, 2020.
7. Hughes, C., **Faskowitz, J.**, Cassidy, B. S., Sporns, O., Krendl, A. C., "Aging relates to a disproportionately weaker functional architecture of brain networks during rest and task states," NeuroImage, p. 116 521, 2020.
8. Pizzagalli, F., Auzias, G., Yang, Q., Mathias, S. R., **Faskowitz, J.**, Boyd, J. D., Amini, A., Rivière, D., McMahon, K. L., Zubicaray, G. I., "The reliability and heritability of cortical folds and their genetic correlations across hemispheres," Communications Biology, vol. 3, no. 1, pp. 1–12, 2020.
9. Puxeddu, M. G., **Faskowitz, J.**, Betzel, R. F., Petti, M., Astolfi, L., Sporns, O., "The modular organization of brain cortical connectivity across the human lifespan," NeuroImage, p. 116 974, 2020.
10. Hughes, C., Cassidy, B. S., **Faskowitz, J.**, Avena-Koenigsberger, A., Sporns, O., Krendl, A. C., "Age differences in specific neural connections within the default mode network underlie theory of mind," NeuroImage, vol. 191, pp. 269–277, 2019.
11. Jahanshad, N., **Faskowitz, J. I.**, Roshchupkin, G., Hibar, D., Gutman, B. A., Tustison, N. J., Adams, H. H., Niessen, W., Vernooij, M. W., Ikram, M. A., "Multi-site meta-analysis of morphometry," IEEE/ACM transactions on computational biology and bioinformatics, 2019.
12. Corlier, F., Hafzalla, G., **Faskowitz, J.**, Kuller, L. H., Becker, J. T., Lopez, O. L., Thompson, P. M., Braskie, M. N., "Systemic inflammation as a predictor of brain aging: Contributions of physical activity, metabolic risk, and genetic risk," Neuroimage, vol. 172, pp. 118–129, 2018.
13. **Faskowitz, J.**, Yan, X., Zuo, X.-N., Sporns, O., "Weighted stochastic block models of the human connectome across the life span," Scientific reports, vol. 8, no. 1, p. 12 997, 2018.
14. Kelly, S., Jahanshad, N., Zalesky, A., Kochunov, P., Agartz, I., Alloza, C., Andreassen, O., Arango, C., Banaj, N., ... **Faskowitz, J.**, ... Donohoe, G., "Widespread white matter microstructural differences in schizophrenia across 4322 individuals: Results from the enigma schizophrenia dti working group," Molecular psychiatry, vol. 23, no. 5, p. 1261, 2018.
15. Van Erp, T. G., Walton, E., Hibar, D. P., Schmaal, L., Jiang, W., Glahn, D. C., Pearlson, G. D., Yao, N., ... **Faskowitz, J.**, ... Turner, J. A., "Cortical brain abnormalities in 4474 individuals with schizophrenia and 5098 control subjects via the enhancing neuro imaging genetics through meta analysis (enigma) consortium," Biological psychiatry, vol. 84, no. 9, pp. 644–654, 2018.
16. Dennis, E. L., **Faskowitz, J.**, Rashid, F., Babikian, T., Mink, R., Babbitt, C., Johnson, J., Giza, C. C., Jahanshad, N., Thompson, P. M., "Diverging volumetric trajectories following pediatric traumatic brain injury," Neuroimage: clinical, vol. 15, pp. 125–135, 2017.

17. Moyer, D., Gutman, B. A., **Faskowitz, J.**, Jahanshad, N., Thompson, P. M., "Continuous representations of brain connectivity using spatial point processes," Medical image analysis, vol. 41, pp. 32–39, 2017.
18. Wang, J., Braskie, M. N., Hafzalla, G. W., **Faskowitz, J.**, McMahon, K. L., Zubicaray, G. I.,Wright, M. J., Yu, C., Thompson, P. M., "Relationship of a common oxtr gene variant to brain structure and default mode network function in healthy humans," Neuroimage, vol. 147, pp. 500–506, 2017.
19. Hibar, D., Westlye, L. T., Erp, T. G., Rasmussen, J., Leonardo, C. D., **Faskowitz, J.**, Haukvik, U. K., Hartberg, C. B., Doan, N. T., Agartz, I., "Subcortical volumetric abnormalities in bipolar disorder," Molecular psychiatry, vol. 21, no. 12, p. 1710, 2016.
20. Lee, P. H., Baker, J. T., Holmes, A. J., Jahanshad, N., Ge, T., Jung, J.-Y., Cruz, Y., Manoach, D. S., Hibar, D. P., **Faskowitz, J**., … "Partitioning heritability analysis reveals a shared genetic basis of brain anatomy and schizophrenia," Molecular psychiatry, vol. 21, no. 12, p. 1680, 2016.
21. Whelan, C. D., Hibar, D. P., Velzen, L. S., Zannas, A. S., Carrillo-Roa, T., McMahon, K., Prasad, G., Kelly, S., **Faskowitz, J.**, deZubiracay, G., "Heritability and reliability of automatically segmented human hippocampal formation subregions," Neuroimage, vol. 128, pp. 125–137, 2016.

Peer-Reviewed Conference Proceedings

1. Ding, L., Zhu, A. H., Saremi, A., **Faskowitz, J. I.**, Håberg, A., Thompson, P. M., Jahanshad, N., "Voxelwise meta-analysis of brain structural associations with genomewide polygenic risk for alzheimer's disease," in 14th International Symposium on Medical Information Processing and Analysis, International Society for Optics and Photonics, vol. 10975, 2018, p. 109750L.
2. Jahanshad, N., Roshchupkin, G., **Faskowitz, J.**, Hibar, D. P., Gutman, B. A., Adams, H. H., Niessen, W. J., Vernooij, M. W., Ikram, M. A., Zwiers, M. P., "Multisite metaanalysis of image-wide genome-wide associations with morphometry," in Imaging Genetics, Academic Press, 2018, pp. 1–23.
3. Pizzagalli, F., Auzias, G., Amini, A., **Faskowitz, J.**, Rashid, F., Moyer, D., Kochunov, P., Rivière, D., Mangin, J.-F., Thompson, P. M., "Sulcal-based morphometry in parkinson's disease: A study of reliability and disease effects," in 14th International Symposium on Medical Information Processing and Analysis, International Society for Optics and Photonics, vol. 10975, 2018, 109750T.
4. Rinker, D. A., Jahanshad, N., Hibar, D. P., **Faskowitz, J.**, McMahon, K. L., Zubicaray, G. I., Wright, M. J., Thompson, P. M., "Genetic connectivity–correlated genetic control of cortical thickness, brain volume, and white matter," in Imaging Genetics, Academic Press, 2018, pp. 25–43.
5. Dennis, E. L., Rashid, F., **Faskowitz, J.**, Jin, Y., McMahon, K. L., De Zubicaray, G. I., Martin, N. G., Hickie, I. B., Wright, M. J., Jahanshad, N., "Mapping age effects along fiber tracts in young adults," in 2017 IEEE 14th International Symposium on Biomedical Imaging (ISBI 2017), IEEE, 2017, pp. 101–104.
6. Hafzalla, G. W., Ragothaman, A., **Faskowitz, J.**, Jahanshad, N., McMahon, K. L., De Zubicaray, G. I., Wright, M. J., Braskie, M. N., Prasad, G., Thompson, P. M., "A comparison of network definitions for detecting sex differences in brain connectivity

using support vector machines," in 2017 IEEE 14th International Symposium on Biomedical Imaging (ISBI 2017), IEEE, 2017, pp. 961–965.

7. Harrison, M. B., Riedel, B. C., Prasad, G., Jahanshad, N., **Faskowitz, J.**, Thompson, P. M., "Utilizing brain measures for large-scale classification of autism applying epic," in 12th International Symposium on Medical Information Processing and Analysis, International Society for Optics and Photonics, vol. 10160, 2017, 101600W.

8. Isaev, D., Gutman, B. A., Moyer, D., **Faskowitz, J.**, Thompson, P. M., "Cortical connectome registration using spherical demons," in 12th International Symposium on Medical Information Processing and Analysis, International Society for Optics and Photonics, vol. 10160, 2017, p. 101600M.

9. Kurmukov, A., Ananyeva, M., Dodonova, Y., Gutman, B., **Faskowitz, J.**, Jahanshad, N., Thompson, P., Zhukov, L., "Classifying phenotypes based on the community structure of human brain networks," in Graphs in Biomedical Image Analysis, Computational Anatomy and Imaging Genetics, Springer, Cham, 2017, pp. 3–11.

10. Mokrov, N., Panov, M., Gutman, B. A., **Faskowitz, J. I.**, Jahanshad, N., Thompson, P. M., "Simultaneous matrix diagonalization for structural brain networks classification," in International Conference on Complex Networks and their Applications, Springer, Cham, 2017, pp. 1261–1270.

11. Petrov, D., Gutman, B., Ivanov, A., **Faskowitz, J.**, Jahanshad, N., Belyaev, M., Thompson, P., "Structural connectome validation using pairwise classification," in 2017 IEEE 14th International Symposium on Biomedical Imaging (ISBI 2017), IEEE, 2017, pp. 451–455.

12. Petrov, D., Ivanov, A., **Faskowitz, J.**, Gutman, B., Moyer, D., Villalon, J., Jahanshad, N., Thompson, P., "Evaluating 35 methods to generate structural connectomes using pairwise classification," in International Conference on medical Image Computing and Computer-Assisted Intervention, Springer, Cham, 2017, pp. 515–522.

13. Pizzagalli, F., Auzias, G., Kochunov, P., **Faskowitz, J. I.**, Thompson, P. M., Jahanshad, N., "The core genetic network underlying sulcal morphometry," in 12th International Symposium on Medical Information Processing and Analysis, International Society for Optics and Photonics, vol. 10160, 2017, p. 101600C.

14. Belyaev, M., Dodonova, Y., Belyaeva, D., Krivov, E., Gutman, B., **Faskowitz, J.**, Jahanshad, N., Thompson, P., "Using geometry of the set of symmetric positive semidefinite matrices to classify structural brain networks," in International Conference on Network Analysis, Springer, Cham, 2016, pp. 257–267.

15. Dennis, E. L., Rashid, F., Villalon-Reina, J., Prasad, G., **Faskowitz, J.**, Babikian, T., Mink, R., Babbitt, C., Johnson, J., Giza, C. C., "Multi-modal registration improves group discrimination in pediatric traumatic brain injury," in International Workshop on Brainlesion: Glioma, Multiple Sclerosis, Stroke and Traumatic Brain Injuries, Springer, Cham, 2016, pp. 32–42.

16. **Faskowitz, J.**, Zubicaray, G. I., McMahon, K. L., Wright, M. J., Thompson, P. M., Jahanshad, N., "Comparison of template registration methods for multi-site meta-analysis of brain morphometry," in Medical Imaging 2016: Biomedical Applications in Molecular, Structural, and Functional Imaging, International Society for Optics and Photonics, vol. 9788, 2016, p. 978 822.

17. Hafzalla, G. W., Prasad, G., Baboyan, V. G., **Faskowitz, J.**, Jahanshad, N., McMahon, K. L., Zubicaray, G. I., Wright, M. J., Braskie, M. N., Thompson, P. M., "The heritability of

the functional connectome is robust to common nonlinear registration methods," in Medical Imaging 2016: Image Processing, International Society for Optics and Photonics, vol. 9784, 2016, 97841R.

18. Kurmukov, A., Dodonova, Y., Burova, M., Mussabayeva, A., Petrov, D., **Faskowitz, J.**, Zhukov, L. E., "Topological modules of human brain networks are anatomically embedded: Evidence from modularity analysis at multiple scales," in International Conference on Network Analysis, Springer, Cham, 2016, pp. 299–308.

19. Moyer, D., Gutman, B. A., **Faskowitz, J.**, Jahanshad, N., Thompson, P. M., "A continuous model of cortical connectivity," in International Conference on Medical Image Computing and Computer-Assisted Intervention, Springer, 2016, pp. 157–165.

20. Pizzagalli, F., Auzias, G., Kochunov, P., **Faskowitz, J. I.**, McMahon, K. L., De Zubicaray, G. I., Martin, N. G., Wright, M. J., Jahanshad, N., Thompson, P. M., "Genetic analysis of cortical sulci in 1,009 adults," in 2016 IEEE 13th International Symposium on Biomedical Imaging (ISBI), IEEE, 2016, pp. 833–837.

21. Zhu, D., Jahanshad, N., Riedel, B. C., Zhan, L., **Faskowitz, J.**, Prasad, G., Thompson, P. M., "Population learning of structural connectivity by white matter encoding and decoding," in 2016 IEEE 13th International Symposium on Biomedical Imaging (ISBI), IEEE, 2016, pp. 554–558.

22. Zhu, D., Lin, B., **Faskowitz, J.**, Ye, J., Thompson, P. M., "Embedded sparse representation of fmri data via group-wise dictionary optimization," in Medical Imaging 2016: Image Processing, International Society for Optics and Photonics, vol. 9784, 2016, 97841K.

23. Moyer, D., Gutman, B., Prasad, G., **Faskowitz, J.**, Ver Steeg, G., Thompson, P., "Blockmodels for connectome analysis," in 11th International Symposium on Medical Information Processing and Analysis, International Society for Optics and Photonics, vol. 9681, 2015, 96810A.

24. Zhan, L., Jahanshad, N., **Faskowitz, J.**, Zhu, D., Prasad, G., Martin, N. G., Zubicaray, G. I., McMahon, K. L., Wright, M. J., Thompson, P. M., "Heritability of brain network topology in 853 twins and siblings," in 2015 IEEE 12th International Symposium on Biomedical Imaging (ISBI), IEEE, 2015, pp. 449–453.

25. Zhu, D., Zhan, L., **Faskowitz, J.**, Daianu, M., Jahanshad, N., De Zubicaray, G. I., McMahon, K. L., Martin, N. G., Wright, M. J., Thompson, P. M., "Genetic analysis of structural brain connectivity using diccol models of diffusion mri in 522 twins," in 2015 IEEE 12th International Symposium on Biomedical Imaging (ISBI), IEEE, 2015, pp. 1167–1171.

Poster Presentations (first author)

1. **Faskowitz, J.**, Esfahlani, F. Z., Jo, Y., Sporns, O., Betzel, R. F., Edge functional connectivity reveals overlapping community structure, Poster presented virtually at OHBM, Montreal, CA, Jun. 2020.

2. **Faskowitz, J.**, Jo, Y., Esfahlani, F. Z., Sporns, O., Betzel, R. F., The edge-centric representation of functional brain networks, Poster presented virtually at OHBM, Montreal, CA, Jun. 2020.

3. **Faskowitz, J.**, Victroy, C., Hunt, D., Delogu, F., Hayashi, S., Betzel, R., Pestilli, F., The brainlife.io cloud-services for functional network neuroscience, Poster presented virtually at OHBM, Montreal, CA, Jun. 2020.

4. **Faskowitz, J.**, Sporns, O., Analyzing the structure of brain networks using stochastic block models, Poster presented at NetSci and Network Neuroscience satellite, Burlington, U.S.A., 2019.
5. **Faskowitz, J.**, Sporns, O., Mapping the community structure of the connectome with weighted stochastic block modeling, Poster presented at OHBM, Rome, IT, Jun. 2019.
6. **Faskowitz, J.**, Yan, X., Zuo, X.-N., Sporns, O., Weighted stochastic blockmodels of the human connectome across the life span, Poster presented at Sf N, San Diego, U.S.A, 2018.
7. **Faskowitz, J.**, Yan, X., Zuo, X.-N., Sporns, O., Development of community structure in the human connectome across the life span: An application of weighted stochastic blockmodels, Poster presented at NetSci and Network Neuroscience satellite, Indianapolis, U.S.A, 2017.
8. **Faskowitz, J.**, Pizzagalli, F., Jahanshad, N., Ching, C., Mwangi, B., Soares, J. C., Thompson, P. M., Cortical investigation of bipolar disorder reveals inferior frontal gyral and sulcal abnormalities, Poster presented at OHBM, Geneva, CH, 2016.
9. **Faskowitz, J.**, Pizzagalli, F., Mwangi, B., Kochunov, P., Thompson, P. M., Soares, J. C., N. J., Cortical abnormalities in patients with bipolar disorder more localized than in those with schizophrenia, Poster presented at Sf N, San Diego, U.S.A, 2016.
10. **Faskowitz, J.**, McMahon, K., Zubicaray, G., Thompson, P. M., Wright, M., Jahanshad, N., Cortical investigation of bipolar disorder reveals inferior frontal gyral and sulcal abnormalities, Poster presented at OHBM, Geneva, CH, 2016.
11. **Faskowitz, J.**, Ching, C., Soares, J. C., Thompson, P. M., Jahanshad, N., Brain white matter integrity in bipolar disorder subtypes assessed with diffusion tensor imaging, Poster presented at Cognitive Neuroscience Society, San Francisco, U.S.A, 2015.
12. **Faskowitz, J.**, Hibar, H., Thompson, P. M., Jahanshad, N., Test-retest reliability of cortical parcellations in 165 healthy adults for multi-site analyses in the enigma consortium, Poster presented at Sf N, Chicago, U.S.A, 2015.
13. **Faskowitz, J.**, Jahanshad, N., Hansell, N., Zubicaray, G., McMahon, K., Martin, N., Wright, M., Thompson, P. M., Cd56+ natural killer cell counts associate with reductions in white matter fractional anisotropy, Poster presented at OHBM, Honolulu, U.S.A, 2015.
14. **Faskowitz, J.**, Ponzio, A., Castrellon, J. J., Mather, M., The influence of emotion on the recognition of change, Poster presented at Western Psychological Association, Portland, U.S.A, 2014.